Kroenke, L. W., Berger, W. H., Janecek, T. R., et al., 1991
Proceedings of the Ocean Drilling Program, Initial Reports, Vol. 130

8. SITE 806[1]

Shipboard Scientific Party[2]

HOLE 806A

Date occupied: 17 February 1990

Date departed: 18 February 1990

Time on hole: 1 day, 15 min

Position: 0°19.11′N, 159°21.68′E

Bottom felt (rig floor; m, drill-pipe measurement): 2531.8

Distance between rig floor and sea level (m): 11.14

Water depth (drill-pipe measurement from sea level, m): 2520.7

Total depth (rig floor; m): 2615.50

Penetration (m): 83.70

Number of cores (including cores with no recovery): 9

Total length of cored section (m): 83.70

Total core recovered (m): 85.95

Core recovery (%): 102.7

Oldest sediment cored:
Depth (mbsf): 83.70
Nature: nannofossil ooze
Oldest age: late Pliocene
Youngest age: Quaternary
Measured velocity (km/s): ND

HOLE 806B

Date occupied: 18 February 1990

Date departed: 22 February 1990

Time on hole: 4 days, 4 hr, 30 min

Position: 0°19.11′N, 159°21.69′E

Bottom felt (rig floor; m, drill-pipe measurement): 2531.0

Distance between rig floor and sea level (m): 11.14

Water depth (drill-pipe measurement from sea level, m): 2519.9

Total depth (rig floor; m): 3274.10

Penetration (m): 743.10

Number of cores (including cores with no recovery): 78

Total length of cored section (m): 743.10 (APC, 320.0; XCB, 423.1)

Total core recovered (m): 666.36 (APC, 335.20; XCB, 331.15.)

Core recovery (%): 89 (APC, 104.8; XCB, 78.3)

Oldest sediment cored:
Depth (mbsf): 743.10
Nature: nannofossil chalk with foraminifers
Oldest age: early Miocene
Youngest age: Quaternary
Measured velocity (km/s): 2.2

HOLE 806C

Date occupied: 22 February 1990

Date departed: 25 February 1990

Time on hole: 2 days, 17 hr, 30 min

Position: 0°19.11′N, 159°21.70′E

Bottom felt (rig floor; m, drill-pipe measurement): 2531.9

Distance between rig floor and sea level (m): 11.14

Water depth (drill-pipe measurement from sea level, m): 2520.8

Total depth (rig floor; m): 3308.30

Penetration (m): 776.40

Number of cores (including cores with no recovery): 62

Total length of cored section (m): 587.60 (APC, 309.6; XCB, 278)

Total core recovered (m): 523.62 (APC, 320.61; XCB, 203.01)

Total section drilled without coring: 188.8

Core recovery (%): 89 (APC, 103.6; XCB, 73)

Oldest sediment cored:
Depth (mbsf): 776.4
Nature: foraminifer nannofossil chalk
Oldest age: late Oligocene
Youngest age: Quaternary
Measured velocity (km/s): 2.1

Principal results: Ocean Drilling Program (ODP) Site 806 (proposed Site OJP-1) is located on the northeastern margin of the Ontong Java Plateau, close to the equator (latitude 0°19.1′N, longitude 159°21.7′E) in 2520 m of water, roughly 125 km northeast of Deep Sea Drilling Project (DSDP) Sites 289/586. The site represents the shallow end member on a transect that was designed to detect depth-related paleoceanographic signals in Neogene sediments. We occupied this site with the objective to obtain a high-resolution carbonate record in an undisturbed setting, which could serve as a standard section for studies of ocean history, including biostratigraphy, chemostratigraphy, and acoustic stratigraphy.

Site 806 was positioned at the proposed location (OJP-1), on a 2-km-wide terrace interrupting a gentle incline sloping to the northeast. We used a single-channel-seismic (SCS) line acquired by the *Thomas Washington* during ROUNDABOUT Cruise 11 (0600 UTC, 21 December 1989). The seismic profile shows a full set of reflectors, comparable with those at Sites 289/586, with little or no disturbance.

Three holes were drilled, using the advanced hydraulic piston corer (APC) and the extended core barrel (XCB), with full recovery with the APC. Hole 806A, a dedicated hole, was cored with the APC to 83.7 mbsf into upper Pliocene sediments. Hole 806B was cored with the APC to 320 mbsf, at which point refusal occurred within the lower upper Miocene. The hole was continued with XCB coring to 743.1 mbsf, with 423.1 m of sediment cored and 331.2 m recovered (78%). Coring ended in the lowermost Miocene because of poor recovery. The hole was then logged. Hole 806C was cored with the APC to 309.6 mbsf and coring with the XCB was then begun. The aim was to core with the XCB to the lower middle Miocene a second time, and then drill ahead to search for the Oligocene/Miocene boundary. The attempt was successful. Drilling terminated in uppermost Oligocene sediments at 776.4 mbsf, with 278 m cored for a recovery rate of 73% and 188.8 m drilled without coring.

[1] Kroenke, L. W., Berger, W. H., Janecek, T. R., et al., 1991. *Proc. ODP, Init. Repts.,* 130: College Station, TX (Ocean Drilling Program).

[2] Shipboard Scientific Party is as given in the list of participants preceding the contents.

The entire sedimentary sequence encountered is considered as one lithologic unit (Unit 1), consisting of upper Oligocene to Pleistocene foraminifer nannofossil ooze and chalk to nannofossil ooze and chalk with foraminifers. Foraminifer abundances mostly range between 15% and 30%, with occasional excursions to 10% and 50%. Radiolarians are a minor constituent throughout the section. The ooze-chalk transition was placed between 338 and 340 mbsf; it is gradational and shows alternation of layers of varying induration, beginning at about 200 mbsf. The age of the sediments at the transition is ca. 10 Ma. Sedimentation throughout the time interval represented seems to have been continuous at this site.

Unit I is divided into two subunits at the ooze-chalk transition, as follows:

Subunit IA (0–339 mbsf) consists of Pleistocene to upper middle Miocene foraminifer nannofossil ooze to nannofossil ooze with foraminifers. Carbonate content generally ranges from 90% to 95%, except in the Pleistocene where it drops to 85%–90%. The dominant color is white, but the topmost several meters are very pale brown grading to light gray below, and then to white. Bioturbation is common throughout, ranging from slight to heavy. Liesegang banding is common throughout the subunit, although it appears to be fainter and more diffuse in appearance than at Sites 803–805. The best examples are near the bottom of the subunit. Authigenic pyrite was found, associated with burrows, and a slight odor of H_2S was occasionally noted on opening the cores. Microfaulting is rare. Sediments are generally soft, but in the lowermost portion of Subunit IA intervals of greater lithification appear (below 200 mbsf). Coring was impeded in one instance because of porcellanite nodules (Core 130-806C-34X) near the level of APC refusal. The shallowest porcellanite nodules were found at 240 mbsf (ca. 8 Ma). A change in the velocity-depth gradient occurs at this level. Deeper in the section, at the ooze-chalk transition, the character of the velocity profile noticeably changes: above this level, high-frequency variations are distinct; below it, they are subdued.

Subunit IB (339–776 mbsf) consists of lower upper Miocene to upper Oligocene foraminifer nannofossil chalk to nannofossil chalk with foraminifers, with a few intervals of nannofossil chalk. Foraminifer content is high (around 30%) down to about 600 mbsf (ca. 20 Ma) and decreases somewhat below that level. Radiolarian content is low. Carbonate content typically fluctuates between 90% and 95%. The color is dominantly white. Color banding occurs throughout; bands become thinner and more distinct with depth in the subunit. Small-scale flaser structures are present. Bioturbation is ubiquitous. Rare, centimeter-size porcellanite nodules were observed at several levels (350 and 510 mbsf). The depth gradient of dissolved silica is reduced at 350 mbsf and between 450 and 550 mbsf, possibly in response to precipitation.

The sediments in the chalk section posed no problem for coring with the XCB, down to the Oligocene/Miocene boundary zone, where recovery decreased. However, even where recovery is very good, core contents are largely broken up and brecciated, with evidence for grinding of chalk on chalk. This type of recovery is typical for the material below 320 mbsf, that is, the section cored with the XCB. The Oligocene/Miocene boundary is located between 740 and 750 mbsf, and apparently is without hiatus (although recovery is poor at this level). Sedimentation rates for the deep chalk section vary between 20 and 30 m/m.y., the same as for the upper portion of the chalk subunit.

The entire Miocene section exhibits little change in foraminifer content, carbonate percentage, and grain size; it also shows a steady increase in density and velocity with depth. The middle Miocene is characterized by rather high foraminifer abundances, with a minimum at the transition to the upper Miocene. Sedimentation rates increase from around 20 m/m.y. in the lower Miocene to more than 40 m/m.y. in the upper Miocene. Above the middle Miocene/upper Miocene boundary, there is a carbonate minimum. This feature correlates with a zone of increased dissolution in the eastern equatorial Pacific. Carbonate values reach a maximum (near 95%) in the middle portion of the upper Miocene and tend to decrease to the present, with increasing variability reflecting increasing fluctuations in the carbon chemistry of the ocean. Sedimentation rates decrease in the late Pliocene (to around 20 m/m.y. for the Pleistocene), despite the fact that the site was further off the equator in the late Miocene.

Magnetostratigraphies were produced for the uppermost section of the two holes. The high productivity experienced at this site, however, is not conducive to the retention of a magnetic signal.

Chemical gradients in interstitial waters at this site are generally similar to those at Site 803 and 805, reflecting the calcareous/siliceous nature of the sediments and the paucity of organic material. A somewhat higher supply of organic matter at this shallower site, close to the equator, tends to produce slightly stronger gradients. Calcium and magnesium gradients, influenced by basalt alteration reactions at depth, show the usual negative correlation. Strontium concentrations reflect recrystallization processes, which appear to be more vigorous at this site than at the other two, because of the higher sedimentation rates and the higher supply of organic matter. Dissolved silica shows a steady increase with depth, except for the minor reversals mentioned.

Excellent logs were obtained for sound velocity and density at Site 806. The fact that this site has continuous sedimentation at high rates will make these logs especially valuable for the interpretation of seismic profiles and for the study of Milankovitch cycles.

BACKGROUND AND OBJECTIVES

Overview

Site 806, the shallow-water anchor site of the Neogene depth transect on the Ontong Java Plateau, was drilled near target Site OJP-1 (2600 m) (Fig. 1). The site lies half-way between Site 805 and DSDP Site 586, and is intermediate in depth between the two. It is well above the present lysocline and just slightly north of the equator, in the region of maximum Pleistocene sediment supply rate. Effects of varying dissolution are expected to be subdued at this depth, and the high rate of accumulation should provide for maximum resolution within the Neogene record. Thus, the productivity history, and its ramifications for physical properties, should be optimally recorded in sediments accumulating at rates of 20–40 m/m.y. We expected to recover rich tropical assemblages of pelagic and benthic microfossils from these sediments, for use in paleoceanographic and biostratigraphic studies of the Neogene.

The site was planned for multiple coring in the upper portion of the section (Neogene and Quaternary), including two APC-cored holes to 250 mbsf, a third hole to 50 mbsf, and XCB-coring to 600 mbsf. The multiple coring was expected to provide for overlap between cores and for sufficient material for concurrent high-resolution studies. Logging was to provide the information necessary to interpret seismic reflection profiles, for correlation between holes, and for three-dimensional reconstruction of sedimentation rates.

Background

The general background to this site is contained in the "Introduction" chapter (this volume; also see Kroenke, 1972). The Ontong Java Plateau is a broad, shallow, mid-ocean highland in the western equatorial Pacific. Its shallowest regions lie above 2000 m, and its flanks reach depths in excess of 4500 m. With an area of 1.5 million km^2, it is the largest of the "classic" Pacific plateaus. The plateau has a crustal thickness on the order of 40 km. Apparently, it roughly maintained its present depth over much of its history, indicating isostatic equilibrium. Crustal seismic velocities are in the range of that of oceanic crust (Hussong et al., 1979).

The pelagic sediment cover of the plateau is uniquely suited for paleoceanographic studies. The maximum thickness of the sediment is over 1200 m and occurs below the top of the plateau, in water depths between 2000 and 2500 m. The sediment thins by roughly 100 m for every 200 m of water depth increase below 2200 m (Berger and Johnson, 1976). At Site 806, the sediment is approximately 1200 m thick.

Site 806 was planned as the shallow-water, end-member site of a Neogene depth transect in the equatorial portion of the On-

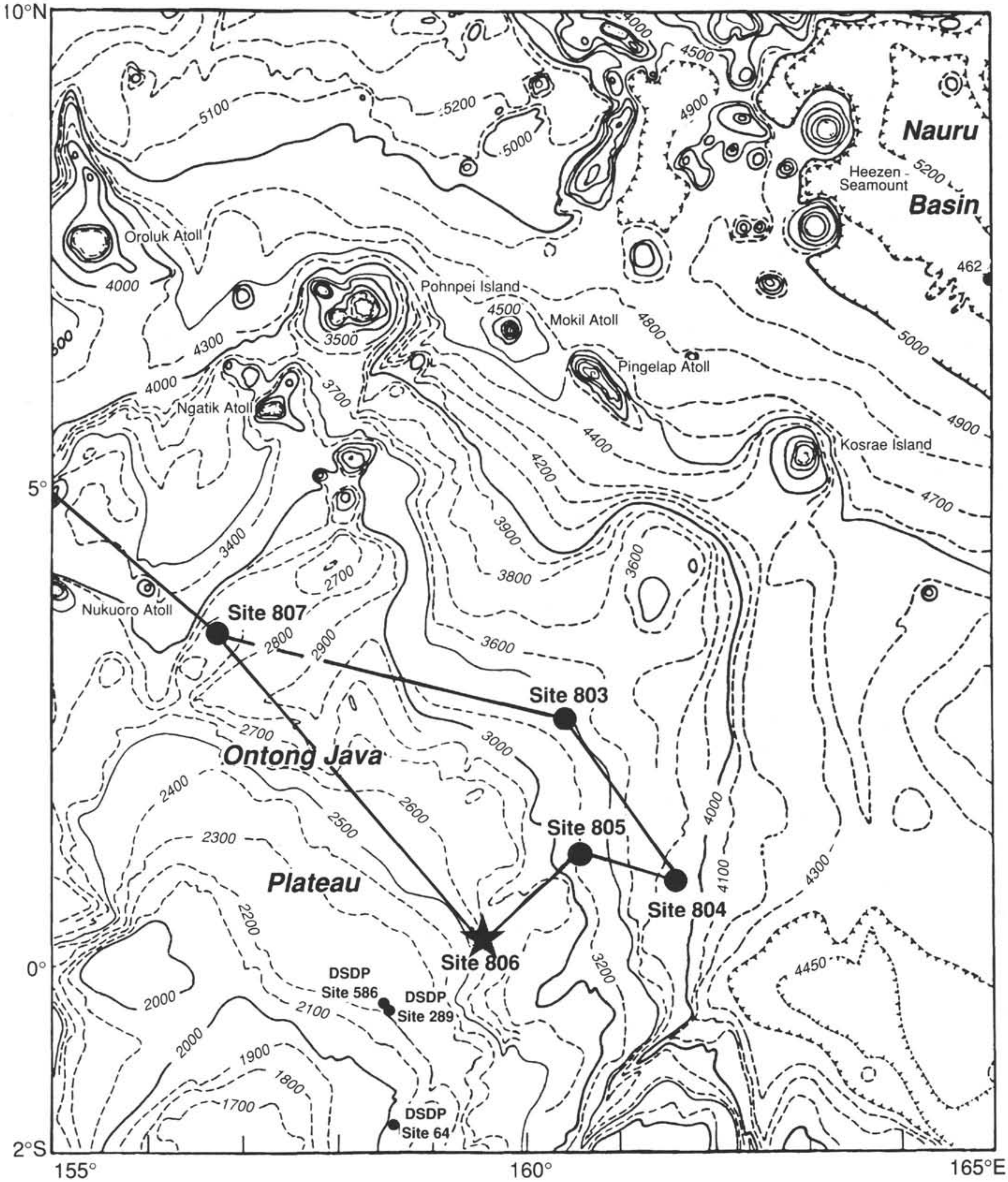

Figure 1. Bathymetry in meters of the northwestern part of the Ontong Java Plateau (after Mammerickx and Smith, 1985). The locations of the Leg 130 sites as well as DSDP Sites 64 and 289/586 are shown. Contour interval is 100 m.

tong Java Plateau, designed for the study of paleoceanographic events of global significance. In this transect, this site should have the highest sedimentation rates and the best preserved carbonates, containing the most complete paleoceanographic record. Problems arising from the creep of large sediment bodies, ubiquitous at water-depths between 3000 and 4000 m, seem to be of much reduced importance at this shallower depth. The site is well above the significant offset between the basement of the plateau and that of the deep ocean floor, which influences sediment stability further down the plateau flank (Fig. 2). Thus, although earthquakes presumably affect the area occasionally, the damage they can do is more restricted in extent (Berger et al., 1977). Selection of a suitable site to drill a continuous record is much less difficult under these conditions than in the deeper sites.

The seismic profiles across Site 806 (taken from the ROUNDABOUT survey conducted in December 1989) show gently dipping parallel reflectors with very little disturbance, except at depths well below the section of interest here, that is, below 800 mbsf (Fig. 3). We therefore expected to encounter a rather complete section at this site.

The plateau has long been the focus of Quaternary paleoceanographic studies based on conventional coring (e.g., Shackleton and Opdyke, 1976; Wu and Berger, 1989). Leg 130 is the fourth drilling expedition to sample the sediment cover here. Three DSDP sites on the plateau were rotary-drilled: participants on Leg 7 drilled and spot-cored Site 64 (Shipboard Scientific Party, 1971); and on Leg 30 the participants drilled and continuously cored Sites 288 and 289 (Shipboard Scientific Party, 1975). The upper 969 m in Site 289 consisted of upper Eocene to Pleistocene nannofossil foraminifer chalks and oozes. The section was found to be continuous from the lower Oligocene on, the top of which was reached at 890 mbsf. Semilithified chalk first appears near 250 mbsf (late Miocene). Results of paleoceanographic studies on Site 289 are reported in Kennett (1985). A fourth DSDP site, Site 586, drilled on Leg 89 next to Site 289, was cored with the hydraulic piston corer to 305 mbsf, reaching upper Miocene sediments (Shipboard Scientific Party, 1986). Well-preserved nannofossil ooze was recovered.

Objectives

Site 806 was planned as the shallowest site within the series of four equatorial sites constituting the Neogene depth transect (Sites 803–806; Fig. 1). The general objective of this transect was to detect depth-related paleoceanographic signals. The sediments sampled along the transect are produced in the same surface-water conditions and thus arrive on the seafloor more or less in the same pelagic rain. Differences in physical, chemical, and paleontological properties, therefore, can be largely attributed to a depth effect.

The depth sampled at Site 806 (Fig. 1), well above the modern lysocline in this region, is that which should show the greatest preservation and the least influence from variations in dissolution intensity. Thus, physical properties should show a signal that can serve as a standard, for comparison with the deeper sites. In turn, this would allow the identification of the factors that are responsible for producing the lithologic changes and which are detectable in the acoustic stratigraphy (productivity changes, dissolution events). The objective was to explore whether through such effects a clear linkage can be established between paleoceanographic events and acoustic stratigraphy (Mayer et al., 1986). Hiatus formation (presumably also linked to paleoceanographic events; Barron and Keller, 1982) should be at a minimum here. Establishing such linkages should allow three-dimensional mapping and correlation into distant sediment sections throughout the Pacific basin.

Regarding biostratigraphic objectives at this site, it was expected that changes in the relative abundance of calcareous and siliceous fossils and in the isotopic composition of planktonic foraminifers should provide clues to changes in intensity of productivity. An important objective is the determination of the original sedimentation rates, as a function of productivity history, with attendant implications for the study of the oceanic carbon cycle. The recovery of benthic foraminifers should allow

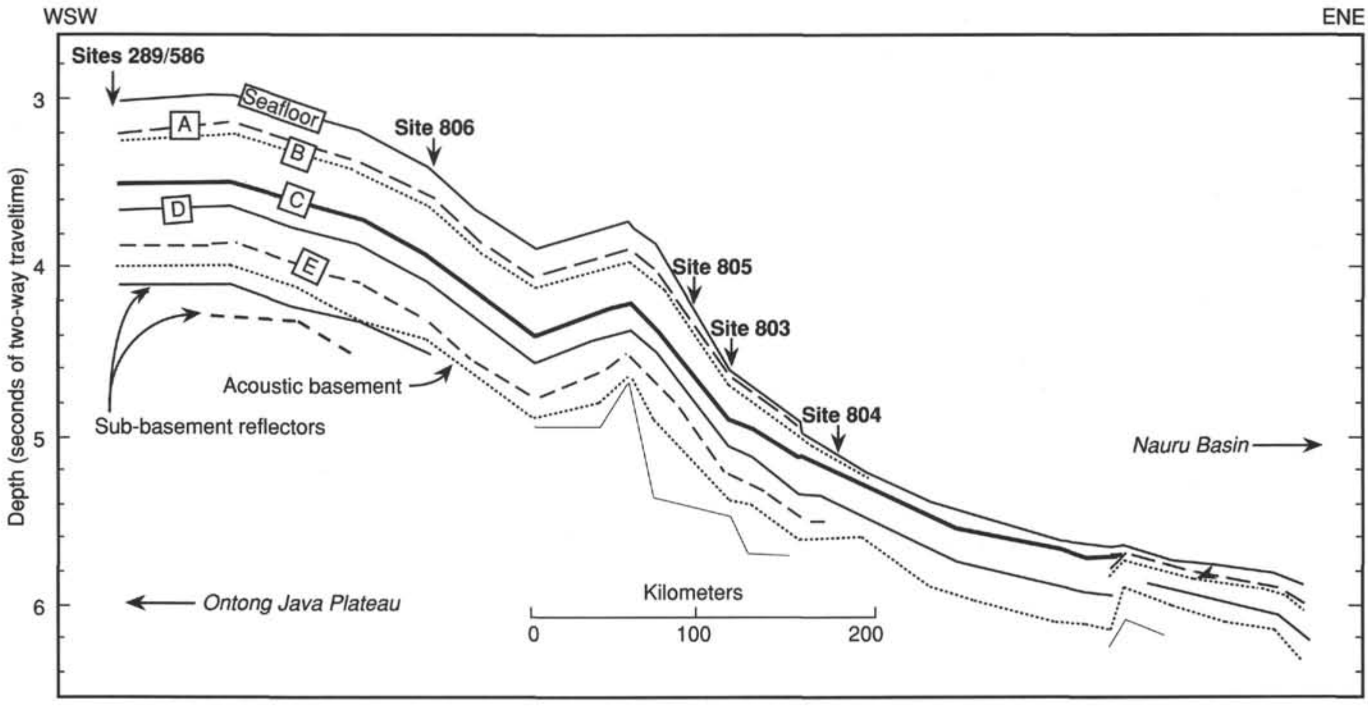

Figure 2. Simplified acoustic stratigraphy for the flank of the Ontong Java Plateau, and approximate location of Sites 803–806 (the depth transect).

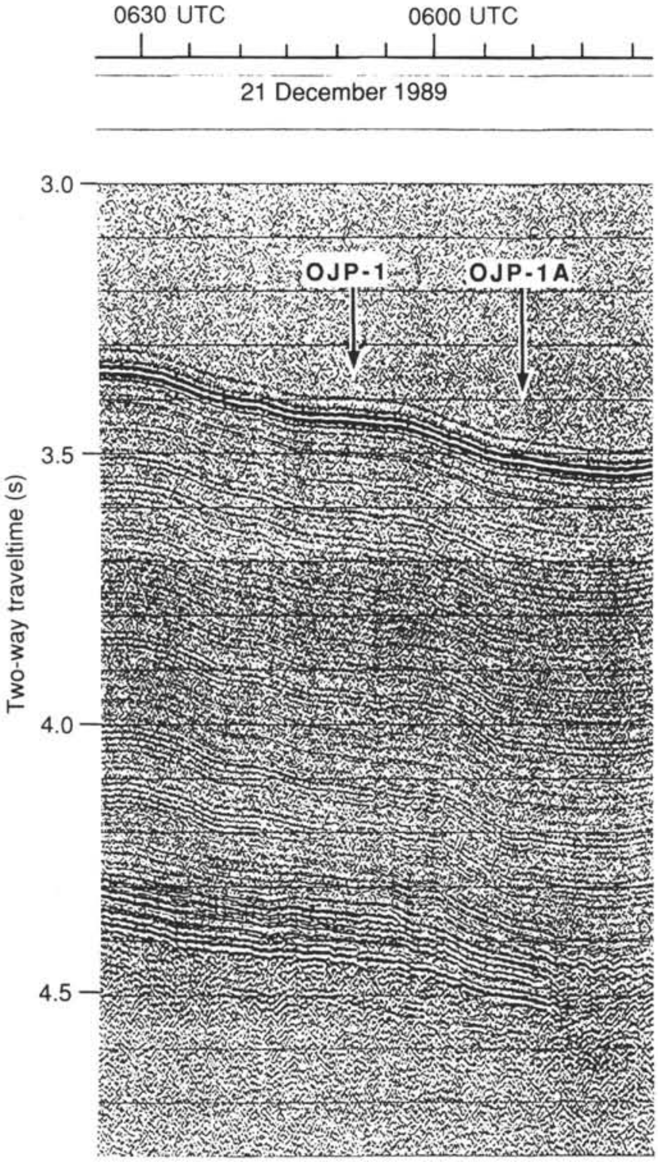

Figure 3. Seismic profiles across proposed drilling site for Site 806, showing evidence of planar disturbance (crinkly horizons) and debris flow (wedges next to basin rim).

reconstruction of upper deep-water properties directly, from their abundances and chemical composition. The effects of partial dissolution on biostratigraphic zonation (by selective removal of marker species) should be no problem at this depth level, allowing the verification and further development of a standard zonation.

OPERATIONS

The transit from Sites 805 to 806 covered 81 nmi in 6.25 hr at an average speed of 13.0 kt. A 17-nmi, pre-site seismic survey was run over the proposed site for 2.0 hr at 8.5 kt (details of site surveys are found in the "Underway Geophysics" chapter, this volume). Good global positioning system (GPS) satellite navigation was available for the site survey. The beacon was dropped at 1052 hr, 17 February 1990, on the proposed site, initiating Site 806.

Hole 806A

The ship was positioned 30 m east of the beacon. After the first core was taken, the core barrel became stuck in the pipe while being retrieved and could not be jarred loose or knocked loose by pumping. The drill string had to be pulled, and the outer-shear-pin sub dogs were found to have broken off and jammed the core barrel in the drill pipe. The core barrel was empty and thus was considered a water core. Core 130-806A-1H was taken at 0530 hr, 18 February 1990, in 2520.7 m of water. Cores 130-806A-1H through -9H (Table 1) were taken from 0 to 83.7 mbsf with 83.7 m of sediment cored and 85.95 m recovered (102.69% recovery). Orientation surveys were conducted during Cores 130-806A-3H through -9H. Hole 806A ended when the depth objective of 83 mbsf was reached. At this point, the pipe was pulled out of the hole, and the bit cleared the seafloor at 1100 hr, 18 February 1990.

Hole 806B

The ship was positioned 60 m east of the beacon. Core 130-806B-1H was taken at 1140 hr, 18 February 1990, in a water depth of 2519.9 m. Cores 130-806B-1H through -34H were taken from 0 to 320.0 mbsf with 320.0 m of sediment cored and 335.20 m recovered (104.75% recovery). Orientation surveys were conducted during Cores 130-806B-3H through -17H. Refusal of the APC was reached at Core 130-806B-34H when the core barrel became stuck and would not pull free, even with 100,000 lb of overpull. At this point, the core barrel was washed over 8 m and finally pulled free with 20,000 lb of overpull.

Cores 130-806B-35X through -78X were taken from 320.0 to 743.1 mbsf with 423.1 m of sediment cored and 331.16 m recovered (78.27% recovery). The XCB bit nozzles started plugging at Core 130-806B-40X (378.2 mbsf), and the sinker-bar assembly was removed to permit pump pressures up to 900 psi. This adjustment succeeded in improving core recovery until Core 130-806B-63X (598.6 mbsf) when the chalk became much harder and started jamming in the shoe. Attempts to improve recovery by reducing weight on bit (WOB) and using different cutting shoes met with mixed results because the formation alternated between hard and soft chalk. The sonic core monitor (SCM) was tested during Core 130-806B-77X, but the target jammed in the liner support sleeve and only 0.35 m of core was recovered. The SCM electronics appeared to work properly and showed that the blockage occurred during the first part of the coring process.

Coring ended in Hole 806B at 743.1 m in lower Miocene sediments, with recovery totaling 666.36 m (89.67% average recovery).

The first air drop in ODP history was made at 0420 hr, 20 February 1990, resulting in the successful delivery of a magnetic susceptibility coil, directional survey camera, and TV camera parts (but no ice cream machine).

Hole 806B Logging

After coring operations ceased, the pipe was pulled to 92 mbsf and a high-viscosity mud sweep was made to clean the hole.

The following logging runs were made:

Run No. 1: NGT/DIT/LSS. Two logs were run successfully from 741.0 to 90.2 mbsf at a rate of 900 ft/hr (306 m/hr). Less than 2 m of fill were found at the base of the hole.

Run No. 2: NGT/ACT/HLDT/GST/TLT. The tool was lowered down the hole to a depth of 740.1 mbsf and pulled back up at a rate of 600 ft/hr (204 m/hr). The GST malfunctioned at

Table 1. Coring summary, Site 806.

Core no.	Date (Feb. 1990)	Time (UTC)	Depth (mbsf)	Cored (m)	Recovered (m)	Recovery (%)
130-806A-						
1H	18	0530	0–7.7	7.7	7.75	100.0
2H	18	0610	7.7–17.2	9.5	9.69	102.0
3H	18	0655	17.2–26.7	9.5	9.89	104.0
4H	18	0730	26.7–36.2	9.5	9.79	103.0
5H	18	0755	36.2–45.7	9.5	9.85	103.0
6H	18	0835	45.7–55.2	9.5	9.76	103.0
7H	18	0915	55.2–64.7	9.5	9.73	102.0
8H	18	0945	64.7–74.2	9.5	9.74	102.0
9H	18	1020	74.2–83.7	9.5	9.75	102.0
Coring totals				83.7	85.95	102.7
130-806B-						
1H	18	1140	0–6.5	6.5	6.54	100.0
2H	18	1210	6.5–16.0	9.5	9.84	103.0
3H	18	1255	16.0–25.5	9.5	9.99	105.0
4H	18	1330	25.5–35.0	9.5	9.92	104.0
5H	18	1415	35.0–44.5	9.5	9.98	105.0
6H	18	1500	44.5–54.0	9.5	10.02	105.5
7H	18	1555	54.0–63.5	9.5	9.96	105.0
8H	18	1640	63.5–73.0	9.5	9.79	103.0
9H	18	1720	73.0–82.5	9.5	10.05	105.8
10H	18	1835	82.5–92.0	9.5	9.81	103.0
11H	18	1930	92.0–101.5	9.5	10.06	105.9
12H	18	2020	101.5–111.0	9.5	9.99	105.0
13H	18	2100	111.0–120.5	9.5	10.03	105.6
14H	18	2150	120.5–130.0	9.5	9.85	103.0
15H	18	2240	130.0–139.5	9.5	9.92	104.0
16H	18	2315	139.5–149.0	9.5	9.94	104.0
17H	19	0005	149.0–158.5	9.5	9.91	104.0
18H	19	0040	158.5–168.0	9.5	10.00	105.2
19H	19	0115	168.0–177.5	9.5	10.02	105.5
20H	19	0200	177.5–187.0	9.5	9.97	105.0
21H	19	0235	187.0–196.5	9.5	9.90	104.0
22H	19	0310	196.5–206.0	9.5	9.91	104.0
23H	19	0345	206.0–215.5	9.5	9.98	105.0
24H	19	0430	215.5–225.0	9.5	10.00	105.2
25H	19	0500	225.0–234.5	9.5	9.96	105.0
26H	19	0535	234.5–244.0	9.5	9.91	104.0
27H	19	0615	244.0–253.5	9.5	9.95	105.0
28H	19	0640	253.5–263.0	9.5	10.00	105.2
29H	19	0715	263.0–272.5	9.5	9.88	104.0
30H	19	0745	272.5–282.0	9.5	10.12	106.5
31H	19	0820	282.0–291.5	9.5	10.01	105.3
32H	19	0850	291.5–301.0	9.5	9.91	104.0
33H	19	0925	301.0–310.5	9.5	9.96	105.0
34H	19	1030	310.5–320.0	9.5	10.12	106.5
35X	19	1120	320.0–329.7	9.7	9.27	95.5
36X	19	1155	329.7–339.4	9.7	9.64	99.4
37X	19	1230	339.4–349.1	9.7	8.45	87.1
38X	19	1310	349.1–358.8	9.7	6.33	65.2
39X	19	1345	358.8–368.5	9.7	8.73	90.0
40X	19	1430	368.5–378.2	9.7	7.46	76.9
41X	19	1510	378.2–387.9	9.7	7.27	74.9
42X	19	1635	387.9–397.5	9.6	9.74	101.0
43X	19	1805	397.5–407.2	9.7	9.62	99.2
44X	19	1915	407.2–416.9	9.7	9.55	98.4
45X	19	2045	416.9–426.5	9.6	9.37	97.6
46X	19	2300	426.5–436.1	9.6	9.50	98.9
47X	20	0005	436.1–445.8	9.7	6.93	71.4
48X	20	0115	445.8–455.5	9.7	9.76	100.0
49X	20	0210	455.5–463.6	8.1	9.74	120.0
50X	20	0315	463.6–473.3	9.7	8.43	86.9
51X	20	0400	473.3–482.6	9.3	9.75	105.0
52X	20	0500	482.6–492.3	9.7	7.73	79.7
53X	20	0620	492.3–501.9	9.6	6.20	64.6
54X	20	0725	501.9–511.6	9.7	9.65	99.5
55X	20	0810	511.6–521.3	9.7	9.77	101.0
56X	20	0910	521.3–530.9	9.6	5.87	61.1
57X	20	1005	530.9–540.5	9.6	9.74	101.0
58X	20	1105	540.5–550.2	9.7	9.72	100.0
59X	20	1205	550.2–559.9	9.7	9.74	100.0
60X	20	1305	559.9–569.6	9.7	6.99	72.0
61X	20	1410	569.6–579.3	9.7	9.73	100.0

Table 1 (continued).

Core no.	Date (Feb. 1990)	Time (UTC)	Depth (mbsf)	Cored (m)	Recovered (m)	Recovery (%)
130-806B- (Cont.)						
62X	20	1530	579.3–589.0	9.7	9.80	101.0
63X	20	1650	589.0–598.6	9.6	9.78	102.0
64X	20	1815	598.6–608.3	9.7	3.03	31.2
65X	20	1945	608.3–617.9	9.6	8.25	85.9
66X	20	2100	617.9–627.5	9.6	9.64	100.0
67X	20	2215	627.5–637.2	9.7	3.35	34.5
68X	20	2340	637.2–646.5	9.3	1.31	14.1
69X	21	0100	646.5–656.2	9.7	6.23	64.2
70X	21	0215	656.2–665.8	9.6	5.17	53.8
71X	21	0335	665.8–675.5	9.7	4.48	46.2
72X	21	0455	675.5–685.2	9.7	6.09	62.8
73X	21	0605	685.2–694.8	9.6	9.75	101.0
74X	21	0710	694.8–704.5	9.7	4.52	46.6
75X	21	0810	704.5–714.1	9.6	8.50	88.5
76X	21	0925	714.1–723.7	9.6	4.93	51.3
77X	21	1045	723.7–733.4	9.7	0.35	3.6
78X	22	1205	733.4–743.1	9.7	1.30	13.4
Coring totals				743.1	666.36	89.7
130-806C-						
1H	22	1840	0–5.6	5.6	5.58	99.6
2H	22	1925	5.6–15.1	9.5	9.93	104.0
3H	22	2020	15.1–24.6	9.5	9.98	105.0
4H	22	2050	24.6–34.1	9.5	9.98	105.0
5H	22	2120	34.1–43.6	9.5	9.11	95.9
6H	22	2210	43.6–53.1	9.5	9.48	99.8
7H	22	2245	53.1–62.6	9.5	9.81	103.0
8H	22	2325	62.6–72.1	9.5	9.91	104.0
9H	23	0000	72.1–81.6	9.5	10.00	105.2
10H	23	0045	81.6–91.1	9.5	9.98	105.0
11H	23	0145	91.1–100.6	9.5	10.07	106.0
12H	23	0215	100.6–110.1	9.5	9.98	105.0
13H	23	0240	110.1–119.6	9.5	9.81	103.0
14H	23	0310	119.6–129.1	9.5	9.72	102.0
15H	23	0340	129.1–138.6	9.5	9.67	102.0
16H	23	0405	138.6–148.1	9.5	9.87	104.0
17H	23	0435	148.1–157.6	9.5	9.92	104.0
18H	23	0500	157.6–167.1	9.5	9.89	104.0
19H	23	0530	167.1–176.6	9.5	9.57	101.0
20H	23	0600	176.6–186.1	9.5	9.79	103.0
21H	23	0630	186.1–195.6	9.5	9.29	97.8
22H	23	0700	195.6–205.1	9.5	9.75	102.0
23H	23	0730	205.1–214.6	9.5	9.94	104.0
24H	23	0800	214.6–224.1	9.5	9.86	104.0
25H	23	0835	224.1–233.6	9.5	9.85	103.0
26H	23	0905	233.6–243.1	9.5	9.97	105.0
27H	23	0935	243.1–252.6	9.5	9.86	104.0
28H	23	1005	252.6–262.1	9.5	10.18	107.1
29H	23	1035	262.1–271.6	9.5	9.91	104.0
30H	23	1105	271.6–281.1	9.5	9.96	105.0
31H	23	1135	281.1–290.6	9.5	9.93	104.0
32H	23	1205	290.6–300.1	9.5	9.94	104.0
33H	23	1235	300.1–309.6	9.5	10.12	106.5
34X	23	1315	309.6–319.3	9.7	0.02	0.2
35X	23	1345	319.3–328.9	9.6	9.09	94.7
36X	23	1425	328.9–338.5	9.6	9.33	97.2
37X	23	1500	338.5–348.2	9.7	6.98	71.9
38X	23	1545	348.2–357.9	9.7	7.64	78.7
39X	23	1625	357.9–367.6	9.7	8.20	84.5
40X	23	1730	367.6–377.3	9.7	6.71	69.2
41X	23	1840	377.3–387.0	9.7	6.69	68.9
42X	23	2000	387.0–396.7	9.7	9.43	97.2
43X	23	2055	396.7–406.3	9.6	9.50	98.9
44X	23	2200	406.3–415.9	9.6	9.47	98.6
45X	23	2300	415.9–425.6	9.7	9.57	98.6
46X	23	2350	425.6–435.2	9.6	9.31	97.0
47X	24	0045	435.2–444.9	9.7	9.43	97.2
48X	24	0140	444.9–454.6	9.7	4.20	43.3
49X	24	0245	454.6–464.5	9.9	6.79	68.6
50X	24	0340	464.5–474.3	9.8	9.54	97.3
51X	24	0445	474.3–483.7	9.4	6.33	67.3
52X	24	0515	483.7–493.3	9.6	5.10	53.1

Table 1 (continued).

Core no.	Date (Feb. 1990)	Time (UTC)	Depth (mbsf)	Cored (m)	Recovered (m)	Recovery (%)
130-806C- (Cont.)						
53X	24	0630	493.3–503.0	9.7	8.19	84.4
54X	24	0740	503.0–512.7	9.7	5.47	56.4
55X	24	0820	512.7–522.4	9.7	6.23	64.2
56X	24	0920	522.4–532.0	9.6	9.32	97.1
57X	24	1140	532.0–541.7	9.7	9.54	98.3
58X	24	1530	599.0–608.5	9.5	9.04	95.1
59X	24	2205	740.0–749.5	9.5	0.81	8.5
60X	24	2340	749.5–759.2	9.7	0.79	8.1
61X	25	0110	759.2–766.7	7.5	9.12	121.0
62X	25	0250	766.7–776.4	9.7	1.17	12.0
Coring totals				587.6	523.62	89.1

702.9 mbsf and was again lowered to 740.7 mbsf to restart the run. The second run up the hole proceeded smoothly until 486.5 mbsf, at which point the GST lost resolution. The tool string was lowered to 504.4 mbsf and the run restarted a third time. This third run was completed to a depth of 88.4 mbsf but the GST did not recalibrate properly. The tool was lowered one final time, to a depth of 334.1 mbsf, in order to restart the GST, but this attempt also was unsuccessful. The tool string was finally pulled on deck, the pipe was pulled out of the hole, and the bottom hole assembly (BHA) cleared the seafloor at 1830 hr, 22 February 1990, ending Hole 806B.

Hole 806C

The ship was positioned 90 m east of the beacon. Core 130-806C-1H was taken at 1840 hr, 22 February 1990, in 2520.8 m of water. Cores 130-806C-1H through -33H were taken from 0 to 309.6 mbsf with 309.6 m of sediment cored and 320.61 m recovered (103.56% recovery). Orientation surveys were taken during Cores 130-806C-3H through -12H. Coring with the APC ended at Core 130-806A-33H (309.6 m) to avoid getting the core barrel stuck in the hole.

Cores 130-806C-34X through -57X were taken from 309.6 to 541.7 mbsf. From that point, the hole was drilled ahead with a center bit to 599.0 mbsf. A spot core (Core 130-806C-58X) was taken from 599.0 to 608.5 mbsf to obtain a sedimentary interval not recovered in the previous hole. The spot core was successful in obtaining the interval. The hole was drilled further with a center bit to a depth of 740.0 mbsf. Cores 130-806C-59X through -62X were taken from 740.0 to 776.4 mbsf. The XCB coring operation drilled 278.0 m and recovered 203.01 m of sediment (73.02% average recovery).

Coring was terminated in Hole 806C after reaching the Miocene/Oligocene boundary. At Hole 806C, a total of 587.6 m of sediment was cored and 523.62 m recovered (89.11% recovery). After coring operations ceased, the pipe was pulled out of the hole and the BHA cleared the rotary table at 0900 hr, 25 February 1990, ending Site 806.

LITHOSTRATIGRAPHY

Introduction

Three holes were drilled at Site 806. Hole 806A was cored with the APC to a sub-bottom depth of 83.7 m. Cores from this hole were not split on board the ship. Hole 806B was cored with the APC to a sub-bottom depth of 320 m and was then cored with the XCB to a total depth of 743.1 mbsf. Hole 806C was cored with the APC to a sub-bottom depth of 309.6 m, cored with the XCB to 541.7 mbsf, drilled to 599 mbsf, cored with the XCB to 608.5 mbsf, drilled to 740 mbsf, and cored again with the XCB to a total sub-bottom depth of 776.4 m. Recovery was 100% in the APC-cored intervals and averaged 78% and 73% in the XCB-cored intervals of Holes 806B and 806C, respectively.

The sediments described from Site 806 are grouped into one lithostratigraphic unit (Unit I), as were the sediments from Sites 804 and 805, and the sediments from equivalent intervals at Sites 289 and 586 (Shipboard Scientific Party, 1975, 1986). This unit is composed of upper Oligocene to Pleistocene foraminifer nannofossil ooze and chalk to nannofossil ooze and chalk with foraminifers (Fig. 4). Foraminifer abundances range between 10% and 50% of the constituent grains in most of the smear slides analyzed (Fig. 5). The cored interval at Site 806 apparently comprises a complete stratigraphic section from the upper Oligocene to the Pleistocene (see "Biostratigraphy" section, this chapter).

Description of Units

Unit I

Intervals: Hole 806B, Cores 130-806B-1H through -62X;
Hole 806C, Cores 130-806C-1H through -78X
Age: Pleistocene–late Oligocene
Depth: 0–776.4 mbsf

Unit I is composed of foraminifer nannofossil ooze and chalk to nannofossil ooze and chalk with foraminifers. The unit is divided into two subunits: (1) Subunit IA (0–339 mbsf) is foraminifer nannofossil ooze to nannofossil ooze with foraminifers, and (2) Subunit IB (339–776.4 mbsf) is foraminifer nannofossil chalk to nannofossil chalk with foraminifers.

Subunit IA

Intervals: Hole 806B, Cores 130-806B-1H through -36X;
Hole 806C, Cores 130-806C-1H through -37X
Age: Pleistocene–early late Miocene
Depth: 0–339 mbsf

Subunit IA is composed of 339 m of foraminifer nannofossil ooze to nannofossil ooze with foraminifers. Foraminifer content, on the basis of smear slide estimates, generally fluctuates between 15% and 30% and only rarely dips below 10% (Fig. 5). These values are significantly higher than the foraminifer abundances at previous Leg 130 sites (Sites 803, 804, and 805). The sediments are, therefore, classified as foraminifer nannofossil ooze to nannofossil ooze with foraminifers.

The sediments of Subunit IA are described texturally as clayey silts to sandy clayey silts. The main constituent of the sediment is nannofossils, as reflected by the predominance of medium silt mean grain sizes determined by shipboard particle size analyses (Fig. 6 and Table 2). The coarser grains (fine sand and coarse silt) at this site are foraminifers, so that fluctuations in the mean grain size are a good indicator of the relative abundances of foraminifers and nannofossils. The foraminifers appear to be well preserved from smear slide observations. The smear slide abundances (Fig. 5) and the grain-size curve (Fig. 6) show large, repeated, and closely spaced fluctuations in the foraminifer content. Other constituents are typically observed in only trace amounts. These grains include radiolarians, siliceous sponge spicules, diatoms, silicoflagellates, volcanic glass, quartz, accessory minerals, and clay, in general order of decreasing abundance.

The carbonate abundance curve for Site 806 is similar to that from Site 805 (Fig. 7; cf. with Fig. 6, "Site 805" chapter, this volume). Carbonate contents range between 83% and 95% and are above 90% through most of the hole. The lowest carbonate values are found at the top of the hole, and X-ray diffraction (XRD) analyses suggest an abundance of terrigenous components (clays, quartz, and feldspars) in this interval. The carbonate

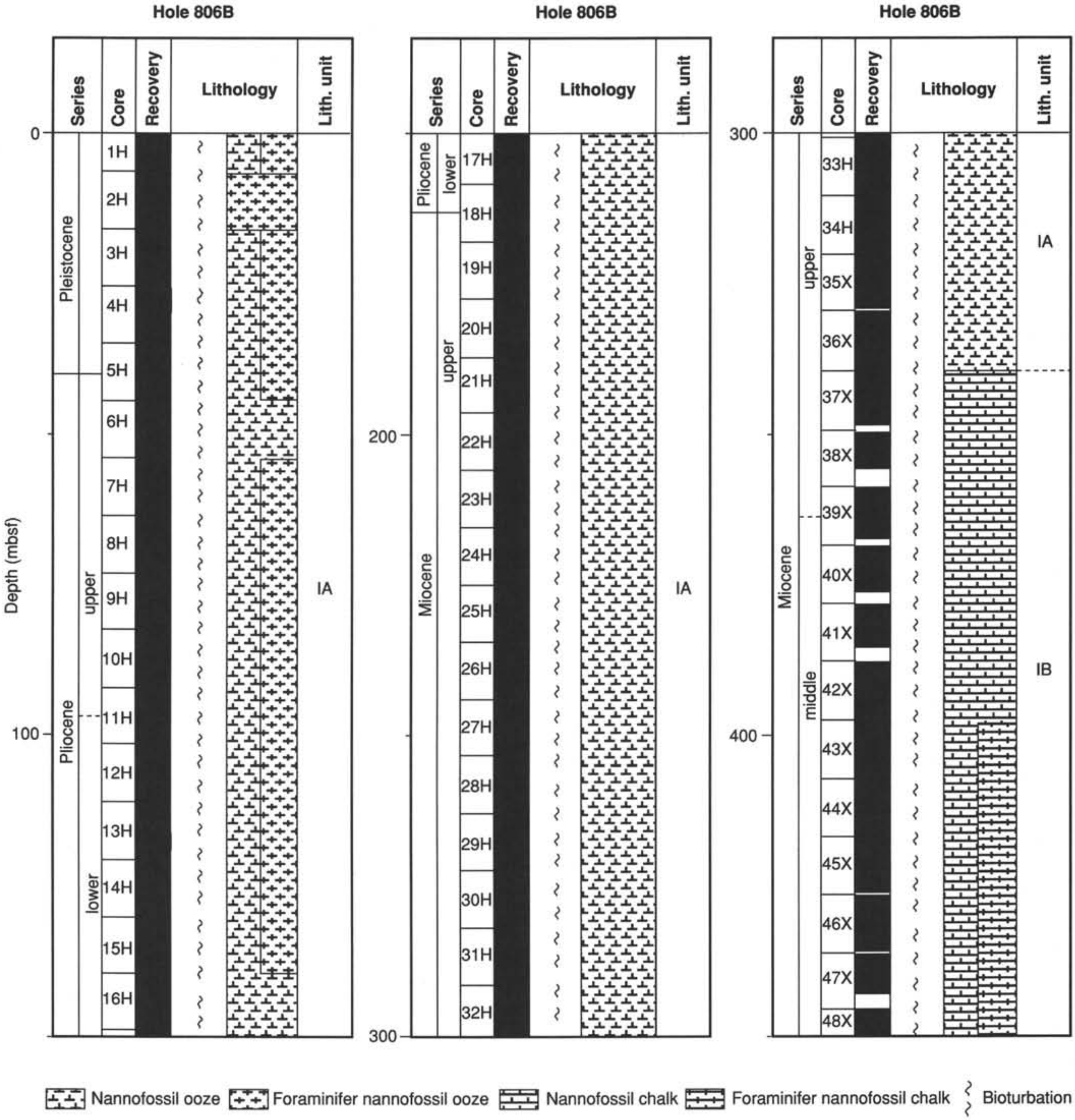

Figure 4. Lithologic summary, Holes 806B and 806C.

content gradually increases with depth to a value of approximately 94% near 250 mbsf, but decreases significantly at 100–120 mbsf (3.5–4.0 Ma), 150–170 mbsf (5.0–5.5 Ma), and 260–320 mbsf (7.0–8.5 Ma). These decreases are not yet explained in terms of dilution versus carbonate dissolution as no obvious relation exists between the carbonate content and the mean grain size, nor between the carbonate and the foraminifer contents (Figs. 5, 6, and 7).

The dominant color of the sediments in Subunit IA is white (2.5Y 8/0, 5Y 8/1, 7.5YR 8/1, and 10YR 8/1). The uppermost several meters at both Holes 806B and 806C are, however, very pale brown (10YR 7/3) and grade rapidly to light gray (10YR 7/2) and then to white. Color banding is common throughout Subunit IA, although the banding appears to be less frequent, fainter, and more diffuse than at Sites 803 to 805. These color bands are typically light greenish gray (5G 7/1) to pale yellowish green (10GY 7/2), light gray (N7/) to reddish gray (5R 6/1), and grayish blue (5PB 5/2) to pale purple (5P 6/2). They are generally 0.5–2 cm thick and horizontal and form groups distributed throughout a core. The groups of color bands are positioned at regular intervals in some parts of Subunit IA, but are apparently randomly distributed in others.

Bioturbation, ranging in intensity from moderate to heavy, is evident throughout the subunit. It is recognized by the presence

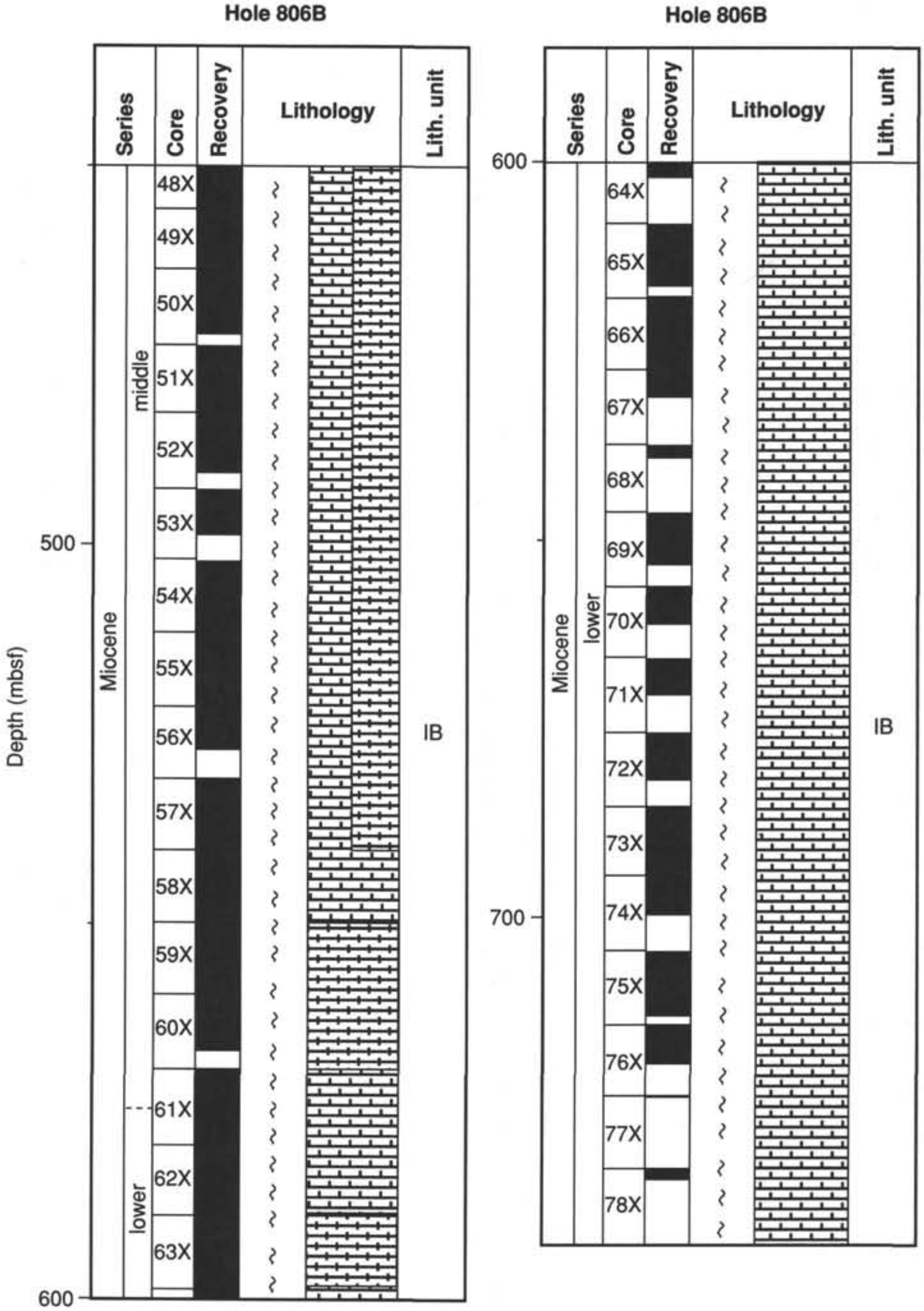

Figure 4 (continued).

of abundant centimeter-scale burrow mottles, discrete trace fossils, and pyritized burrow fillings. The burrow mottles are light gray (2.5Y 7/2) or pale purple (5P 6/2). The light gray mottles are typically 1-3 cm in diameter, aligned subhorizontally, and infilled with coarser and softer material than the surrounding matrix. The pale purple mottles form swirling patterns approximately 1 cm in diameter and are oriented at steep angles to the horizontal. The pale purple color is also present as halos and borders around obvious burrow structures, many of which are filled with authigenic pyrite. Pale purple color rings, greater than 10 cm in diameter, are also apparent in the cores. Bioturbation structures appear to be larger and more abundant than at Sites 803 and 804, though comparable with those observed at Site 805. A slight odor of H_2S was noted upon opening most cores from Subunit IA.

Within the fairly uniform sedimentary sequence of Subunit IA are several anomalies, the most significant of which are the rare occurrences of centimeter-size porcellanite nodules or concretions (Fig. 8). The shallowest concretion was found in the upper Miocene sequence at 240 mbsf in Hole 806C (Sections 130-806C-26H-5 and -6). Similar concretions are found only rarely below this level, except in Core 130-806C-34X, where coring was impeded and recovery was limited to a number of microcrystalline porcellanite concretions (Fig. 8). Smear slide analyses of scrapings from the split surface of a concretion showed the presence of nannofossils, and the concretion contains 14% $CaCO_3$.

Other features worthy of note within Subunit IA are microfaults, pumice, and thin (centimeter-scale) beds of well-sorted foraminifer ooze. Microfaults were observed as offsets in color bands at 290 mbsf in Hole 806B (Section 130-806B-31H-6) and

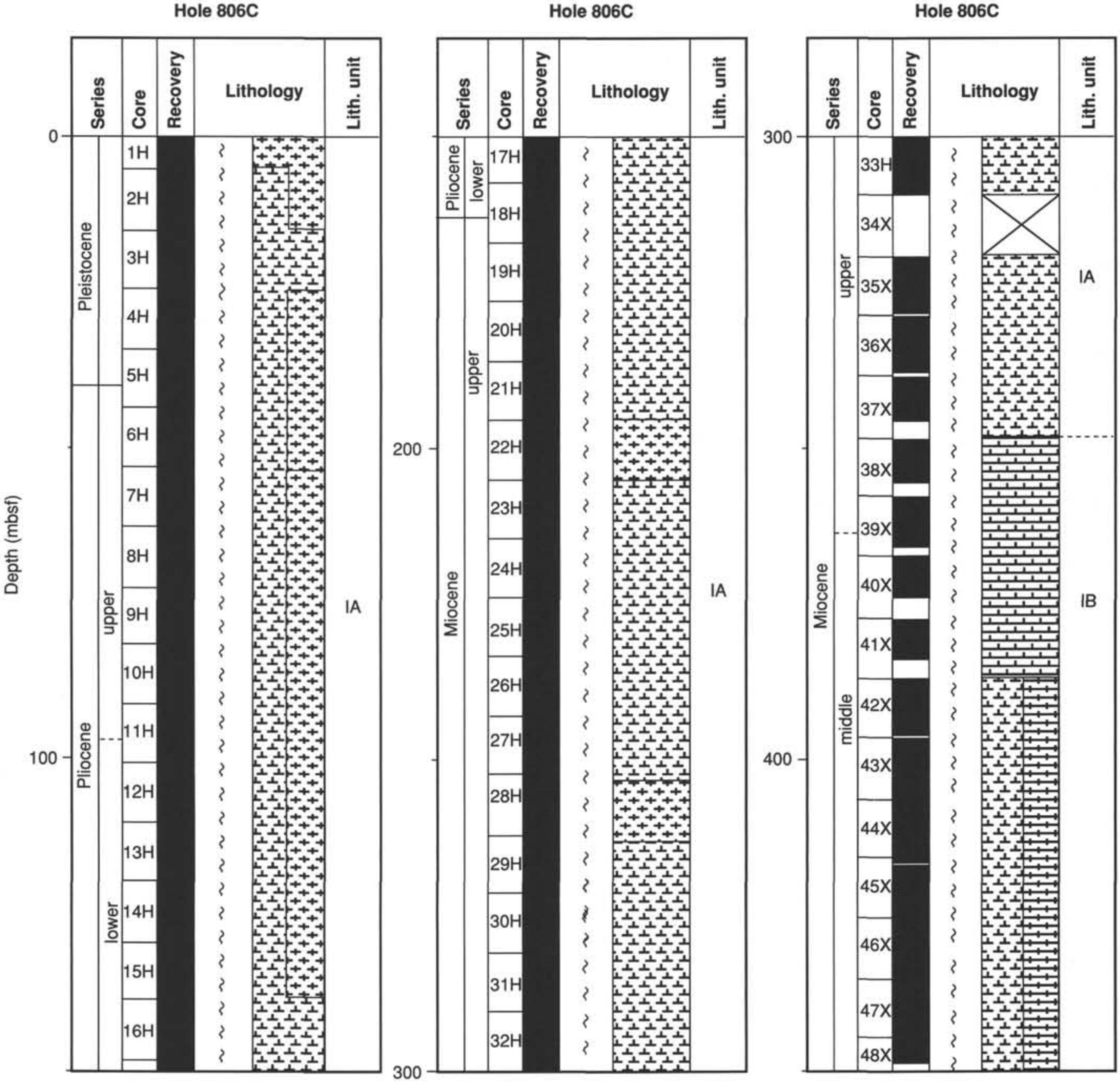

Figure 4 (continued).

at 190 and 299 mbsf in Hole 806C (Sections 130-806C-21H-4 and -32H-6). A pumice pebble, 2–3 cm in diameter, was found at 56.6 mbsf in Hole 806C (Section 130-806C-7H-3, 52 cm; Fig. 9). At 39.4 and 45.1 mbsf within Hole 806C (Sections 130-806C-5H-4 and -6H-2, respectively), thin (1 and 3 cm) beds of well-sorted foraminifer tests were observed. The lower contacts of these beds are sharp and even, and the upper contacts are obscured by bioturbation. The material within the beds is primarily whole foraminifer tests and grading is not obvious. Grain size analyses were conducted on samples from the bed at 39.4 mbsf (Fig. 10) and demonstrate the coarser, well-sorted nature of the bed relative to the surrounding sediment.

At approximately 200 mbsf (upper Miocene) in Holes 806B and 806C, the first signs of sediment induration were observed as thin (centimeter-scale), stiff to hard layers interspersed within the softer ooze matrix. These harder intervals appear to be nodular rather than continuous, although it is not known if this pattern is primary or a function of the coring process. With increasing depth these stiff intervals gradually become harder and thicker. The placement of the ooze-chalk transition is subjective, but it normally coincides with the level at which the saw, rather than the pull-wire, is necessary to split the core. Given this criterion, the ooze-chalk transition at Site 806 was placed at approximately 340 mbsf in both holes, even though sediments at this level are still interbedded chalks and oozes. Several additional lines of evidence, however, support placing this transition at 320 mbsf:

1. The downhole caliper log shows that the hole is narrower and more stable at 320 mbsf than above, perhaps because of the

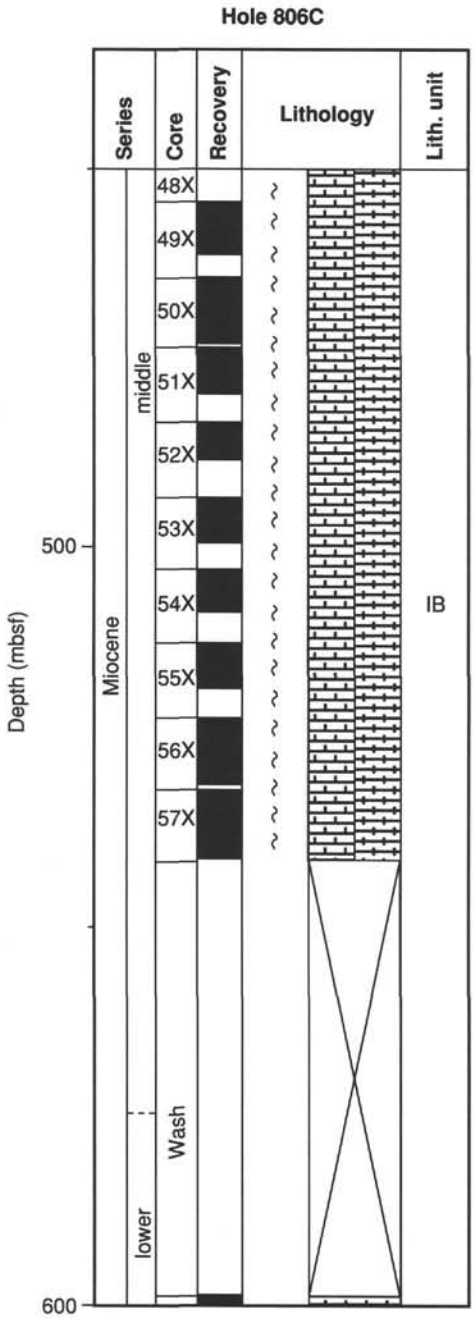

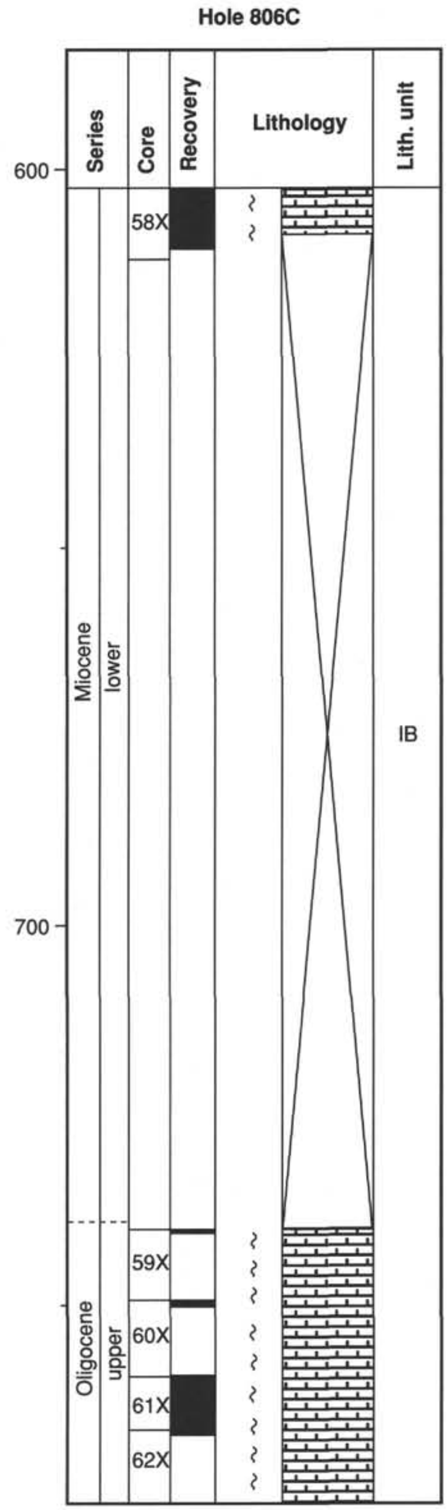

Figure 4 (continued).

transition from ooze to chalk (see "Logging" section, this chapter).

2. Sonic velocities measured on board ship increase markedly for samples recovered below 320 m (see "Physical Properties" section, this chapter), but these measurements have not been corrected for *in-situ* conditions. Because porosity rebound caused by the removal of overburden is greater in unlithified material than in cemented chalks, this velocity increase is a function of cementation and correlates well with the ooze-chalk transition chosen from evidence in the recovered sediments. Sonic velocities from the downhole velocity log increase gradually and show no obvious correlation with the onset of lithification, since these measurements were made under conditions of existing overburden.

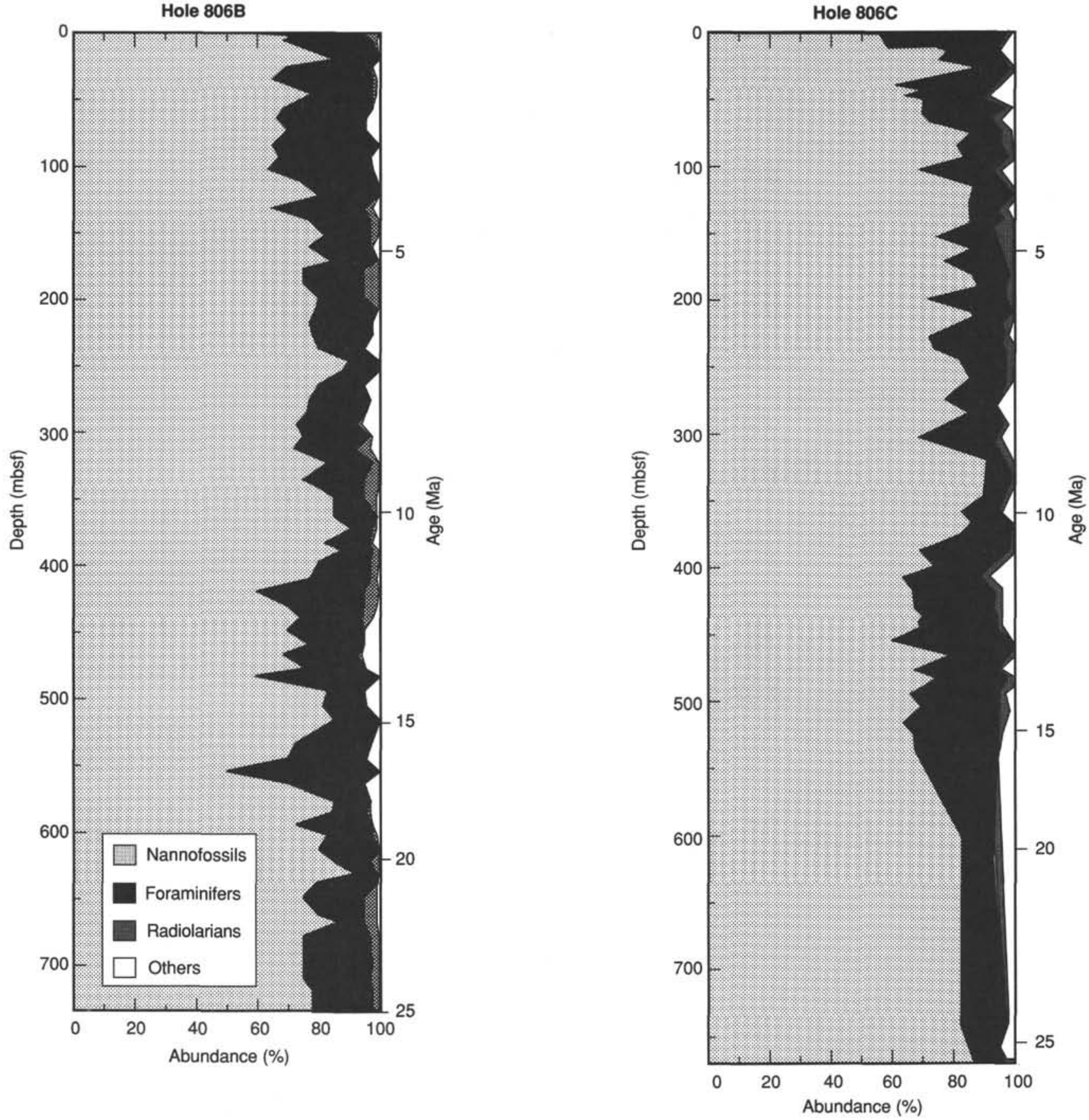

Figure 5. Abundances of major components, Holes 806B and 806C, as determined from smear slide analyses. Age designations are from the sedimentation rate data provided in the "Sedimentation Rates" section (this chapter).

Subunit IB

Intervals: Hole 806B, Cores 130-806B-37X through -78X;
Hole 806C, Cores 130-806C-38X through -62X
Age: early late Miocene–late Oligocene
Depth: 339–776.4 mbsf

Subunit IB, from 339 to 560 mbsf (lower upper Miocene to lower Miocene), is composed of foraminifer nannofossil chalk to nannofossil chalk with foraminifers, with a few intervals of nannofossil chalk. From 560 mbsf to the base of Hole 806C at 776.4 mbsf (lower Miocene to upper Oligocene), Subunit IB contains nannofossil chalk with foraminifers. The foraminifer content of Subunit IB, which varies between 10% and 50%, is high relative to that of equivalent intervals at Sites 803, 804, and 805 (Fig. 5). The amounts of other components, such as radiolarians, remain low (<5% to trace), as in Subunit IA. The mean carbonate content in this interval (Fig. 7) remains high at approximately 94%, but the short-term fluctuations are more extreme than in Subunit IA, ranging between values of 88% and 95%.

The dominant sediment color of Subunit IB is white (2.5Y 8/0 and 10YR 8/1). A few intervals (20–30 cm thick) are pale pink (5RP 8/2) to light pale purple (5P 6/2) in color. Thin (<0.1–1 cm thick), faint, and distinct color bands are common. These bands are light gray (5Y 7/2), pale blue (5PB 7/2), pale purple (5P 6/2), and greenish gray (5G 7/1) in color. The color

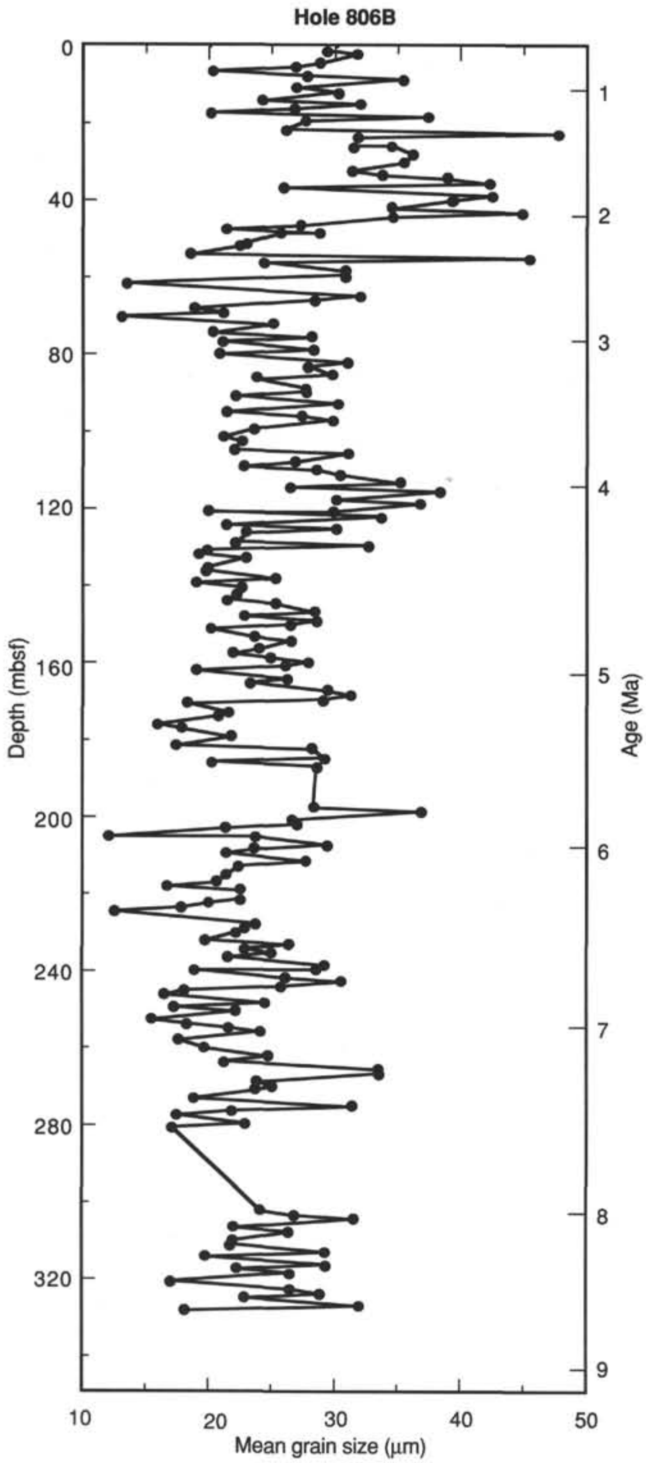

Figure 6. Mean grain-size curve, Hole 806B. Age designations are from the sedimentation rate data provided in the "Sedimentation Rates" section (this chapter).

bands become thinner, more distinct, and wavy in shape (approaching flaser structures) with depth in the subunit.

The sediments of Subunit IB are moderately to heavily bioturbated, as evident from burrow mottles, pyrite-filled trace structures and burrows, and discrete trace fossils (e.g., *Zoophycos*) (Fig. 11). Rare, centimeter-size porcellanite nodules were observed within this subunit, located at approximately 350 mbsf in Hole 806C (Sections 130-806C-38X-1 and -2), and at 509 mbsf and 514 mbsf in Hole 806B (Sections 130-806B-54X-5 and -55X-2).

The top of Subunit IB consists of soft chalk with interbeds of ooze. Color bands at this depth are faint, diffuse, and typically about 1 cm thick. The chalk intervals gradually become thicker and more lithified with depth. The color banding is millimeter-scale in thickness and very distinct by about 370 mbsf. By approximately 530 mbsf the sediment is composed of 100% chalk (no ooze) and is well lithified. Burrow traces at this depth are flattened, and color bands are very thin ($\ll$0.1 cm) and wavy in appearance, forming flaser structures. The bands typically occur in groups from about 1 to 3 cm thick (Fig. 12), and become thinner and more braided with increasing depth. Furthermore, single, very thin ($\ll$0.1 cm) light gray (N7/), slightly wavy bands are apparent (Fig. 13). Fracturing occurs readily along these surfaces.

Discussion

The sedimentary column at Site 806 is composed of homogeneous nannofossil oozes and chalks with foraminifers to foraminifer nannofossil oozes and chalks. The foraminifer abundances are high relative to those observed at the sites drilled in deeper water during Leg 130 (Sites 803–805), and typically range between 15% and 30%. The foraminifer tests are generally well preserved in comparison with those from Sites 803–805 (Fig. 14). This evidence, combined with biostratigraphic data (see "Biostratigraphy" section, this chapter) and the absence of primary sedimentary structures, suggests that the sedimentary section at this site was deposited by biogenic pelagic processes since the late Oligocene, without interruption or significant dissolution.

The most significant variation in the sediments at Site 806 is the change in foraminifer content, and consequently in mean grain size. On a large scale, foraminifer abundance is low in the upper Oligocene and lower Miocene, highest in the middle Miocene, low again in the upper Miocene, and high through the Pliocene and Pleistocene (Fig. 5). On a smaller scale, the high-frequency variations in foraminifer content appear on a scale of meters to tens of meters. Higher resolution grain-size and smear slide information, however, will be necessary to describe or quantify this variability adequately.

The fluctuations in the foraminifer content and mean grain size reflect the interplay of several factors, including overall productivity and the relative production rates of the different fossil groups, climatic conditions, changes in surface-water circulation, and changes in the effects preservation/dissolution and/or winnowing. It is difficult to determine the importance of each of these processes at this time. The good state of preservation of foraminifers and the water depth of this site suggest that dissolution has been of minor importance, but detailed work is required to document degrees of dissolution. The sediments exhibit little evidence of winnowing, although heavy bioturbation may have obscured such sedimentary structures. Two thin beds of well-sorted foraminifer ooze in Hole 806C (39.4 and 45.1 mbsf) may provide limited evidence for bottom current activity. These beds are well sorted, contain whole foraminifer tests, and are apparently ungraded. Because of their ungraded nature and uniform composition of foraminifers, these beds are interpreted as lag deposits formed by strong winnowing events, rather than as turbidites. In contrast, the turbidites at Site 804 contain numerous fragments of foraminifers mixed with other constituents and are graded (see "Lithostratigraphy" section, "Site 804" chapter, this volume).

Foraminifer abundance fluctuations may also be explained by changes in relative productivity, but it is difficult to imagine a bloom in foraminifers without an accompanying bloom in the

Table 2. Mean grain size of sediments from Subunit IA, as determined by shipboard analyses.

Core, section, interval (cm)	Depth (mbsf)	Mean grain size (μm)
130-806B-		
1H-1, 112	1.12	29.3
1H-2, 110	2.60	31.8
1H-3, 96	3.96	29.0
1H-4, 110	5.60	26.8
1H-5, 23	6.23	20.4
2H-1, 108	7.58	27.7
2H-2, 109	9.09	35.2
2H-3, 110	10.60	27.1
2H-4, 111	12.11	30.1
2H-5, 111	13.61	24.5
2H-6, 111	15.11	32.0
2H-7, 49	15.99	27.0
3H-1, 75	16.75	20.4
3H-2, 75	18.25	37.3
3H-3, 75	19.75	27.6
3H-4, 75	21.25	26.1
3H-5, 75	22.75	47.5
3H-6, 75	24.25	31.9
3H-7, 74	25.74	31.5
4H-1, 70	26.20	34.4
4H-2, 70	27.70	36.1
4H-4, 70	30.70	35.7
4H-5, 70	32.20	31.3
4H-6, 70	33.70	33.6
4H-7, 60	35.10	39.0
5H-1, 75	35.75	42.2
5H-2, 75	37.25	26.0
5H-3, 75	38.75	42.3
5H-4, 75	40.25	39.3
5H-5, 75	41.75	34.6
5H-6, 75	43.25	44.7
6H-1, 10	44.60	34.6
6H-2, 10	46.10	27.3
6H-3, 10	47.60	21.4
6H-4, 10	49.10	28.8
6H-4, 10	49.10	25.8
6H-5, 10	50.60	23.4
6H-6, 10	52.10	22.6
6H-7, 10	53.60	18.7
7H-1, 109	55.09	45.5
7H-2, 110	56.60	24.8
7H-3, 110	58.10	30.7
7H-4, 109	59.59	30.6
7H-5, 111	61.11	13.5
8H-1, 110	64.60	31.9
8H-2, 110	66.10	28.6
8H-3, 110	67.60	18.9
8H-4, 110	69.10	21.1
8H-5, 110	70.60	12.9
8H-6, 110	72.10	24.9
9H-1, 109	74.09	20.4
9H-2, 109	75.59	28.2
9H-3, 109	77.09	21.1
9H-4, 109	78.59	28.2
9H-5, 109	80.09	20.8
9H-6, 109	81.59	31.0
10H-1, 69	83.19	28.0
10H-2, 110	85.10	29.6
10H-3, 109	86.59	23.9
10H-4, 109	88.09	27.3
10H-5, 110	89.60	27.6
10H-6, 109	91.09	22.3
11H-1, 110	93.10	30.0
11H-2, 110	94.60	21.4
11H-3, 109	96.09	27.3
11H-4, 125	97.75	29.6
11H-5, 111	99.11	23.7
12H-1, 10	101.60	21.2
12H-2, 10	103.10	22.4
12H-3, 10	104.60	22.1
12H-4, 10	106.10	31.0
12H-5, 10	107.60	26.8

Table 2 (continued).

Core, section, interval (cm)	Depth (mbsf)	Mean grain size (μm)
130-806B- (Cont.)		
12H-6, 10	109.10	22.8
12H-7, 10	110.60	28.8
13H-1, 59	111.59	30.3
13H-2, 59	113.09	35.1
13H-3, 59	114.59	26.6
13H-4, 59	116.09	38.2
13H-5, 59	117.59	30.0
13H-6, 59	119.09	36.7
13H-7, 59	120.59	29.7
14H-1, 40	120.90	20.0
14H-2, 40	122.40	33.6
14H-3, 36	123.86	21.3
14H-4, 34	125.34	30.1
14H-5, 34	126.84	23.1
14H-6, 36	128.36	22.2
14H-7, 24	129.74	32.7
15H-1, 35	130.35	19.9
15H-2, 35	131.85	19.2
15H-3, 35	133.35	22.9
15H-4, 40	134.90	20.1
15H-5, 41	136.41	19.7
15H-6, 40	137.90	25.3
15H-7, 40	139.40	19.1
16H-1, 110	140.60	22.4
16H-2, 110	142.10	22.1
16H-3, 110	143.60	21.8
16H-4, 110	145.10	25.3
16H-5, 110	146.60	28.2
16H-6, 110	148.10	22.9
16H-7, 75	149.25	28.6
17H-1, 110	150.10	26.6
17H-2, 109	151.59	20.2
17H-3, 110	153.10	23.5
17H-4, 110	154.60	26.3
17H-5, 110	156.10	23.9
17H-6, 110	157.60	22.0
17H-7, 40	158.40	24.8
18H-1, 96	159.46	27.8
18H-2, 96	160.96	26.0
18H-3, 96	162.46	18.9
18H-4, 96	163.96	26.1
18H-5, 96	165.46	23.2
18H-6, 96	166.96	29.4
19H-1, 10	168.10	31.1
19H-2, 10	169.60	29.1
19H-3, 10	171.10	18.5
19H-4, 10	172.60	21.4
19H-5, 10	174.10	20.8
19H-6, 10	175.60	16.0
20H-1, 15	177.65	18.0
20H-2, 15	179.15	21.7
20H-3, 110	181.60	17.5
20H-4, 110	183.10	28.3
20H-5, 110	184.60	29.1
20H-6, 110	186.10	20.4
20H-7, 15	186.65	28.5
22H-1, 110	197.60	28.3
22H-2, 110	199.10	36.7
22H-3, 110	200.60	26.6
22H-4, 110	202.10	26.9
22H-5, 110	203.60	21.3
22H-6, 110	205.10	12.3
22H-7, 10	205.60	23.6
23H-1, 105	207.05	29.3
23H-2, 109	208.59	23.6
23H-3, 38	209.38	21.4
23H-4, 109	211.59	27.7
23H-5, 105	213.05	22.4
23H-6, 105	214.55	21.5
24H-1, 110	216.60	20.7
24H-2, 110	218.10	16.9

Table 2 (continued).

Core, section, interval (cm)	Depth (mbsf)	Mean grain size (μm)
130-806B- (Cont.)		
24H-3, 109	219.59	22.5
24H-4, 106	221.06	22.5
24H-5, 110	222.60	20.2
24H-6, 110	224.10	18.0
24H-7, 40	224.90	12.5
25H-2, 108	227.58	23.6
25H-3, 108	229.08	22.8
25H-4, 109	230.59	22.2
25H-5, 119	232.19	19.8
25H-6, 111	233.61	26.2
25H-7, 48	234.48	22.7
26H-1, 108	235.58	24.9
26H-2, 104	237.04	21.7
26H-3, 109	238.59	29.0
26H-4, 109	240.09	28.5
26H-4, 109	240.09	19.1
26H-5, 110	241.60	26.1
26H-6, 109	243.09	30.3
26H-7, 39	243.89	25.7
27H-1, 110	245.10	18.2
27H-2, 110	246.60	16.6
27H-3, 110	248.10	24.4
27H-4, 105	249.55	17.4
27H-5, 105	251.05	21.9
27H-6, 108	252.58	15.4
27H-7, 40	253.40	18.2
28H-1, 109	254.59	21.7
28H-2, 109	256.09	24.0
28H-3, 115	257.65	17.6
28H-5, 115	260.65	19.7
28H-6, 109	262.09	24.6
29H-1, 109	264.09	21.2
29H-2, 109	265.59	33.5
29H-3, 113	267.13	33.4
29H-4, 99	268.49	23.8
29H-5, 104	270.04	25.1
29H-6, 116	271.66	23.8
30H-1, 111	273.61	18.6
30H-2, 111	275.11	31.2
30H-3, 111	276.61	21.9
30H-4, 111	278.11	17.6
30H-5, 110	279.60	22.7
30H-6, 111	281.11	17.1
33H-1, 110	302.10	24.1
33H-2, 110	303.60	26.7
33H-3, 110	305.10	31.6
33H-4, 110	306.60	21.9
33H-5, 110	308.10	26.5
33H-6, 110	309.60	21.9
34H-1, 102	311.52	21.8
34H-2, 109	313.09	29.4
34H-3, 110	314.60	19.9
34H-4, 110	316.10	29.4
34H-5, 110	317.60	22.2
34H-6, 110	319.10	26.2
35X-1, 104	321.04	17.1
35X-2, 104	322.54	26.6
35X-3, 106	324.06	28.9
35X-4, 107	325.57	23.1
35X-5, 108	327.08	31.7
35X-6, 91	328.41	18.2

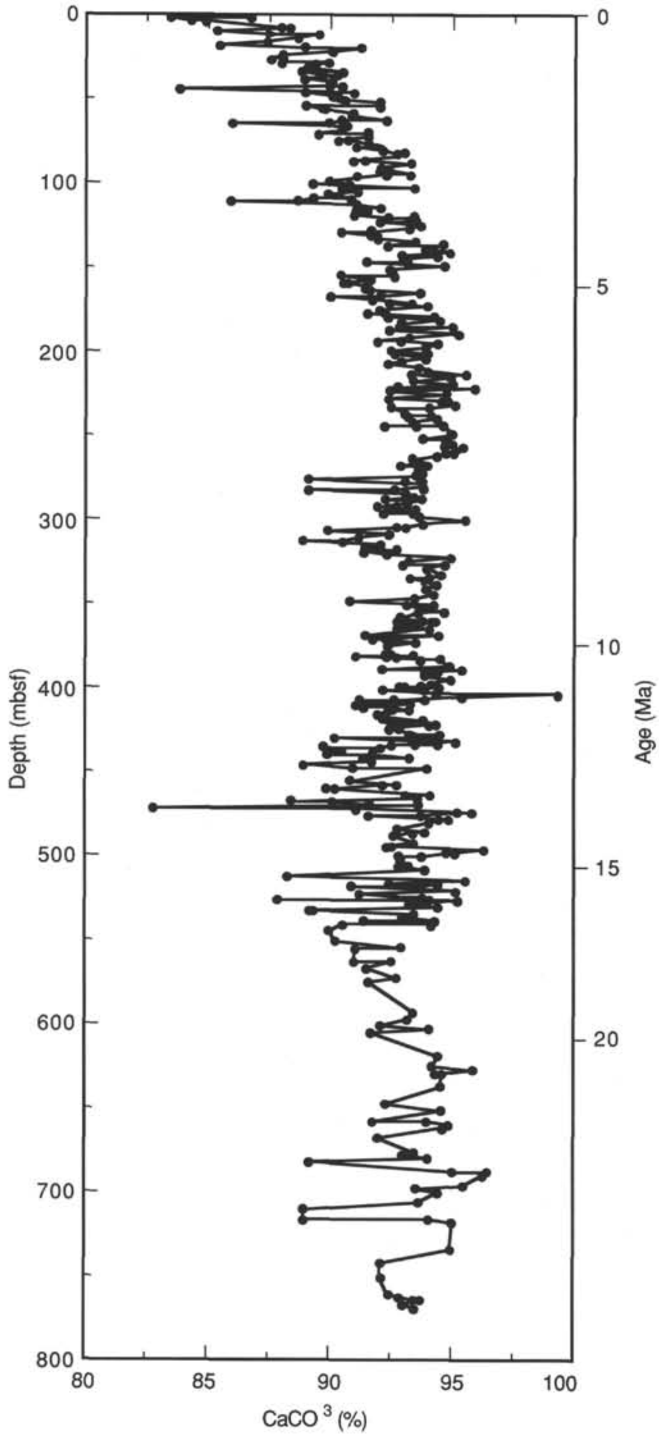

Figure 7. Carbonate contents, Hole 806B. Age designations are from the sedimentation rate data provided in the "Sedimentation Rates" section (this chapter).

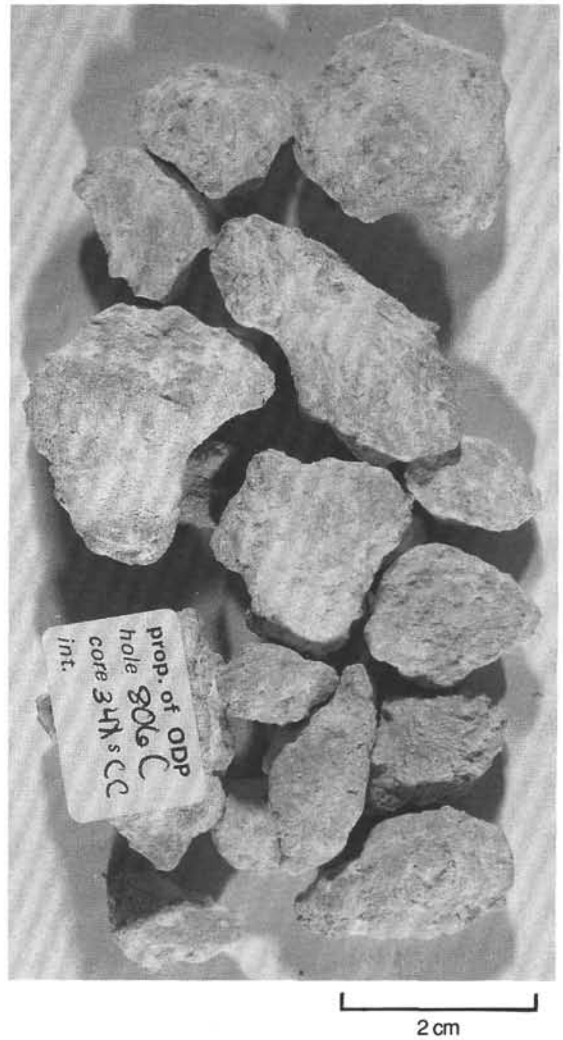

Figure 8. Porcellanite nodules (Core 130-806C-34X; 309.6 mbsf; upper middle Miocene). These nodules were the only material recovered in Core 130-806C-34X.

nannofossils. In addition, the intervals with high sedimentation rates do not correlate well with the periods of higher foraminifer abundance (see "Sedimentation Rates" section, this chapter). Instead, the intervals with low sedimentation rates correlate with high foraminifer abundances, supporting the winnowing hypothesis for the concentration of foraminifers. Further detailed work is necessary before the relative effects of productivity and winnowing on sedimentation rates and foraminifer abundances can be quantified. Changes in climate or surface-water masses may alter the composition of an assemblage, resulting in the production of more resistant forms that are preserved in the sedimentologic record. As a result, the grain-size change would reflect this change in foraminifer assemblage composition.

The abundance of foraminifers, which affects the grain size and is, in part, controlled by productivity and dissolution, may also affect the lithification process by influencing the diagenetic potential of the sediment. The processes involved in the ooze to chalk transition are, however, not well understood (Schlanger and Douglas, 1974). At Site 806, the transition was placed at 340 mbsf (lower upper Miocene), which is deeper and younger than the ooze-chalk transitions at Sites 803, 804, and 805. In fact, the transition occurs gradually over an interval of approximately 250 m. The first significant evidence of lithification is the presence of thin intervals of stiffer material within softer ooze. These intervals become thicker and harder downsection until they become chalk, which is intercalated with stiff ooze. The transition proceeds by a reduction in the abundance of ooze, until the sediment is eventually all converted to chalk. Smear slide observations of lithified samples provide little evidence of grain-to-grain cementation, although the difficulty of disaggregating those grains when making smear slides suggests that some cementation has occurred. The potential for cementa-

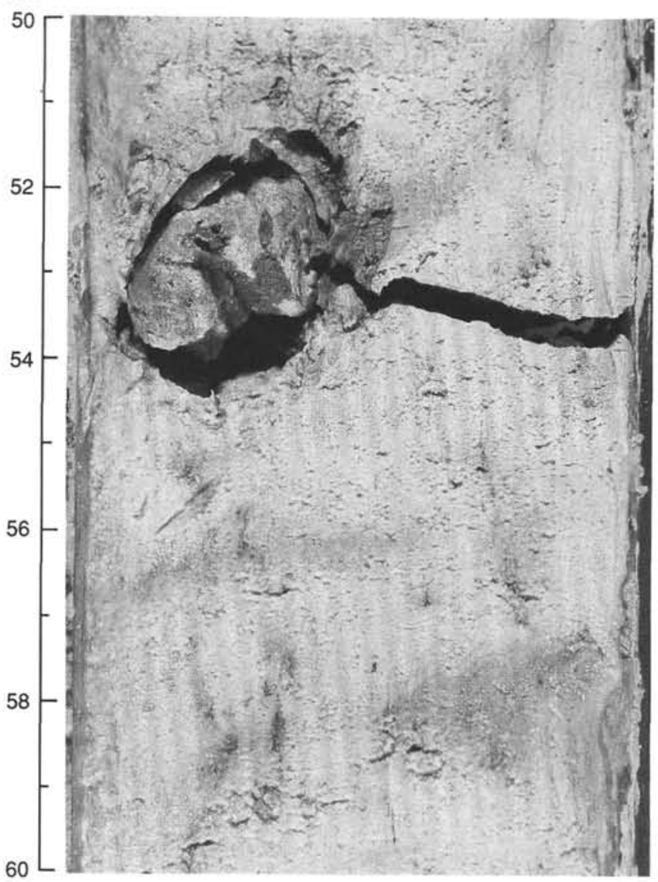

Figure 9. A dropstone of pumice (Section 130-806C-7H-3, 52 cm; 56.6 mbsf).

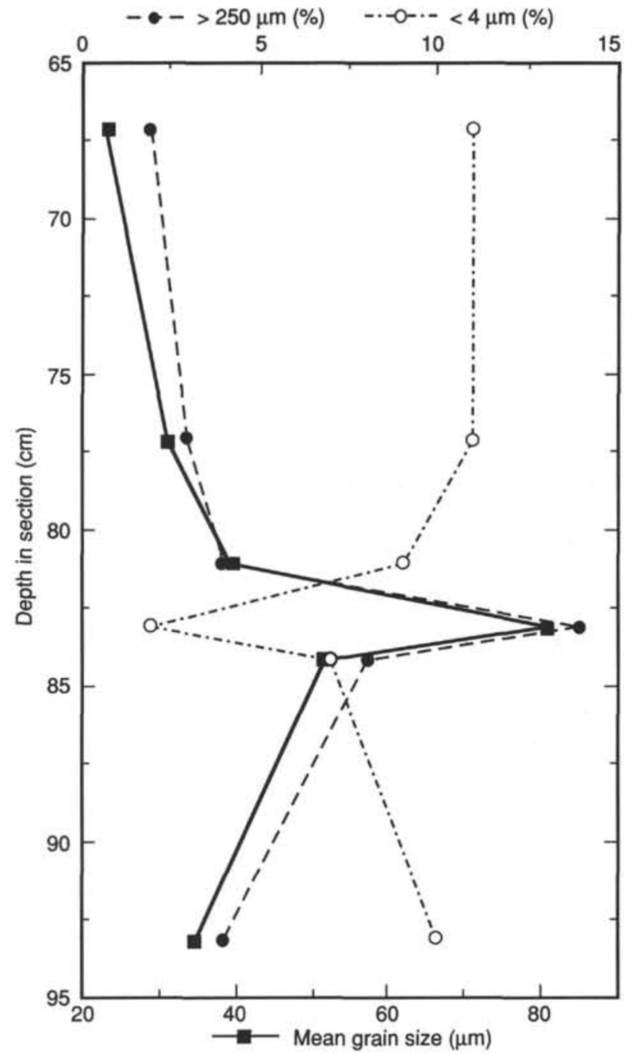

Figure 10. Profiles of mean grain size and coarse sand (>250 μm) and clay (<4 μm) abundances found in a well-sorted bed of foraminifer tests at Section 130-806C-5H-4, 83 cm (39.4 mbsf). Depth is measured as the position within Section 130-806C-5H-4. This bed is interpreted as having been formed by a strong winnowing event.

tion is also demonstrated by the significant amounts of calcite precipitated onto nannofossil tests during lithification, which gradually make the nannofossils appear thicker downhole (Fig. 15).

Other signs of lithification include porcellanite concretions that are distributed in low abundances below 240 mbsf. The silica comprising these nodules appears to have been precipitated. Although pore-water silica concentrations are not significantly higher at the levels where concretions were recovered, the pore-water silica levels are consistently high enough to allow precipitation (see "Inorganic Geochemistry" section, this chapter). It is not known at this time why the concretion abundances are so low nor what the catalyst is for their formation.

The chalk becomes more lithified below approximately 500 mbsf. Sediment compaction, both mechanical and chemical, results in the flattened appearance of bioturbation structures and color-band thinning. Below 600 mbsf the color bands become wavy and braided in appearance (Fig. 14), probably because of chemical compaction by dissolution and reprecipitation, which produces flaser structures. These features are not interpreted as primary sedimentary structures, caused by oceanic bottom currents, as was suggested for Site 289 on the Ontong Java Plateau (Shipboard Scientific Party, 1975). We interpret these structures as postdepositional for three reasons: (1) the color bands thin and intensify with depth; (2) the color bands frequently cross bioturbation structures, suggesting that they formed after the bioturbation; and (3) the color bands are braided at depth in Site 806, whereas primary sedimentary structures cannot cross and intertwine with one another.

Thin (<0.1 mm), single, gray, wavy color bands were also observed occasionally (Fig. 15). Fracturing occurred readily along the irregular contacts formed by these bands. These bands cross bioturbation features in some cases, such as is shown in Figure 13. In these cases, the trace fossil is slightly offset across the band, implying that some material has been lost through chemical compaction. This observation supports the interpretation of these structures as incipient stylolites.

Summary

The sedimentary section at Site 806, which extends from the upper Oligocene to the Pleistocene, is a complete stratigraphic section of biogenic pelagic sediments, with no evidence of interruption, hiatus, or significant reworking other than bioturbation. As a result, this site offers an excellent type section for correlation to sites lower on the slope of the Ontong Java Plateau. The sedimentary column was classified as one lithostratigraphic unit (Unit I), but was divided into two subunits on the basis of the states of lithification. Subunit IA is composed of foramini-

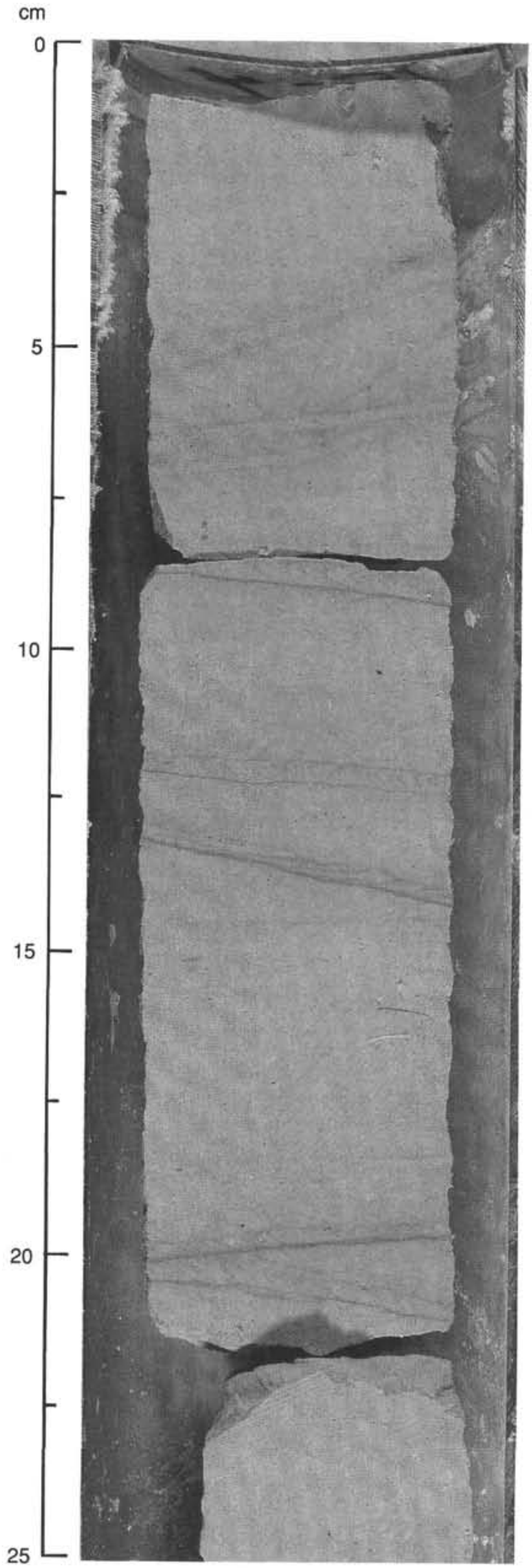

Figure 11. Distinct *Zoophycos* trace fossils common in the chalks deep in Site 806 (Section 130-806B-70X-4, 0–25 cm; 662 mbsf).

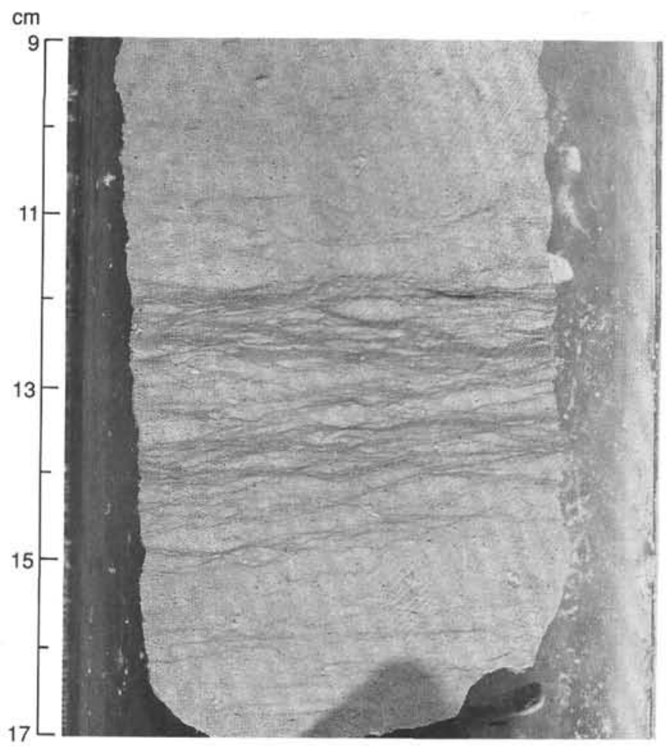

Figure 12. Photograph of color bands (Section 130-806B-70X-CC, 9–17 cm; 656 mbsf). These bands are described as flaser structures because of their wavy, braided appearance and are interpreted as resulting from chemical compaction.

fer nannofossil ooze to nannofossil ooze with foraminifers, with some intervals of nannofossil ooze. Subunit IB is composed of foraminifer nannofossil chalk to nannofossil chalk with foraminifers.

BIOSTRATIGRAPHY

Introduction

Site 806, in a water depth of 2520 m, is nearest to the equator and is the shallowest site on the Ontong Java Plateau depth transect. Three holes were drilled at Site 806. Hole 806A penetrated sediments of Quaternary to Pliocene age, and an apparently complete sequence was retrieved. The Pliocene/Pleistocene boundary was placed within Core 130-806A-5H on the basis of the calcareous nannofossil evidence. Hole 806B was drilled to a depth of 743.1 mbsf and retrieved an apparently continuous sequence of sediments of Pleistocene to early Miocene age (Fig. 16). The deepest hole at this site, Hole 806C, penetrated sediments of Pleistocene to late Oligocene age (Fig. 16). Much of the lower Miocene was not cored at this hole, which was washed ahead below 542 mbsf to retrieve the Oligocene/Miocene boundary. This boundary was placed within Core 130-806C-59X (interval 740.0–749.5 mbsf) on the basis of the planktonic foraminifer and diatom evidence. As at Site 805, this site has an unusually thick middle and lower Miocene section (approximate thickness = 380 m).

The microfossils show various states of preservation. Calcareous nannofossils, planktonic foraminifers, diatoms, and radiolarians are generally well to moderately well preserved throughout much of the sediment sequence. However, the preservation of diatoms and radiolarians is generally moderate to poor in the lower Miocene. Poor preservation of foraminifers, diatoms, and radiolarians was seen in Oligocene samples.

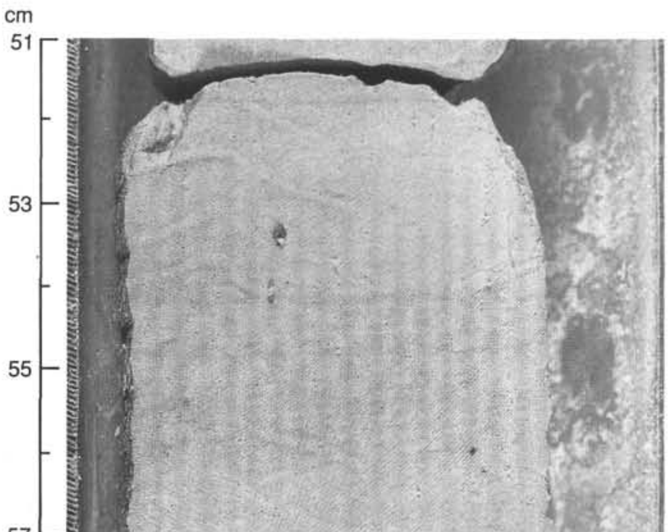

Figure 13. A photograph of very thin (≪0.1 cm), wavy, gray bands observed in the highly consolidated chalks deep in Site 806 (Section 130-806B-70X-3, 51–65 cm; 659 mbsf). Fractures occur readily along these bands, which are interpreted as incipient stylolites. Note that the color band crosses through the *Zoophycos* trace fossil without interruption; the trace fossil, however, is offset slightly across the band, suggesting the loss of material through chemical compaction.

Details on biostratigraphy as well as on abundance and preservation of the different microfossil groups are presented below.

Calcareous Nannofossils

The sediments at Site 806 yielded abundant calcareous nannofossils from an apparently continuous Neogene and uppermost Oligocene sequence. The section can be characterized as presenting a "text-book" type of stratigraphy with virtually all zonal markers present and no signs of sedimentological or drilling disturbance. Only three markers in the zonal schemes of Martini (1971) and Okada and Bukry (1980) were observed to be missing, namely *Helicosphaera ampliaperta* (NN4/NN5 boundary), *Helicosphaera recta* (NP25/NN1 boundary), and *Dictyococcites bisectus* (CP19/CN1 boundary).

Preservation is good in the Pleistocene and the upper Pliocene, and moderate in the remainder of the section. The chief problem was that primary morphological characters of the discoasters commonly were blurred by calcite overgrowth. The calcareous dinoflagellate genus *Thoracosphaera* was observed in low but varying abundances throughout the section.

The following discussion represents a composite summary of the nannofossil biostratigraphy as recognized in the Quaternary to upper Pliocene (Hole 806A), the lower Pliocene to lower Miocene (Hole 806B), and the middle Miocene to upper Oligocene sections (Hole 806C). Figure 16 summarizes the calcareous nannofossil zones of the three holes drilled at Site 806 and their correlation to those of the planktonic foraminifers, diatoms, and radiolarians.

Hole 806A

Pleistocene

Sample 130-806A-1H-CC contains a late Pleistocene to Holocene assemblage, including such forms as *Calcidiscus leptoporus, Ceratolithus telesmus, Helicosphaera carteri, Syracosphaera,* and abundant small *Gephyrocapsa*. This sample lies above the stratigraphic range of *Pseudoemiliania lacunosa* and was placed in the NN20/NN21 zonal interval, therefore. This interval was not subdivided because *Emiliania huxleyi* cannot be reliably identified using light microscopy. The presence of abundant *Pseudoemiliania lacunosa* and the absence of discoasters place Samples 130-806A-2H-CC through -4H-CC in Zone NN19. Among these samples, Sample 130-806A-3H-CC contains many specimens of *Pontosphaera,* even though it is still referred to as "few" in abundance (0.1%–1.0 % of the total assemblage). Sample 130-806A-4H-CC contained the first downhole observations of *Coccolithus pelagicus, Calcidiscus macintyrei,* and *Helicosphaera sellii,* and therefore corresponds to the lower part of Zone NN19. One reworked specimen (*Discoaster variabilis*) was also observed in this core-catcher sample.

Pliocene

The Pliocene/Pleistocene boundary was placed in Core 130-806A-5H. Sample 130-806A-5H-CC contained a few specimens of *Discoaster brouweri* and was assigned to the upper Pliocene Zone NN18. *Discoaster brouweri* and *D. pentaradiatus* co-occur in Sample 130-806A-6H-CC (Zone NN17). Below this level, the assemblage is characterized by a more diversified discoaster association, including *Discoaster surculus*. Samples 130-806A-7H-CC through -9H-CC were assigned to the upper Pliocene Zone NN16. Rare *Discoaster asymmetricus* and *D. tamalis* were observed in Sample 130-806A-8H-CC. *Discoaster variabilis* was absent in this discoaster-rich sample, placing this sample in the upper half of Zone NN16. Hole 806A ended within Zone NN16 of the upper Pliocene (Core 130-806A-9H).

Hole 806B

Pliocene

The last occurrence (LO) of *Discoaster brouweri* is in the lower part of Core 130-806B-5H. The onset of the acme interval of *Discoaster triradiatus* appears to begin in Section 130-806B-6H-1, and the NN18/NN17 zonal boundary falls between Samples 130-806B-7H-1, 70 cm, and 130-806B-7H-2, 70 cm. The single specimen of *Discoaster pentaradiatus* observed in Sample 130-806B-6H-CC was considered to be reworked. Sample 130-806B-7H-CC contains *Discoaster surculus*. Samples 130-806B-7H-CC through -10H-CC are all placed in Zone NN16. Within that interval, Sample 130-806B-9H-CC yielded such diversified

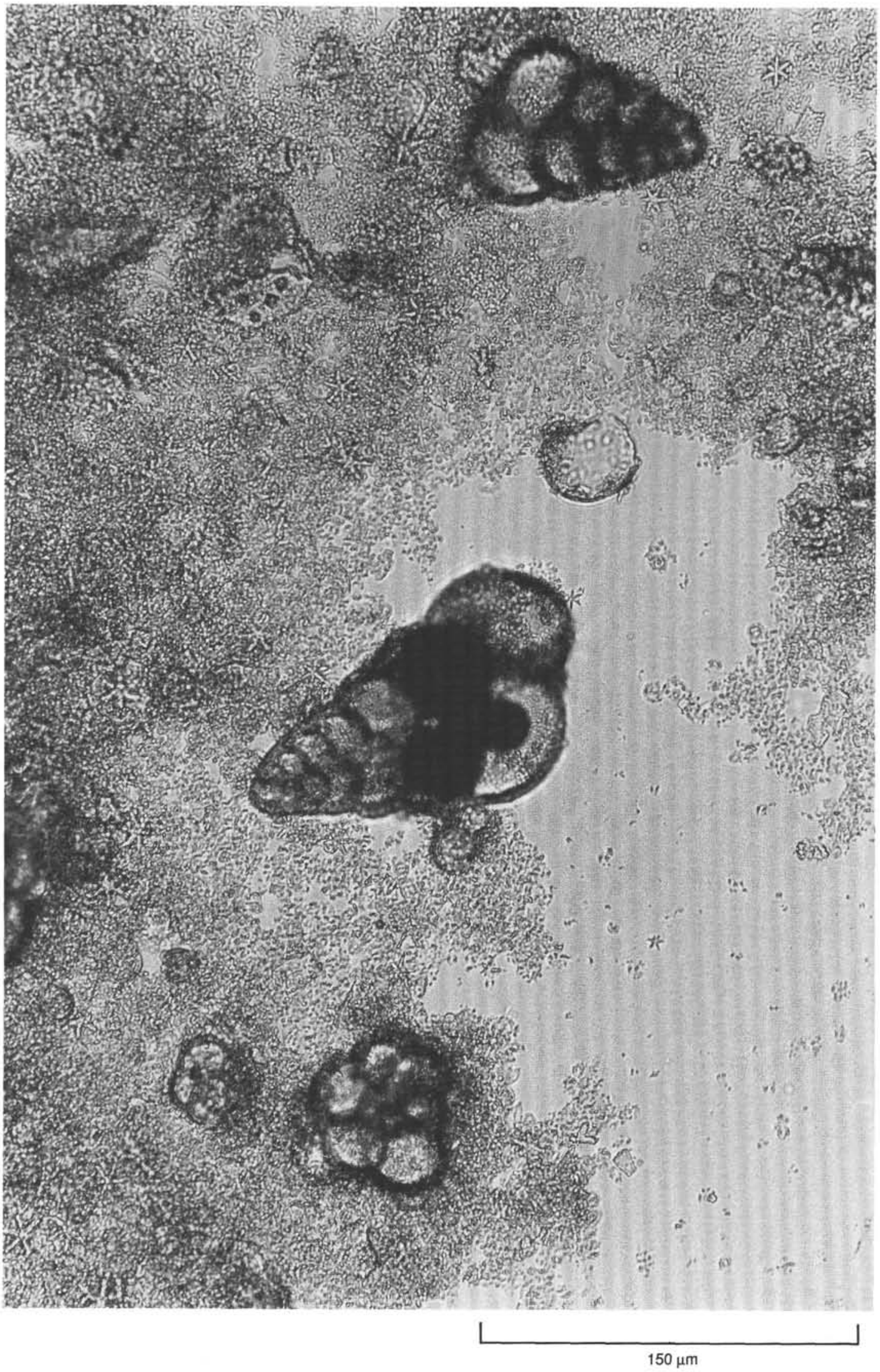

Figure 14. Photomicrograph of well-preserved foraminifer tests abundant in all of the sediments recovered from Site 806 (Section 130-806B-24H-3, 74 cm; 218 mbsf). Pyrite infilling of test chambers is also abundant. The prominent biserial foraminifers are *Streptochilus latum*.

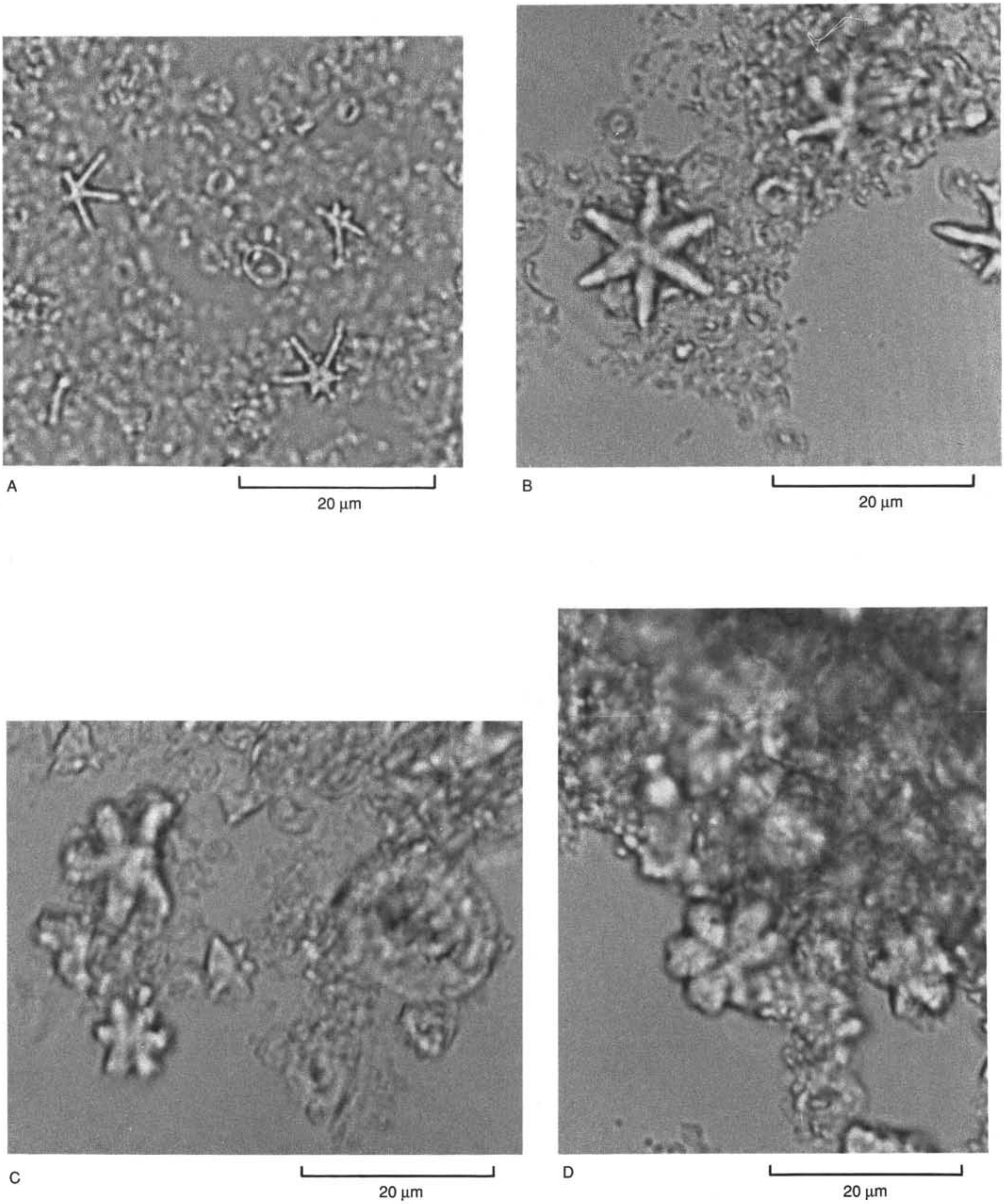

Figure 15. Photomicrographs showing the calcification of nannofossil tests (*Discoaster*) as the sediment in transformed from ooze to chalk. **A.** Section 130-806A-6H-CC; 54 mbsf. **B.** Section 130-806B-24H-3; 219 mbsf. **C.** Section 130-806C-51X-3; 478 mbsf. **D.** Section 130-806B-65X-3; 611 mbsf. Note the gradual thickening of the arms of the *Discoaster* tests with depth in the hole, which results from calcite precipitation onto the tests.

discoaster species as *Discoaster asymmetricus, D. brouweri, D. challengeri, D. decorus, D. surculus, D. tamalis, D. triradiatus,* and *D. variabilis.* Some specimens of *D. challengeri* and *D. variabilis* are unusually large in size.

The LO of *Sphenolithus abies* is between Samples 130-806B-10H-5, 75 cm, and -6, 75 cm, indicating an approximate position of the upper/lower Pliocene boundary. The highest occurrence of *Reticulofenestra pseudoumbilica* was observed between Samples 130-806B-11H-2, 75 cm, and -3, 75 cm, indicating the NN15/NN16 zonal boundary. Samples 130-806B-12H-CC through -14H-CC contain *R. pseudoumbilica* and *Discoaster asymmetricus,* placing these samples in the NN15/NN14 zonal interval. This interval is not subdivided because members of the genus *Amaurolithus* are rare or absent in this section. *Sphenolithus abies* and *S. neoabies* are abundant in these samples belonging to the upper part of the lower Pliocene. A bloomlike abundance of small reticulofenestrid placoliths (<3 μm) was observed in Sample 130-806B-14H-4, 40 cm.

Ceratoliths are comparatively rare in the lower Pliocene. Nevertheless, the change from the descendant *Ceratolithus rugosus* to the ancestral form *Ceratolithus acutus* was observed between Samples 130-806B-16H-6, 40 cm, and -7, 40 cm. Thus, these samples mark the NN12/NN13 zonal boundary. *Triquetrorhabdulus rugosus* has its LO in Section 130-806B-17H-5, indicating a position within the bottom part of Zone NN12 and near the Miocene/Pliocene boundary.

Sediments between Samples 130-806B-14H-CC and -16H-CC are characterized by fairly abundant occurrences of peculiar subcircular *Reticulofenestra* specimens in addition to abundant *Scyphosphaera* spp., *Sphenolithus abies,* and *S. neoabies.*

Miocene

Samples 130-806B-18H-CC down to -29H-CC contain *Discoaster quinqueramus,* the total range of which defines the late Miocene Zone NN11. The uppermost part of the range of *D. quinqueramus* was difficult to recognize, partly because of calcite overgrowth that blurred the distinct and characteristic central knob of this species, but partly also because the critical central knob was less clearly developed among the uppermost representatives of what we take to be *D. quinqueramus.* The lowermost occurrence of *Amaurolithus* was observed in Sample 130-806B-24H-CC, which lies in the middle part of Zone NN11. Representatives of this genus are consistently rare in the upper Miocene sediments of the Ontong Java Plateau. Yet, by judging from the results of the previous Leg 130 sites, one would expect a somewhat lower position for the evolutionary appearance of *Amaurolithus.*

Discoaster neohamatus disappears in Core 130-806B-29H. Sample 130-806B-30H-CC contains rare *Discoaster quinqueramus* together with *D. berggrenii.* Samples 130-806B-31H-CC through -35X-CC contain neither *Discoaster quinqueramus* nor *D. hamatus,* indicating a position of the NN10/NN11 zonal boundary in the former core. The lower part of Zone NN11 and the upper part of Zone NN10 (i.e., Samples 130-806B-29H-CC through -31H-CC) are characterized by bloomlike abundances of small *Sphenolithus abies* and *S. neoabies. Minylitha convallis* and sphenoliths are abundant in Sample 130-806B-33H-CC, whereas *Thoracosphaera* is rather common in Sample 130-806B-34H-CC.

Samples 130-806B-36X-CC through -38X-CC are characterized by continuous occurrences of *Discoaster hamatus,* the total range of which defines Zone NN9. Sample 130-806B-39X-CC is characterized by the presence of *Catinaster coalitus* and the absence of *Discoaster hamatus,* and hence belongs to Zone NN8; the middle/late Miocene boundary was placed within Zone NN8.

The sediments from Sample 130-806B-40X-CC through Sample -44X-CC lack primary marker species except for a single specimen of *Discoaster* cf. *D. kugleri* in Sample 130-806B-43X-CC. This interval, however, is characterized by a typical upper middle Miocene assemblage, including *Calcidiscus leptoporus* and abundant *Calcidiscus macintyrei,* few *Coccolithus miopelagicus,* common to abundant members of the *Discoaster variabilis* group, common to abundant *Reticulofenestra pseudoumbilica* and *Reticulofenestra gelida,* and few to common *Triquetrorhabdulus rugosus.* The LO of *C. miopelagicus* appears to fall immediately below Zone NN8. The NN6/NN7 zonal interval is difficult to subdivide because of the absence or rare occurrence of the nominate species *Discoaster kugleri.* If present, calcite overgrowth on discoasters tends to prevent accurate identification of *D. kugleri.*

Coronocyclus nitescens was observed in and below Sample 130-806B-45X-CC. The LO of this species is supposed to lie near the first occurrence (FO) of *Discoaster kugleri.* Samples 130-806B-45X-CC down to 130-806B-50X-CC contains *Coronocyclus nitescens* but not *Sphenolithus heteromorphus,* and therefore these samples may belong to Zone NN6. The LOs of *Cyclicargolithus floridanus* and *Sphenolithus heteromorphus* are both observed between Samples 130-806B-50X-CC and 130-806B-51X-CC. Samples 130-806B-51X-CC through 130-806B-61X-CC contain *S. heteromorphus.*

Helicosphaera ampliaperta, the last occurrence of which is used to define the top of Zone NN4, has not been observed in any of the Leg 130 samples taken from the pertinent stratigraphic interval and must have been ecologically excluded from this region. It follows that the combination of Zones NN4 and NN5 results in a long biostratigraphic interval that straddles the lower/middle Miocene boundary. Bukry's (1973) end-of-acme concept of *Discoaster deflandrei,* that recently was quantified and defined by Rio et al. (in press) as the decrease to $<30\%$ of *D. deflandrei* of the total discoaster assemblage, allows splitting of the NN4/NN5 zonal interval into two parts of approximately equal duration. This abundance transition was observed in Core 130-806B-57X.

The FO of *Sphenolithus heteromorphus* occurs in Core 130-806B-62X, a core that also contains the LO of *Sphenolithus belemnos,* and thus marks the NN3/NN4 zonal boundary. Sample 130-806B-63X-CC also contains *Sphenolithus belemnos,* indicating that the FO of this species lies above Sample 130-806B-64X-CC. Rare specimens of *Triquetrorhabdulus carinatus* were observed in this former sample (reworked?). The first observation of common *T. carinatus* was made in Sample 130-806B-66X-CC, which probably marks the top of the lower Miocene Zone NN2.

The nannofossil assemblages in the deepest part of Hole 806B are abundant but moderate to poorly preserved (Samples 130-806B-64X-CC to 130-806B-78X-CC). This rather monotonous flora is composed of abundant *Discoaster deflandrei, Cyclicargolithus floridanus* and forms belonging to the *Sphenolithus moriformis* group. A few specimens of *Discoaster druggii* were observed in Samples 130-806B-66X-CC and 130-806B-77X-CC, placing this interval in Zone NN2. Sample 130-806B-78X-CC, which was taken from the bottom of the Hole 806B, contains neither *D. druggii* nor *Sphenolithus ciperoensis.* The lack of *D. druggii* in this sequence, however, does not necessarily imply a position within Zone NN1 because of calcite overgrowth problems.

Hole 806C

Sphenolithus heteromorphus disappears together with *Cyclicargolithus floridanus* in Core 130-806C-50X; the NN5/NN6 zonal boundary thus lies in this core. *Discoaster deflandrei* is abundant in and below Sample 130-806C-56X-CC, accounting

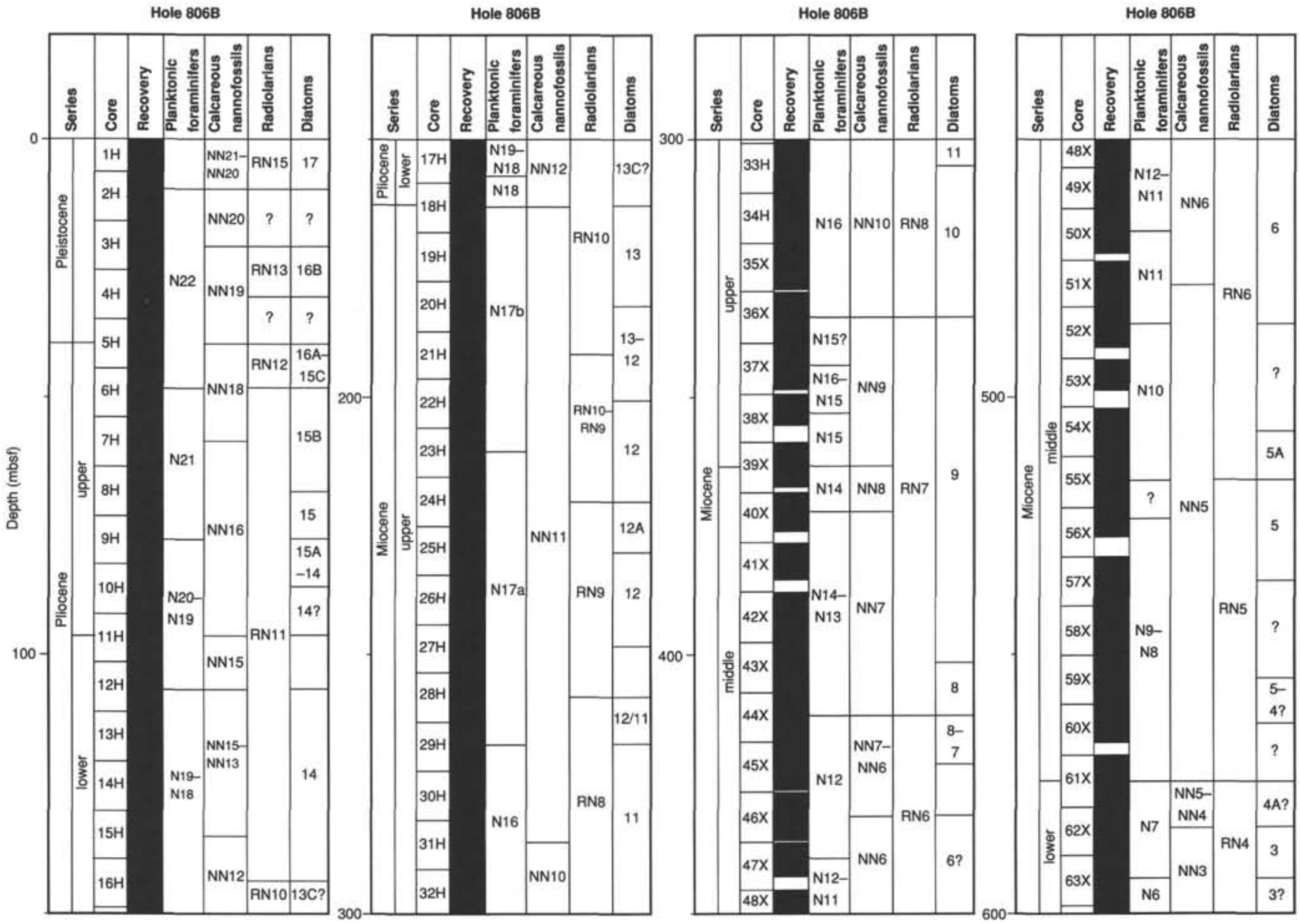

Figure 16. Biostratigraphic hole summaries, Site 806. RN = radiolarian Neogene zone, NTD = Neogene tropical diatom zone, RP = radiolarian Paleogene zone, and NN = nannofossil Neogene zone.

for >30% of the total discoaster assemblage. The decrease in abundance to values that are substantially less than 30% in Core 130-806C-56X approximately indicates the lower/middle Miocene boundary and the NN4/NN5 zonal boundary. *Sphenolithus heteromorphus* is abundant in Sample 130-806C-57X-CC, which lies at 541.7 mbsf.

Core 130-806C-58X was recovered after washing down to 599.0 mbsf. This core contains the FO of *Sphenolithus belemnos* between Samples 130-806C-58X-1, 75 cm, and -58X-CC, implying that the FO of *Sphenolithus heteromorphus* and the LO of *Sphenolithus belemnos* (NN3/NN4 boundary) fall in the washed interval. Both *Triquetrorhabdulus carinatus* and *Discoaster druggii* were observed in Sample 130-806C-58X-CC; *T. carinatus* was observed also from the top of this core, in Sample 30-806C-58X-1, 5 cm, together with *S. belemnos,* placing the core in the lower Miocene Zone NN2.

The interval from 608.5 to 740.0 mbsf was drilled without coring. Sample 130-806C-59X-CC contains a typical upper Oligocene/lower Miocene assemblage, with common to abundant *Coccolithus pelagicus, Cyclicargolithus floridanus, Discoaster deflandrei,* and sphenoliths, including abundant *Sphenolithus moriformis,* common *S. dissimilis,* and rare *S. delphix* and *S. conicus.* Sample 130-806C-61X-CC was dominated by *Cyclicargolithus floridanus* and *Sphenolithus moriformis.* A few specimens of *Sphenolithus ciperoensis* were also observed in this sample. *Helicosphaera recta* and *Dictyococcites bisectus* are absent in the upper Oligocene sediments from the Ontong Java Plateau. The rare occurrences of *Sphenolithus ciperoensis,* however, suggest that Core 130-806C-61X belongs to upper Oligocene Zone NP25. Sample 130-806C-62X-CC represents the bottom of Hole 806C; the assemblage is similar to that observed in the next higher core and is considered to represent Zone NP25 despite the fact that *Sphenolithus ciperoensis* was not observed.

Planktonic Foraminifers

Planktonic foraminifers are abundant in the Pleistocene to lower Pliocene sequence of Hole 806A, and the preservation is good. Exceptions to this are the Samples 130-806A-7H-CC and -8H-CC where the preservation is poor.

Hole 806B penetrated an apparently continuous sequence of sediments of Pleistocene to early Miocene age (Fig. 16). With the exception of Sample 130-806B-1H-CC where the preservation of planktonic foraminifers is poor, abundance and preservation are generally good from the top of the section through Sample 130-806B-38X-CC in the middle Miocene. In the remainder of the middle Miocene sequence, from Sample 130-806B-38X-CC to -56X-CC, planktonic foraminifers are abundant and the preservation is moderate to good. Below Core 130-806B-58X-CC, abundance and preservation of planktonic foraminifers are more variable but in general are also good.

The sediment recovered in Hole 806C ranges in age from Pleistocene to late Oligocene (Fig. 16). Like Hole 806B, this hole possesses an expanded middle and lower Miocene section. Much of the lower Miocene (N4 and N5) was not cored at this

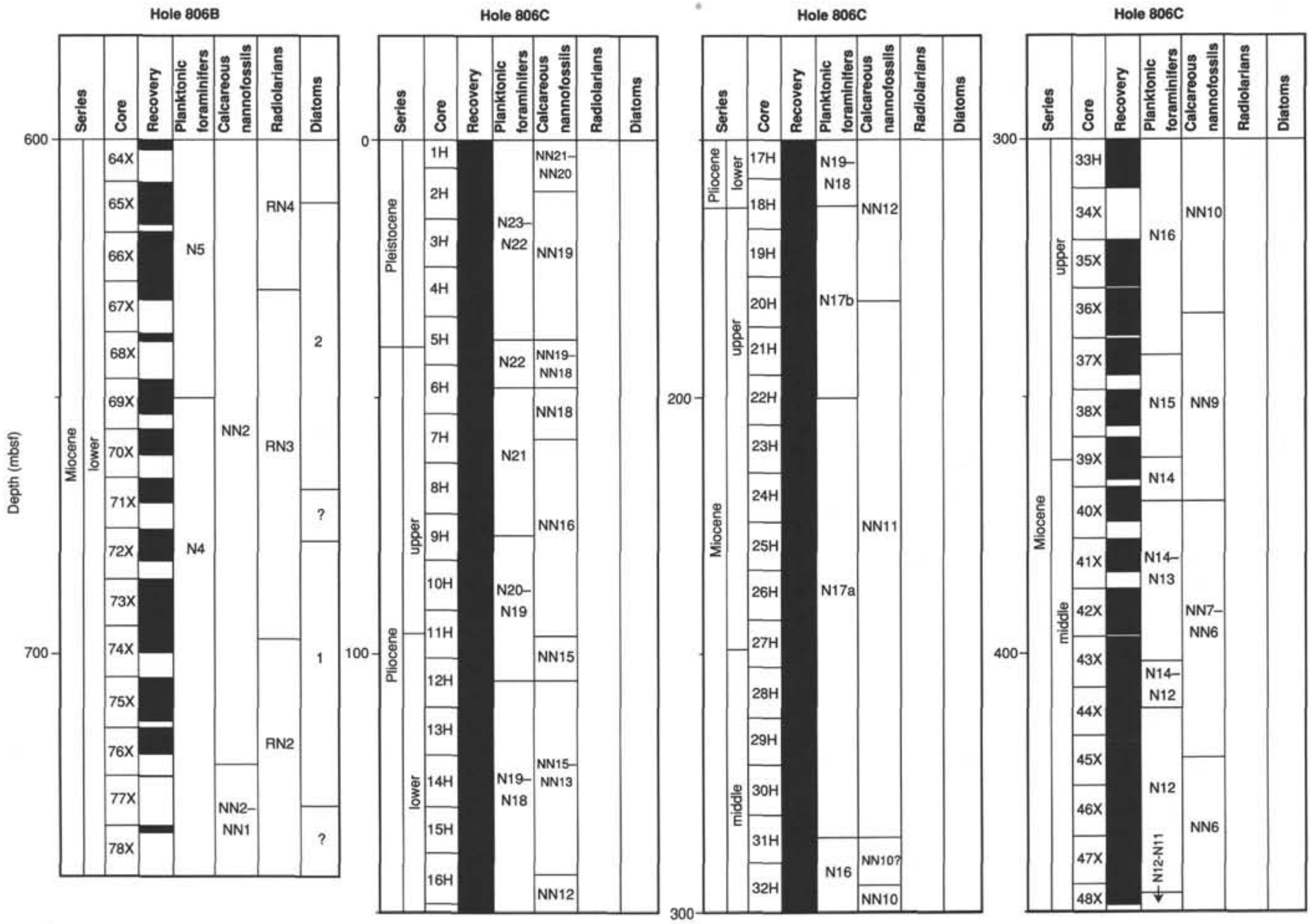

Figure 16 (continued).

hole. Planktonic foraminifers are generally abundant and well preserved. Preservation is poor only in the bottom two samples in the hole (upper Oligocene).

Hole 806A

Sample 130-806A-1H-CC is void of the Pleistocene–latest Pliocene marker species *Globorotalia truncatulinoides*. This absence may be environmentally controlled, as there was no sign of dissolution in this sample. However, *G. truncatulinoides* is present in stratigraphically lower samples. The Pliocene/Pleistocene boundary was placed within Core 130-806A-4H on the basis of the LO of *Globigerinoides fistulosus*.

Hole 806B

The Pliocene/Pleistocene boundary was placed in Core 130-806B-5H on the basis of the FO of *G. truncatulinoides*. The base of the upper Pliocene was placed within Core 130-806B-9H on the basis of the FO of *G. tosaensis*. The base of Zone N19–N20 occurs within Core 130-806B-12H. The FO of *Globorotalia tumida* occurs in Sample 130-806B-17H-CC; therefore, the base of Zone N18 and the lower Pliocene is within Core 130-806B-18H. The base of Subzone 17b occurs within Core 130-806B-23H on the basis of the FO of *Pulleniatina primalis*. Subzone 17a extends to within Core 130-806B-29H (i.e., the core below the last core-catcher sample to contain *Globorotalia plesiotumida*). The FO of *Neogloboquadrina acostaensis* occurs within Core 130-806B-38X, which therefore defines the base of Zone N16. The zonal marker *Globorotalia siakensis* defines the base of Zone N15 and is found within Core 130-806B-39X. Therefore, Zone N15, typically of short duration, occupies an attenuated interval of sediment between these two marker species. The base of Zone N14 is defined on the basis of the FO of *Globigerina nepenthes*. This species was not observed in the core-catcher samples of Hole 806B and so it is not possible to subdivide the N14/N13 interval.

The LO of the *Globorotalia fohsi* plexus was observed in Sample 130-806B-44X-CC; therefore, the base of Zone N13 occurs within Core 130-806B-44X. Members of the *G. fohsi* lineage are well developed at Site 806, although they do not form a dominant part of the fauna. Gradational forms are common, making the distinction between *G. fohsi* and *G. praefohsi*, and therefore the Zone N12/N11 transition, difficult to recognize. For practical purposes, however, we placed this boundary in Core 130-806B-47X. Zone N11 (based on the FO of *G. praefohsi*) covers the interval from Cores 130-806B-48X to -52X. Zone N10 was defined on the FO of *G. peripheroacuta*, which occurs in Core 130-806B-55X. However, Core 130-806B-55X itself is chalky and difficult to disaggregate, so that no age-diagnostic taxa were observed within it.

No members of the *Orbulina* lineage were observed in the lower middle Miocene part of this hole; therefore, it is not possible to distinguish the boundary between Zones N8 and N9. Assemblages diagnostic of Zone N7 were identified in Cores 130-806B-61X and -62X. Although *Praeorbulina sicanus* was not observed in this hole, these two samples are devoid of *Catapsydrax dissimilis*, indicating an approximate Zone N7 age. The

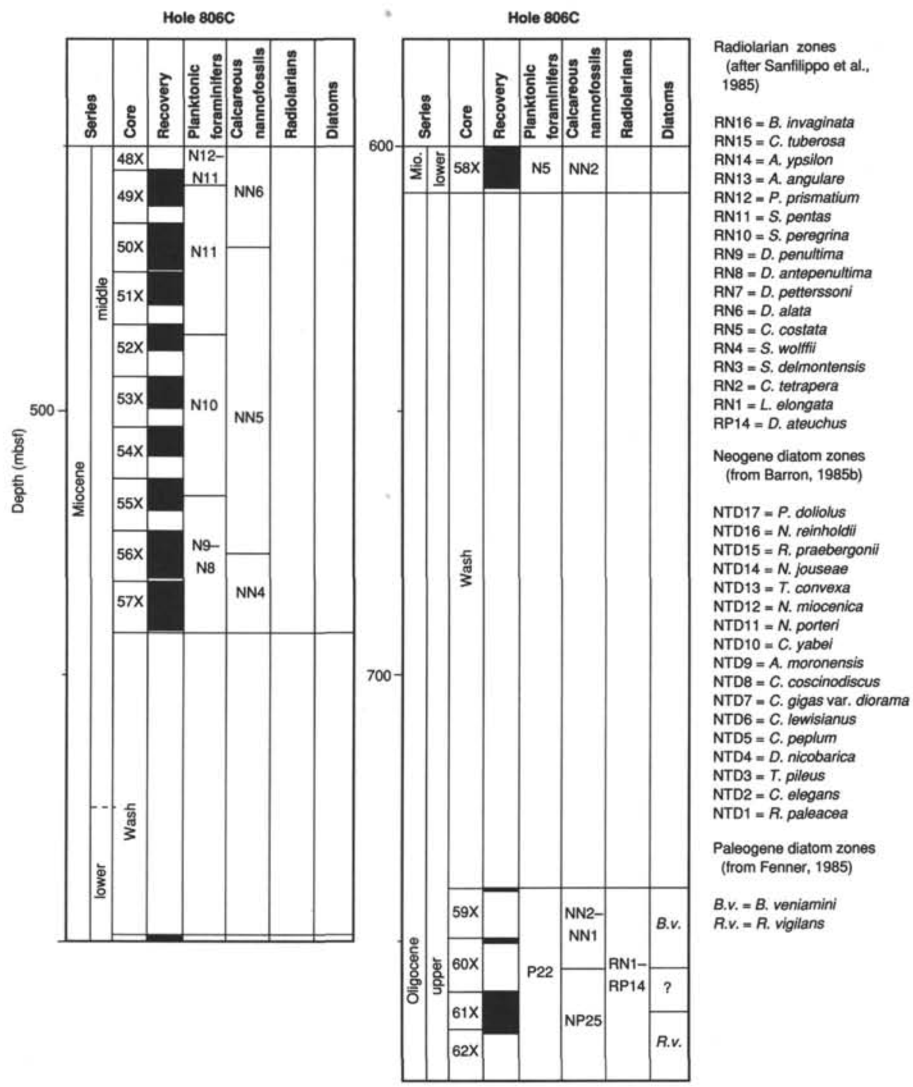

Figure 16 (continued).

LO of *C. dissimilis* was placed in Sample 130-806B-63X-CC, and this event marks the base of Zone N7. Core 130-806B-63X, therefore, contains part of Zone N6. An indicator species that has been used as a proxy for Zone P5 is the presence of *Globoquadrina binaiensis* in the absence of *Globorotalia kugleri*. The LO of *G. binaiensis* was observed in Sample 130-806B-64X-CC, and Zone N5 extends down to Core 130-806B-69X or Sample 130 806B-69X-CC, where the LO of *G. kugleri* was observed. Zone N4 was recognized in sediment from Core 130-806B-69X to the base of the hole in Sample 130-806B-78X-CC.

Hole 806C

Cores 130-806C-1H through -5H were placed in Pleistocene–uppermost Pliocene Zone N22. The FO of *G. truncatulinoides* occurs within Core 130-806C-6H. Core 130-806C-6H to within Core 130-806C-9H-CC were placed within Zone N21. Because of the absence of *G. tosaensis* in Sample 130-806C-6H-CC and -7H-CC, this zone was also recognized on the presence of *G. fistulosus*. The distinction between Zones N19/20 and N18 was difficult to recognize in this hole because of the sporadic occurrence of *S. dehiscens*. However, on the basis of the change from sinistral to dextral coiling within the *Pulleniatina* lineage, we placed the Zone N19–N20 to Zone N18–N19 boundary within Core 130-806C-12H. The base of Zone N18 (the FO of *G. tumida*) occurs within Core 130-806C-18H. The boundary between Subzones N17a and N17b (the FO of *P. primalis*) occurs within Core 130-806C-22H. The boundary between Subzone N17a and N16 was based on the FO of *G. plesiotumida*, which occurs within Core 130-806C-31H.

The base of Zone N16 was defined according to the FO of *N. acostaensis*, which occurs within Core 130-806C-37X, as it was first observed in Sample 130-806C-36X-CC. The LO of *G. siakensis* (and therefore the base of N15) occurs within Core 130-806C-39X. The base of Zone N14 is normally defined on the FO of *G. nepenthes*, but because of the paucity of this taxon in Leg 130 material, it was not possible to discriminate Zone N13 from Zone N14 reliably on the basis of the core-catcher samples. The LO of the subspecies *Globorotalia fohsi lobata* and *Globorotalia fohsi robusta* occurs within Core 130-806C-43X and thus defines the base of Zone N13. Zone N12 extends to Core 130-806C-48X, although precise recognition of this zonal boundary was obscured by the occurrence of transitional morphotypes between *Globorotalia praefohsi* and *G. fohsi*. The FO of *G. praefohsi* occurs within Core 130-806C-52X. This event defines the base of Zone N11. Zone N10 in this hole was found from Cores 130-806C-52X to -56X. The FO of *G. peripheroa-*

cuta, which defines the base of Zone N10, occurs within Core 130-806C-56X.

Members of the *Orbulina* lineage are not well represented in Hole 806C (as was the case in Hole 806B); therefore, it was not possible to distinguish Zones N8 and N9. Together, these two zones occupy Cores 130-806C-56X and -57X. The hole was drilled without coring much of the lower Miocene. The next sample examined (Sample 130-806C-58X-CC at 608.5 mbsf) is within Zone N5, the base of which is defined by the LO of *G. kugleri.* Further washing took place below this sample, and the next sample to be examined (Sample 130-806C-59X-CC at 749.5 mbsf) contains a planktonic foraminifer fauna of upper Oligocene age (Zone P22). The critical marker species designating P22 is *Globorotalia pseudokugleri* in the absence of *G. kugleri* s.s. Samples 130-806C-60X-CC and -61X-CC are also of Zone P22 age.

Diatoms

Diatoms were examined in Holes 806B (Samples 130-806B-1H-CC through -78X-CC) and 806C (Samples 130-806C-59X-CC through -62X-CC). Quaternary through lower Miocene diatoms are present in Hole 806B (Fig. 16). The sediment recovered in Hole 806C ranges in age from Pleistocene to Oligocene. Much of the lower Miocene section was drilled without coring to retrieve the Oligocene/Miocene boundary. Oligocene diatoms are present in the four samples analyzed from Hole 806C (Fig. 16).

Diatoms are common to abundant and preservation generally is moderate from the Pleistocene (Sample 130-806B-1H-CC) through the middle Miocene (Sample 130-806B-51X-CC). Large fluctuations in abundance (abundant to few) and preservation (moderate to poor) were seen below Core 130-806B-52X. Furthermore, only one fragment of *Synedra jouseana* and one fragment of *Craspedodiscus coscinodiscus* (coarse form) were found in Sample 130-806C-78X-CC. Preservation is poor in uppermost Oligocene Samples 130-806C-59X-CC and -60X-CC.

As at Site 805, Site 806 has a complete and expanded sediment sequence, from the Quaternary NTD 17 *Pseudoeunotia doliolus* Zone (Sample 130-806B-1H-CC) throughout the Oligocene *Rocella vigilans* Zone (Sample 130-806C-62X-CC). However, the *Rocella gelida* Zone across the Miocene/Oligocene boundary may be missing. This also has been the case in all the previous sites (803, 804, and 805).

The Pliocene/Pleistocene boundary, as defined on the basis of diatoms, is within Core 130-806B-5H, as Sample 130-806B-5H-CC does not contain specimens of *P. doliolus.* Samples 130-806B-5H-CC through 130-806B-9H-CC are all referable to the NTD 15 *R. praebergonii* Zone in the upper Pliocene.

The Pliocene/Miocene boundary was located in the NTD 13 *Thalassiosira convexa* Zone, and it coincides with the FO of *T. oestrupii* in Sample 130-806B-18H-CC.

The late Miocene/middle Miocene boundary falls within the NTD 9 *Actinocyclus moronensis* Zone and may be contained in Core 130-806B-39X. Poor preservation and low diatom abundance hinders exact recognition of the middle Miocene/lower Miocene boundary. It may be placed in Core 130-806B-59X as the next downcore sample analyzed (Sample 130-806B-59X-CC) contains the LO of *Raphidodiscus marylandicus* (16.7 Ma) within the lower Miocene. The thick Miocene section at Site 806 allowed us to recognize two diatom zones previously missing at Sites 803 and 804: the NTD 4 *Denticulopsis nicobarica* Zone and the NTD 3 *Triceratium pileus* Zone (Samples 130-806B-57X-CC (?) to -63X-CC).

The Oligocene flora of Hole 806C is preserved poorly. Sample 130-806C-59X-CC tentatively was assigned to the *Borgorovia veniamini* Zone, and Samples 130-806C-61X-CC and -62X-CC were assigned to the *Rocella vigilans* Zone.

Radiolarians

Radiolarians recovered from Site 806 ranged from well to poorly preserved, and most of the samples provided useful age information. All core-catcher samples from Hole 806B were examined. Four core-catcher samples recovered from Hole 806C (the bottom of which is at 776.4 mbsf) were also examined. The following discussion concerns the zonal assignments of the stratigraphically important taxa and the age of their datum levels. The radiolarian datums with absolute ages cited in the discussion are taken from those listed by Nigrini in the Leg 117 "Explanatory Notes" chapter (Prell et al., 1989). Figure 16 summarizes the radiolarian zonation of Holes 806B and 806C and correlates these zonations with the zones of the other microfossil groups. The radiolarian zones are continuous at least from the lower Pleistocene to the early lower Miocene. No evidence for significant sediment reworking is found at this site.

Quaternary

Sample 130-806B-1H-CC was placed in the *Collosphaera tuberosa* Zone of the Quaternary, given the presence of *C. tuberosa* and the absence of *Buccinosphaera invaginata.* The uppermost Pleistocene section appears to be condensed. Samples 130-806B-2H-CC and -4H-CC did not contain enough key radiolarian taxa to assign ages. Core 130-806B-3H-CC, which contains *A. angulare* and *Theocorythium trachelium,* was placed in the *Anthocyrtidium angulare* Zone.

Pliocene

The LO of *Pterocanium prismatium* (1.52–1.56 Ma) was observed in Sample 130-806B-5H-CC, which places it in the upper part of the *P. prismatium* Zone. Samples 130-806B-6H-CC through -15H-CC were assigned to the *Spongaster pentas* Zone. This zone contains the following radiolarian events: the LO of *S. pentas* (3.74–3.82 Ma) in Sample 130-806B-6H-CC; the LO of *Stichocorys peregrina* (2.62–2.64 Ma) in Sample 130-806B-7H-CC; the FO of *Amphirhopalum ypsilon* (3.77–3.79 Ma) in Sample 130-806B-8H-CC; the FO of *Spongaster tetras* (3.83–3.85 MA) in Sample 130-806B-11H-CC; and the LO of *Spongaster berminghami* (3.85–3.87 Ma) in Sample 130-806B-16H-CC. Samples 130-806B-16H-CC through -20H-CC were placed in the *Stichocorys peregrina* Zone. Radiolarian events found in this zone include the LO of *Solenosphaera omnitubus* (4.7–4.8 Ma) in Sample 130-806B-16H-CC; the FO of *S. pentas* (4.2–4.3 Ma) in Sample 130-806B-18H-CC; and the LO of *Acrobotrys tritubus* (5.3–5.4 Ma) in Sample 130-806B-20H-CC.

Upper Miocene

Samples 130-806B-21H-CC through -23H-CC were assigned to the *Didymocyrtis penultima* or the *S. peregrina* Zones, which cannot be differentiated. These samples contain the following key taxa: *S. peregrina, S. berminghami, S. omnitubus, A. tritubus,* and *D. penultima.* Samples 130-806B-24H-CC through -27H-CC belong to the *D. penultima* Zone. Radiolarian events found in these samples include the LO of *Calocycletta caepa* (6.2–6.6 Ma) in Sample 130-806B-24H-CC and the FO of *S. omnitubus* (6.3–6.5 Ma) in Sample 130-806B-26H-CC. Samples 130-806B-28H-CC through -35X-CC were placed in the *Didymocyrtis antepenultima* Zone. The LOs of the following five taxa were found: *Diartus hughesi* (7.1–7.2 Ma) in Sample 130-806B-29H-CC; *Dictyocoryne ontogenesis* (7.2–7.7 Ma) in Sample 130-806B-31H-CC; *Didymocyrtis laticonus* (8.1–8.2 Ma) in Sample 130-806B-31H-CC; *Diartus petterssoni* (8.1–8.2 Ma) in

Sample 130-806B-34H-CC; and *Stichocorys wolffii* (8.1–8.2 Ma) in Sample 130-806B-35H-CC. Also, the FO of *S. berminghami* (7.9–8.0 Ma) was observed in Sample 130-806B-35X-CC.

Middle Miocene

Samples 130-806B-36X-CC through -43X-CC were assigned to the *D. petterssoni* Zone. In this zone, the FO of *D. hughesi* (8.7–8.8 Ma) in Sample 130-806B-35X-CC and the LO of the following three taxa were observed: *Cyrtocapsella japonica* (10.0–10.3 Ma) in Sample 130-806B-38X-CC, *Lithopera thornburgi* (10.3–11.6 Ma) in Sample 130-806B-42X-CC, and *Cyrtocapsella cornuta* (11.6–11.9 Ma) in Sample 130-806B-43X-CC. The *Dorcadospyris alata* Zone begins in Sample 130-806B-44X-CC and extends through Sample 130-806B-54X-CC. Several LOs and FOs of *Dorcadospyris* species are in this zone, but exact datum levels are yet to be determined.

Lower Miocene and Oligocene

Samples 130-806B-56X-CC through -60X-CC were placed in the *Calocycletta costata* Zone. Around this depth and below, radiolarian preservation is generally moderate to poor; however, age assignments are still possible because of the preservation of sufficient key taxa. The *Stichocorys wolffii* Zone occurs between the base of *C. costata* and the base of *S. wolffii* (Riedel and Sanfilippo, 1978), and Samples 130-806B-61X-CC through -66X-CC were placed in it. *S. wolffii* was generally found in high abundance in this zone. A critical evaluation of *S. wolffii* morphology (i.e., the number of pores in the cephalis that are <12) was needed to bracket this zone because other morphological features of this taxon are identical to those of *Stichocorys delmontensis* (Riedel and Sanfilippo, 1978).

Samples 130-806B-67X-CC through -73X-CC were placed in the *S. delmontensis* Zone, which is followed by the *Cyrtocapsella tetrapera* Zone in Samples 130-806B-74X-CC through -77X-CC. Sample 130-806B-78X-CC (743.1 mbsf) and Samples 130-806C-59X-CC (749.5 mbsf) through -62X-CC (776.4 mbsf) were assigned to either the *Dorcadospyris ateuchus* or the *C. tetrapera* Zone, which cannot be differentiated. It is notable that *Dorcadospyris riedeli* appears just above the occurrence of *Dorcadospyris papilio,* which has been noted at other sites. The radiolarian evidence suggests that the bottom of Hole 806C may or may not be in the Oligocene because of the zonal assignment, which ranges from the middle Oligocene to the early lower Miocene.

PALEOMAGNETISM

Introduction

Stable magnetic polarity at Site 806 can be traced downward with confidence only to about 10 mbsf in Holes 806B and 806C and does not extend to the Brunhes/Matuyama Chron boundary in either hole, representing the trend toward a shorter magnetostratigraphic record with decreasing water depth in the three near-equatorial sites (804, 805, and 806). Two factors combine to reduce the age limit of the preserved magnetostratigraphy: (1) an increase in sedimentation rates extending the record, so that a given magnetic datum occurs at a greater subbottom depth; and (2) a decrease in the sub-bottom depth at which the primary magnetic remanence fades to the point that polarity information is lost (Fig. 17). In response to this behavior, detailed paleomagnetic analysis at Site 806 was curtailed at any early stage.

Natural remanent magnetization (NRM) and 15-mT alternating field (AF) demagnetized runs were measured in the cryogenic magnetometer at 1-cm intervals in the first two cores in both Holes 806B and 806C (Cores 130-806B-1H and -2H and Cores 130-806C-1H and -2H). The measurement interval was expanded to 3 cm for the third and fourth cores (Cores 130-806B-3H and -4H and Cores 130-806C-3H and -4H), and to 5 cm for the fifth core (Cores 130-806B-5H and 130-806C-5H). Measurement was expanded to 10-cm intervals from Core 130-806B-11H in Hole 806B, and from Core 130-806C-7H in Hole 806C, whereas demagnetization was restricted to one section per core. Paleomagnetic measurements in Hole 806C were discontinued after Core 130-806C-10H.

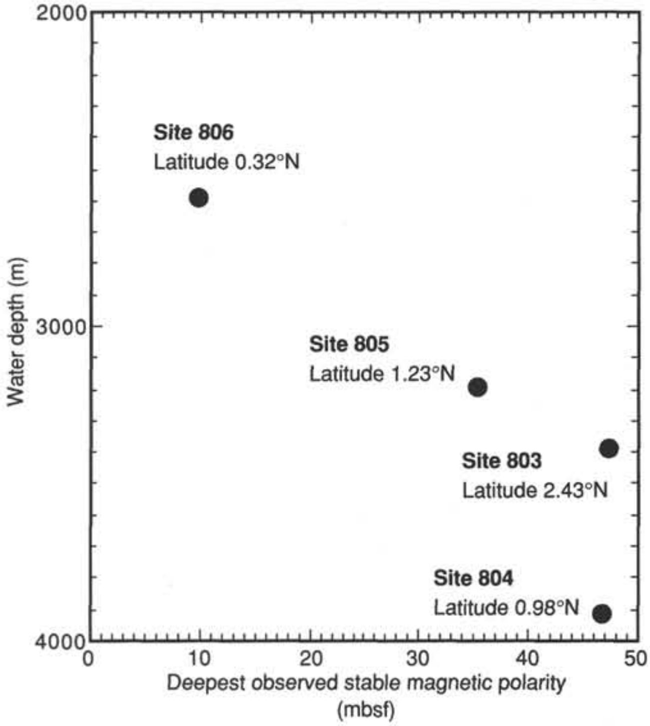

Figure 17. Relationship between water and sub-bottom depths to the deepest point at which stable magnetic polarity was observed for Sites 803–806. The depth to which magnetic polarity is preserved lessens with decreasing water depth and increased proximity to the equatorial zone of high biogenic productivity.

Magnetization Record

Plots of AF-demagnetized declination, inclination and intensity for Holes 806B and 806C are shown in Figure 18. Cores 130-806B-1H and -2H and Cores 130-806C-1H and -2H were not oriented; these cores represent the upper 16 m in Hole 806B and the upper 15.3 m in Hole 806C. The intensity record in cores from Hole 806B, subjected to 15-mT magnetic cleaning, remains fairly constant at values of 2–4 mA/m from the surface to 10.3 mbsf, at which point the intensity values decrease to 0.1–0.2 mA/m over an interval of about 0.5 m. Demagnetized intensity in Hole 806B then increases with sub-bottom depth, peaking at values of 0.5 mA/m at 20 mbsf, before declining again to 0.01–0.02 mA/m by 30 mbsf, and recovering to about 0.5 mA/m at about 37 mbsf. Demagnetized intensities of cores from Hole 806C also decrease sharply at 10 mbsf, declining from 3 mA/m at 9.8 mbsf to 0.3 mA/m at 10.5 mbsf. Below 10.5 mbsf, intensity declines more steadily in Hole 806C than in Hole 806B.

Although both the declination and inclination records are noisy, AF-cleaned magnetizations in Holes 806B and 806C appear to be stable down to about 10 mbsf, the depth at which intensity values suddenly decline. Continuity of the declination record from within a meter of the seafloor implies that the polarity to 10 mbsf is normal, despite the lack of orientation over

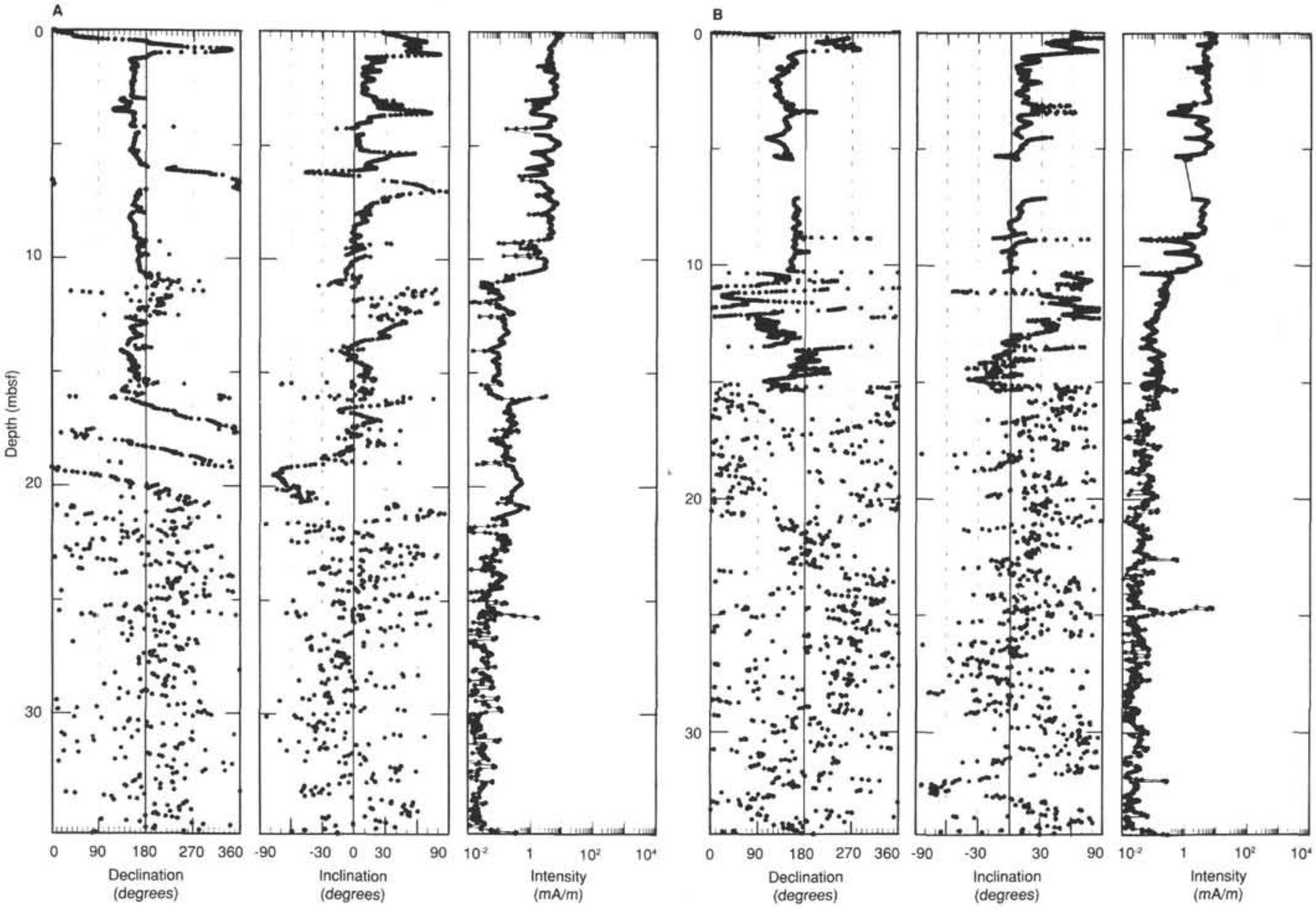

Figure 18. Unoriented, AF-demagnetized declination, inclination, and intensity charts for the first four cores in Holes 806B and 806C. **A.** Cores 130-806B-1H to -4H. **B.** Cores 130-806B-1H to -4H.

this interval, and that the Brunhes/Matuyama boundary is deeper than 10 mbsf in both holes. Below 10 mbsf, the AF-cleaned magnetization records in both holes are difficult to interpret. Within Core 130-806B-2H, immediately below the sharp drop in intensity at 10.5 mbsf, the AF-cleaned declination and inclination records are complex and remain so until about 12.5 mbsf. Inclination values reach about +80° at 11.2 mbsf before decreasing to 0° at 13.6 mbsf. Declination and inclination records remain constant from 13.6 mbsf to the base of Core 130-806B-2H at 16.0 mbsf.

Declination values follow an extraordinary spiraling path through three complete revolutions from the top of Core 130-806B-3H at 16.0 mbsf down to 21 mbsf. Over this interval, inclination varies from about +60° to about −70° in a continuous but complex fashion, and intensity increases as noted above. Below 21 mbsf the AF-cleaned record in Hole 806B becomes chaotic, and intensities decrease again. Complex magnetization features also appear in the record from Hole 806C, beginning immediately below the sharp drop in intensity values at 10.3 mbsf. Between 10.3 and ~12.3 mbsf in Core 130-806C-2H, the AF-cleaned declination record swings through a series of short-wavelength, large variations, whereas the inclination data form a noisy grouping around +60°. From 12.3 mbsf to the base of Core 130-806C-2H at 15.1 mbsf, declination data continue to oscillate, with a wavelength of about 30 cm and a range of about 60°–140°, whereas the inclination values trend downward from about +80° to about −30°.

Visual examination of these intervals of complex magnetization in Holes 806B and 806C shows no evidence for physical disruption or internal rotation of the cores. It is difficult to envisage how these features could have arisen as part of the primary magnetization of the sediments. It is also clear from an examination of the records from Sites 803, 804, and 805 that the loss of recognizable polarity normally accompanies a sudden drop in intensity of the type seen at about 10 mbsf in Holes 806B and 806C. NRM measurements have steep negative inclinations over each of these intervals of complex magnetization (Fig. 19), similar to those identified as drilling-induced remanence in other, deeper cores (see below). The spiraling declination values seen in Core 130-806B-3H may be artifacts caused by the passage of the core past a locally intense field source while the source was rotating relative to the core. Intervals of less disturbed, apparently normal polarity below 10 mbsf in Holes 806B and 806C may have been magnetized by viscous remanence acquired during the Brunhes Chron.

It appears unlikely that any of the magnetization measured either as NRM or after 15-mT cleaning in the magnetically complex region between about 10 and 20 mbsf in Holes 806B and 806C is of primary origin. The unusual magnetization pattern of these intervals, their apparent susceptibility to VRM and drilling-related remanences, and the resistance of these secondary magnetizations to AF cleaning (i.e., their high coercivity) may indicate an unusual magnetic mineralogy in this interval.

The NRMs of many of the cores below 30 mbsf in Holes 806B and 806C have inclinations of about −60° to −80° (Fig. 20), a pattern similar to that seen at Site 805. Drilling-induced remanence reported by Sallomy and Briden (1975) in a borehole core was aligned with the borehole axis, although drilling in this

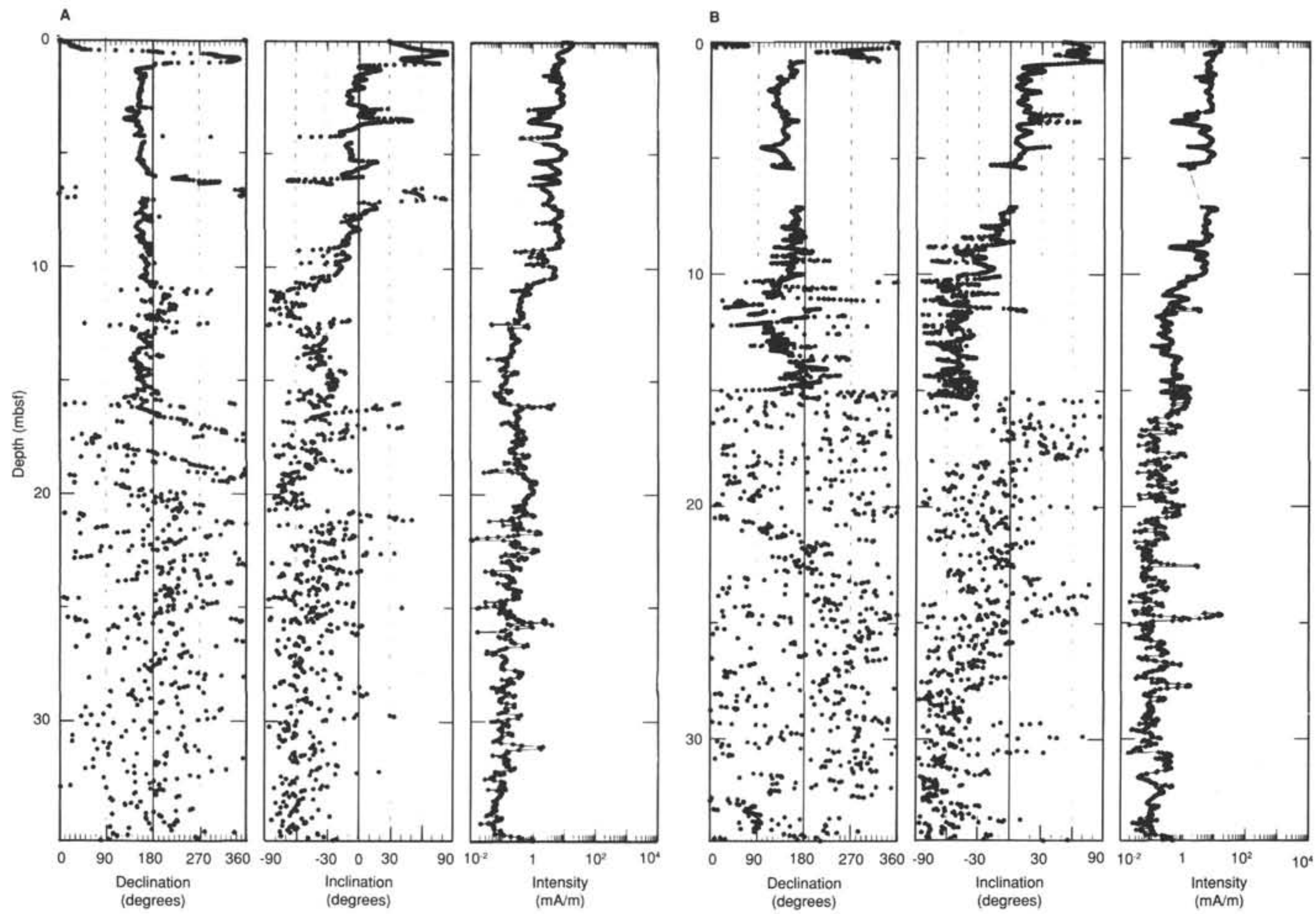

Figure 19. Unoriented NRM declination, inclination, and intensity charts for the first four cores in Holes 806B and 806C. **A.** Cores 130-806B-1H to -4H. **B.** Cores 130-806C-1H to -4H.

case was in harder rocks in which drilling-induced heating was a likely factor in the magnetization. Steeply negative NRM inclinations in weakly magnetized cores from Leg 130 sites probably reflect the presence of a similar borehole-parallel component dominating a presumably shallowly inclined pre-drilling remanence.

SO_4^{2-} Reduction and Magnetization Intensity

Interstitial water SO_4^{2-} levels and remanence intensity in Hole 806B appear to be positively correlated (Fig. 21). The abundance of the SO_4^{2-} ion has a trend similar to that of the log intensity, particularly after demagnetization. An SO_4^{2-} concentration of about 26.6 mM appears to be critical; as this value is first crossed at about 10.3 mbsf, the demagnetized remanence intensity drops sharply from about 3 to about 0.15 mA/m. An upward inflection in the SO_4^{2-} abundance at a sub-bottom depth of 20 mbsf is accompanied by a local increase in intensity, as noted above. Remanence intensities of 0.02 mA/m are reached when the SO_4^{2-} concentration drops to about 25 mM, at which point remanence measurements reach the limit of resolution of the shipboard cryogenic magnetometer.

Reduction of magnetite, producing dissolved and reduced Fe, and the reduction of sulfate to sulfide (both of which were caused by microbial activity) result in the precipitation of iron sulfide minerals, principally pyrite. These reactions appear to be the possible mechanism that links the decline in remanence intensity to the decrease in SO_4^{2-} concentration (e.g., Karlin and Levi, 1983, 1985). Two successive phases of downhole alteration of the magnetic mineralogy in Hole 806B are implied by the presence of the interval of complex magnetization between the sharp decrease in intensity at about 10.3 mbsf and the beginning of random weak magnetizations at 20 mbsf.

Little dissolution of magnetite occurs from the surface to about 10 mbsf, at which point rapid dissolution over the next 0.5 m appears to remove almost all magnetite much larger than the critical "blocking diameter" of 0.025 μm (Dunlop, 1981). At this point, primary magnetization becomes too weak to measure. The interval between 10 and 20 mbsf, in which high coercivity secondary components appear to have been acquired, may correspond to an interval observed by Sager (1988) in carbonate oozes in Holes 632A and 633A from ODP Leg 101. Mean destructive fields increased in these holes as intensities decreased downhole. Sager attributed this behavior to the possible development of a metastable, magnetic iron sulfide such as greigite or pyrrhotite along with pyrite as the sulfate reduction reactions progress.

A similar mechanism may operate between 10 and 20 mbsf in Holes 806B and 806C. The local inflection in SO_4^{2-} concentration at 20 mbsf is presumably related to changes in the rate of SO_4^{2-} reduction over the interval in which these metastable iron sulfides are produced. The accompanying peak in magnetic intensity in both the NRM and AF-cleaned records is a function of the acquisition of high-coercivity secondary remanences by these metastable phases. Below 20 mbsf, magnetite may be

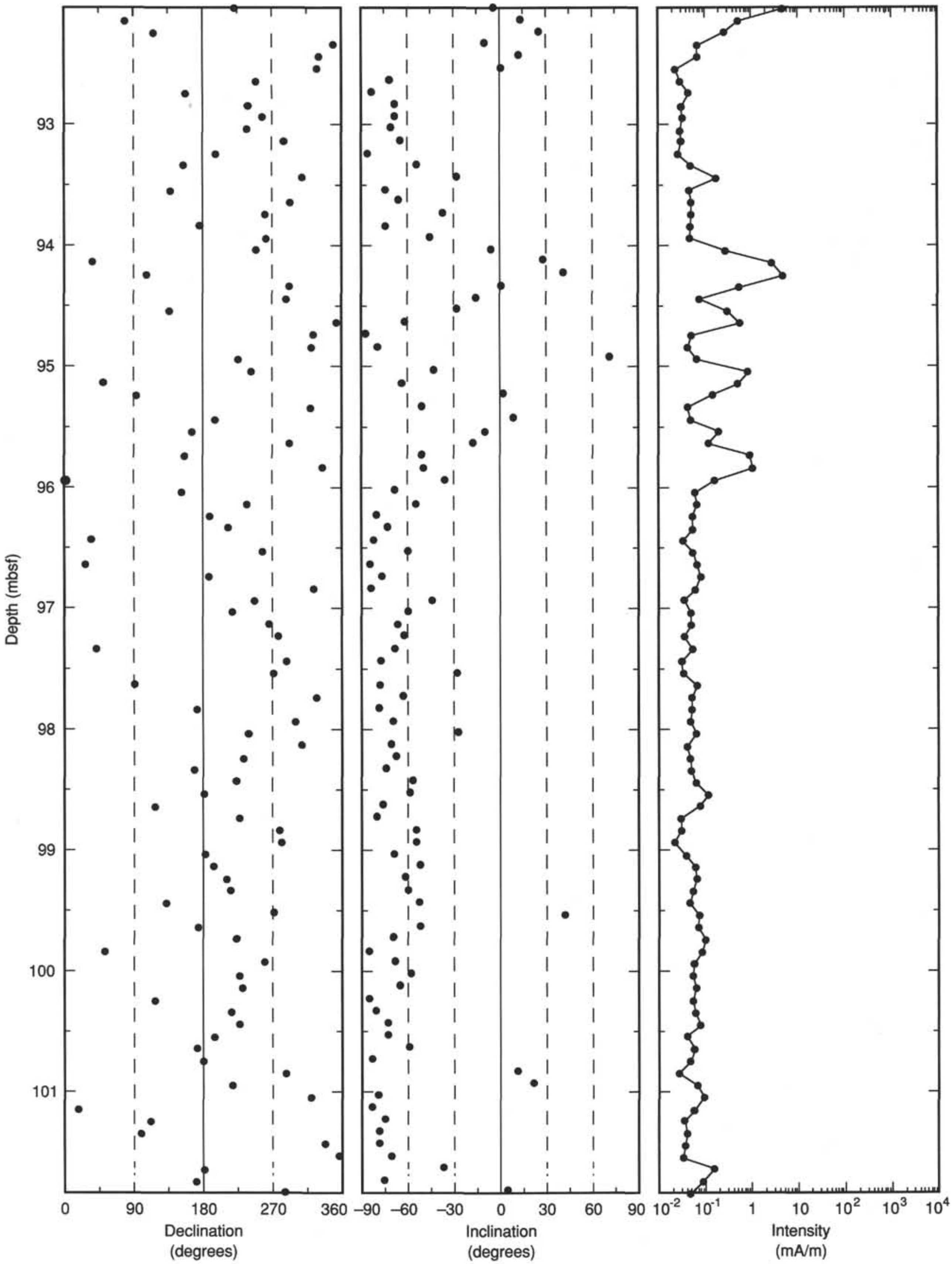

Figure 20. Declination, inclination, and intensity chart of the NRM of Core 130-806B-11H. Note the steeply negative inclinations.

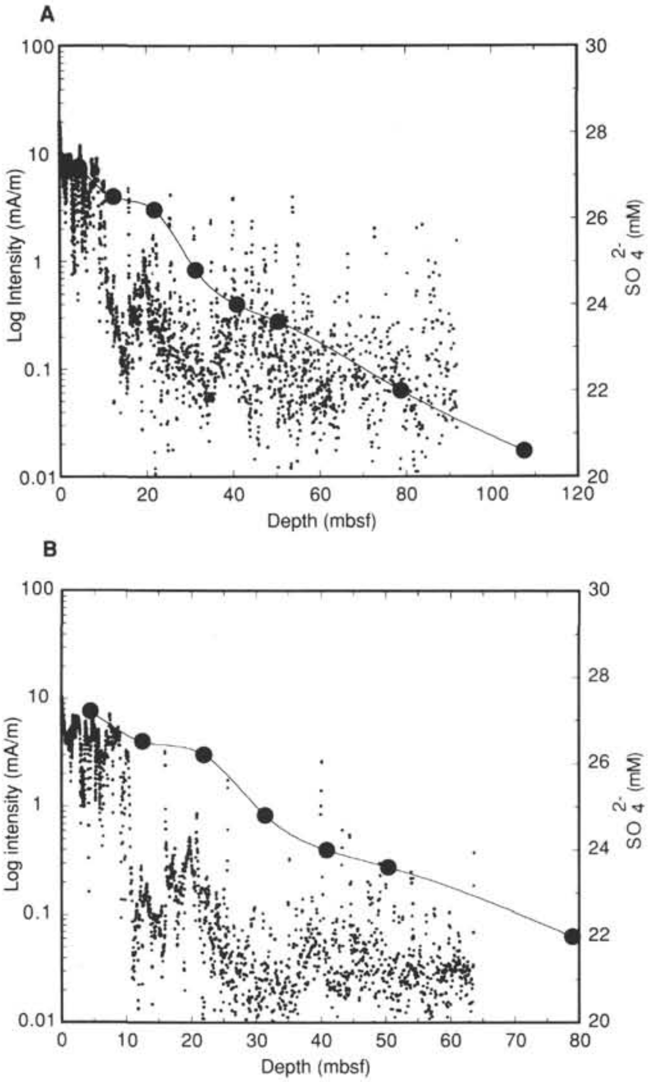

Figure 21. Correlation between remanence intensity (dots) and sulfate ion concentration (closed circles, fitted by cubic splines) (see "Inorganic Geochemistry" section, this chapter) vs. depth, Hole 806B, for (A) NRM and (B) after 15-mT demagnetization. Note the increase in demagnetized intensity and the change in the rate of SO_4^{2-} reduction around 20 mbsf.

present as very fine-grained relicts within pyrite, and large proportions of the remanence may be carried by magnetite grains with low coercivities and short relaxation times.

Fine-grained pyrrhotite may also persist and contribute a higher coercivity component to the remanence. Although Lowrie and Heller (1982) noted that pyrrhotite was rarely a significant source of remanence in marine limestones, pyrrhotite, occurring as minute inclusions within pyrite, has been reported as the major magnetic carrier in the Helvetic Limestones (Kligfield and Channell, 1981). The pervasive drilling-induced remanence observed in the weakly magnetized cores may be carried by either or both of these minerals. Shore-based studies of the magnetic mineralogy should clarify these matters.

SEDIMENTATION RATES

An apparently continuous uppermost Oligocene through Holocene sediment sequence was cored at Site 806. The average sedimentation rate is about 30 m/m.y., as estimated from the biostratigraphic information (see "Biostratigraphy" section, this chapter). All datum events that were recognized in the three holes cored at Site 806 are listed in Table 3. The biostratigraphic age-depth indicators from Holes 806B and 806C are shown graphically in Figures 22 and 23. The large depth uncertainties for some early Miocene datums of Hole 806C (Fig. 23) represent two washed intervals separated by a single spot core.

Age-depth data representing calcareous and siliceous microfossil groups are available from Hole 806B. These data have been replotted for shorter time and depth intervals in Figures 24, 25, and 26, so that every individual biostratigraphic datum listed in Table 3 can be identified, and so that points where sedimentation rate changes occur can be selected. The different microfossil groups commonly provide age discrepancies of about 1 m.y. for identical sample depths (i.e., Fig. 24). These discrepancies consequently are on the order of 10%–20% of the age of the sediment even in the upper Miocene and Pliocene intervals. Presumably, they largely reflect problems associated with the assigned ages to the biostratigraphic events.

Sedimentation rates from all three holes that have been calculated from selected calcareous biostratigraphic events and are presented in Table 4. These rates are plotted vs. age in Figure 27. The shape of this age/rate curve is similar to those obtained from previous Leg 130 sites (Sites 803, 804, and 805). This similarity implies that the rate histories indeed were alike at the different sites, but to some extent it also reflects the fact that, if possible, the same series of control points were chosen for the sedimentation rate calculations at the different sites. Minor differences in the rate histories between Holes 806B and 806C (Fig. 27) primarily stem from the large sample intervals used. The greatest rate difference between the two holes falls in the 20–25 Ma interval and is probably caused by the use of different datums: the LO of *Globorotalia kugleri* in Hole 806B, and the LO of *Sphenolithus ciperoensis* in Hole 806C.

The marked increase in sedimentation rates at about 8.7 Ma has been also observed at all of the deeper transect sites. Assuming the change at the fairly shallow Site 806 is associated with moderate to little carbonate dissolution, it follows that the major portion of that signal represents a significant productivity increase in the early part of late Miocene time.

INORGANIC GEOCHEMISTRY

Thirty interstitial water samples were collected at Site 806, twenty-nine from Hole 806B at depths ranging from 4.5 to 706.0 mbsf and one from Hole 806C at 765.1 mbsf, which was patched into the profile. Interstitial water samples cover most of the depth range of the nannofossil ooze and chalk of Unit I, the single lithologic unit recognized at Site 806 (see "Lithostratigraphy" section, this chapter). Chemical gradients in the interstitial waters at this site (Table 5) are similar to those at the first three sites drilled on this leg, being governed by the biogenic-rich, organic-carbon-poor character of the sediments and by the diffusive influence of basalt alteration reactions at depth. The magnitude of the chemical gradients at Site 806, the site nearest to the equator and at the shallowest depth drilled on this leg, is generally equal to or larger than those at the first three sites. The differences in gradients are consistent with the differences in geography, water depth, and sedimentation rates.

Going downhole, chlorinity increases by almost 2% to 565 mM at 41.0 mbsf (Core 180-806B-5H) and increases further to values close to 600 mM at depths >500 m, for a total increase of 8.5% over the sampled interval (Fig. 28). Salinity, measured refractively as total dissolved solids, is fairly constant with depth at 35.0–35.5 g/kg over the interval from 4.5 to 564.4 mbsf, with the exception of a high, possibly errant, value of 40 g/kg at 450.2 mbsf (Core 130-806B-48X); there are a few higher values in the interval from 594.9 to 679.9 mbsf (Table 5).

Table 3. Biostratigraphic events observed at Site 806.

Event	Upper depth (mbsf)	Lower depth (mbsf)	Age (Ma)
130-806A-			
LO *P. lacunosa* (N)	7.7	17.2	0.46
LO *G. tosaensis* (F)	7.7	17.2	0.60
LO *C. macintyrei* (N)	26.7	36.2	1.45
LO *G. fistulosus* (F)	26.7	36.2	1.60
LO *D. brouweri* (N)	36.2	45.7	1.89
OA *D. triradiatus* (N)	36.2	45.7	2.07
LO *D. pentaradiatus* (N)	45.7	55.2	2.35
LO *D. surculus* (N)	55.2	64.7	2.45
LO *D. tamalis* (N)	64.7	74.2	2.65
LO *G. multicamerata* (F)	64.7	74.2	2.90
LO *G. altispira* (F)	64.7	74.2	2.90
FO *G. fistulosus* (F)	74.2	83.7	2.90
130-806B-			
LO *P. lacunosa* (N)	6.5	16.0	0.46
FO *C. tuberosa* (R)	6.5	16.0	0.50
LO *G. tosaensis* (F)	6.5	16.0	0.60
LO *N. reinholdii* (D)	16.0	25.5	0.65
LO *A. angulare* (R)	25.5	35.0	0.99
LO *C. macintyrei* (N)	32.3	35.0	1.45
LO *P. prismatium* (R)	35.0	44.5	1.54
FO *A. angulare* (R)	16.0	25.5	1.58
LO *G. fistulosus* (F)	35.0	44.5	1.60
LO *R. praebergonii* var. *robusta* (D)	35.0	44.5	1.55
LO *D. brouweri* (N)	38.8	41.8	1.89
FO *G. truncatulinoides* (F)	44.5	54.0	1.90
OA *D. triradiatus* (N)	44.5	46.8	2.07
LO *T. convexa* var. *aspinosa* (D)	44.5	54.0	2.10
LO *D. pentaradiatus* (N)	54.7	56.2	2.35
LO *N. jouseae* (D)	73.0	82.5	2.60
LO *S. peregrina* (R)	54.0	63.5	2.63
LO *G. multicamerata* (F)	44.5	54.0	2.90
LO *G. altispira* (F)	63.5	73.0	2.90
FO *G. fistulosus* (F)	73.0	82.5	2.90
LO *Sphaeroidinellopsis* spp. (F)	73.0	82.5	3.00
FO *R. praebergonii* (D)	73.0	82.5	3.00
FO *S. dehiscens* (F)	73.0	82.5	3.00
FO *G. tosaensis* (F)	73.0	82.5	3.10
LO *P. fistula* (R)	92.0	101.5	3.27
LO *G. margaritae* (F)	73.0	82.5	3.40
LO *Sphenolithus* (N)	89.3	90.8	3.45
LO *P. doliolum* (R)	92.0	101.5	3.54
LO *R. pseudoumbilica* (N)	94.3	95.8	3.56
FO *A. ypsilon* (R)	73.0	82.5	3.78
FO *S. tetras* (R)	101.5	111.0	3.84
LO *S. berminghami* (R)	139.5	149.0	3.86
FO *A. elegans* (D)	73.0	82.5	3.90
FO *S. pentas* (R)	168.0	177.5	4.25
LO *N. cylindrica* (D)	139.5	149.0	4.35
FO *N. jouseae* (D)	139.5	149.0	4.50
LO *C. acutus* (N)	147.4	148.9	4.60
LO *S. omnitubus* (R)	139.5	149.0	4.75
LO *D. quinqueramus* (N)	158.5	168.0	5.00
LO *S. delmontensis* (R)	196.5	206.5	5.00
LO *S. corona* (R)	215.5	225.0	5.05
FO *S. dehiscens* (F)	92.0	101.5	5.10
FO *G. tumida* (F)	158.5	168.0	5.20
FO *P. spectabilis* (F)	158.5	168.0	5.20
LO *A. acutiloba* (D)	158.5	168.0	5.40
LO *A. tritubus* (R)	177.5	187.0	5.35
LO *N. miocenica* (D)	168.0	177.5	5.60
LO *T. praeconvexa* (D)	168.0	177.5	5.80
FO *P. primalis* (F)	206.0	215.5	5.80
LO *C. caepa* (R)	215.5	225.0	6.40
FO *S. omnitubus* (R)	244.0	253.5	6.40
FO *Amaurolithus* (N)	215.5	225.0	6.70
FO *G. plesiotumida* (F)	263.0	272.5	7.10
LO *D. hughesi* (R)	263.0	272.5	7.15
FO *D. quinqueramus* (N)	263.0	282.0	7.50
LO *C. yabei* (D)	301.0	310.5	7.50
LO *D. ontogenesis* (R)	282.0	291.5	7.50
FO *S. berminghami* (R)	329.7	339.4	7.95
LO *A. ellipticus* var. *javanica* (D)	263.0	272.5	8.00
LO *B. miralestensis* (R)	320.0	329.7	8.15

Table 3 (continued).

Event	Upper depth (mbsf)	Lower depth (mbsf)	Age (Ma)
130-806B- (Cont.)			
LO *D. laticonus* (R)	282.0	291.5	8.15
LO *D. petterssoni* (R)	310.5	320.0	8.15
LO *S. wolffii* (R)	320.0	329.7	8.15
LO *C. yabei* (D)	301.0	310.5	8.60
LO *D. hamatus* (N)	329.7	339.4	8.70
FO *D. hughesi* (R)	329.7	339.4	8.75
LO *A. moronensis* (D)	329.7	339.4	8.90
LO *C. japonica* (R)	349.1	358.8	10.15
FO *N. acostaensis* (F)	349.1	358.8	10.20
LO *G. siakensis* (F)	358.8	368.5	10.40
FO *D. hamatus* (N)	358.8	368.5	10.50
LO *C. coscinodiscus* (D)	397.5	407.2	10.70
LO *L. thornburgi* (R)	387.9	397.5	11.00
FO *C. coalitus* (N)	368.5	378.2	11.10
LO *A. moronensis* (D)	329.7	339.4	11.30
LO *G. fohsi lobata/robusta* (F)	407.2	416.9	11.50
LO *C. cornuta* (R)	397.5	407.2	11.75
LO *C. coscinodiscus* (D)	397.5	407.2	12.20
LO *C. nitescens* (N)	426.5	436.1	12.80
LO *C. lewisianus* (D)	426.5	436.1	12.90
FO *G. fohsi fohsi* (F)	445.8	455.5	13.10
LO *C. floridanus* (N)	473.3	482.6	13.10
LO *C. lewisianus* (D)	426.5	436.1	13.50
LO *S. heteromorphus* (N)	473.3	482.6	13.60
FO *D. hustedtii* (D)	455.5	463.6	13.70
FO *G. praefohsi* (F)	501.9	511.6	13.90
LO *C. peplum* (D)	501.9	511.6	14.10
LO *A. californicus* (D)	501.9	511.6	14.80
FO *G. peripheroacuta* (F)	511.6	521.3	14.90
LO *C. lewisianus* var. *similis* (D)	511.6	521.3	15.70
TA *D. deflandrei* (N)	530.9	540.5	16.10
LO *R. marylandicus* (D)	550.2	559.9	16.70
LO *C. dissimilis* (F)	589.0	598.6	17.60
FO *S. heteromorphus* (N)	579.3	589.0	18.60
LO *C. elegans* (D)	608.3	617.9	18.70
LO *S. belemnos* (N)	579.3	589.0	18.80
FO *S. belemnos* (N)	598.6	608.3	20.00
LO *G. kugleri* (F)	646.5	656.2	21.80
FO *R. paleacea* (D)	733.4	743.1	22.70
130-806C-			
LO *P. lacunosa* (N)	5.6	11.6	0.46
LO *G. tosaensis* (F)	0	5.6	0.60
LO *C. macintyrei* (N)	34.1	43.6	1.45
LO *G. fistulosus* (F)	34.1	43.6	1.60
LO *D. brouweri* (N)	34.1	43.6	1.89
FO *G. truncatulinoides* (F)	43.6	53.1	1.90
OA *D. triradiatus* (N)	43.6	53.1	2.07
LO *D. pentaradiatus* (N)	53.1	62.6	2.35
LO *D. surculus* (N)	53.1	62.6	2.45
LO *G. altispira* (F)	62.6	72.1	2.90
FO *G. fistulosus* (F)	72.1	81.6	2.90
LO *Sphaeroidinellopsis* spp. (F)	72.1	81.6	3.00
FO *S. dehiscens* (F)	72.1	81.6	3.00
FO *G. tosaensis* (F)	72.1	81.6	3.10
LO *G. margaritae* (F)	72.1	81.6	3.40
LO *Sphenolithus* (N)	81.6	91.1	3.45
LO *R. pseudoumbilica* (N)	91.1	100.6	3.56
LO *C. acutus* (N)	138.6	148.1	4.60
FO *C. acutus* (N)	176.6	186.1	4.90
LO *D. quinqueramus* (N)	176.6	186.1	5.00
FO *S. dehiscens* (F)	81.6	91.1	5.10
FO *G. tumida* (F)	157.6	167.1	5.20
FO *P. primalis* (F)	195.6	205.1	5.80
FO *Amaurolithus* (N)	233.6	243.1	6.70
FO *G. plesiotumida* (F)	281.1	290.6	7.10
FO *D. quinqueramus* (N)	281.1	290.6	7.50
LO *D. hamatus* (N)	328.9	338.5	8.70
LO *Catinaster* (N)	328.9	338.5	8.80
FO *D. neohamatus* (N)	338.5	348.2	9.00
FO *N. acostaensis* (F)	338.5	348.2	10.20
LO *G. siakensis* (F)	357.9	367.6	10.40
FO *D. hamatus* (N)	367.6	377.3	10.50
FO *Catinaster* (N)	367.6	377.3	11.10

Table 3 (continued).

Event	Upper depth (mbsf)	Lower depth (mbsf)	Age (Ma)
130-806C- (Cont.)			
LO *G. fohsi lobata/robusta* (F)	406.3	415.9	11.50
LO *C. nitescens* (N)	415.9	425.6	12.80
FO *G. fohsi fohsi*	444.9	454.6	13.10
LO *C. floridanus* (N)	464.5	474.3	13.10
LO *S. heteromorphus* (N)	464.5	474.3	13.60
FO *G. praefohsi* (F)	483.7	493.3	13.90
FO *G. peripheroacuta* (F)	512.7	522.4	14.90
TA *D. deflandrei*	522.4	532.0	16.10
LO *C. dissimilis* (F)	541.7	608.5	17.60
FO *S. heteromorphus* (N)	541.7	608.5	18.60
LO *S. belemnos* (N)	541.7	608.5	18.80
FO *S. belemnos* (N)	599.8	608.5	20.00
LO *G. kugleri* (F)	608.5	749.5	21.80
FO *G. kugleri* (F)	608.5	749.5	23.70
LO *S. ciperoensis* (N)	759.2	766.7	25.20

Notes: The depth uncertainty predominantly represents sample intervals used. References for the age estimates are presented in the "Explanatory Notes" chapter (this volume). N = nannofossil, F = foraminifer, D = diatom, R = radiolarian, FO = first occurrence, LO = last occurrence, OA = onset acme, and TA = termination acme. Magnetostratigraphic reversal boundaries followed by the designation (T) or (O) refer to "termination" and "onset," respectively.

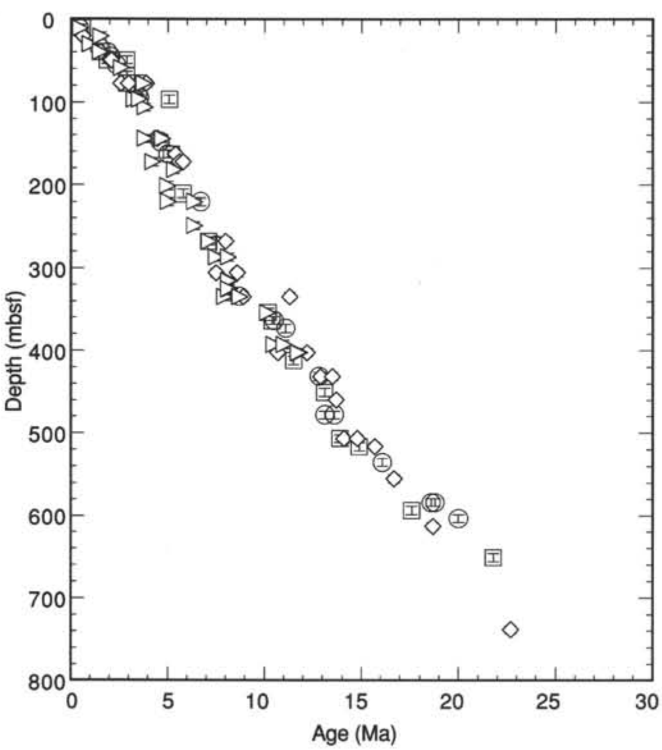

Figure 22. Age-depth relationships of biostratigraphic markers, Hole 806B. Circles = nannofossil, squares = foraminifer, diamonds = diatom, and triangles = radiolarian.

Sodium concentrations measured by flame emission spectrophotometry (Table 5) and those estimated by charge balance calculations generally agree to within <1.5%. Sodium concentrations increase from 471 mM at 4.5 mbsf to ~520 mM at 650.9–706.0 mbsf, a total increase of 10%. Sodium concentrations at

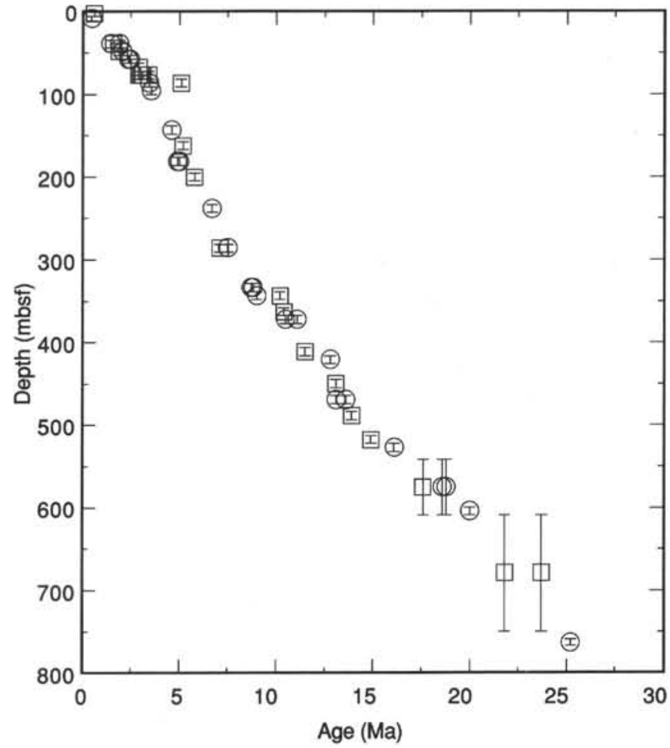

Figure 23. Age-depth relationships of biostratigraphic markers, Hole 806C. Large error bars show uncored interval. Symbols used are as in Figure 22.

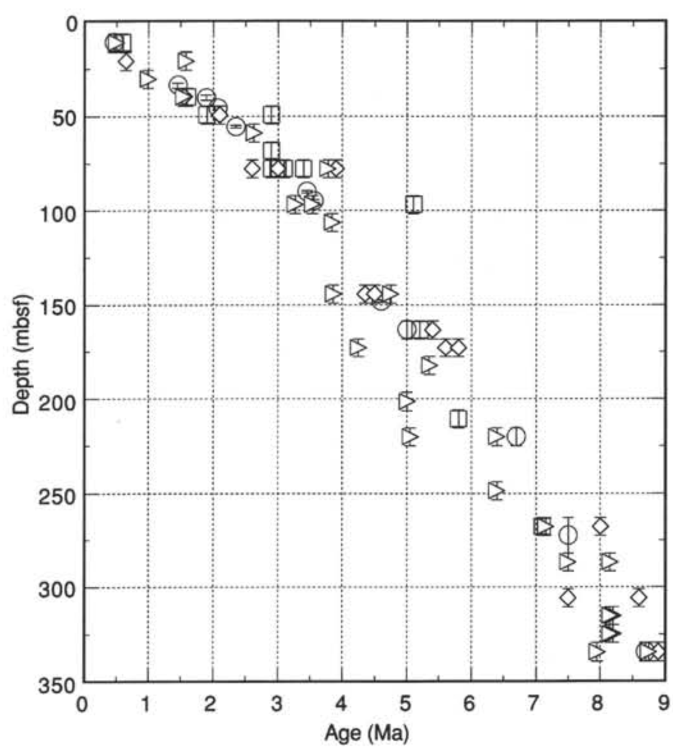

Figure 24. Age-depth relationships of biostratigraphic markers from the upper Miocene through Holocene interval, Hole 806B. Error bars show sample interval uncertainties. Symbols used are as in Figure 22.

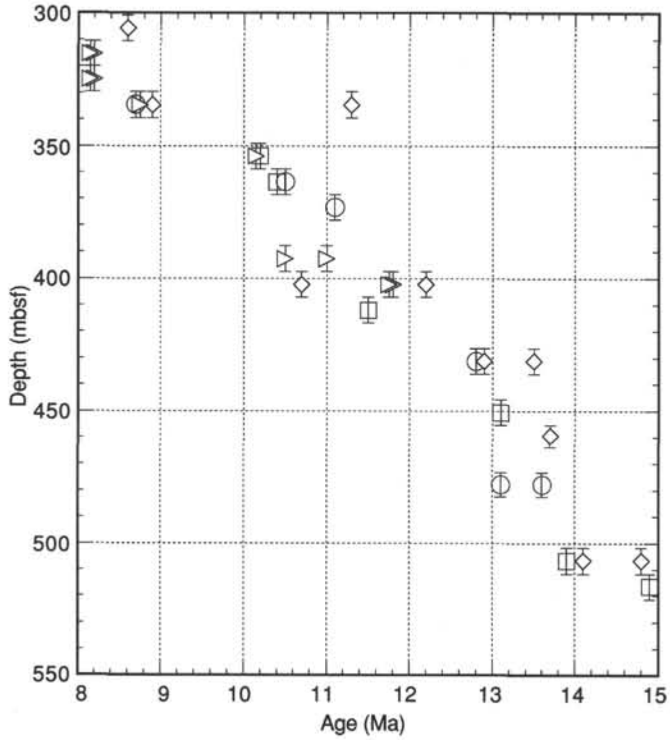

Figure 26. Age-depth relationships of biostratigraphic markers from the lower through middle Miocene interval, Hole 806B. Error bars show sample interval uncertainties. Symbols used are as in Figure 22.

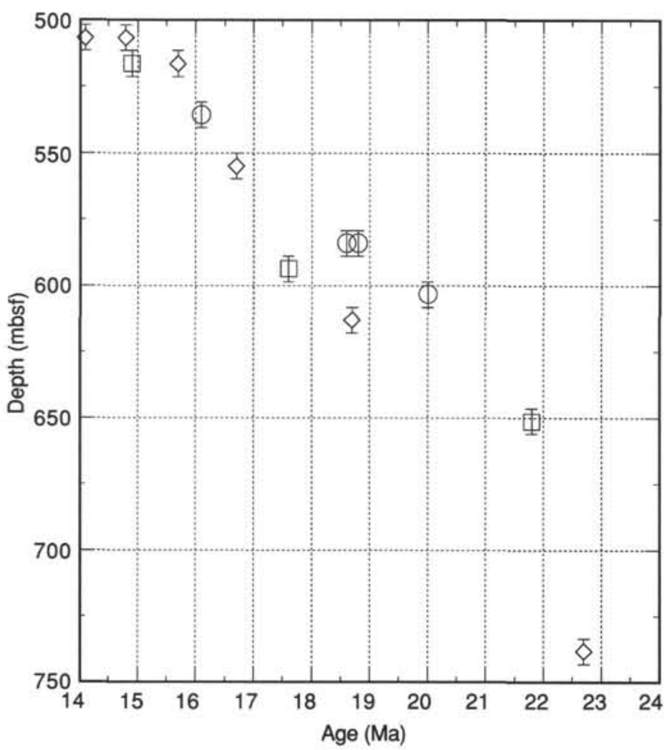

Figure 25. Age-depth relationships of biostratigraphic markers from the middle through lower upper Miocene interval, Hole 806B. Error bars show sample interval uncertainties. Symbols used are as in Figure 22.

Table 4. Estimated sedimentation rates, Site 806, and the control points determining those rates.

Control points	Depth (mbsf)	Age (Ma)	Sedimentation rate (m/m.y.)
130-806A-			
Top section	0	0	
OA D. triradiatus	41.05	2.07	19.8
LO G. altispira	69.55	2.90	34.3
Terminal depth	83.70	3.31	
130-806B-			
Top section	0	0	
LO D. brouweri (N)	40.25	1.89	21.3
LO R. pseudoumbilica (N)	95.00	3.56	32.8
LO D. hamatus (N)	334.55	8.70	46.6
LO S. heteromorphus (N)	477.95	13.60	29.3
FO S. belemnos (N)	603.45	20.00	19.6
LO G. kugleri (F)	651.35	21.80	26.6
Terminal depth	743.10	25.25	
130-806C-			
Top section	0	0	
OA D. triradiatus (N)	48.35	2.07	23.4
LO R. pseudoumbilica (N)	95.85	3.56	31.9
LO D. hamatus (N)	333.70	8.70	46.3
LO S. heteromorphus (N)	469.40	13.60	27.7
FO S. belemnos (N)	603.38	20.00	20.9
LO S. ciperoensis (N)	762.95	25.20	30.7
Terminal depth	776.40	25.64	

Notes: References for the age estimates are presented in the "Explanatory Notes" chapter (this volume). N = nannofossil, F = foraminifer, D = diatom, R = radiolarian, FO = first occurrence, LO = last occurrence, and OA = onset acme. Magnetostratigraphic reversal boundaries followed by the designation (T) or (O) refer to "termination" and "onset," respectively.

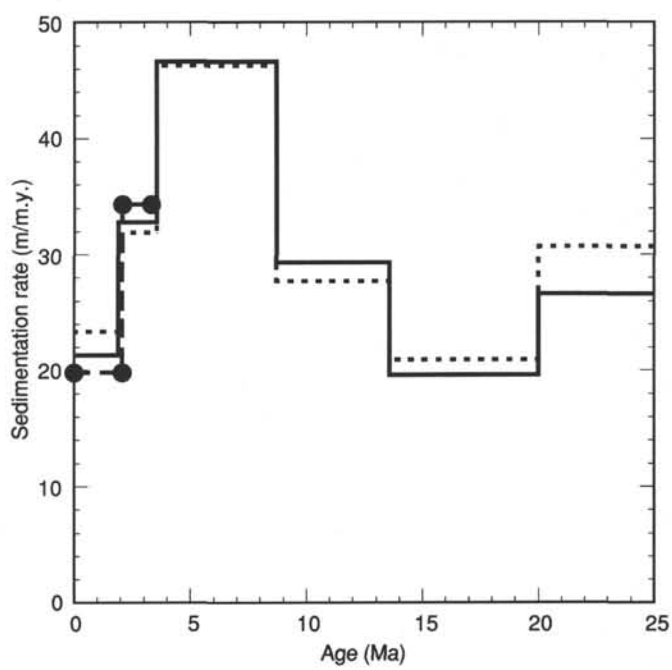

Figure 27. Sedimentation rate history, Site 806. Dashed line with filled circle = Holes 806A; solid line = Hole 806B; and dashed line = Hole 806C.

Table 5. Interstitial water geochemical data, Holes 806B and 806C.

Core, section, interval (cm)	Depth (mbsf)	pH	Alk. (mM)	Sal. (g/kg)	Cl^- (mM)	Na (mM)	SO_4^{2-} (mM)	PO_4^{3-} (μM)	NH_4^+ (μM)	SiO_2 (μM)	Mn (μM)	Ca^{2+} (mM)	Mg^{2+} (mM)	Sr (μM)	Li (μM)	K (mM)	Rb (μM)
130-806B-																	
1H-3, 145–150	4.45	7.6	3.73	35.5	553	471	27.2	2.9	37	469	9	10.7	52.3	140	24.5	10.8	1.62
2H-4, 145–150	12.45	7.6	4.07	35.5	559	472	26.5	2.7	92	506	4	10.7	51.9	223	22.8	10.9	1.68
3H-4, 145–150	21.95	7.6	4.53	35.5	562	483	26.2	2.5	140	539	3	10.9	51.0	317	22.3	11.1	1.58
4H-4, 145–150	31.45	7.6	4.72	35.5	563	475	24.8	2.3	182	552	3	11.1	50.2	396	21.9	11.1	1.72
5H-4, 145–150	40.95	7.6	5.08	35.5	565	479	24.0	LD	218	595	LD	11.3	49.3	475	21.0	11.3	1.74
6H-4, 145–150	50.45	7.6	5.25	35.5	564	487	23.6	LD	247	637	LD	11.4	48.5	540	20.6	11.4	1.76
9H-4, 145–150	78.95	7.6	5.80	35.5	564	484	22.0	LD	325	676	LD	12.3	45.9	723	18.9	11.1	1.70
12H-4, 145–150	107.45	7.6	6.23	35.0	568	490	20.6	LD	379	728	LD	13.2	43.5	861	17.2	10.8	1.70
15H-4, 145–150	135.95	7.6	6.31	35.0	567	484	20.1	LD	430	796	LD	14.3	41.6	983	15.9	10.6	1.70
18H-4, 145–150	164.45	7.6	6.43	35.0	567	492	19.2	LD	462	842	LD	15.2	39.7	1055	15.4	10.6	1.66
21H-4, 145–150	192.95	7.6	6.33	35.0	569	488	18.4	LD	502	871	LD	16.2	37.7	1069	14.1	10.5	1.69
24H-4, 145–150	221.45	7.1	6.34	35.0	578	493	17.4	LD	528	896	LD	16.9	36.6	1070	13.7	10.3	1.71
27H-4, 145–150	249.95	7.6	6.33	35.0	576	491	17.3	LD	543	956	LD	17.8	35.8	1048	13.3	10.3	1.70
30H-5, 145–150	279.95	7.6	6.24	35.0	575	500	17.1	LD	579	995	LD	18.6	34.3	1057	13.3	10.3	1.74
33H-4, 145–150	306.95	7.6	5.93	ND	576	503	17.3	LD	589	1010	LD	19.6	34.1	1082	12.8	10.3	1.72
36X-4, 145–150	335.65	7.8	5.74	35.0	577	498	16.9	LD	601	1033	LD	20.2	33.1	1094	13.7	10.7	1.72
39X-4, 140–150	364.70	7.1	5.67	35.0	580	503	16.9	LD	610	1022	LD	21.2	32.3	1102	14.1	10.1	1.70
42X-3, 140–150	392.30	7.6	5.63	35.0	581	503	16.7	LD	618	1058	LD	21.7	31.0	1089	15.4	10.0	1.72
45X-3, 140–150	421.30	7.0	5.14	35.5	584	506	16.4	LD	644	1109	LD	22.7	30.5	1106	16.7	10.0	1.69
48X-3, 140–150	450.20	7.6	5.60	40.0	591	519	16.7	LD	646	1147	LD	23.7	29.7	1132	18.4	10.0	1.69
52X-4, 140–150	488.50	ND	ND	ND	592	506	16.3	ND	644	1132	ND	24.9	28.5	1148	20.9	9.63	1.62
54X-5, 140–150	509.30	7.6	4.46	ND	596	511	16.1	LD	649	1132	LD	25.1	28.2	1138	21.8	9.78	1.60
57X-2, 140–150	533.80	ND	ND	ND	599	511	16.3	ND	642	1139	ND	26.1	27.5	1143	23.9	9.77	1.65
60X-4, 0–7	564.40	6.8	ND	35.5	582	501	16.1	LD	611	1136	LD	26.1	26.6	1111	26.5	9.56	1.65
63X-4, 140–150	594.90	7.7	3.88	37.5	597	517	15.9	LD	648	1192	LD	27.7	25.0	1172	27.3	9.53	1.55
66X-4, 140–150	623.80	7.1	3.75	36.0	594	514	15.6	ND	657	1263	LD	28.6	24.4	1180	29.0	9.30	1.53
69X-3, 140–150	650.90	ND	ND	ND	595	519	15.6	ND	646	1248	LD	29.9	23.5	1197	28.6	9.09	1.40
72X-3, 140–150	679.90	7.6	3.13	35.5	597	525	16.0	ND	631	1242	LD	30.0	23.3	1172	26.9	9.16	1.40
75X-2, 0–10	706.00	ND	ND	ND	604	522	15.4	ND	633	1221	ND	30.0	23.4	1165	26.5	9.03	1.42
130-806C-																	
61X-4, 140–150	765.10	ND	ND	ND	590	519	14.3	ND	708	1347	ND	31.5	20.5	1191	24.2	9.08	1.33

Notes: LD = concentration lower than detection limit, and ND = not determined.

Site 806 below 300 mbsf are higher than those at Site 805, which in turn were higher than those at Sites 803 and 804.

Alkalinity increases from 3.7 mM at 4.5 mbsf to a broad maximum (>6 mM) from 107.5 to 280.0 mbsf; it then decreases with depth to 3.1 mM at 679.9 mbsf (Fig. 28). Site 806 has a deeper and broader alkalinity maximum with higher concentrations than Sites 803, 804, and 805, suggesting a larger supply of organic matter for oxidation at this fairly shallow site, the closest to the equator of those drilled on the Ontong Java Plateau.

Sulfate concentrations decrease by almost 50% from 27.2 mM at 4.5 mbsf to 14.3 mM at 765.1 mbsf; most of the decrease occurs by 221.5 mbsf, where the concentration is 17.4 mM (Fig. 28). The sulfate depletion at this site is nearly a factor of 2 larger than at Sites 803 and 805 and larger still than that at the deepest site (804), consistent with the patterns of the alkalinity profiles for these sites.

Phosphate concentrations are 2–3 μM in the upper 31.5 mbsf, with concentrations at greater depths below the detection limit of 1–2 μM (Table 5).

Ammonia concentrations increase to a broad maximum >610 μM by 392.3 mbsf, persisting at these levels throughout the depth range sampled (Fig. 28). These concentrations are twice those at Site 805, which are in turn higher than those at Sites 803 and 804.

Measurable phosphate concentrations in the shallowest samples, higher ammonia concentrations, higher alkalinities, and greater sulfate depletion all suggest a greater supply of organic matter to the sediments at Site 806, which is then oxidized downcore.

Dissolved silica concentrations increase with depth to 1200 μM or greater by 623.8 mbsf (Fig. 28) . The depth profile, both in shape and concentration, is similar to those at Sites 803, 804, and 805. No decreases in dissolved Si are seen, but there are only sparse occurrences of porcellanite below 240 mbsf (see "Lithostratigraphy" section, this chapter).

Dissolved manganese concentrations are generally below the detection limit of 2–3 μM, with the exception of samples in the depth range from 4.5 to 31.5 mbsf. The higher dissolved manganese concentrations are consistent with the reduction of manganese oxides during organic matter oxidation shallow in the core. There is no increase in dissolved Mn with the dissolved Si increase, perhaps because of the organic-carbon-poor nature of the sediments (Gieskes, 1981).

Calcium concentrations increase with depth, with an average gradient of 2.7 mM/100 m (Fig. 28), smaller than those observed at Sites 803, 804, and 805. Magnesium concentrations decrease with depth, with an overall gradient of −4.2 mM/100 m (Fig. 28), similar to gradients observed at Sites 803, 804, and 805. Although the Ca and Mg concentrations are linearly correlated overall ($R^2 = 0.96$), with a $\Delta Ca/\Delta Mg$ ratio approximately equal to −0.7, there is clear evidence in a plot of this relationship for nonconservative behavior of Mg in the upper 136 m. The extent of Mg depletion relative to Ca increase in that depth range is greater than expected from a strictly linear correlation, indicating that there must be an additional sink for Mg in the shallowest sediments, such as dispersed volcanic ash (McDuff and Gieskes, 1976). Nonconservative Mg behavior was also observed in the upper section of Site 289 on the Ontong Java Plateau (Leg 30), though not at Site 288 (Elderfield et al., 1982). The correlation of Mg and Ca below 136 mbsf is linear ($R^2 = 0.99$) with a $\Delta Ca/\Delta Mg$ ratio approximately equal to −0.9.

Strontium concentrations increase with depth to >1000 μM by 164.5 mbsf and to maximum values of >1100 μM by 364.7 mbsf, persisting to the deepest sample (Fig. 28). The maximum concentrations here are higher than at Sites 803, 804, and 805, where sediments accumulate more slowly.

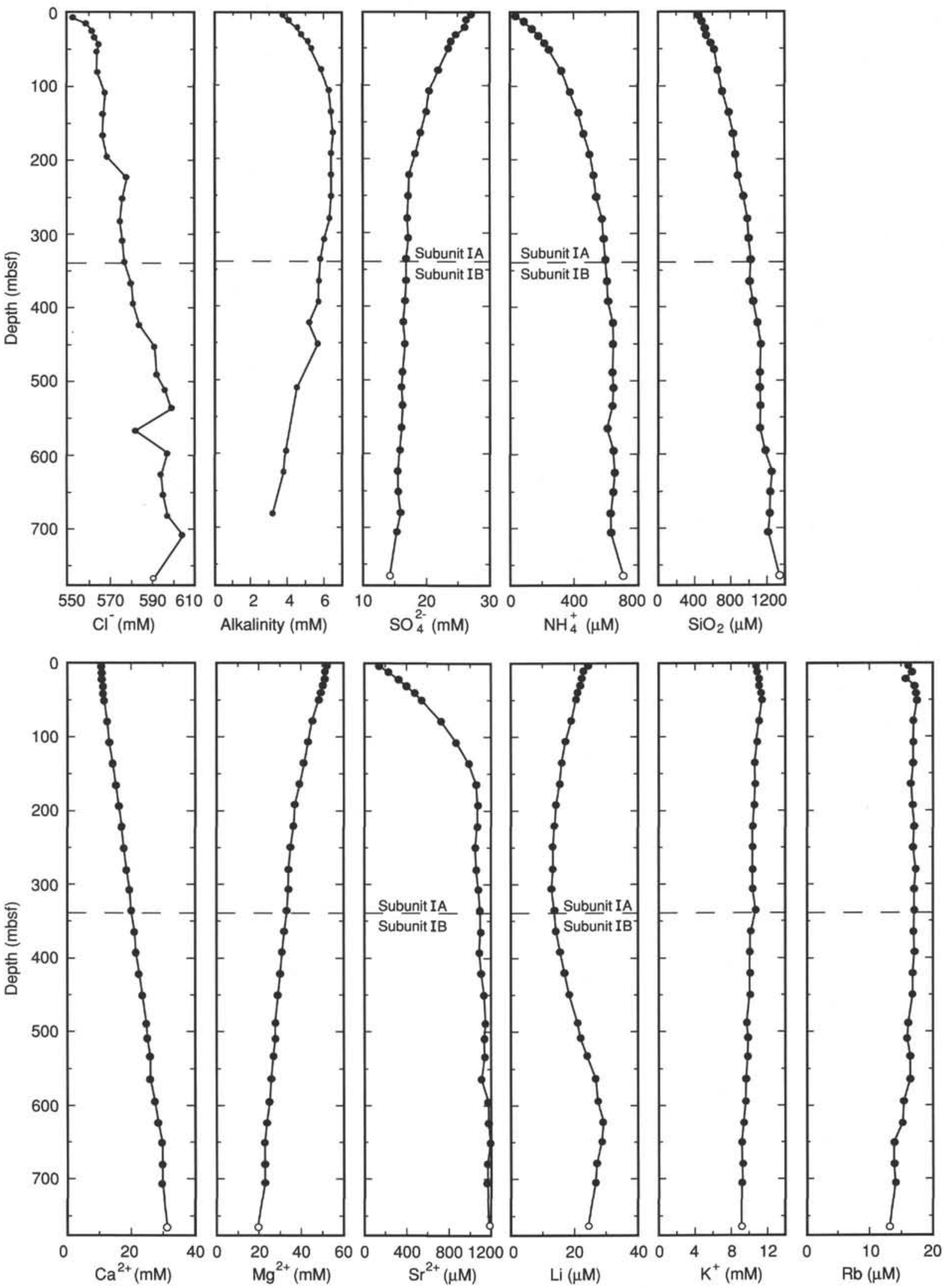

Figure 28. Interstitial water geochemical data, Site 806. Filled circles = Hole 806B and open circle = Hole 806C. The depth at the base of the plots is that of the deepest sediment drilled.

Lithium concentrations decrease from 24.5 μM at 4.5 mbsf to a broad minimum of <15 μM from 193.0 to 364.7 mbsf; values then increase to 24–29 μM from 564.4 to 765.1 mbsf (Fig. 28). The Li minimum at this site has lower concentrations persisting to somewhat greater depths than those at Sites 803, 804, and 805.

Potassium concentrations decrease with depth from 10.8 mM at 4.5 mbsf to values around 9.0–9.1 mM from 650.9 to 765.1 mbsf (Fig. 28) and correlate well with the increase in Ca (R^2 = 0.93). Rubidium concentrations also decrease with depth from 1.6 μM at 4.5 mbsf to 1.3 μM at 765.1 mbsf (Fig. 28). The K and Rb decreases with depth are smaller than those observed at Sites 803, 804, and 805. The differences between Site 806 and the first three sites drilled in the magnitudes of Ca increases with depth and K and Rb decreases with depth suggest that there must be differences in the history of basalt alteration at Site 806 compared with the others.

CARBON GEOCHEMISTRY

The shipboard carbon geochemical analyses included determinations of inorganic carbon (342 samples), total carbon (50 samples), and volatile hydrocarbons (43 samples). A detailed description of the analytical methods used is given in the "Explanatory Notes" chapter (this volume) and by Emeis and Kvenvolden (1986). Volatile hydrocarbons were routinely monitored every third core. The samples were taken using the headspace-technique and were measured for the occurrence of methane, ethane, and propane. As at the previous Leg 130 sites, no significant amounts of these gases were detected.

Inorganic carbon (IC) analyses were conducted on physical properties samples. Percent $CaCO_3$ was calculated as IC · 8.334, assuming that all carbonate is calcite. The results are summarized in Table 6 and presented in Figure 7. The sediments at Site 806 contain very high amounts of $CaCO_3$, with values ranging from 85% to 97%. The range and variation of the values is much lower when compared with previous sites on Leg 130. Carbonate contents increase downhole from 85% to 95% over the interval from 0 to 250 mbsf, similar to the trend seen at all of the previous Leg 130 sites. In the lower part of the section (250–740 mbsf), $CaCO_3$ values average 92%. Table 6 is on microfiche in back pocket.

Total organic carbon (TOC) was calculated as the difference between total carbon (TC) values (as determined by means of the Carlo Erba NCS Analyzer) and inorganic carbon. The downhole distribution of total organic carbon in the sediments of Site 806 is characterized by very low values ranging between 0.02% and 0.6%. Most of the shipboard organic carbon data are near the detection limit of the analytical methods used. They will have to be verified by independent shore-based analyses.

PHYSICAL PROPERTIES

Introduction

At a depth of 2520 mbsl, Site 806 is the shallowest of the four sites devoted to the Neogene transect of the Ontong Java Plateau. GRAPE and *P*-wave velocity (using the multisensor track), and thermal conductivity measurements were made on whole rounds from all cores at Site 806. Physical property measurements were made on split cores from Holes 806B and 806C (cores from Hole 806A were not split on board the ship). These measurements included undrained shear strength, index properties (wet-bulk density, porosity, grain density, water content), and *P*-wave velocity.

The intensive physical properties program conducted on Leg 130 concentrated on making closely spaced laboratory measurements and afforded little time for processing data. Problems caused by improper needle calibration led to a significant scatter in the thermal conductivity data at Site 806. Correction of these thermal conductivity values will be attempted on shore. GRAPE and *P*-wave logger (PWL) data were recorded in the three holes at Site 806, but only a few intervals of the GRAPE data set were processed on board. No comparison of the GRAPE data with index properties is attempted in this chapter. The entire GRAPE and PWL data set also will be processed on shore.

Shear Strength

Undrained shear strength was typically measured at a sampling interval of one per split section in Holes 806B and 806C, using a motorized minivane apparatus (see "Explanatory Notes" chapter, this volume). Between 0 and approximately 200 mbsf, measurements were performed by inserting the vane in the soft sediment. Below 200 mbsf, shear strength was measured in undisturbed coherent blocks of sediment (or "biscuits") interspersed within the softer ooze matrix. Measurements were made until the sediment became too stiff (at approximately 315 mbsf in Hole 806B and 310 mbsf in Hole 806C).

Residual shear strength data were obtained at points where cracking did not dominate the sediment failure (see discussion of vane shear strength data interpretation in the "Physical Properties" section, "Site 803" chapter, this volume). Shear strength results are presented in Table 7, and Figure 29 shows a plot of the variations of shear strength with depth. Table 7 is on microfiche in backpocket.

Shear strength measured at Site 806 ranges from 5 to 25 kPa. Profiles from the two holes are similar; some minor differences, however, are possibly a result of coring-induced disturbance (see detailed discussion of disturbance effects on shear strength in the "Physical Properties" section, "Site 803" chapter, this volume).

Between 0 and 200 mbsf, shear strength values generally range between 5 and 15 kPa. Below 200 mbsf, the constant increase in shear strength reflects the progressive induration of the sediment. High-amplitude, low-frequency shear strength fluctuations (wavelength of around 40–60 m) and high-amplitude, high-frequency fluctuations (wavelength of around a few meters to 10 m) are superimposed on the general trend described above. Below 200 mbsf, the low-frequency fluctuations in shear strength data decrease in amplitude. High-frequency fluctuations, however, begin to dominate the record and may be the result of interspersed layers of different induration states. Some

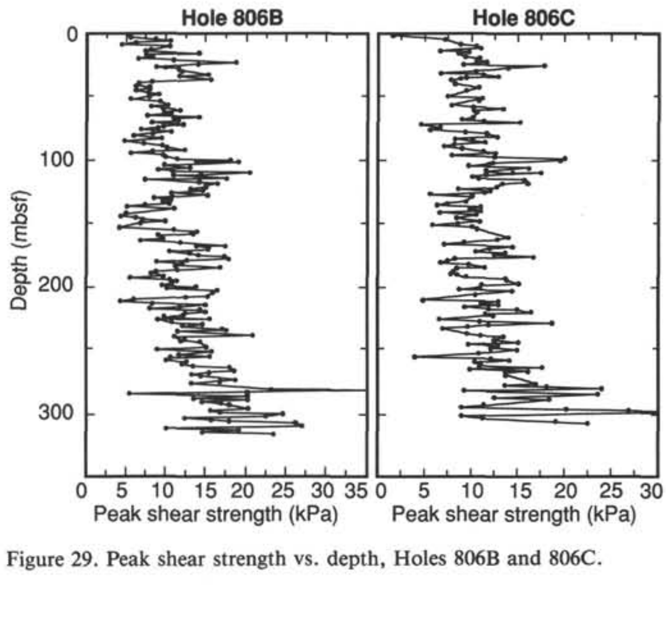

Figure 29. Peak shear strength vs. depth, Holes 806B and 806C.

of the lower values are probably caused by internal cracking in the stiffer intervals.

Index Properties

In Hole 806B, the sampling frequency for index property measurements in soft sediments was two samples per section until Core 130-806B-15H (139 mbsf), and one sample per section in the deeper cores. The sampling frequency in Hole 806C was generally one sample per section in APC cores and less frequently in the chalk interval. Index property samples were always taken at the same locations as the velocity measurements. Intervals showing evidence of "flow-in" or any other coring disturbance were not sampled (usually, the top of Section 1 in many cores). Results of index property measurements are presented in Table 8. Figures 30 through 33 show the downhole profiles of wet-bulk density, porosity, water content and grain density in each hole; superimposed on Figure 34 are the merged porosity curve for Site 806 (Holes 806B and 806C) and a generalized porosity curve for calcareous sediments (Hamilton, 1976). Table 8 is on microfiche in back pocket.

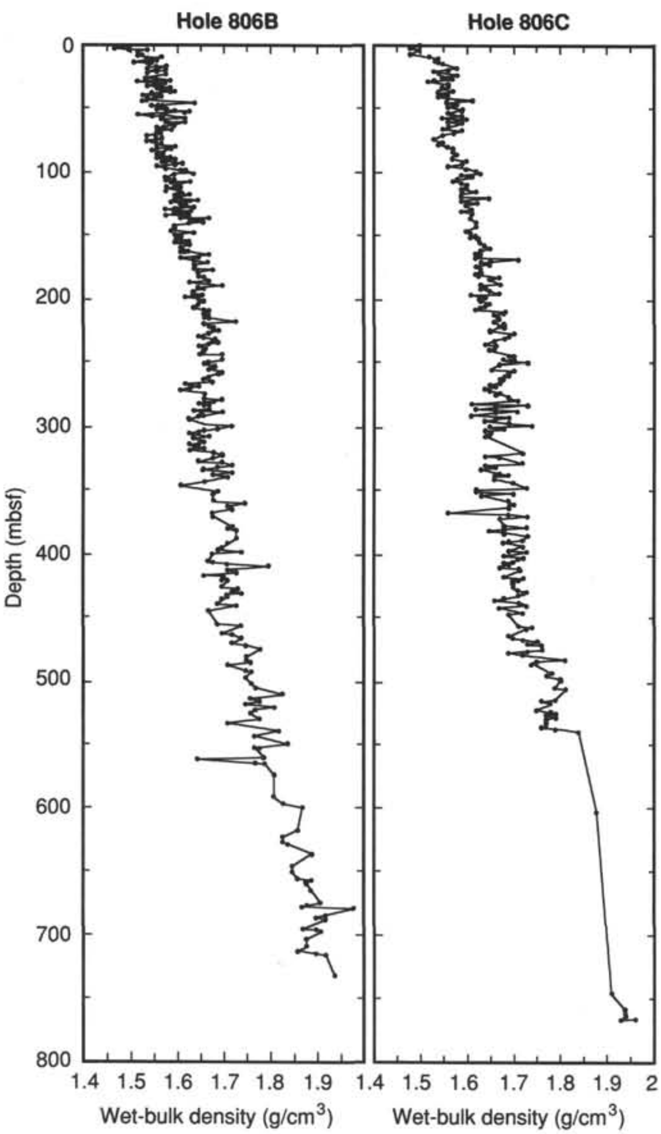

Figure 30. Wet-bulk density vs. depth, Holes 806B and 806C.

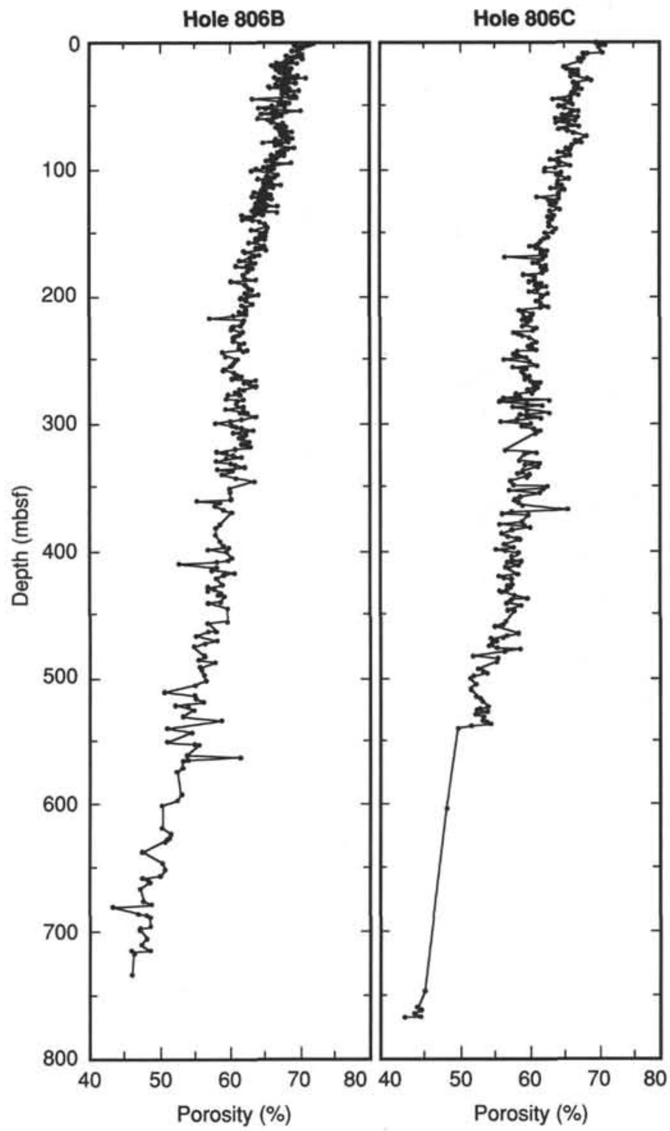

Figure 31. Porosity vs. depth, Holes 806B and 806C.

Wet-bulk density values at Site 806 range from 1.47 to 1.97 g/cm^3, generally increasing with depth. This increase is not linear but shows several changes in the gradient. Porosity and water content have similar trends with depth but are inverted from that of wet-bulk density. The grain density is generally near 2.7 g/cm^3, reflecting the high carbonate content of the sediments cored at Site 806 (around 85%–95%).

In the uppermost 60 mbsf of the sediment column, consolidation effects lead to a rapid change in index properties. Over this interval, porosity decreases from 72% at the mud line to ~66% at 60 mbsf (water content decreases from 100% to 75% and wet-bulk density increases from 1.47 to 1.58 g/cm^3). The trend of the porosity-depth curve in this interval is similar to the generalized curve of Hamilton (1976) for calcareous sediments (Fig. 34).

At about 60 mbsf, a small step in the index property curves (a decrease in bulk density and an increase in porosity) marks the beginning of an important divergence from the general trend of the Hamilton curve. Between 60 and ~240 mbsf, consolidation effects on the index properties were still observed but with diminished amplitude. Compared to the Hamilton curve, the re-

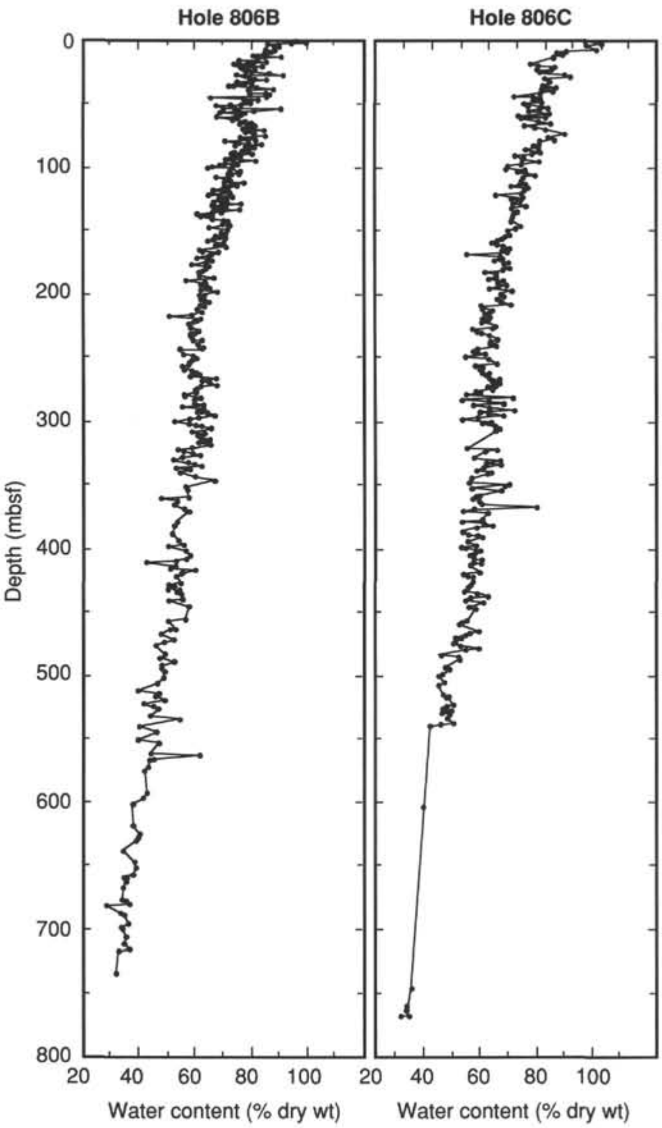

Figure 32. Water content vs. depth, Holes 806B and 806C.

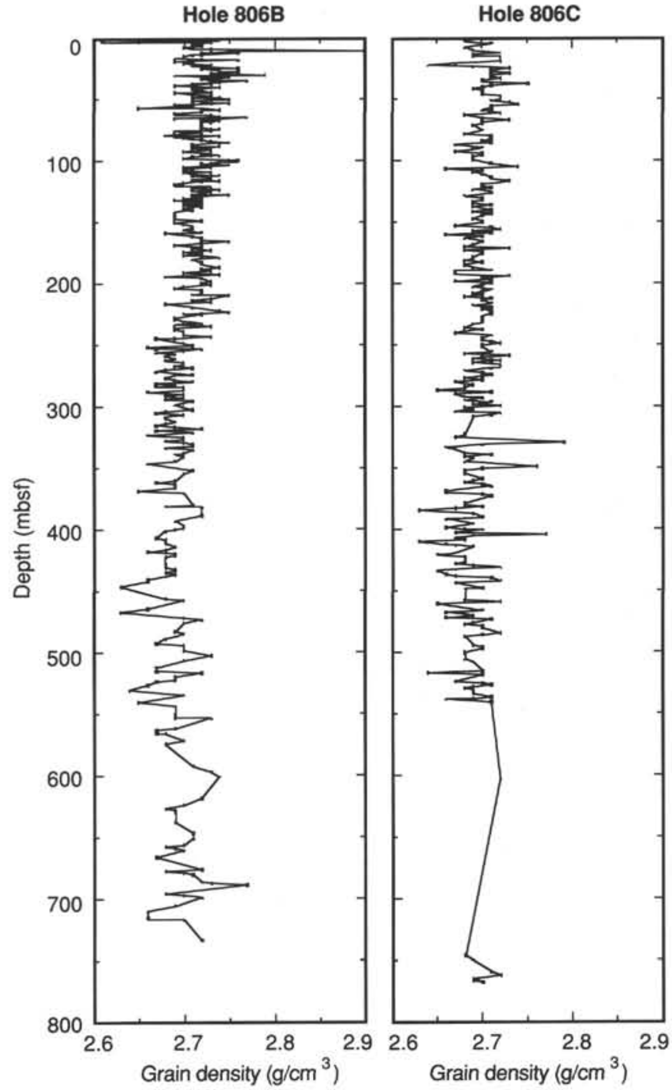

Figure 33. Grain density vs. depth, Holes 806B and 806C.

duction of porosity with depth at Site 806 is low (Fig. 34). At 240 mbsf, the porosity at Site 806 reaches 61% and is, therefore, 10% higher than the porosity value in the Hamilton curve. An increase of sediment rigidity because of early cementation may explain the small reduction of porosity in this depth interval. The low shear strength values measured in this interval do not, however, support this argument. Another possible explanation for this low gradient in the porosity-depth curve is the fact that the sediment is richer in foraminifers at Site 806 than at the previous Leg 130 sites (see "Lithostratigraphy" section, this chapter).

An important contribution to the porosity measured at Site 806 may come from intraparticle porosity (foraminifer chambers). Between 0 and 60 mbsf, consolidation effects led to a rapid reduction of the interparticle porosity. At about 60 mbsf, the sediment may become grain supported and thus further interparticle porosity reduction below 60 mbsf would be less important. Intraparticle porosity in foraminifer tests is not reduced by mechanical compaction; total porosity is, therefore, unaffected by compaction until breakdown of foraminifer tests occurs or test are filled by remobilized calcite.

The interval between 240 and ~440 mbsf shows little reduction of porosity and water content and little increase in wet-bulk density with depth (Figs. 30 through 32). The first occurrence of "biscuits" interspersed in soft ooze was observed slightly above the beginning of this interval (around 200 mbsf) and reflects the visible onset of lithification (see "Lithostratigraphy" section, this chapter). The ooze-chalk transition occurs at about 340 mbsf. The small amount of compaction between 240 and 440 mbsf is, therefore, probably a result of the progressive increase of cementation over this interval. Cementation increases the rigidity of the sediment, thereby improving its resistance to compaction.

A slight increase in porosity (decrease in density) was observed between approximately 250 and 320 mbsf (Figs. 30 and 31), which correlates with a major decrease in carbonate content. This trend also was observed in the index property curves at previous Leg 130 sites.

Below 440 mbsf, bulk density increases rapidly with depth. Reduction of porosity because of mechanical compaction is presumably very low, as it was in the previous interval (240–440 mbsf). Thus, the reduction of porosity with depth (and the increase in bulk density) was possibly a result of pore spaces infilling with calcite as the chalk became more indurated.

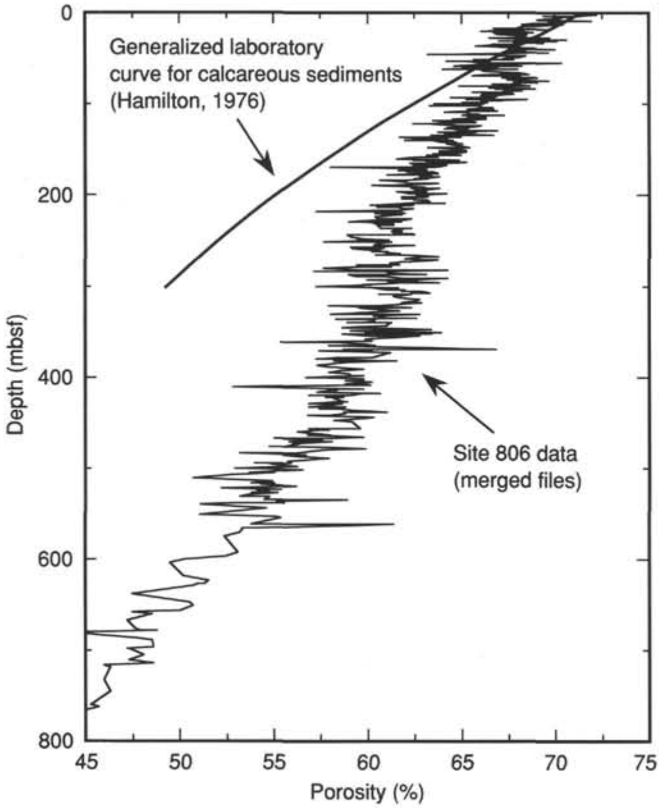

Figure 34. Merged porosity (Holes 806B and 806C) vs. depth for Site 806 and generalized laboratory curve for calcareous sediments (Hamilton, 1976).

High-frequency fluctuations (wavelength of around a few meters to 30 m) are superimposed on the general index property trends described above (Figs. 30 through 32). The study of the origin of major seismic reflectors at Site 806 (see "Seismic Stratigraphy" section, this chapter) shows that these fluctuations in index property values result from a complex interplay of at least three major factors: carbonate content, mean grain size, and sediment induration.

Compressional Wave Velocity

Horizontal (parallel to bedding) and vertical (perpendicular to bedding) *P*-wave velocities were measured on split cores at Site 806. The DSV apparatus was replaced by the Hamilton Frame at 324 mbsf in Hole 806B and at 387 mbsf in Hole 806C. Results of velocity analyses are shown in Table 9 and listed in Figure 35. Figure 36 shows changes with depth of horizontal *P*-wave velocity and mean grain size in the top 350 mbsf at Hole 806B, and Figure 37 shows a smoothed version of these two curves (5-point running average). Table 9 is on microfiche in back pocket.

Velocities measured at Site 806 range from 1530 to about 2400 m/s, generally increasing with depth. In the upper part of the section, however, between 0 and 120 mbsf, velocity actually decreases slightly. In this depth interval, the general trend and the high-amplitude, low-frequency fluctuations of *P*-wave velocities correlate well with changes in mean grain size (Fig. 37). The trend of slightly decreasing velocity corresponds to the progressive decrease in mean grain size over this interval.

Below 120 mbsf, velocity and mean grain size are poorly correlated, with the mean grain size trend showing only minor changes with depth whereas velocity values increase. This increase in the velocity values is presumably caused by consolidation and cementation.

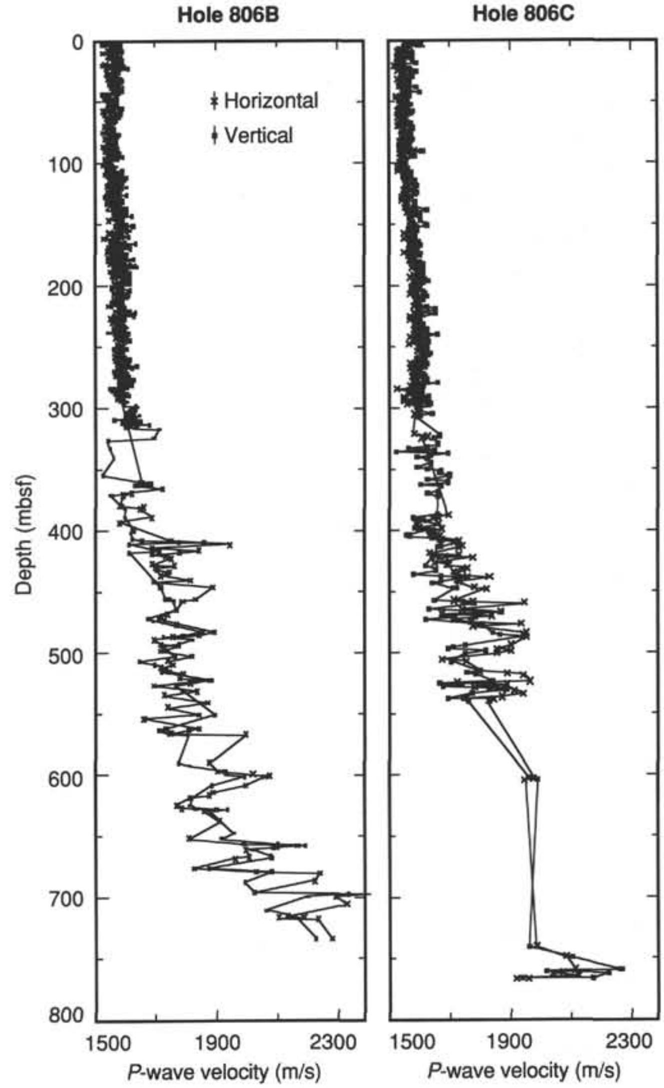

Figure 35. *P*-wave velocity (vertical and horizontal) vs. depth, Holes 806B and 806C.

The gradient of laboratory *P*-wave velocities is weak between 120 and 310 mbsf. It begins to increase rapidly below about 310 mbsf, slightly above the ooze/chalk transition (340 mbsf). Very low velocity values recorded between 320 and 340 mbsf in Hole 806B and at about 390 mbsf in Hole 806C correspond to the first measurements made with the Hamilton Frame and are probably the result of chalk fracturing.

LOGGING

Logging at Site 806 followed the same protocol as at Site 805 and achieved similar results (Tables 10 and 11). The first tool string was the Leg 130 geophysical string consisting of an NGT (natural gamma-ray), LSS (long spaced sonic), and DITE (electrical resistivity) combination. Logging data were collected from the base of the hole (741 mbsf) to pipe (90.2 mbsf; Table 10). All data on this run are of good quality.

The next tool string consisted of the NGT (natural gamma-ray), ACT (aluminum clay tool), HLDT (lithodensity tool), GST (geochemical spectral tool), and TLT (temperature) combination. After reaching the bottom of the hole at 741 mbsf and beginning this logging run, the GST would not calibrate properly. The tool string was lowered back to the bottom of the hole, recalibrated, and the logging run started from 740 mbsf with all

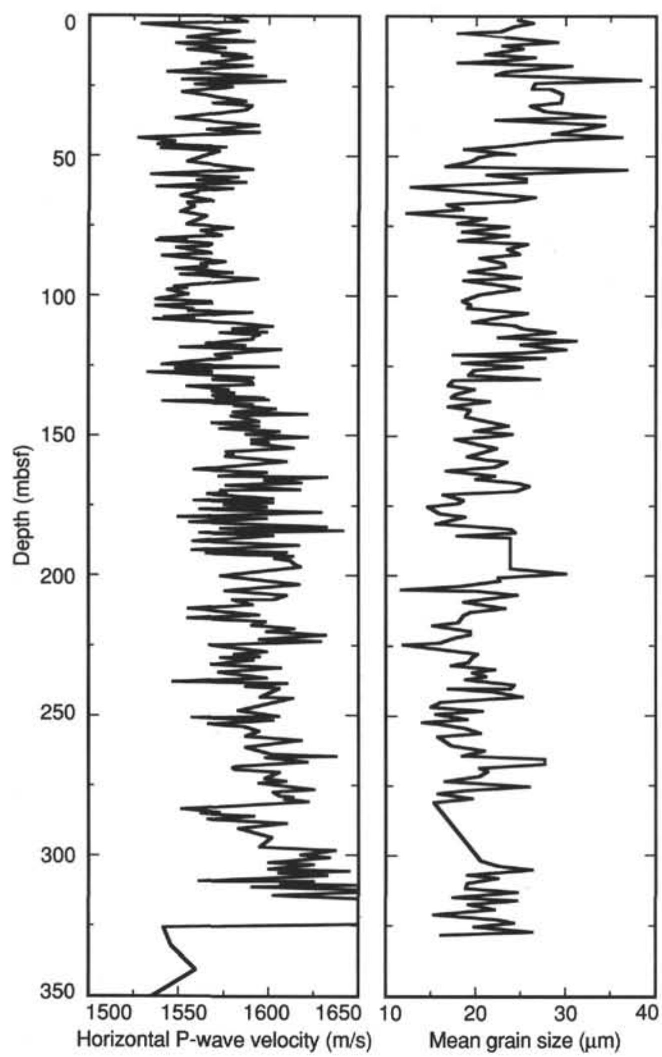

Figure 36. Horizontal *P*-wave velocity and mean grain size vs. depth, Hole 806B.

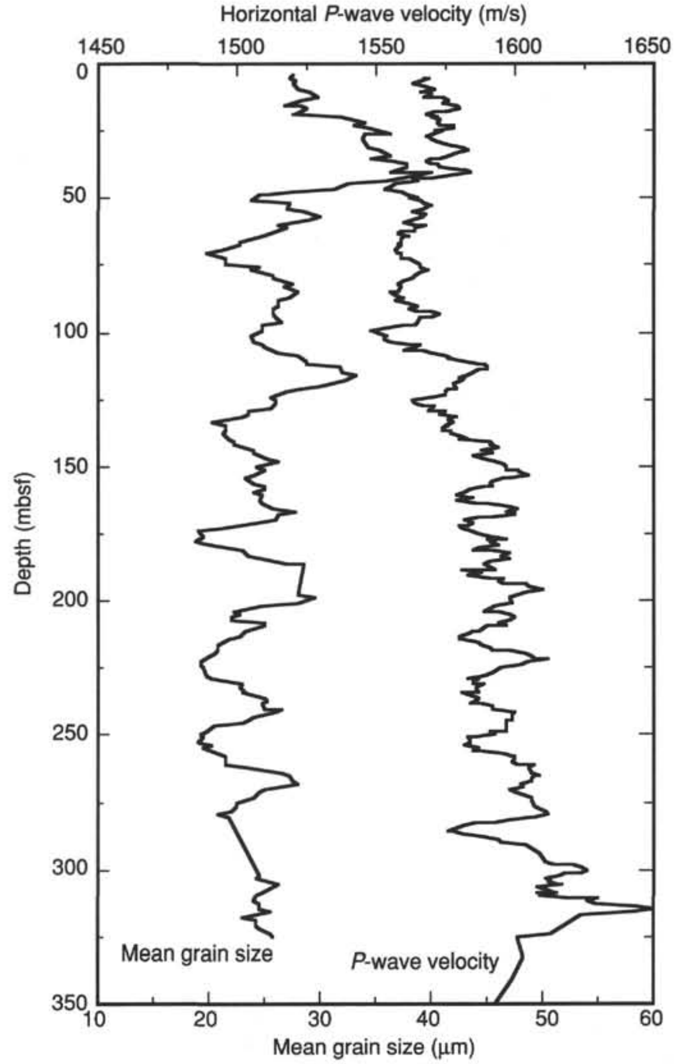

Figure 37. Smoothed curves (5-point running average) of horizontal *P*-wave velocity and mean grain size vs. depth, Hole 806B.

tools functioning. Because the formation was activated by the GST on the first (aborted) pass, the NGT and ACT logs of the bottom 38 m (741–703 mbsf) are suspect. The decay of unstable nuclei created by the high neutron flux from the GST produced gamma radiation that was measured by these two tools.

Logging proceeded smoothly until about 485 mbsf, where the GST again began to show poor resolution. By 442 mbsf, resolution was sufficiently bad to require the loggers to stop logging operations. The tool string was lowered back down to 496 mbsf and an attempt was made to recalibrate the GST. The GST would not function properly after 30 min of recalibration effort, so the GST was shut down and logging continued upward with the other tools. The tool string entered pipe at 88.4 mbsf.

The GST, when checked in pipe, appeared to function. For this reason, the tool string was lowered to repeat the section not logged with the GST. The tool string was lowered to 334 mbsf, but after an additional 15 min of recalibration the GST still malfunctioned. The tool string was raised to 244 mbsf for a repeat logging section (without the GST) of the NGT/ACT/HLDT/TLT from 244 to 121 m without the heave compensator as swells were low. Apparently, the caliper on the HLDT jammed into the wall of the hole on a down swell and broke off at about 160 mbsf during this final run.

Because of GST failures, the geochemical logs of Hole 806B are not continuous and are pieced together in sections. Spikes in the natural gamma activity logs and the aluminum logs may be present because of GST-induced hot spots in the hole. Nevertheless, the NGT and ACT logs are of good quality for the most part. The density log suffers from one major dropout between 290 and 320 mbsf and from suspect intervals between 290 and 180 mbsf. On the repeat section, the density log data is useless above 160 mbsf, the point at which the caliper broke off.

Log Stratigraphic Units

The stratigraphic column recovered at Site 806 is nannofossil ooze with foraminifers, grading into chalk at about 320 mbsf. We recognized three logging units, similar to the top three units at Site 805 (Fig. 38 and Site 805, Figs. 30–32).

Logging Unit A

Unit A (90–340 mbsf) is marked by low resistivity values that remain at about 0.8 ohmm throughout the interval. Wet-bulk density values increase downcore only slightly, from 1.6 to 1.7 g/cm^3. A comparison of log and laboratory density reveals unreliable logging data from 190 to 320 mbsf (Fig. 49, "Seismic

Table 10. Logging operations, Hole 806B.

Local day	Local time	Cumulative hours	[a]Depth (mbsf)	
2/21/90	22:30			Last core on deck
2/22/90	7:50	0.0		RIH with geophysical tool string (NGT/DIT/LSS)
2/22/90	8:53	1.0	96.3	Out of pipe; start downlog to base of hole
2/22/90	9:37	1.8	741.0	On bottom of hole, <2 m fill
2/22/90	9:38	1.8	741.0	Main log pass; NGT/DIT/LSS all working; up at 900 ft/hr; heave compensator not on
2/22/90	12:11	4.3	71.9	Tool in pipe at 90.2 mbsf (600 ft), end up log at 71.9 mbsf
2/22/90	12:11	4.3		Run down for repeat section
2/22/90	12:20	4.5	212.1	Start up on repeat section; NGT/DIT/LSS all working; 900 ft/hr
2/22/90	12:46	4.9	71.9	Tool in pipe at 90.2 mbsf (8,600 ft); POOH
2/22/90	13:50	6.0		Tool string on deck
2/22/90	14:52	7.0		RIH with geochemical tool string (NGT/ACT/HLDT/GST/TLT)
2/22/90	16:15	8.4	740.1	At bottom of hole; heave compensator on; start log up, 600 ft/hr
2/22/90	16:31	8.7	702.9	Trouble with GST; stop up log at 10,610 fbrf; this section neutroned
2/22/90	16:46	8.9	740.7	Dropped back to this depth; got GST started, HLDT caliper closed
2/22/90	16:57	9.1	716.9	HLDT caliper fully open, all logs good
2/22/90	18:28	10.6	486.5	GST starts to lose resolution
2/22/90	18:37	10.8	442.9	Stop up log, go back down to 9,960 fbrf (504.4 mbsf)
2/22/90	19:09	11.3	495.6	Start up log; GST would not recalibrate, not functioning
2/22/90	21:24	13.6	88.4	Enter pipe; end repeat geochemical string
2/22/90	21:27	13.6	82.3	Stop in pipe for recalibration; some response
2/22/90	22:03	14.2	334.1	Run back in hole to try to GST started; no luck, run back up for repeat
2/22/90	22:03	14.2	244.1	Repeat up log (NGT/ACT/HLDT/TLT) GST not functioning; heave compensator sticky, not turned on
2/22/90	23:05	15.2	120.7	End repeat section; POOH
2/23/90	0:00	16.2		Geochemical string at wellhead
2/23/90	1:15	17.4		Rigged down from logging runs

[a] Based on a seafloor depth of 2531 mbrf.

Table 11. Acronyms used in text describing logging at Hole 806B.

Acronym	Definition or meaning
ACT	Aluminum clay tool
API units	American Petroleum Institute standard units for gamma-ray activity calibrated to test pit in Houston, TX
BHC	Borehole compensated sonic tool
DIT	Phasor dual induction tool
fbrf	Feet below rig floor
FMS	Formation microscanner
GST	Geochemical spectral tool
HLDT	High-temperature lithodensity tool
LSS	Long-spaced sonic digital tool
mbrf	Meters below rig floor
mbsf	Meters below seafloor
NGT	Natural gamma tool
POOH	Pull out of hole
RIH	Run into hole
SDT	Long-spaced sonic digital tool
TLT	LDGO temperature logging tool

Stratigraphy" section, this chapter). Most of the large-amplitude variations observed in the HLDT density data between 190 and 320 mbsf are suspect.

Natural gamma-ray activity decreases throughout the entire interval of Unit A, indicative of increasing calcite contents with depth. To a certain extent, a similar pattern was observed for aluminum. As in Hole 805C, however, the Al trend stops before that of the natural gamma-ray activity, at about 280 mbsf. The lowermost part of the unit between 300 and 320 mbsf has some of the highest Al values.

Velocities in Unit A increase from just above 1.6 km/s at 90 mbsf to about 1.95 km/s at the base of this unit. Superimposed upon this linear velocity change are high-frequency (10–20 m period) velocity variations of about 0.1 km/s. These high-frequency variations may, in part, be artifacts resulting from hole-width variations or coring (see below). The transition between Units A and B also has a section of very high-frequency velocity variations between 320 and 340 mbsf. A few porcellanite nodules were the only recovered material in this interval in Hole 806C. In Hole 806B, which was logged, a single porcellanite nodule was found in a full core of chalk. We speculate that the high-frequency velocity variations are indicative of one or more chert-rich horizons at this depth.

Logging Unit B

Unit B (340–600 mbsf) is characterized by gradients in all physical properties and flat chemical logs. Resistivity values increase from 0.8 to 1.1 ohmm and have larger amplitude fluctuations than in Unit A. The velocity gradient also is greater in this unit. In the lower portion of the unit, between 460 and 600 mbsf, small-amplitude, low-frequency (30–40 m period) variations were observed. The density gradient increases somewhat from Units A to B, and the density log is marked by low-frequency variations. In the lower part of Unit B, between 500 and 600 m, the low-frequency density and velocity variations are inversely correlated. However, there is no correlation between the two data sets over the entire unit, except for the compaction-imposed linear increase of both density and velocity with depth.

Logging Unit C

Unit C (600–720 mbsf) is marked by a decrease in resistivity, velocity, and density gradients with depth and by high-amplitude, low-frequency (30–40 m period) variations in density and resistivity. The chemical logs show little distinction between logging Units B and C. Unit C, in Hole 806B, resembles logging Unit C in Hole 805C and may represent a common depositional lithology. The Unit B-C transition, located at 380 mbsf in Hole 805C, marks the level of a condensed section between 17 and 20 Ma (see "Sedimentation Rates" section, "Site 805" chapter, this

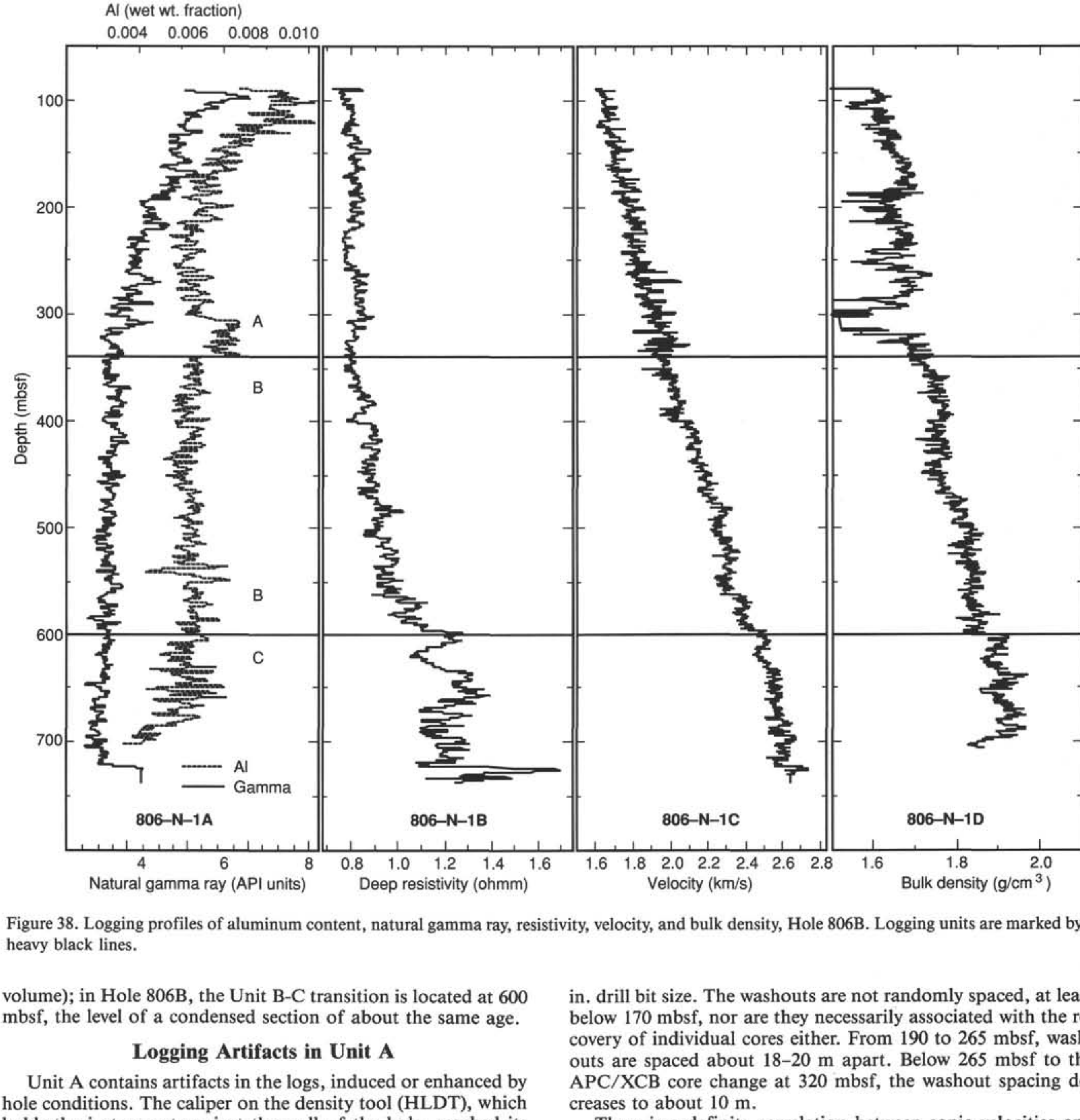

Figure 38. Logging profiles of aluminum content, natural gamma ray, resistivity, velocity, and bulk density, Hole 806B. Logging units are marked by heavy black lines.

volume); in Hole 806B, the Unit B-C transition is located at 600 mbsf, the level of a condensed section of about the same age.

Logging Artifacts in Unit A

Unit A contains artifacts in the logs, induced or enhanced by hole conditions. The caliper on the density tool (HLDT), which holds the instrument against the wall of the hole, reached its maximum extension of 18 in. at depths above 350 mbsf, and gave little information about the size of the upper part of the hole. The separate travel paths from the long-spaced sonic tool, however, gave information about hole width in the upper part of Hole 806B (Fig. 39). The LSS has three different source-receiver spacings: 8, 10, and 12 ft. Thus, at any point in the hole we can perform a small refraction experiment. If the sound velocity for fluid in the borehole is known, the distance to the wall of the borehole can be solved. Assuming that Hole 806B was filled with seawater, the hole width varied as shown in Figure 39.

The mechanical and sonic calipers give similar information qualitatively, although there is some offset between the two. Above 320 mbsf the hole has washed out more than the $11^{3}/_{4}$-in. drill bit size. The washouts are not randomly spaced, at least below 170 mbsf, nor are they necessarily associated with the recovery of individual cores either. From 190 to 265 mbsf, washouts are spaced about 18–20 m apart. Below 265 mbsf to the APC/XCB core change at 320 mbsf, the washout spacing decreases to about 10 m.

There is a definite correlation between sonic velocities and hole width (Fig. 40), based upon a comparison between the sonic caliper and the upper part of the sonic log. A narrow hole is correlated with higher velocities. This in itself is not necessarily an artifact, since better indurated horizons should have higher sound velocities than neighboring units and, because of their competence, should be less prone to washout. There is a definite 9.5-m periodicity in the velocity record over the interval from 100 to 340 mbsf that does not correlate with the washouts except below 250 mbsf. The largest amplitudes occur when the washouts also have about a 10-m spacing. This is best illustrated in Figure 41, in which the core breaks are marked by the verticals of a square wave. At each core break, we can recognize a couplet of high- and low-velocity spikes. In most cases, the

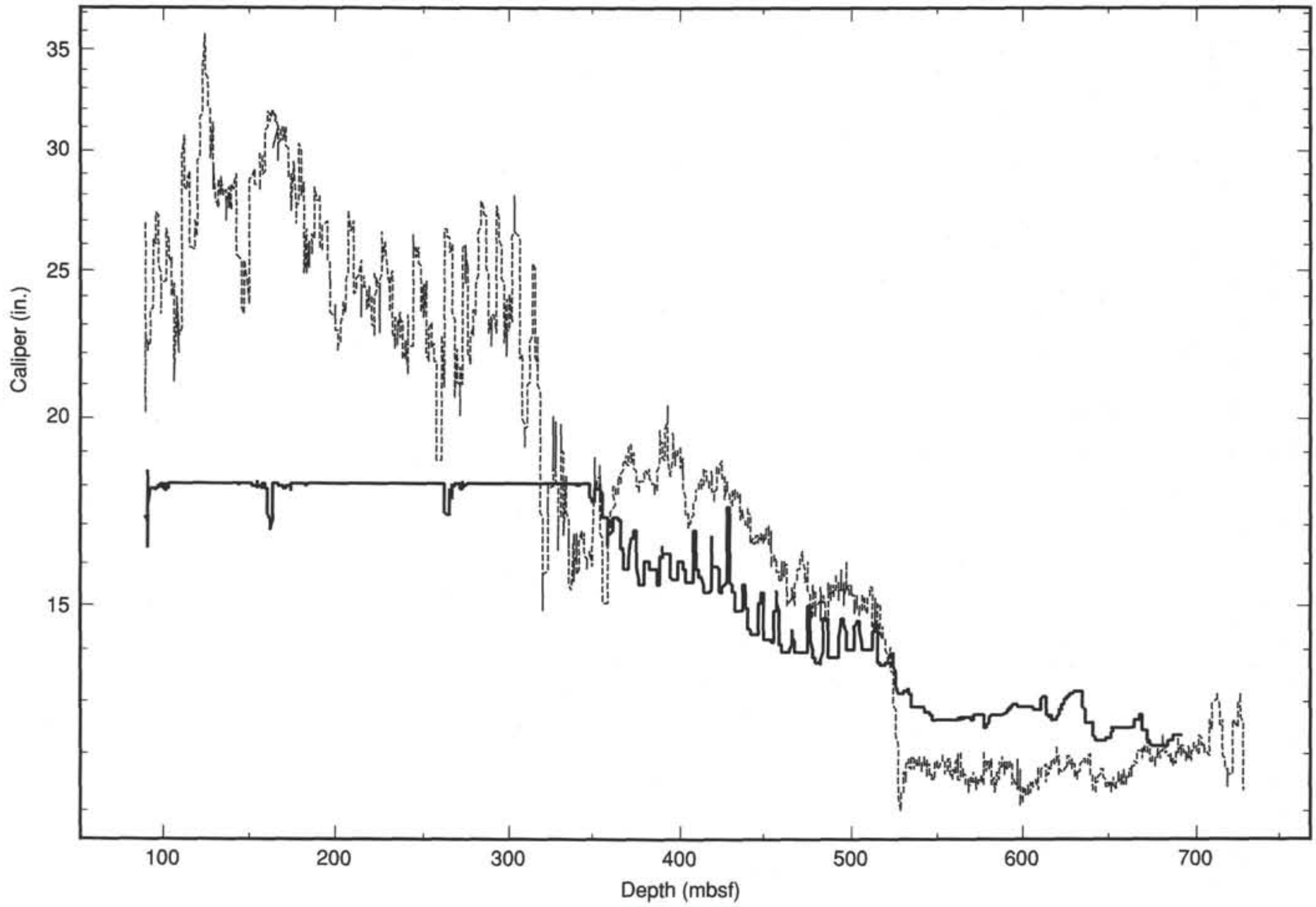

Figure 39. HLDT hole width measured by caliper (solid line) compared with hole width inferred from the sonic velocity log (dashed line) (see text), Hole 806B. The HLDT caliper has a maximum extension of 18 in. All information about hole width in the upper portion of the hole must be based upon the sonic velocity measurements.

high-velocity spike is most prominent. The 9.5-m couplets most probably are coring artifacts, as they are precisely the length of the APC.

The strong density artifacts in Unit A are probably the hole width. The HLDT can only get accurate density readings when positioned near the core wall. Figure 38 shows a large dropout that occurred between 290 and 320 mbsf. Above this interval, between 180 and 290 mbsf, comparison with lab data shows that the logging data are invalid (see "Seismic Stratigraphy" section, this chapter).

Chemical Logging at Site 806

In addition to the ACT aluminum data and the natural gamma-ray activity data already described, a geochemical spectral tool (GST) log was obtained over the interval from 445 to 735 mbsf. This represents a time interval from about 12.4 to 25.5 Ma. As at Site 805, only Ca and Si are present in sufficient abundance in the solid phases for the data to be considered reliable. Figure 42 shows the GST counts of Ca normalized to the total Ca + Si counts, an indicator of calcite abundance in the sediments. Two main features are apparent from the logging data: (1) a trend to higher calcite toward the base of the hole and (2) abundant high-frequency variations of calcite throughout the interval.

By simple inspection (Fig. 43), it appears that much of this high-frequency variation may occur at the 100-k.y. Milankovitch period. Figure 43 incorporates a 100-k.y. signal based upon sedimentation rates from Table 11 (see "Sedimentation Rates" section, this chapter). The large-amplitude signal in this part of the record appears to occur at this periodicity. Spectral analysis techniques provide an objective approach to examine the periodicity, as shown in Figure 44. In this case, we have used only eight nannofossil datum levels to establish a time scale for Hole 806B. Despite the crude time scale, 100-k.y. periodicity is apparent in the 13-m.y. long record. Weak, but significant, power occurs near the 41-k.y. Milankovitch period. Strong power also occurs at 313, 209, 84, 68, and 49.5 k.y. Some of these periodicities may be resonant periods of the climate system amplifying harmonics of the orbital periods. All or part of them could be artifacts introduced by the crude time scale, however.

Correlation Between Sites 586, 805, and 806

Comparison of Sites 586 and 806

Site 586 (0°29.84′S, 158°29.89′E, 2208 m water depth; Shipboard Scientific Party, 1986a, 1986b) and Site 806 (0°19.11′N, 159°21.69′E, 2521 m water depth) are both located on the top of the Ontong Java Plateau, on opposite sides of the equator but within 75 nmi of each other. The two sites should have highly similar records. Figure 45 is a comparison of the two velocity profiles. A simple linear stretch of the Site 586 depth axis with respect to depth in Site 806 has been used for the comparison. Note also that the velocity axes have been offset so that the two records could lie side by side. From the excellent correlation of the two records, one can infer that the two sites had the same depositional history over the entire common interval, essentially

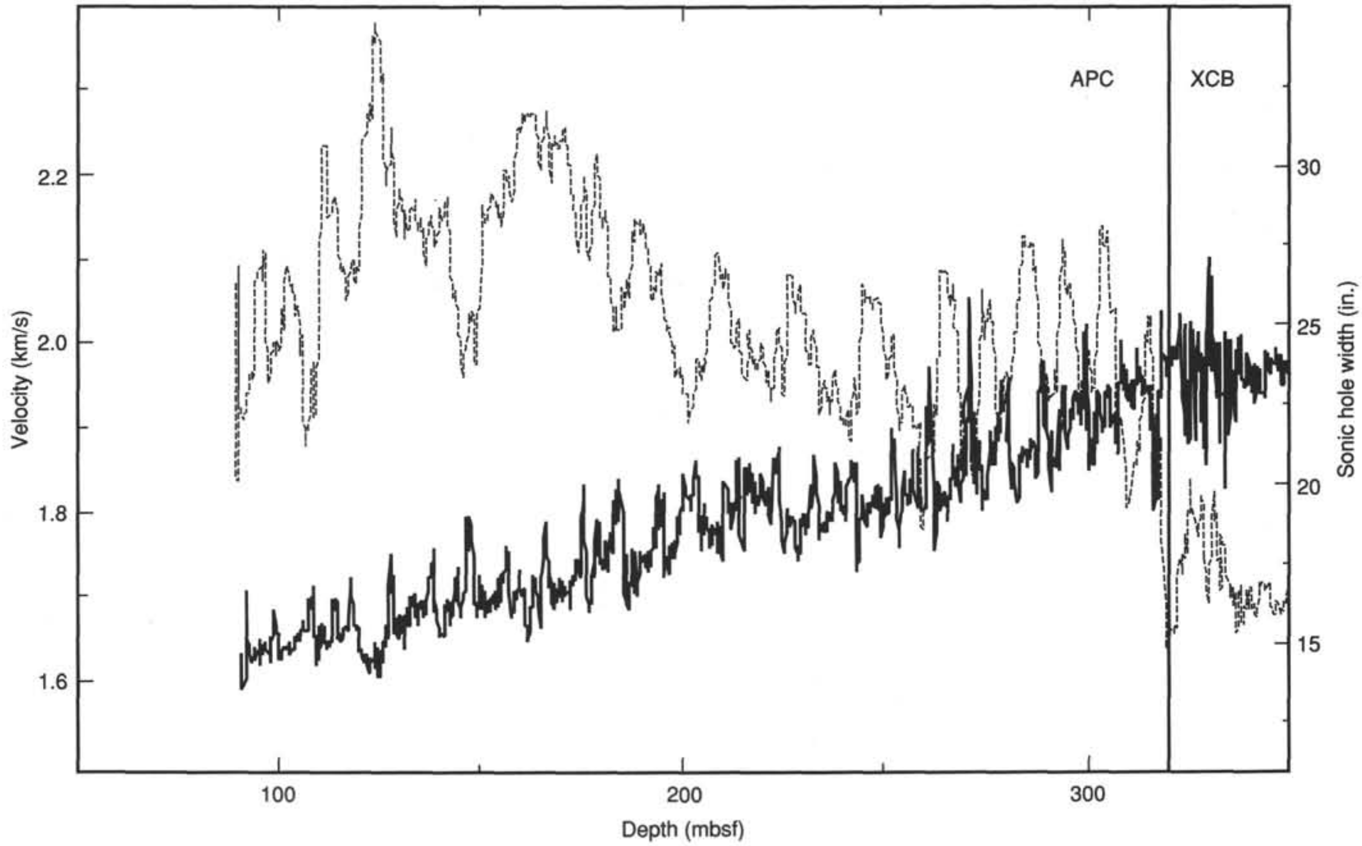

Figure 40. Comparison of velocity profile (solid line) to sonic hole width (dashed line) from the same logging data, Hole 806B. A narrow hole is generally correlated with fast sonic velocities. Coring artifacts, with a 9.5-m spacing, can also be seen.

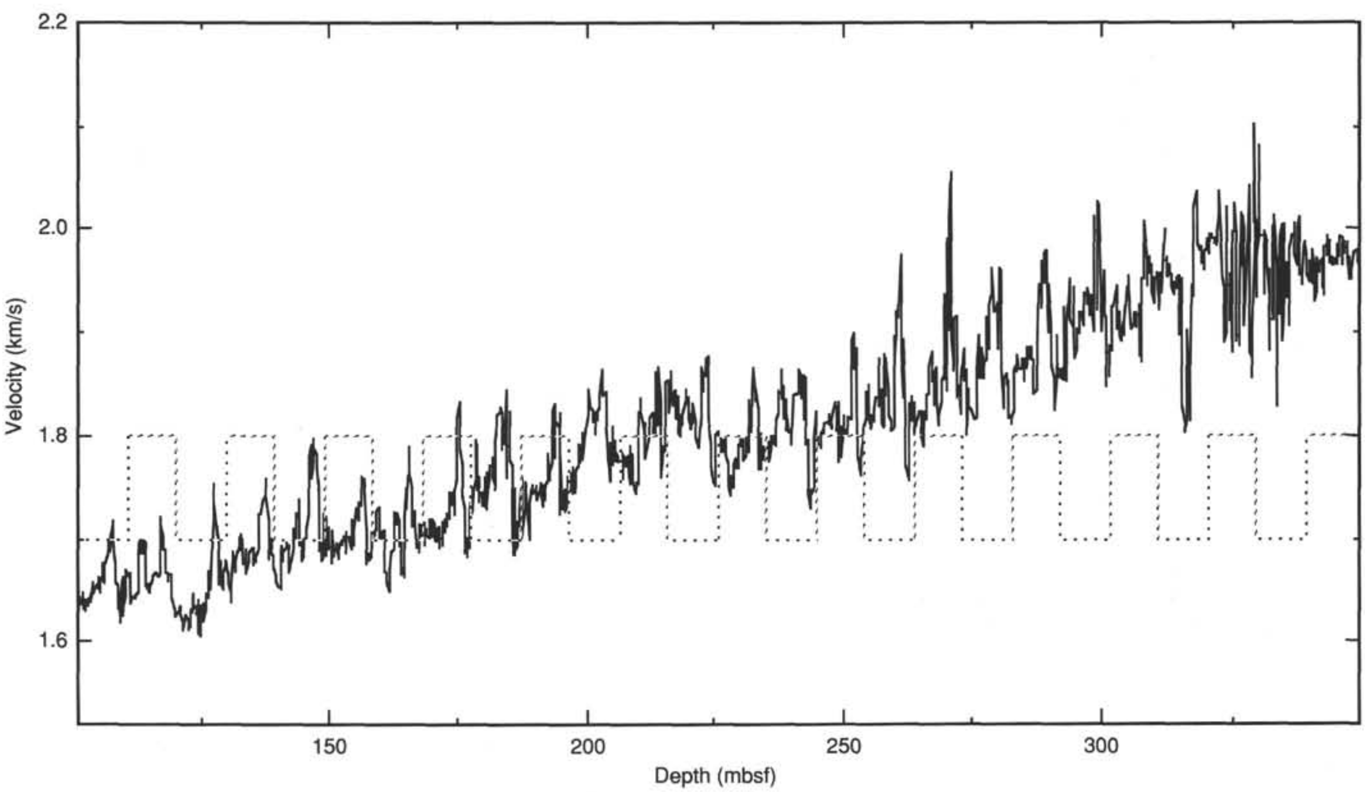

Figure 41. Velocity profile from Hole 806B compared with core breaks in the hole. Core breaks are marked by vertical lines of the square wave. Note that a couplet of high- and low-velocity spikes are consistently associated with the core breaks.

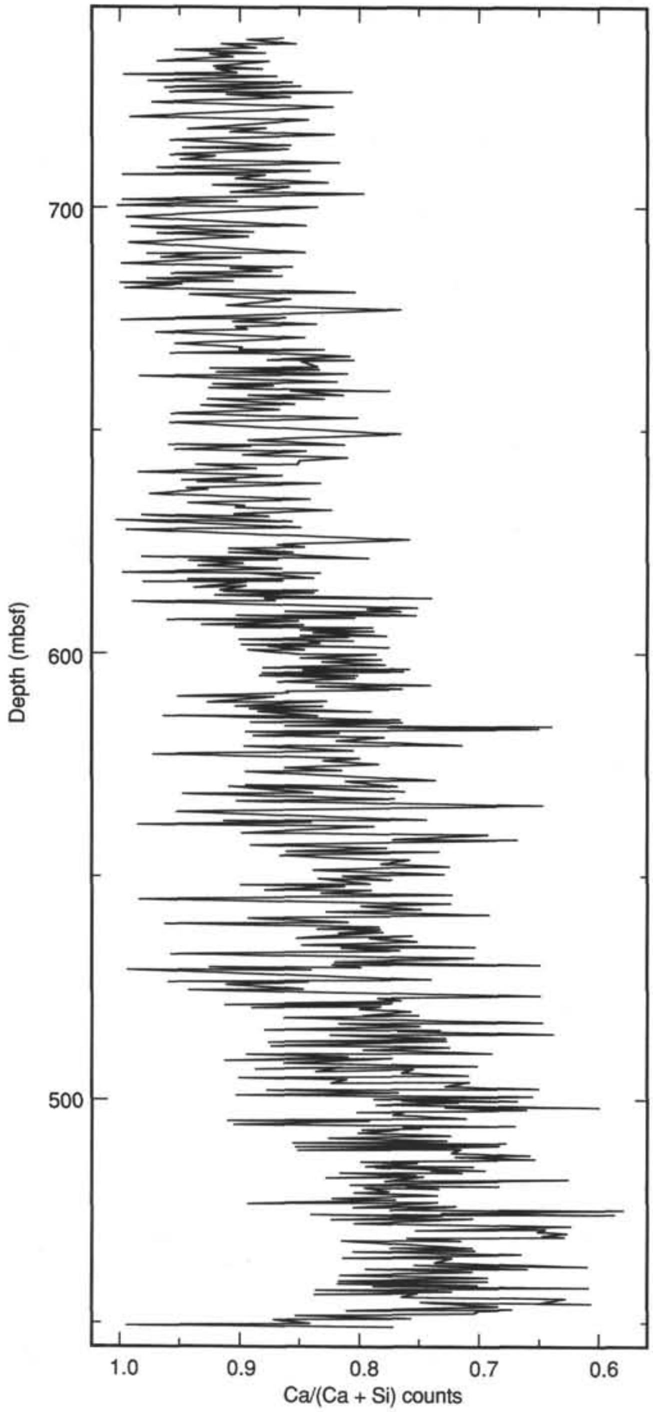

Figure 42. GST record of calcium variations, Hole 806B. The data are presented as Ca/(Ca + Si) counts to normalize borehole effects in the shipboard-processed data. There is a trend throughout the interval toward higher calcium in older sediments. In addition, there are abundant large-amplitude, high-frequency variations.

all of the Miocene. This observation argues against local winnowing events at either site. Instead, any resuspension or other sediment loss must be regional in scale.

Site 586 does have lower sedimentation rates than Site 806 for the entire logged interval, consistent with their positions relative to the equator. Assuming an absolute latitudinal motion for the Ontong Java Plateau of about 0.25°/m.y. northward during the Neogene (R. Musgrave, pers. comm.) Site 806 was located about 1°S, and Site 586 was located about 2°S when the sediments at the top of the logged interval were being deposited. The difference in sediment deposition at the two sites may in part reflect the sedimentation rate gradient away from the equator. Expansion and contraction of the equatorial high-productivity zone during the Miocene may eventually be discerned from detailed correlations of these two sites.

Even though velocity data from Holes 586C and 806C were offset for clarity in Figure 45, they converge at depth. The two records apparently have different velocity gradients. This is an artifact of the presentation in the figure, however. Common depths have similar velocities at either site. Thus, the two sites have similar compaction trends, which are mostly a result of burial depth. Superimposed upon the compaction trend are the variations in the physical properties caused by changes in sedimentation. These variations, which have paleoceanographic significance, will be easy to separate from the diagenetic information.

Comparison of Sites 805 and 806

Correlation of Sites 805 and 806 should yield important insights about dissolution gradients in the Miocene. Dissolution- and sedimentation-induced differences between Sites 805 and 806 make the correlation more difficult than for the sites on top of the Ontong Java Plateau, however. The correlation will be dependent upon stratigraphic ties and age control provided by micropaleontological studies. This should pose little problem, as the two sites have two of the best Neogene micropaleontological records ever recovered in ODP (see "Biostratigraphy" section, this chapter and Site 805 chapter).

The comparisons between Site 805 and 806 velocity and density, respectively, are illustrated in Figures 46 and 47. Both figures are drawn assuming that Site 806 averages a factor of 1.44 higher sedimentation rate than Site 805. An examination of either figure indicates that there have been many relative changes in sedimentation rate between the sites. Mesoscale features, such as the small 30–40-m wavelength velocity variations in the interval from 420 to 640 mbsf in Hole 806B and from 300 to 440 mbsf in Hole 805C will provide a means to refine the correlation and look for higher frequency ties between the records.

SEISMIC STRATIGRAPHY

The seismic section at Site 806, the shallowest of the Ontong Java Plateau depth transect sites, is characterized by a thick sequence of parallel, closely spaced reflectors that mirror the gently sloping seafloor and basement topography (Fig. 48). The section shows little evidence of disturbance or mass wasting, and individual reflectors can be traced continuously to Sites 289/586 (Shipboard Scientific Party, 1975b, 1986a), 139 km west and 400 m shallower than Site 806. The section at Site 806 is only slightly thinner than those at Sites 289/586, and its thickness exceeds that at Site 805 by a factor of 1.35. Between Sites 289/586 and 806, the minor thinning that was observed occurs in the deep (pre-Oligocene) part of the section; between Sites 806 and 805 the thinning takes place throughout the section, with the possible exception of the Oligocene (see Mayer et al., this volume).

As at the previous sites, we have used the results of laboratory and logging measurements to convert seismic traveltime to depth-in-section, and we have employed seismic modeling to check on the accuracy of this traveltime-to-depth conversion. Site 806 laboratory measurements of velocity and density were made approximately every 75 cm (see "Physical Properties" section, this chapter), and velocity and density logs (15-cm sample interval, 60-cm sensor spacing) were run for the section between 100 and 710 mbsf (see "Logging" section, this chapter). Labo-

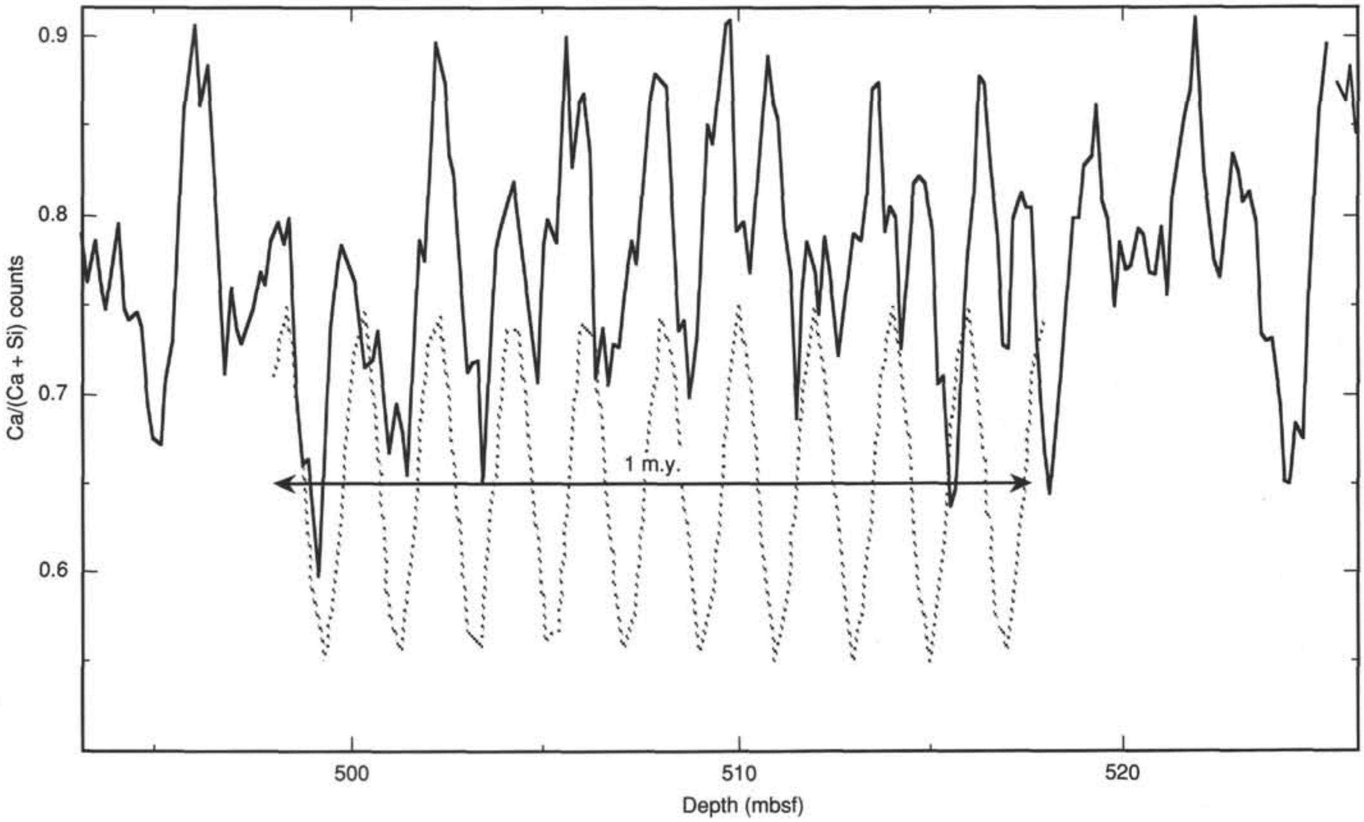

Figure 43. A plot of a small interval of the GST Ca/Ca+ Si (solid line) data (Hole 806B), which shows that much of the variation in calcium occurs at a period of approximately 100 k.y. The dashed line represents a 100-k.y. cycle based on sedimentation rates listed in Table 4.

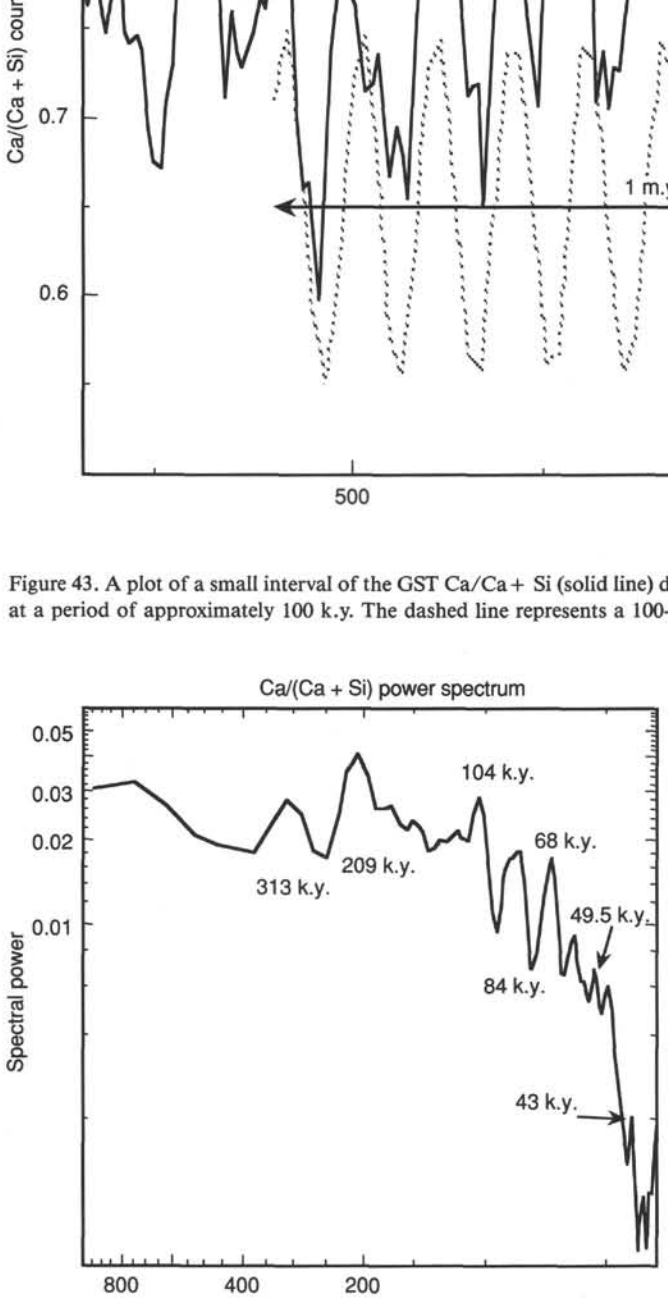

Figure 44. Power spectrum of the GST calcium record interpolated to a 7500-yr sample spacing. The time scale used for the spectral analysis is based upon only eight nannofossil age control points (Table 4). Milankovitch-type periodicity near 41 and 100 k.y. can be found, as well as a large amount of power in lower frequencies.

ratory measurements of velocity and density were converted to *in-situ* values using the methods described in Mayer et al. (1985) and merged with the logging data. A comparison of *in-situ* corrected laboratory data with log data reveals several inconsistencies that must be addressed before the data can be properly merged (Fig. 49).

If we assume that the log-derived velocities and densities represent *in-situ* values, then laboratory measurements, properly corrected to *in situ,* should be the same as the logging values. At the previous sites, the corrected laboratory values have, for the most part, been in good agreement with the logging data, implying that the procedure used to correct laboratory data to *in-situ* values is reasonable. Discrepancies between the laboratory and logging values (e.g., at Site 805 between 140 and 160 mbsf; see "Logging" section, "Site 805" chapter, this volume) have been attributed to poor hole conditions that have degraded the logs in certain intervals.

A comparison of log and laboratory velocity measurements (Fig. 49) reveals that between 100 and 180 mbsf the logging data are also in agreement with the corrected laboratory measurements and below 180 mbsf the two data sets diverge. Deeper than about 180 mbsf, the laboratory velocities are consistently lower than the logged velocities, but we have little confidence in the *in-situ* correction process at these depths (once cementation begins). A detailed look at several indicators of borehole conditions reveals that there are changes in the borehole behavior at 180 and 340 mbsf (see "Logging" section, this chapter). A full understanding of the effect of these borehole changes will have to await further study.

Comparing the logs from Site 806 with the laboratory data reveals that between 100 and 180 mbsf the corrected density values are in good agreement with the logging data; however, below

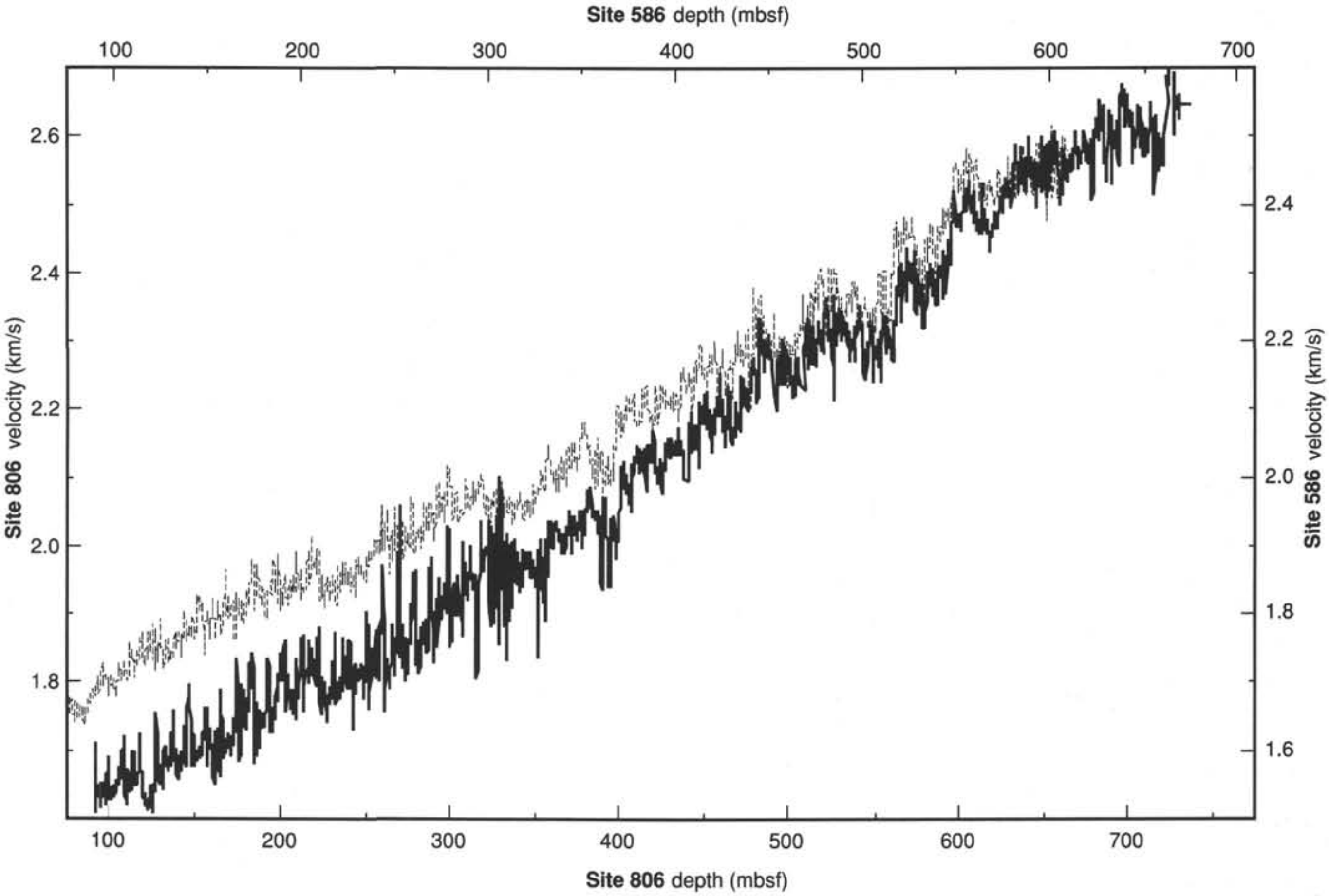

Figure 45. Comparison of velocity profiles, Holes 586C (dashed line) and 806B (solid line). Site 586 is approximately 135 km to the southwest of Site 806. Note that the two sites have separate depth axes so as to eliminate first-order sedimentation rate differences between the two sites. In the figure, the Site 586 velocity data have been offset by 0.1 km/s for clarity.

that depth the logging values are significantly lower than the lab measurements (Fig. 49). Between 280 and 340 mbsf, the logged densities are so low that they are unquestionably in error.

To obtain the best possible data base for the seismic model, we have used laboratory density data from the seafloor to 360 mbsf (and downhole density data deeper than that) and laboratory velocity data from the seafloor to 180 mbsf (and downhole velocity data deeper down). The compromise that we make in doing this is the loss of detailed density sampling provided by logging, particularly in the interval from 200 to 360 mbsf where the laboratory sampling interval was reduced (Fig. 49).

The merged, corrected laboratory and logging data (velocity and density) were used to calculate acoustic impedance (Fig. 50), which was then convolved with a seismic source signature to generate a synthetic seismogram (see "Seismic Stratigraphy" section, "Site 803" chapter, this volume, or Mayer et al., 1985, for details). The synthetic seismogram was compared with the field seismic profile to evaluate the accuracy of the traveltime-to-depth conversion. The field records used for this study are those collected by the *Thomas Washington* (ROUNDABOUT Cruise 11) during the site surveys for Leg 130 (see Mayer et al., this volume).

As at previous sites, we have looked in detail at several representative reflectors within the section. By examining the age and possible origin of these reflectors, we hope to place the seismic record in a stratigraphic framework. The criteria for the selection of these reflectors is simply that they have large amplitudes and are laterally coherent within the immediate area of Site 806. No effort has been made to select reflectors that are regionally correlatable (e.g., see Mayer et al., this volume), although the regional distribution of the named reflector patterns is evident (see "Summary and Conclusions" section, this chapter). As at Site 805, we will refer to the six named reflector series (Panama, Tethys, Antarctic, Drake, Texas, and Ontong Java; see "Seismic Stratigraphy" and "Summary and Conclusions" sections, "Site 805" chapter, this volume) to place the selected reflectors within a regional stratigraphic framework.

The comparison of the synthetic seismogram to the field profile at Site 806 (Fig. 50) produces a reasonable match, though not one that is without ambiguities. In the absence of a clear tie point such as basement or chert (as at Site 803), there are several possible fits of the synthetic record to the field data. We have chosen a fit that maximizes the number of matches, particularly in the deeper part of the section (Fig. 50). We have selected 13 reflectors in the 740 m of logged section; they are labeled on the plot of reflection coefficient vs. traveltime (Fig. 51), and their traveltimes, depths, and ages are listed in Table 12.

The three shallowest reflectors picked (6-1, 6-2, and 6-3) are associated with the "Panama Series" of reflectors. The youngest two (6-1, ca. 1.9–2.0 Ma., and 6-2, ca. 2.4 Ma.) are correlated with large grain size, low carbonate, high velocity, and low density (Figs. 52 and 53), a physical property association that appears to indicate winnowing. Increased currents remove the fine components (which may preferentially remove nannofossils and could reduce the measured carbonate content, depending

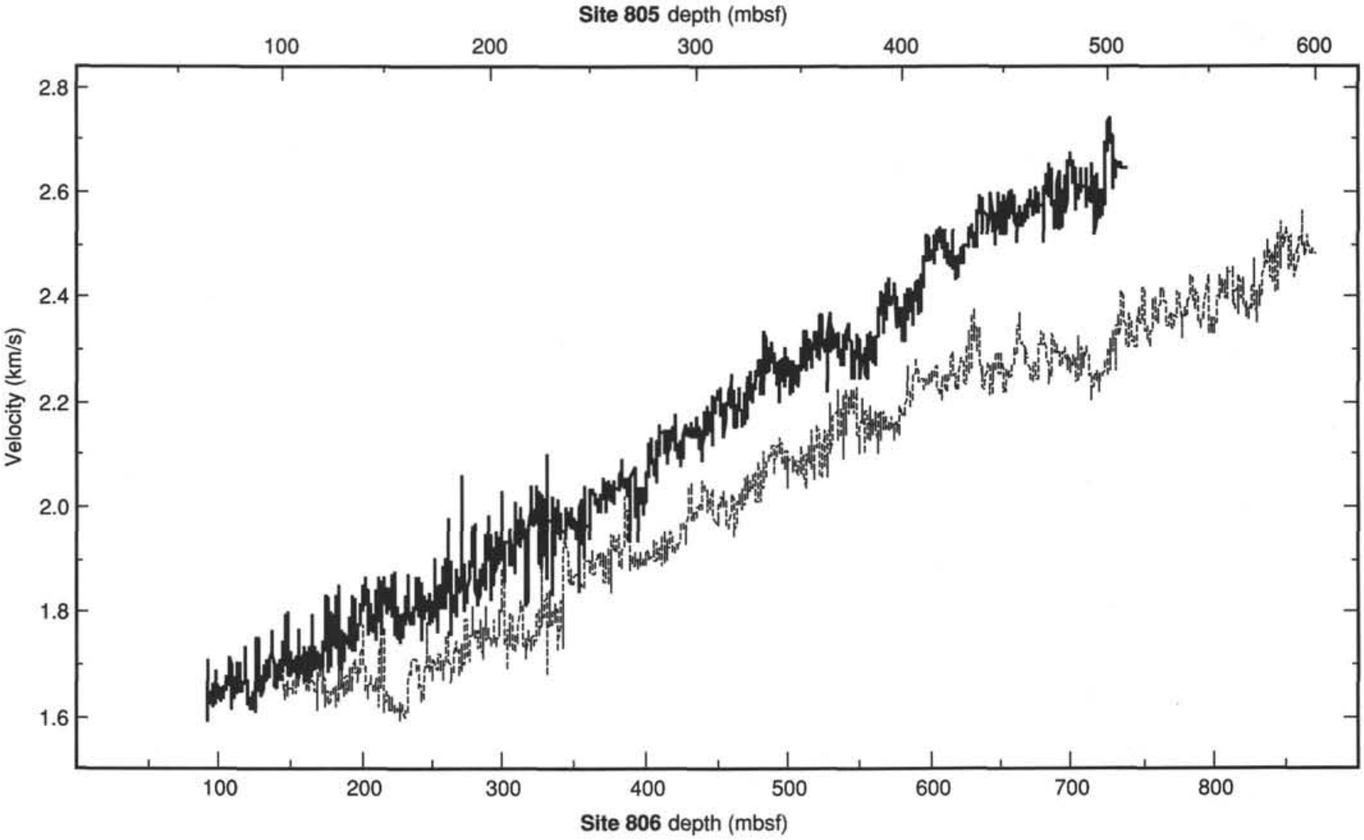

Figure 46. Comparison of velocity profiles, Holes 805C (dashed line) and 806B (solid line). The offset in the data at 220 mbsf in the Hole 805C profile is an artifact of the logging data (see "Seismic Stratigraphy" section, "Site 805" chapter, this volume).

on the composition of the noncarbonate components), resulting in a coarse-grained system that does not pack well (thus, the low density) and yet has a high velocity (because of the large grain size). The third reflector of this group (6-3, ca. 3.8–3.9 Ma) has the same set of physical property relationships except that it is associated with a high carbonate content, which may indicate that it is the result of increased productivity rather than winnowing.

Within the "Tethys Series," six reflectors (6-4 through 6-9) have been picked. The youngest of these (6-4, ca. 5.1 Ma) shows the physical property association that we suggest represents winnowing (high in grain size and velocity with a low in carbonate content and density; Figs. 52 and 53). The next deepest reflector (6-5, ca. 5.8–6 Ma) is the only one associated with a marked low in grain size (and thus velocity); density and carbonate content vary only slightly (Figs. 52 and 53). This interval may represent a period of particularly quiescent current activity. At about the same depth (200 mbsf), there is a marked change in the shape of the velocity vs. depth curve with a sharp increase in velocity (Fig. 52). The rapid increase in velocity with depth is probably indicative of the onset of cementation (induration is first reported by the sedimentologists at about 200 mbsf, see "Lithostratigraphy" section, this chapter).

At about the same level, we also see a change in the slope of the density curve with density increasing at a slower rate below 200 mbsf (Fig. 52). This change in the shape of the density curve may also be indicative of a change from a compaction-dominated system (above 200 mbsf) to one where grain-to-grain contacts and induration begin to support the sediment column, or it may simply be a reflection of the increase in carbonate content with depth (Fig. 53).

Deeper than 200 mbsf, the state of induration begins to play an important role in reflector formation. Reflector 6-6 (265 mbsf, ca. 7.2 Ma) still shows some indication of a grain-size influence (large grain size and high velocity), but at this depth there is also a peak in density, perhaps the result of enhanced cementation. Deeper than 250 mbsf, induration variations become the dominant mechanism for reflector formation. Reflector 6-7 (280 mbsf, ca. 7.5–7.6 Ma) is associated with rapid, in-phase, alternations between high and low velocity, density, and carbonate content. These variations in induration (as shown by the rapid, large-amplitude changes in velocity and density) apparently are a response to fluctuations in carbonate content (and thus more fundamental oceanographic factors such as dissolution and productivity). Reflector 6-8 (320 mbsf, ca. 8.2–8.4 Ma), with its low velocity and density, probably represents the unindurated end member of this system.

All of the deeper reflectors (6-9 through 6-13), which include representatives of the "Antarctic," "Drake," and "Texas" series, are characterized by synchronous, large-amplitude fluctuations in velocity, density, and carbonate content that appear to represent the diagenetic enhancement of an original carbonate signal. Interestingly, the "Texas Interval," which has been characterized by few large-amplitude reflectors at previous sites, shows a number of large-amplitude events here. It is possible that this is a result of the increased thickness of the section here and thus the increased potential for diagenetic enhancement of the original sediment variability.

The logging record at Site 806 ends at approximately 740 mbsf. We can, however, use the results of Site 803 to estimate that the Eocene/Oligocene boundary is at about 120 m below Reflector 6-13, at approximately 0.88 s below seafloor (sbsf).

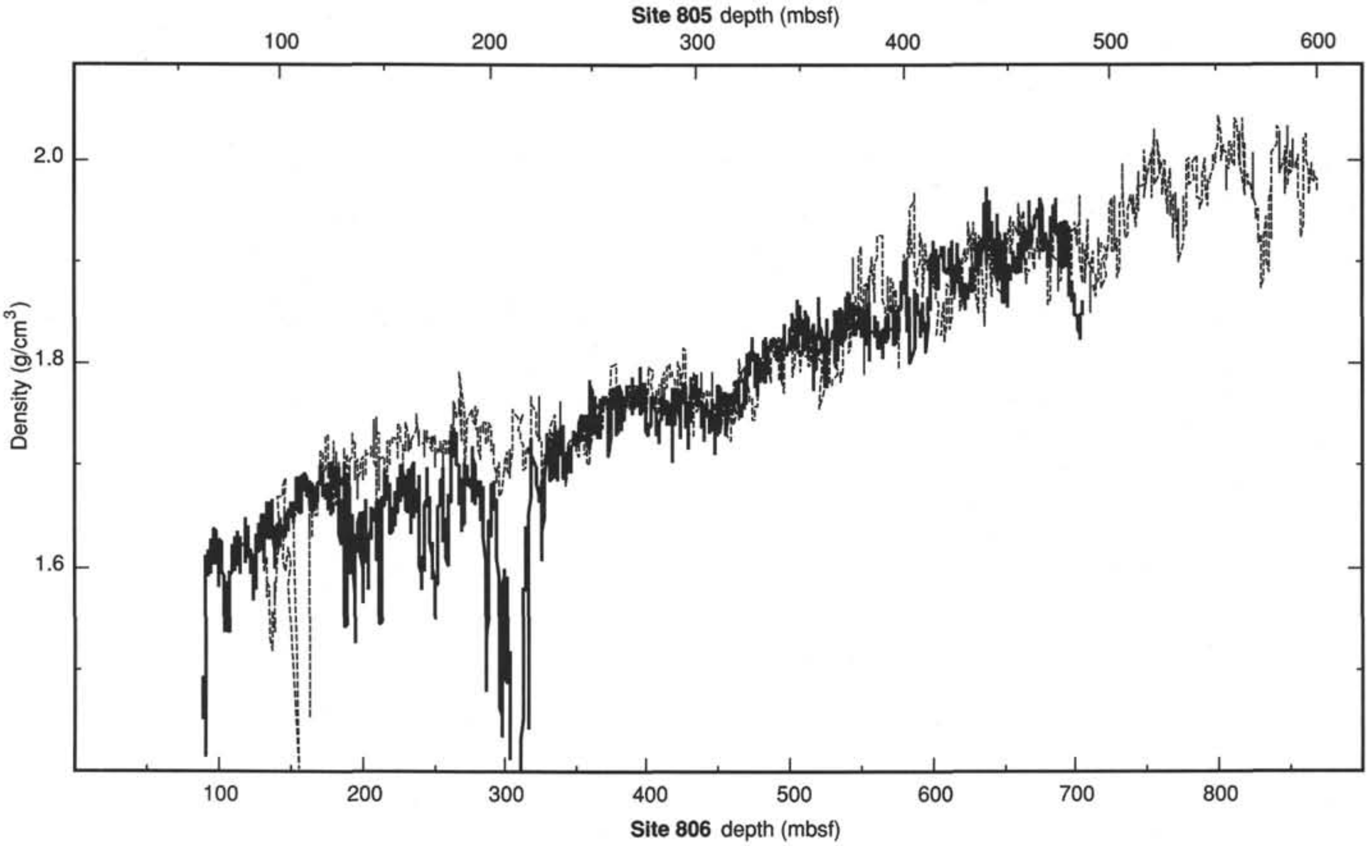

Figure 47. Comparison of wet-bulk density profiles, Holes 805C (dashed line) and 806B (solid line). The overall shape of the two records is similar.

Basement should then be at 1.03 sbsf or approximately 1000 mbsf.

SUMMARY AND CONCLUSIONS

Site 806 is located on the northeastern margin of the Ontong Java Plateau, close to the equator (latitude 0°19.1′N, longitude 159°21.7′E) in 2520 m of water. The site represents the shallow end member on a transect that was designed to detect depth-related paleoceanographic signals in Neogene sediments. The objective in drilling at this location was to obtain a continuous record in an undisturbed setting, with maximum sedimentation rates, that could serve as a standard section against which all others could be measured. The setting was considered ideal for high-resolution studies of ocean history, including biostratigraphy, chemostratigraphy, and acoustic stratigraphy. This expectation proved well founded.

Positioning was based on a SCS line acquired by the *Thomas Washington* during ROUNDABOUT Cruise 11 (0600 UTC, December 21 1989). The site is located at the proposed location (OJP-1) on a 2-km-wide terrace interrupting a gentle incline sloping to the northeast. The sedimentary sequence apparently is complete and undisturbed, with the seismic profile showing a full set of reflectors that are readily correlatable with those at Sites 289/586.

Coring Results

We spent 7.5 days at this site, drilling three holes and coring 1414 m of sediment, of which 1276 m were recovered. Hole 806A, a dedicated hole, was cored with the APC to 83.7 mbsf into upper Pliocene sediments, with 103% recovery. Hole 806B was cored with the APC to 320.0 mbsf, where refusal occurred, within the lower upper Miocene; recovery was 105%. The hole was continued with XCB coring to 743.1 mbsf, with 423.1 m of sediment cored and 331.2 m recovered (78% recovery). Coring was terminated within lowermost Miocene sediments when the objective (recovery of the Neogene section) was judged to have been reached. The hole was then logged, with the pipe pulled to 92 mbsf.

Hole 806C was cored with the APC to 309.6 mbsf (104% recovery), at which point coring with the XCB was initiated. Cores were taken from 309.6 to 541.7 mbsf; from that point, we drilled ahead with a center bit to 599.0 mbsf, where a spot core was taken to obtain sediments from an interval with poor recovery in Hole 806B. A full core was obtained. Drilling was then continued with a center bit to 740 mbsf, at which point four cores were taken (740.0–776.4 mbsf), spanning the Oligocene/Miocene boundary. The XCB-coring operation drilled 278 m and recovered 203 m of sediment (73% recovery) at this hole.

The sediment retrieved is Neogene in age, except for the three deepest cores in Hole 806C, which recovered Oligocene chalk (Cores 130-806C-60X to -62X). The entire column, from the oldest deposits to the seafloor, is considered as one lithologic unit and was classified as foraminifer nannofossil ooze and chalk to nannofossil ooze and chalk with foraminifers. No stratigraphic breaks were detected; apparently depositional history was continuous between the upper Oligocene (ca. 27 Ma) and the present. The average sedimentation rate over the entire Neogene may be estimated as 32 m/m.y, the highest of any site drilled on Leg 130. Depending on assumptions made about the age of biostratigraphic tie points, the range of fluctuation lies between 15 and 55 m/m.y., or between 20 and 45 m/m.y.

Two subunits were recognized in this rather uniform section of bioturbated ooze and chalk, on the basis of degree of consolidation. They are separated by the ooze-chalk transition, placed

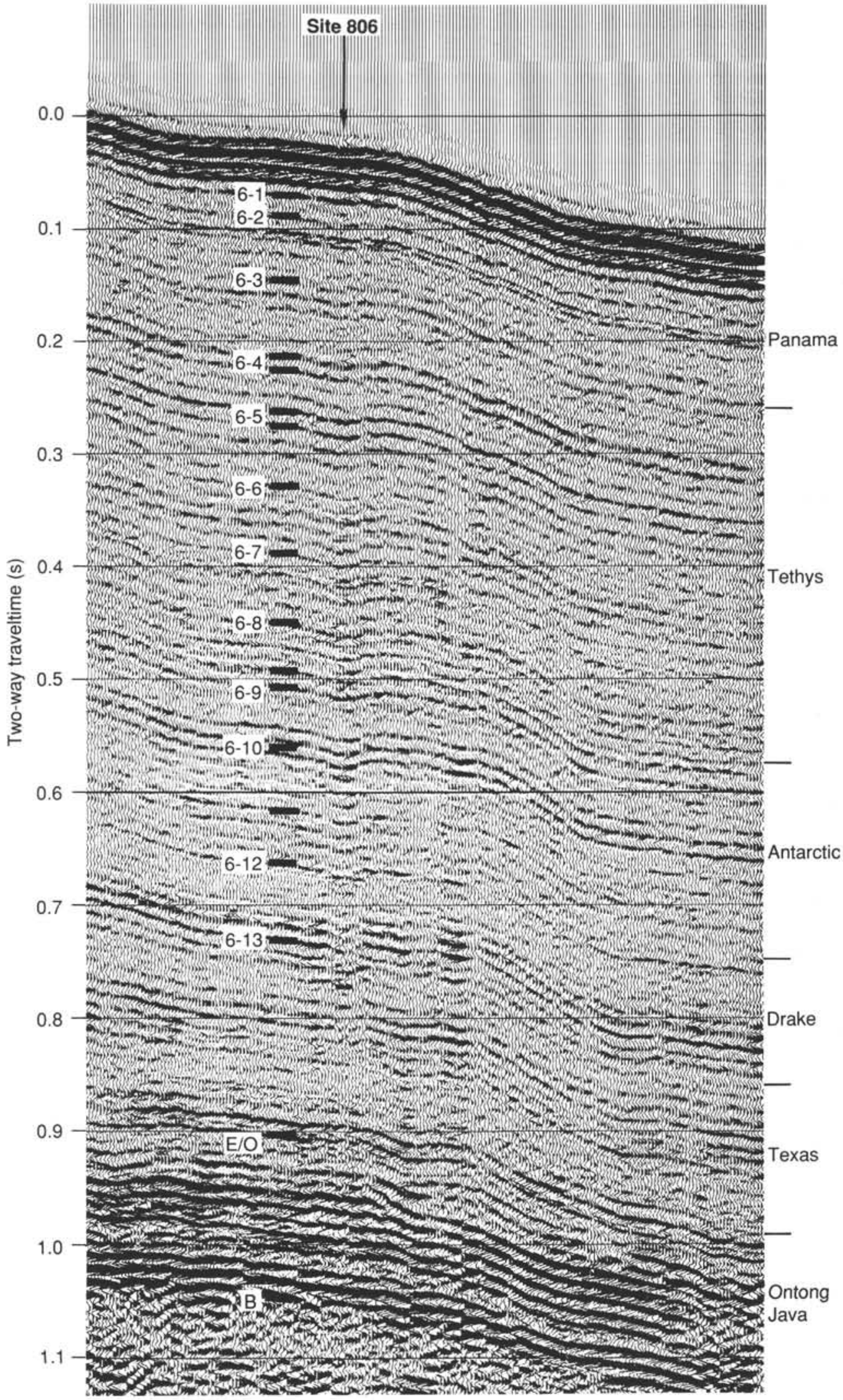

Figure 48. Seismic record collected on the ROUNDABOUT Cruise 11 site survey over Site 806, using the 80-in.^{3} water gun, 70–250 Hz band-pass filter. For details of reflector picks, see Table 12. E/O = Eocene/Oligocene boundary and B = basement.

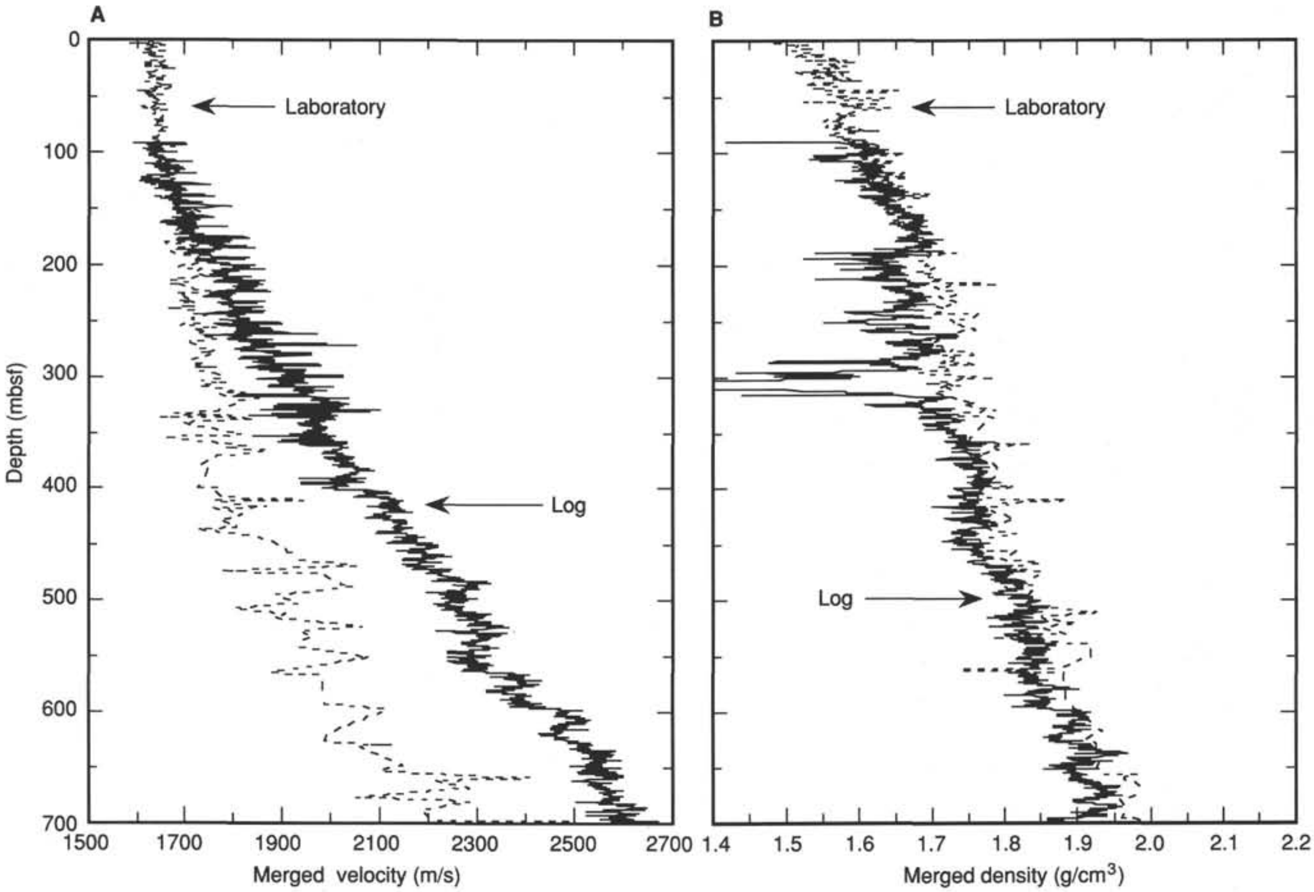

Figure 49. **A.** Merged laboratory (dashed line) and log velocity (solid line) profiles. Laboratory values were used from 0 to 180 mbsf, log values from 180 to 740 mbsf. **B.** Merged laboratory (dashed line) and log density (solid line) profile. Laboratory values were used from 0 to 360 mbsf, log values from 360 to 750 mbsf.

at 339.4 mbsf in Hole 806B (Core 130-806B-37X) and at 338.5 mbsf in Hole 806C (Core 130-806C-37X) (lowermost upper Miocene, ca. 10 Ma). The transition is gradational and shows alternating layers of varying degree of lithification, beginning at about 200 mbsf in both holes, looking downhole.

The younger section of the unit (Subunit IA, 0–339 mbsf) comprises Pleistocene to upper middle Miocene foraminifer nannofossil ooze to nannofossil ooze with foraminifers. Foraminifer content is significantly higher than at previous Leg 130 sites (Sites 803–805) and is estimated to be between 15 and 30%, on average. Radiolarian content is low throughout. Bioturbation is common throughout; it appears to be more strongly expressed than at the previous sites (803–805). Liesegang banding is common throughout the subunit, although it appears to be fainter and more diffuse in appearance than at Sites 803–805. The best examples are near the bottom of the subunit. Authigenic pyrite was found, associated with burrows, and a slight odor of H_2S was noted on occasion, upon opening the cores. Microfaulting is rare. Sediments are generally soft, but in the lowermost portion of Subunit IA more lithified intervals appear (below 200 mbsf). Coring was impeded in one instance because of porcellanite nodules (310 mbsf, ca. 8.2 Ma, Core 130-806C-34X) near the level of APC refusal. The shallowest porcellanite nodules were found at 240 mbsf (ca. 6.7 Ma). A marked change in the velocity-depth gradient (associated with a brief reversal) occurs just above this depth level (at 220 mbsf). At the ooze-chalk transition (339 mbsf), the character of the velocity profile changes: above this level, high-frequency variations are pronounced; below it, they are indistinct.

The older section of the unit, Subunit IB (339–776 mbsf), consists of 437 m of foraminifer nannofossil chalk to nannofossil chalk with foraminifers, with a few intervals of nannofossil chalk, ranging from the lower upper Miocene to the upper Oligocene. Foraminifer content is high down to about 600 mbsf (ca. 20 Ma) and decreases below that level. Radiolarian content is low throughout. The color is predominantly white. Color banding occurs throughout; bands become thinner and more distinct with depth in the subunit. Small-scale flaser bedding is present. Bioturbation is ubiquitous. Rare, centimeter-size porcellanite nodules were observed at several levels (350 and 510 mbsf). The depth gradient of dissolved silica is reduced at 350 mbsf and between 450 and 550 mbsf, possibly in response to precipitation.

The sediments in the chalk section posed no problem for XCB-coring down to the Oligocene/Miocene boundary zone, at which point recovery decreased. However, even where recovery is very good, the chalk is broken up and brecciated by drilling, with evidence for grinding of chalk on chalk. This type of recovery is typical for the material below 320 mbsf, that is, the section cored with the XCB. The Oligocene/Miocene boundary is located between 740 and 750 mbsf and apparently is without hiatus (although recovery is poor at this level). Sedimentation rates for the deep chalk section vary between 20 and 30 m/m.y., the same as for the upper portion of the chalk subunit.

Special Studies

An attempt was made to construct magnetostratigraphies for the uppermost section of Holes 806B and 806C. Although the

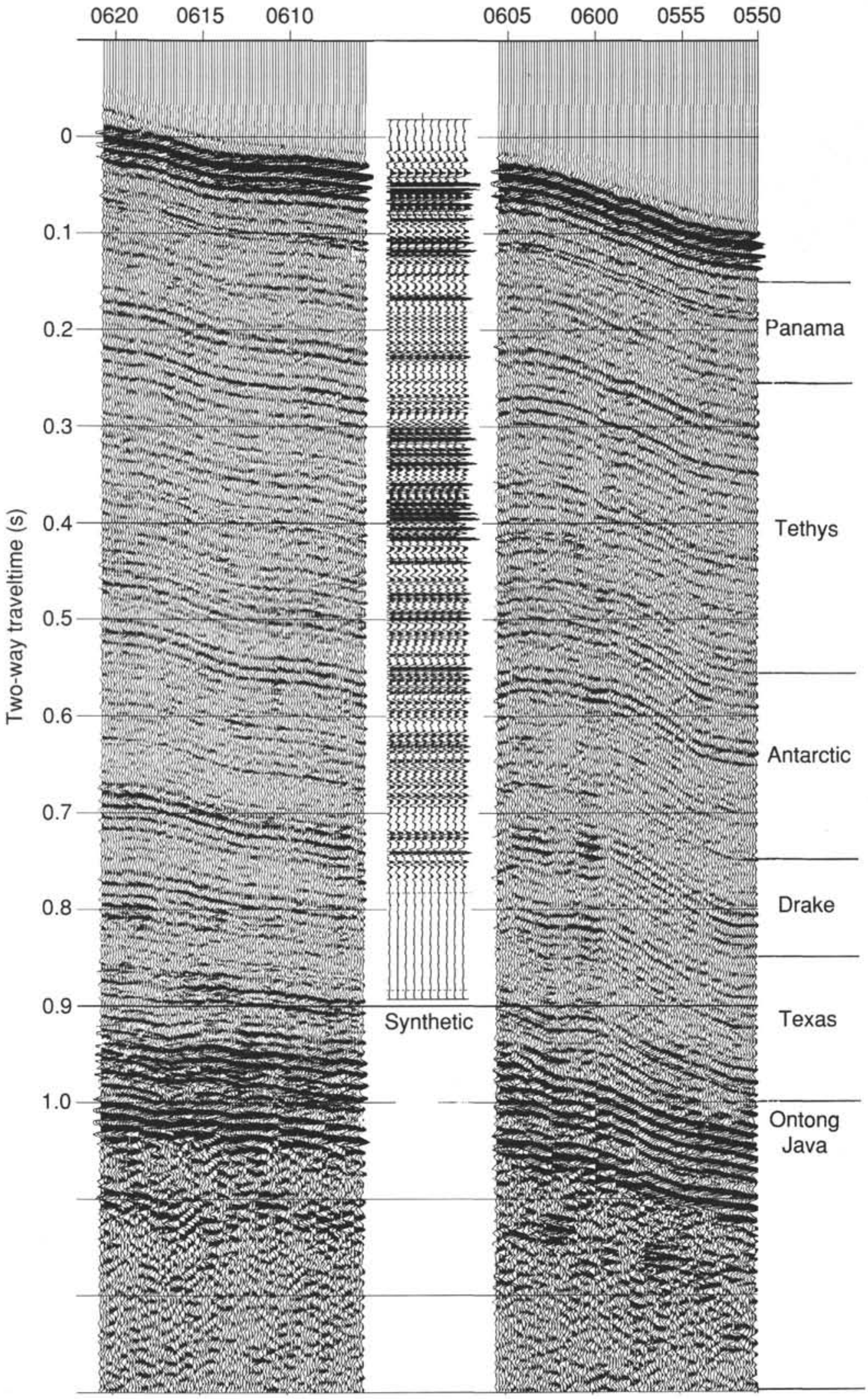

Figure 50. Comparison of synthetic seismogram and field record at Site 806. Names to the right of the diagram refer to groups of reflectors or zones with reflector groups. See Site 805 "Summary and Conclusions" section for significance of names.

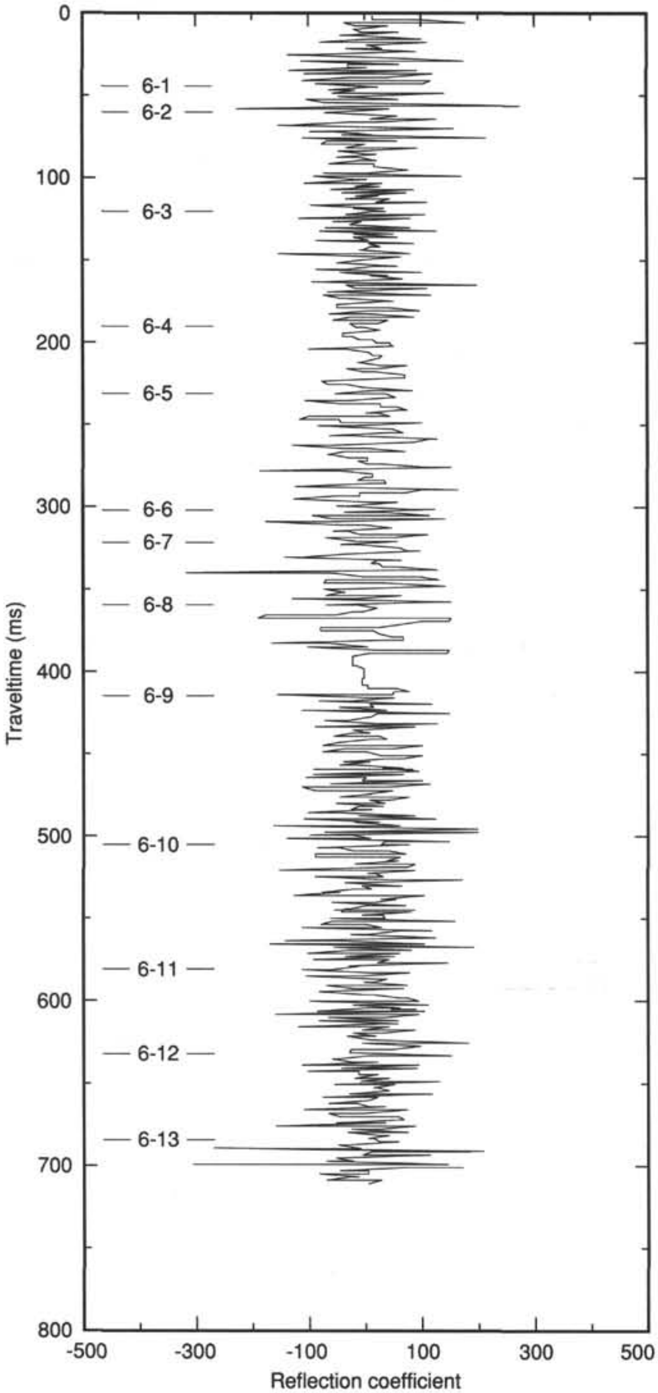

Figure 51. Reflection coefficient vs. traveltime, Site 806. For details of reflector picks, see Table 12.

Brunhes/Matuyama boundary could not be identified, magnetic susceptibility seems to be measurable well into the Pliocene, opening the possibility for the study of Milankovitch-type cycles using magnetic properties.

Chemical gradients in interstitial waters at this site are generally similar to those at Sites 803–805, reflecting the calcareous/siliceous nature of the sediments and the paucity of organic material. A somewhat higher supply of organic matter at this site, presumably because of the shallower depth, tends to produce slightly stronger gradients. Sulfate concentrations, especially, show this influence of organic supply. Concentrations decrease by almost 50% over the length of Hole 806C, with most of the decrease occurring by 222 mbsf. Alkalinity increases correspondingly in the upper section but decreases below 250 mbsf, presumably in response to precipitation of carbonate. Calcium and magnesium gradients are influenced by basalt alteration reactions at depth and show the usual negative correlation. Strontium concentrations reflect recrystallization processes, which apparently are more vigorous here than at the previous sites because of the higher sedimentation rates. Dissolved silica shows a steady increase with depth, except for a minor reversal of this trend near the ooze/chalk transition (350–360 mbsf).

Excellent logs were obtained for sound velocity and density at Site 806. The fact that this site has continuous sedimentation makes these logs especially valuable. Laboratory velocities and bulk densities provide control for the upper portion of the record, which could not be logged. Bulk density and sound velocity increase with depth more or less as expected. Bulk density values are near 1.6 g/cm^3 at 100 mbsf and increase to 1.9 g/cm^3 by 700 mbsf. If expressed as average density increase per age interval (0.15 g/cm^3 per 10 Ma) the overall gradient is exactly identical to that in Site 586. It is noticeably higher than that in Site 805, which has a distinctly lower sedimentation rate. Thus, both depth of burial and age govern this parameter. Sound velocity is 1.65 km/s at 100 mbsf and increases by 0.13 km/s per 100 m down to 250 mbsf, where the gradient changes to 0.18 km/s. The stronger gradient, presumably, shows the effects of carbonate precipitation below 250 mbsf, as seen in the interstitial water measurements.

Table 12. Summary of traveltimes, depth, and ages for Site 806 reflectors.

Reflector	Traveltime Seismic (s)	Traveltime Synthetic (s)	Depth Seismic (m)	Depth Synthetic (m)	Age (Ma)
6-1	0.050	0.055	41	45	1.9–2.0
6-2	0.068	0.070	56	57	2.4
6-3	0.129	0.131	106	108	3.8
6-4	0.200	0.200	167	167	5.1
6-5	0.235–0.24	0.24–0.024	196	213	5.7–6.1
6-6	0.310	0.312	264	265	7.2
6-7	0.326	0.332	278	284	7.5–7.6
6-8	0.360	0.370	311	321	8.2–8.4
6-9	0.425	0.425	375	375	10.8
6-10	0.514	0.515	469	470	13.3
6-11	0.591	0.590	556	555	17.6
6-12	0.635	0.641	610	617	20.3–20.5
6-13	0.690	0.694	678	685	22.8–22.9

Notes: Depths and traveltimes to seismic events are picked on both the synthetic seismograph (synthetic) and the field record (seismic). Ages are from sedimentation rate curves (see "Sedimentation Rates" section, this chapter).

Seismic Stratigraphy

Site 806 is characterized by the highest sedimentation rate of any of the Leg 130 sites. A complete section, without hiatuses, is also present, as is true for Site 805. This site, therefore, is of great interest with respect to a central objective of the leg: to determine the nature of the acoustic reflectors seen on seismic profiles.

The reflector groups identified at Site 805 can also be recognized at Site 806, in the SCS profiles taken by the *Thomas Washington* during the ROUNDABOUT pre-site survey (Fig. 54). In addition, there are others, not seen in the Site 805 profiles. Dating shows that at least some reflectors are associated with paleoceanographic events, as suggested by Mayer et al. (1986) for the central equatorial Pacific. They proposed the

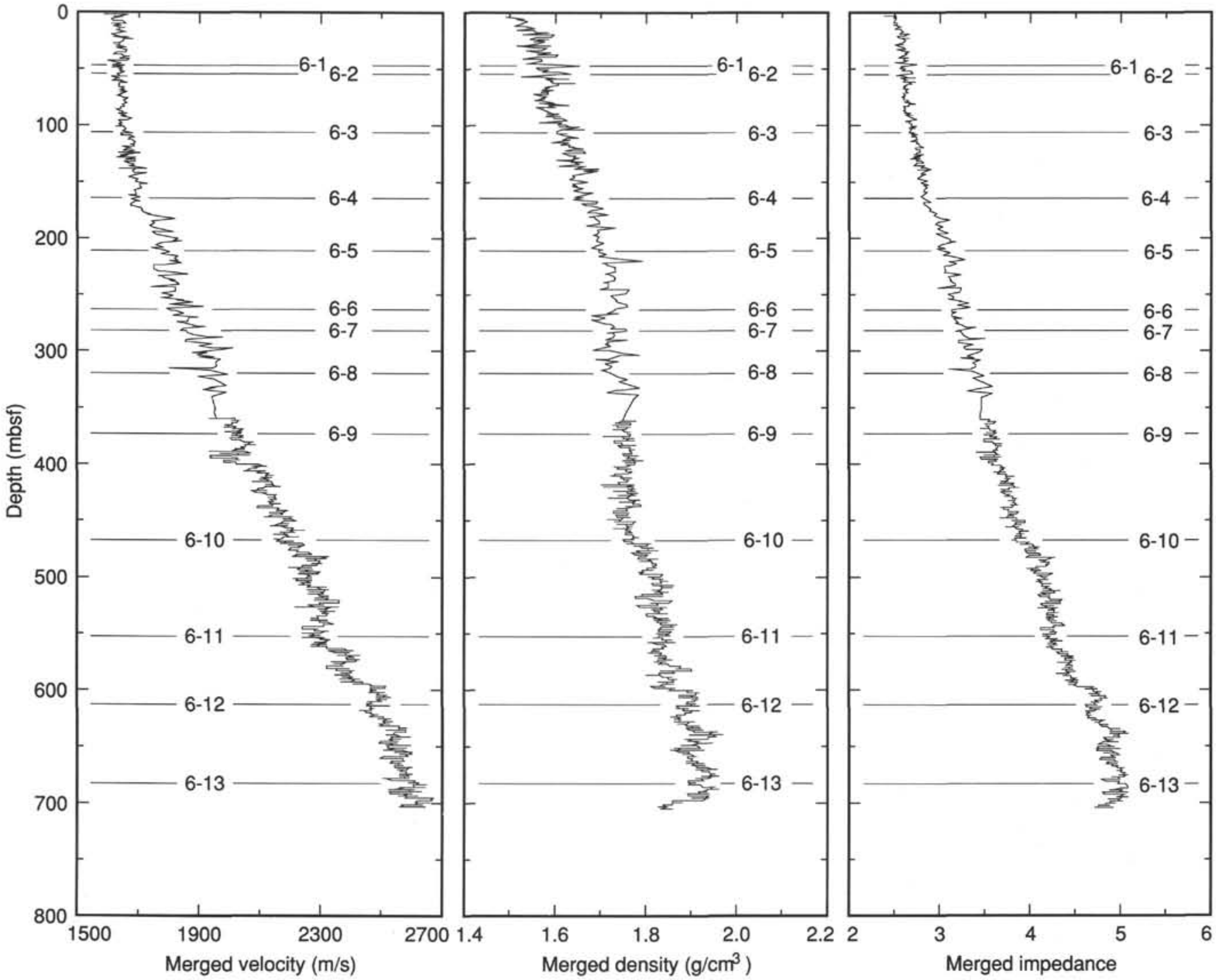

Figure 52. Merged velocity, density, and acoustic impedance used to generate synthetic seismogram, Site 806. For details of reflector picks, see Table 12.

closing of the Panama Isthmus, reorganization of deep circulation in the Atlantic, climatic events surrounding the Antarctic, and the opening of the Drake Passage as important paleoceanographic themes reflected in the acoustic properties of Pacific pelagic sediments. The names for three reflector groups were chosen for these propositions (without necessarily implying endorsement). The advantage of considering groups of reflectors in addition to single members is obvious: it is then the variability of sediment properties within a given section that is being addressed, rather than an individual excursion of velocity and/or density. For explanation of the names "Tethys Interval" and "Texas Interval," see the "Summary and Conclusions" section of the Site 805 chapter (this volume).

The match of reflectors shown in Figure 54 is readily obtained by assuming that the traveltime to equivalent reflectors in Site 806 is 1.37 times that in Site 805. The success of the match allows dating by correlation and also allows the statement that sedimentation rates between these two sites are likely to differ by a certain factor for the entire Neogene and Oligocene. This result is quite surprising, considering that the effects of dissolution are thought to be responsible for the difference in overall sedimentation rate, and that dissolution intensity might be expected to have a long-term trend, producing a corresponding trend in differences in sedimentation rates.

The general match proposed in Figure 54 predicts that the age of 22.0 Ma found at .50 sbsf at Site 805 should appear at 0.685 sbsf at Site 806 (0.5 · 1.37), which corresponds to 676 mbsf, using a generalized velocity profile for Site 806 (based on logging). In fact, the biostratigraphic age of 22.0 Ma in Site 806 appears at 665 mbsf (with an uncertainty of 5 m). At 676 mbsf (the guess), the age is 22.3 Ma according to shipboard biostratigraphy. The result of this exercise suggests that the matching of reflectors on the Ontong Java Plateau produces correlations that are comparable in quality with those from biostratigraphic control. To check this proposition, additional matches were picked as follows (each comparison shows Site 805 first, then Site 806):

1. 0.044 sbsf, 35 mbsf, 1.95 Ma; 0.061 sbsf, 48 mbsf, 2.05 Ma;
2. 0.128 sbsf, 103 mbsf, 4.44 Ma; 0.170 sbsf, 139 mbsf, 4.49 Ma;
3. 0.258 sbsf, 216 mbsf, 7.17 Ma; 0.332 sbsf, 285 mbsf, 7.64 Ma; and

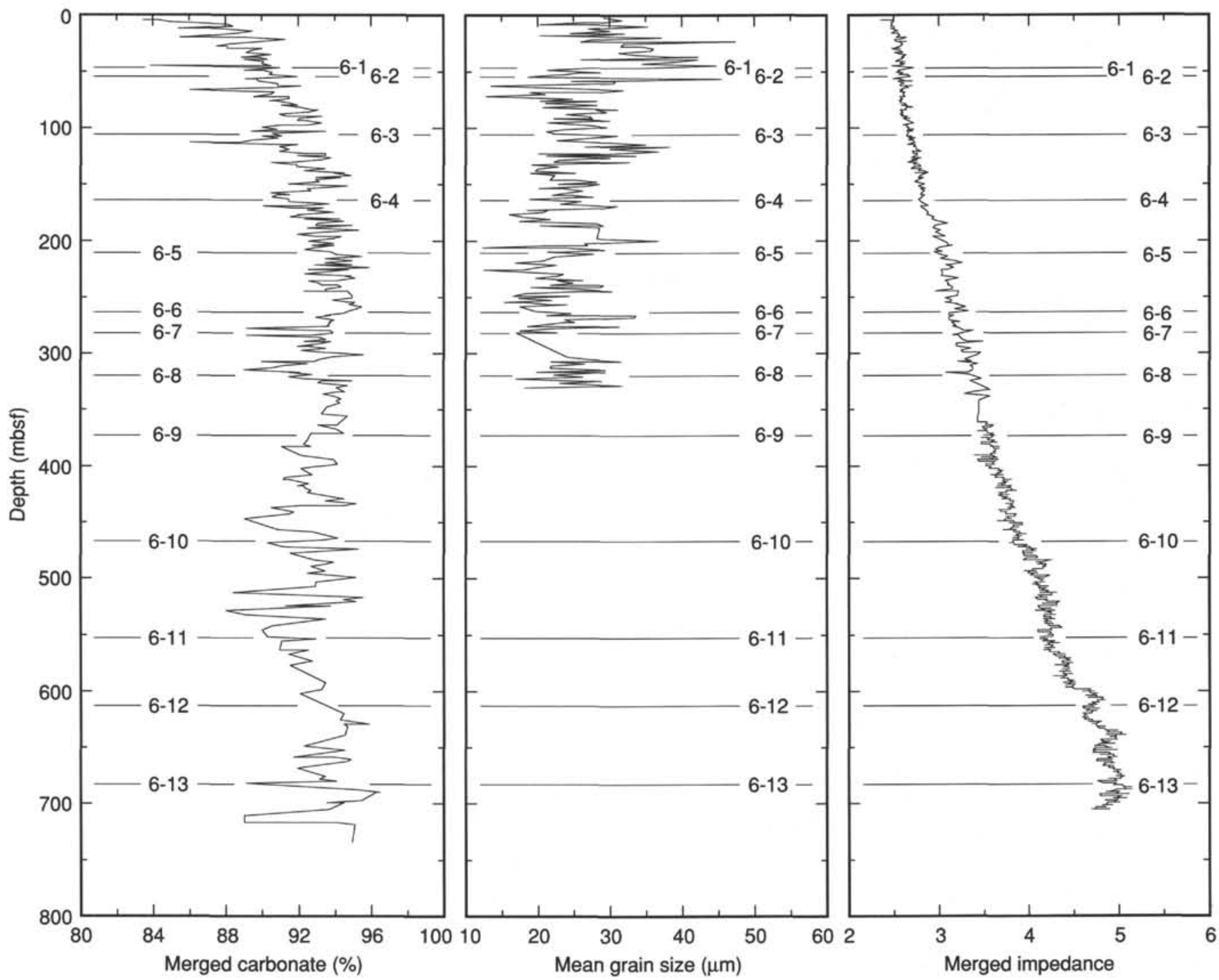

Figure 53. Merged carbonate content, mean grain size, and merged acoustic impedance vs. depth, Site 806. For details of reflector picks, see Table 12.

4. 0.363 sbsf, 315 mbsf, 12.70 Ma; 0.480 sbsf, 435 mbsf, 12.34 Ma.

The average difference between the age estimates is 0.23 m.y. for the five determinations. A repeat of the exercise using a continuous velocity profile, and picking different levels independently, gave virtually identical results. An error of between 0.2 and 0.3 m.y. is within the interpolation errors of the biostratigraphic age; it is the uncertainty found if one hole of Site 806 is used to predict the age at the same depth in the other hole. Thus, as far as we can tell, the correlative reflectors of Sites 805 and 806 are identical in age. The demonstration of this synchroneity is an important result; it is greatly simplified by the fact that near-equivalent levels in the two sites are readily found because of the similarity of sedimentation rate patterns (Fig. 55).

The Panama Series (Fig. 54) contains reflectors that we dated near 2, 2.4, and 3.7 Ma. The age of 2.4 Ma corresponds to a deep-water cooling event and the onset of North Atlantic ice buildup (Backman, 1979; Shackleton et al., 1984). The reflectors dated at 2.4 and 3.7 Ma can be identified in the seismic record from DSDP Site 586 using the velocity profile provided by the logging of DSDP Site 586 (Shipboard Scientific Party, 1986a). The Tethys Interval contains a number of lesser reflectors, two of which (just above and below 0.4 sbsf) do not seem to have corresponding reflectors in Site 805 and may be related to lithification at that depth (near 350 mbsf).

The next group of strong reflectors, going downsection, is the upper group of the Antarctic Series, centered on the middle Miocene (13 Ma; 0.49 sbsf, ca 450 mbsf). The lower group of this series is somewhat less prominent and belongs to the uppermost lower Miocene and lowermost middle Miocene (560–500 mbsf, 18–15 Ma). This entire zone is characterized by major climatic change and associated excursions in carbonate content and other sediment properties (Barron et al., 1985). These changes, presumably, are associated with the onset of Antarctic Bottom Water production at that time. The group of reflectors immediately below the Antarctic Series, the Drake Series, has the strongest reflector members. Dates range from about 22.5 Ma for the deepest of the group (680 mbsf) to 18.5 for the uppermost (570 mbsf).

Below this group there is a thick section, the Texas Interval (250–270 m thick), which shows another series of reflectors, almost as strong as the Drake Series. At Site 805 these reflectors are much less pronounced. The reason for the difference is not known; it may be related to the higher diagenetic potential in Site 806, which could be stemming from better preservation of

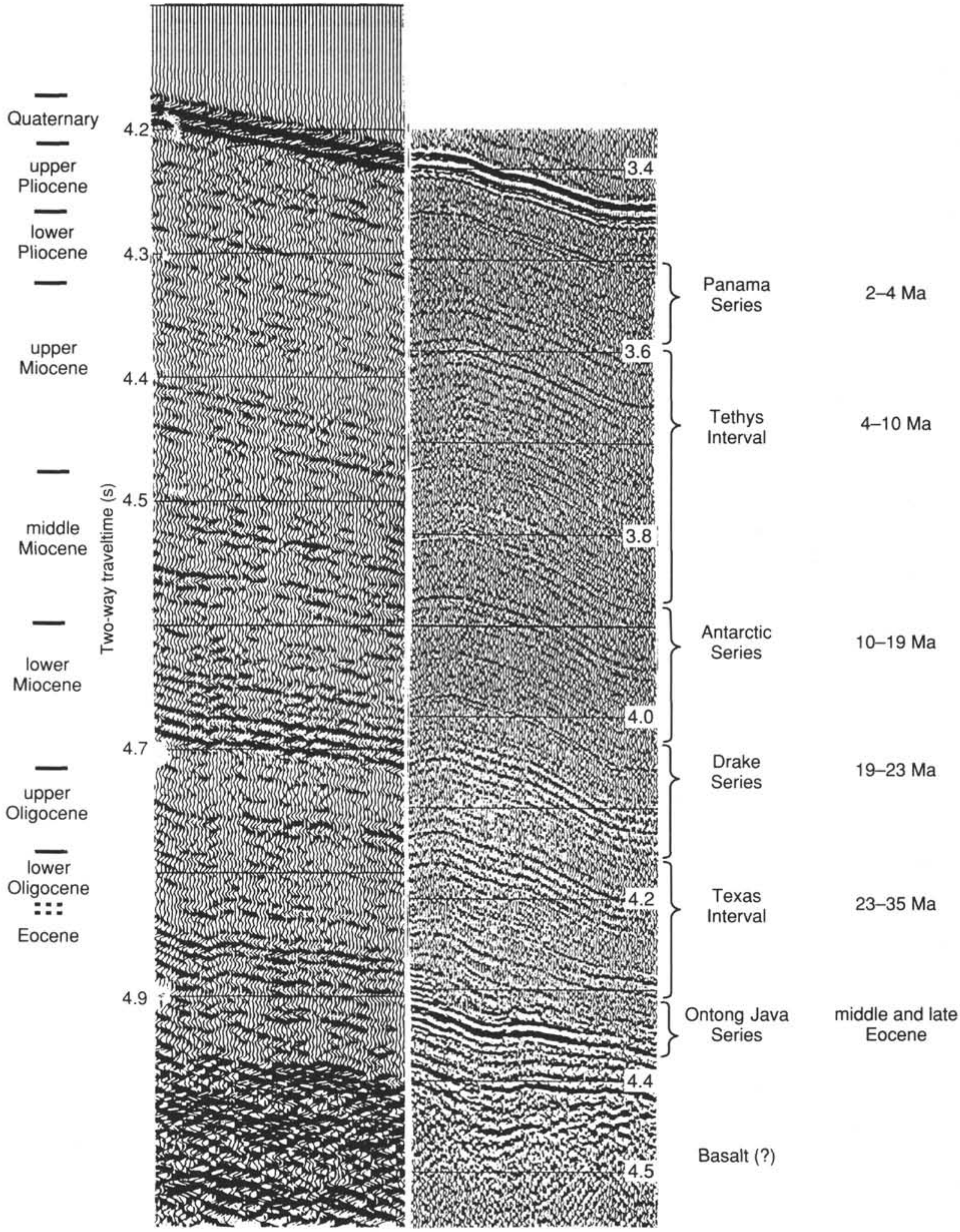

Figure 54. Comparison of seismic profiles at Sites 805 and 806. Profiles taken by the *Thomas Washington* on ROUNDABOUT Cruise 11 (see "Seismic Stratigraphy" section, this chapter), with time scale assigned from drilling and logging results as well as biostratigraphic studies (see "Biostratigraphy" section, this chapter). Names to the right refer to groups of reflectors ("series") and zones with less distinct groups ("intervals"). See the "Summary and Conclusions" section of the Site 805 chapter (this volume) for the significance of names. The record of Site 806 is to the right; its traveltime scale was reduced by a factor of 0.73 to match reflectors as best as possible without individual adjustments.

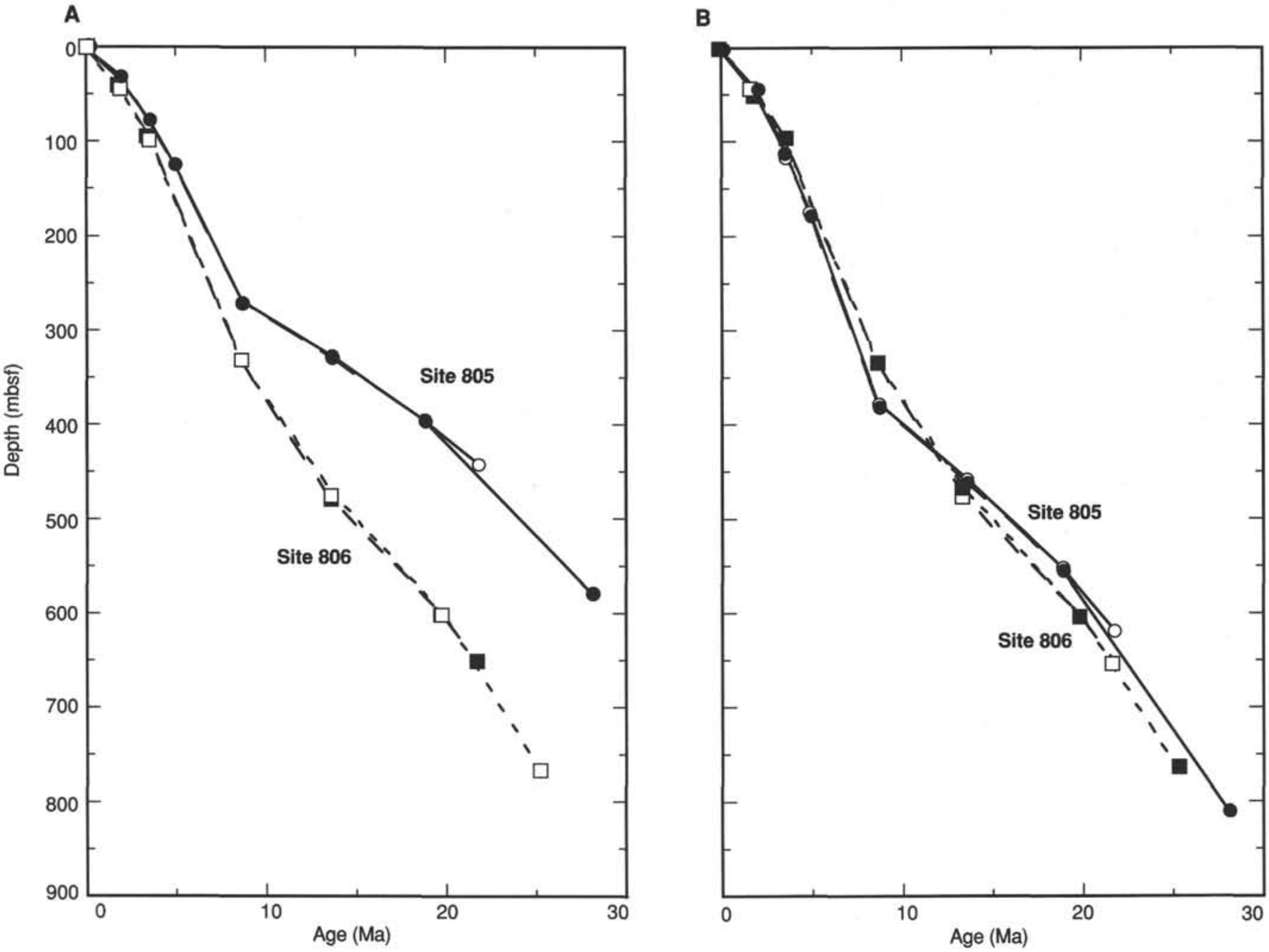

Figure 55. Age-depth plots, Sites 805 (solid line) and 806 (dashed line), as given by biostratigraphic tie points (**A**) and after mapping Site 805 onto 806 by multiplying depth by a factor of 1.4 (**B**). Solid squares = Hole 806B, open squares = Hole 806C, solid circles = Hole 805C, and open circles = Hole 805B.

carbonate or from a greater supply of organic matter, or both. Below this interval is the Ontong Java Series, which is thought to represent the change from chalk to limestone in the lowermost Oligocene, and—somewhat deeper in the section—the occurrence of chert. As at Site 805, acoustic basement lies a short distance below this sequence.

In summary, there is good correlation between Sites 805 and 806, and good agreement in biostratigraphic dates for equivalent reflectors or reflector groups, regardless of the overall difference in sedimentation rates. This observation provides strong support for the hypothesis that many reflectors represent the effects of paleoceanographic events felt over a wide depth range and, hence, are of global significance. Other reflectors may be regionally strong expressions of minor events or may be related to diagenetic processes that are not synchronous.

Sedimentation Rates

The oldest sediments cored, at 776 mbsf in Hole 806C, were of latest Oligocene age (Zones NP25 and P22). The distance to acoustic basement below this level (0.75 sbsf) may be estimated as approximately 0.23 s two-way traveltime, which corresponds to roughly 340 m of sediment at that depth. Assuming that the uncored section represents at least 80 Ma of time, the presence of condensed intervals or hiatuses, or both, would seem to be indicated for the early Paleocene and Upper Cretaceous.

Since late Oligocene time, Site 806 has received nannofossil ooze with, on the whole, rather minor admixtures of siliceous fossils. Sedimentation rates typically varied between 20 (lower Miocene) and 46 m/m.y. (upper Miocene), the overall average being near 30 m/m.y. (Fig. 56). These numbers are somewhat misleading, inasmuch they are not corrected for mass flux, and contain the trend of decreasing porosity with depth. If one corrects for this trend, one will find that the mass flux in the late Oligocene is of the same magnitude as in the late Neogene. Spikes in sedimentation rate may be present between 8 and 6 Ma (uppermost Miocene), and between 14 and 13 Ma (middle Miocene) (see "Sedimentation Rates" section, Figs. 22 through 26) but cannot be fully substantiated at this time because of uncertainties in absolute ages for biostratigraphic tie-points. The two intervals in question are characterized by maximum carbonate values. There seem to be no condensed sections at Site 806 (whereas thinning was observed at Site 805 for the upper lower Miocene).

Comparisons Between Sites 805 and 806

Carbonate Stratigraphy

Of the sites drilled during Leg 130, Sites 805 and 806 are the most similar with respect to reflector patterns (Fig. 54) and sedimentation rate patterns (Figs. 55 and 56). The lithologies of the

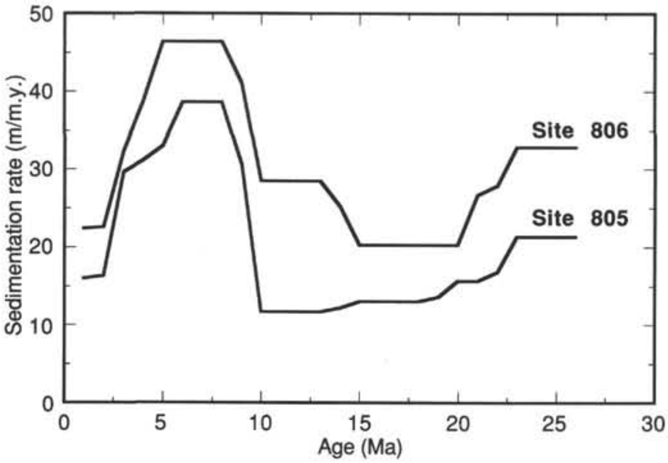

Figure 56. Sedimentation rates, Sites 805 and 806, based on biostratigraphic tie-points (see "Sedimentation Rates" section, this chapter).

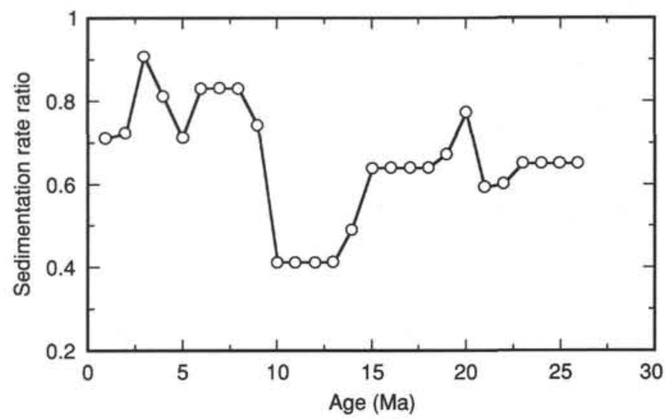

Figure 57. Sedimentation rate ratio between Sites 805 and 806, based on biostratigraphic tie-points (see "Sedimentation Rates" section, this chapter). The circles are 1-m.y. interpolation steps.

two sites, in essence, are identical. These two sites, therefore, offer a unique opportunity to study one central objective of the Neogene program, that is, the depth effect on the deposition of carbonate. A question that arises in this context is to what extent are fluctuations in sedimentation rate caused by variations in the intensity of carbonate dissolution. The following brief analysis addresses this question, using the biostratigraphic tie-points provided in the "Sedimentation Rate" sections of the site chapters for 805 and 806 and the carbonate data available on 15 March 1990 and listed in the "Carbon Geochemistry" sections of the same site chapters.

The overall Neogene sedimentation rate ratio (SRR) between Sites 806 and 805 is ~ 1.4, according to biostratigraphic correlation (Fig. 55). The inverse—that is, SRR (805/806)—is then 0.71, which means that on average there are 7.1 m of sediment at Site 805 for every 10 m at Site 806. Based on biostratigraphy, it appears that there are marked fluctuations in this ratio, ranging from around 0.4 to 0.85, when considering time spans of several million years (Fig. 57). There is a general resemblance of the (bio-)SRR curve to the sedimentation rate curves of both sites (cf. Figs. 56 and 57). This indicates that the depth factor reducing sedimentation at Site 805 (presumably carbonate dissolution) tends to be less important during intervals when sedimentation rates are high. If this proves to be true, one would conclude that dissolution gradient and supply rate are negatively correlated. This is opposite actual expectations (van Andel et al., 1975; Berger, 1979).

Carbonate dissolution, presumably, is largely responsible for the average SRR of 0.71, that is, the reduction of sedimentation at Site 805 with respect to that at Site 806. To explore further the importance of this factor as a source of variability in sedimentation pattern, we next turn to the carbonate record. By multiplying depths between 0 and 200 mbsf in Site 805 by 1.35, a tolerably good match between the two carbonate records is obtained for this interval (Fig. 58). Likewise, multiplying depths between 200 and 400 mbsf in Site 805 by 1.28 matches the carbonate records closely enough for the purpose of the discussion that follows (Fig. 58).

The carbonate content at Site 806 typically fluctuates between 90% and 95% throughout the section except in the Pleistocene portion, where it drops to values as low as 86% (Fig. 58). Values below 90% also are seen in the lower upper Miocene (280-320 mbsf, 7.5-8.5 Ma) (Fig. 58), and again in the lower middle Miocene (490-550 mbsf, 14-16.5 Ma). The pattern in Site 805 is quite similar, percentage values being commonly 1%%-2% lower and amplitudes slightly greater. Strong lows in carbonate at Site 806 typically line up with strong lows at Site 805, although lows at Site 805 do not necessarily have a partner in Site 806.

The major carbonate minimum periods are initiated by a sudden drop in the carbonate content, which can be extremely steep, especially at Site 805 (e.g., near 170 mbsf) (Fig. 58). Termination of low carbonate acme events can be equally sudden. In detail, large carbonate fluctuations are superimposed on these steep ramps, accentuating differences in physical properties (the figure shows 7-point averages). Ten sudden drops in carbonate values ("carbonate reduction events" [CREs]) are readily recognized (numbered with Roman numerals, CRE-I through CRE-X).

CRE-I, near 10 mbsf (ca. 0.5 Ma), presumably initiates the "Brunhes Dissolution Cycle" of Adelseck (1977). CRE-II (1-2 Ma; not well matched on the figure) apparently leads into the Dissolution Acme Event M17, described by Saito et al. (1975). CRE-III (ca. 2.4 Ma) is correlative with a major glacial buildup event in the North Atlantic (Backman 1979; Shackleton et al., 1984), and is seen as a strong reflector in the Panama Interval. CRE-IV (ca. 3.2 Ma) is correlative to a period of cooling and increase in North Atlantic Deep Water production. The event presumably leads into the GU3 minimum in the carbonate stratigraphy of Saito et al. (1975). It marks the time of the closure of the Panama Straits (Keigwin, 1978).

The next three major CREs each mark a descent into a different substantial minimum carbonate period. CRE-V (ca. 4.0 Ma) apparently coincides with a major warming and transgression (Ingle, 1973; Whitman, 1989). The deepest of the Panama Series reflectors, near 3.7 Ma, may mark recovery from this event. CRE-VI (ca. 4.4 Ma) apparently is associated with that same warming, representing an earlier step. CRE-VII (ca. 5.2 Ma) leads into a major dissolution acme, labeled "X" in Saito et al. (1975). This event is associated with a strong reflector, identified at 0.17 mbsf in Site 586 (labeled 150 m/N17-N18/5-6 m.y.), by Shipboard Scientific Party (1986a). Our own data show a strong triple reflector at 0.20-0.22 sbsf (5.1-5.4 Ma) in the upper part of the Tethys Series. A moderate cooling is indicated in the oxygen isotope data for Site 586 at this level (Whitman, 1989) as well as a rapid increase in sand content, which peaks shortly thereafter (Whitman, 1989). Hiatus formation in the central Pacific is indicated for this period (NH7 of Keller and Barron, 1987).

The next deeper CRE (VIII) is not strongly expressed, possibly because of the very high initial carbonate values. It occurs near 245 mbsf (ca. 6.8 Ma). Site 806 does not show a strong reflector here, but Site 805 does (0.25 sbsf; 6.9 Ma). The event ap-

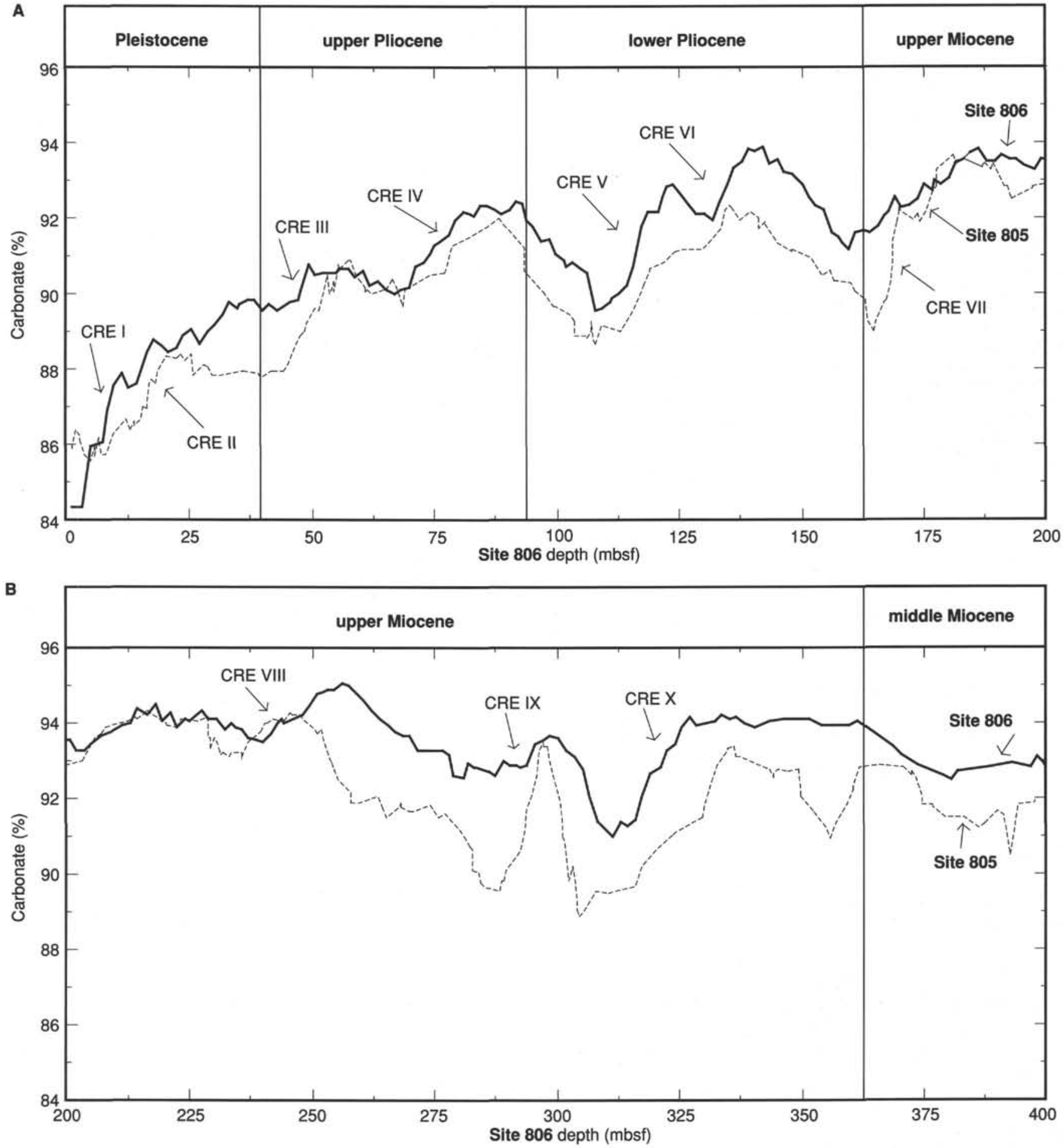

Figure 58. Comparison of the carbonate stratigraphies, Sites 805 and 806 (upper 400 mbsf). The carbonate reduction events are numbered from CRE-I in the upper Pleistocene to CRE-X at the beginning of the upper Miocene. The events are characterized by a sudden decrease in carbonate in one or both of the sites (see text). From 0 to 200 mbsf, the depth-in-hole values of Site 805 were multiplied by 1.35 for an approximate match; from 200 to 400 mbsf, the depth-in-hole values of Site 805 were multiplied by 1.28.

pears correlative with Hiatus NH6 of Keller and Barron (1987). CRE-IX and CRE-X are major events, occurring within the N16 Zone, notorious for poor preservation elsewhere in the Pacific. At Site 806 they are dated near 7.5 Ma and 8.5 Ma, respectively, suggesting a close association with Hiatus NH5 (Keller and Barron (1987). The extreme carbonate minimum in the eastern central Pacific labeled 10e (Barron et al., 1985) and Hiatus NH5 appear to be correlative. Thus, CRE-IX or CRE-X, or both, appear to be equivalent to 10e and NH5. A cooling step is reported for this interval at Site 289 (Savin et al., 1985). A moderately strong reflector is seen at Site 806 at the level of CRE-X (0.37 sbsf; Fig. 54), but only a weak one shows up in Site 805.

With regard to carbonate reduction events, then, we note that they have Pacific-wide significance, in lining up with carbonate lows in the central Pacific, as well as with Pacific hiatus events. Also, acoustic reflectors tend to be associated with CREs, presumably because they are responsible for creating surfaces of contrasting physical properties, within the sediment stack. As to causes, we note that several of the events appear to be associated with cooling, and at least one (CRE-V) with a pronounced warming. Cooling and warming changes the sites of carbonate deposition of the ocean, leading to a reorganization of sedimentation patterns. In principle, this could lead to either an increase or a decrease in carbonate deposition at a given site. On the flanks of the Ontong Java Plateau, in the tropical Pacific, a cooling event apparently produces sudden carbonate reduction (although the cooling trend, after 10 Ma, is associated with increased carbonate sedimentation rates). The response to warming seen at CRE-V may stem from a change in the partitioning of carbonate between shelf and deep-ocean (Berger and Winterer, 1974; Davies et al., 1977) environments, or from sharply reduced carbonate production. These findings lend strong support to the hypothesis that many acoustic reflectors on the Ontong Java Plateau are the result of paleoceanographic events (Schlanger and Douglas, 1974; Berger and Mayer, 1978; Mayer et al., 1985, 1986).

Curve Matching and Difference in Carbonate Content

The close correspondence of the carbonate stratigraphies of Sites 805 and 806 permits a detailed feature-for-feature matching on a scale somewhat finer than that provided by biostratigraphy alone. Figure 59 shows such a match, based on peak-to-peak and ramp-to-ramp correlations. Although all available data were used to make the match, only paired data are shown, that is, values that have a partner within 4 m of the matched level (i.e., Site 806 depth-in-hole). Resolution varies depending on the variability of the record; it is taken to be about 1 Ma. The stratigraphy of differences in the carbonate content in the two sites (based on paired, averaged data) shows fluctuations with a typical range between 0% and 3% (the carbonate content of Site 806 minus the carbonate content of Site 805, at equivalent depth levels). The greatest differences, and the most variable portions of the record, are associated with major CREs, such as CRE-II, CRE-V, CRE-VII, and the CRE-IX/X interval, discussed above.

The maximum difference is seen at 510 mbsf (Site 806), near 15.5 Ma (CRE-XVI). This event coincides with the rapid change in oxygen isotopes that marks the acme of the Antarctic cooling event (Zones N9/N10; Savin et al., 1985; Vincent and Berger, 1985). The maximum is preceded (in time) by two smaller peaks (belonging to CRE-XVII and CRE-XVIII), one near 550 mbsf (ca. 17.5 Ma), the other near 585 mbsf (19 Ma). CRE-XVII is centered on Zone N8, which marks the onset of the Antarctic cooling event (Savin et al., 1985) and the maximum of the Monterey carbon isotope excursion (Vincent and Berger, 1985). Hiatus formation is common in this interval (NH2 of Keller and Barron, 1987). CRE-XVIII occurs in the uppermost lower Miocene, in Zone N7. Cooling and ^{13}C enrichment is correlated with this event, as well as a carbonate minimum in the central Pacific (16g; Barron et al., 1985). CRE-XVI through CRE-XVIII define a period of reduced sedimentation rate in Site 806, whereas at Site 805 there is a condensed section, and at Sites 803 and 804 the interval is not represented in the record at all.

Surprisingly, the events surrounding CRE-XVI to CRE-XVIII are not strongly expressed in the acoustic reflection records of Sites 805 and 806. There is, however, a strong double reflector in the profile at Site 586, farther up on the plateau. It is labeled 550/N6/19 m.y. (Shipboard Scientific Party, 1986a) and probably corresponds to CRE XVII/CRE XVIII. At Site 806, there is a group of strong reflectors in the middle of the Antarctic Series (at ca. 3.9 sbsf; Fig. 54) near 435 mbsf (Site 806). This series apparently belongs to the interval between CRE-XIII and CRE-XIV (12–13 Ma), which corresponds to a period of hiatus formation in the central Pacific (NH3 of Keller and Barron, 1987). The differences in carbonate content between matching depth levels of Sites 806 and 805 imply a loss of carbonate at the deeper site. Assuming that this loss occurred by carbonate dissolution, and that noncarbonate material was not affected, we can calculate the proportion of sediment lost at the deeper site ("Loss") from the carbonate fluxes in the shallow site ("initial carbonate") and in the deeper one ("final carbonate"), at corresponding depth levels:

$$\text{Loss} = (\text{Initial carb.}) - (\text{Final carb.}) = 1 - NC_i/NC_f,$$

where NC_i and NC_f are initial and final percent of noncarbonate, respectively. To determine the percentage loss of carbonate, "Loss" would have to be multiplied by the percentage of carbonate content at Site 806.

The "Loss" curve should repeat the pattern of the carbonate difference curve (Fig. 59A), as it is a function of the difference in carbonate. The result of calculating the loss of sediment by the above equation is shown in Figure 59B, together with the two smoothed carbonate curves, on the same scale. First, one should note that small differences in carbonate between the two sites are translated into large losses. The reason for this is the great sensitivity of "Loss" in the above equation to the quotient NC_i/NC_f when these numbers are small. This also means that errors in measurement, or in matching the carbonate curves, are greatly amplified. Second, it is evident that losses are pulsed rather than being smoothly distributed through time. We know this is true for the Milankovitch scale, where dissolution cycles are common (e.g., Thompson, 1976; Moore et al., 1977; Farrell and Prell, 1989). Apparently, unless the results shown here are artifacts stemming from spotty data and poor matching, similar pulsing is indicated on scales between 0.5 and 1 Ma in our carbonate curves (cf. van Andel et al., 1975). Finally, this analysis reveals that loss by carbonate dissolution in the manner assumed (that is, without involving loss of noncarbonate) cannot account for the overall difference in sedimentation rates between Sites 805 and 806.

If the stratigraphy of Site 805 were to be generated from that of Site 806 solely according to carbonate dissolution, the differences in carbonate percentages would have to be greater than observed. For a general sedimentation rate ratio of 0.71, the average loss would have to come out as 29% (100% − 71%). In fact, we get about one-half of that (Pleistocene, 8.5%; upper Pliocene, 6.3%; lower Pliocene, 13.9%; upper Miocene, 13.9%, middle Miocene, 13.0%, and lower Miocene, 16.8%). We shall next adduce further evidence regarding this discrepancy and subsequently discuss possible causes for its origin.

Sedimentation Rate Ratios from Curve Matching

The match of carbonate curves shown in Figure 59 implies that we know which depth levels at Sites 805 and 806 correspond to each other. If this knowledge is accurate, we can next turn to the ratios in sedimentation rates that are implied for each 10-m section in Site 806 (10 m is an arbitrary interpolation interval). Note that the resulting curve (Fig. 60) is independent of age assignments. The overall SRR is given as 0.71, from biostratigraphy. Down to about 400 mbsf (Site 806), the SRR found by carbonate matching agrees well with that based on biostratigraphy. Below this depth, the carbonate data have too many gaps for confident matching.

Down into the uppermost upper Miocene, the deviations of the SRR from the average are minor. For the Quaternary, there

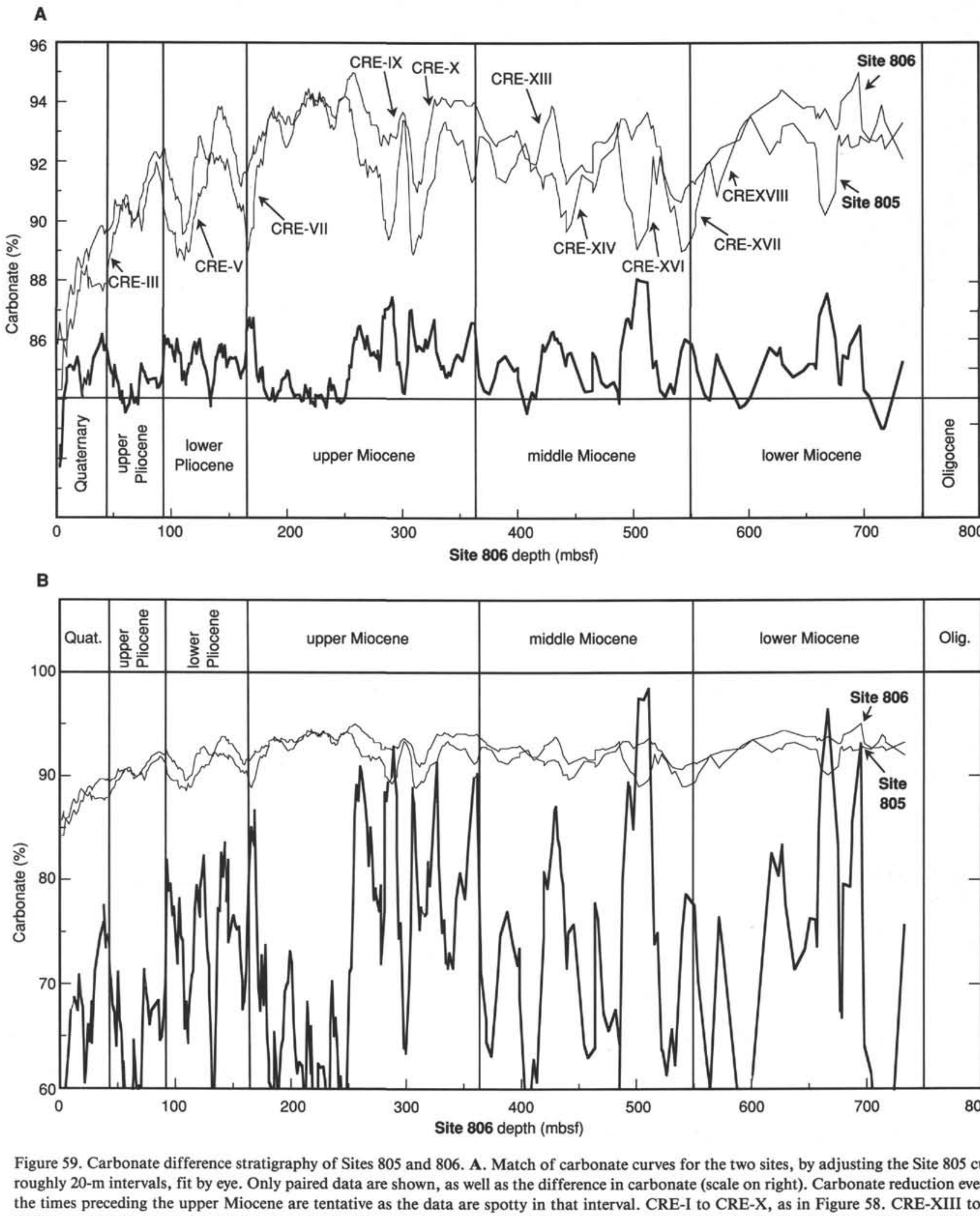

Figure 59. Carbonate difference stratigraphy of Sites 805 and 806. **A.** Match of carbonate curves for the two sites, by adjusting the Site 805 curve at roughly 20-m intervals, fit by eye. Only paired data are shown, as well as the difference in carbonate (scale on right). Carbonate reduction events for the times preceding the upper Miocene are tentative as the data are spotty in that interval. CRE-I to CRE-X, as in Figure 58. CRE-XIII to CRE-XVIII, see text. **B.** Loss of sediment calculated on the assumption that the difference between the sedimentation rates of Sites 805 and 806 is entirely a result of the dissolution of carbonate and that the initial supply of sediment is the same at both sites. The uppermost two curves are the paired carbonate data, for orientation.

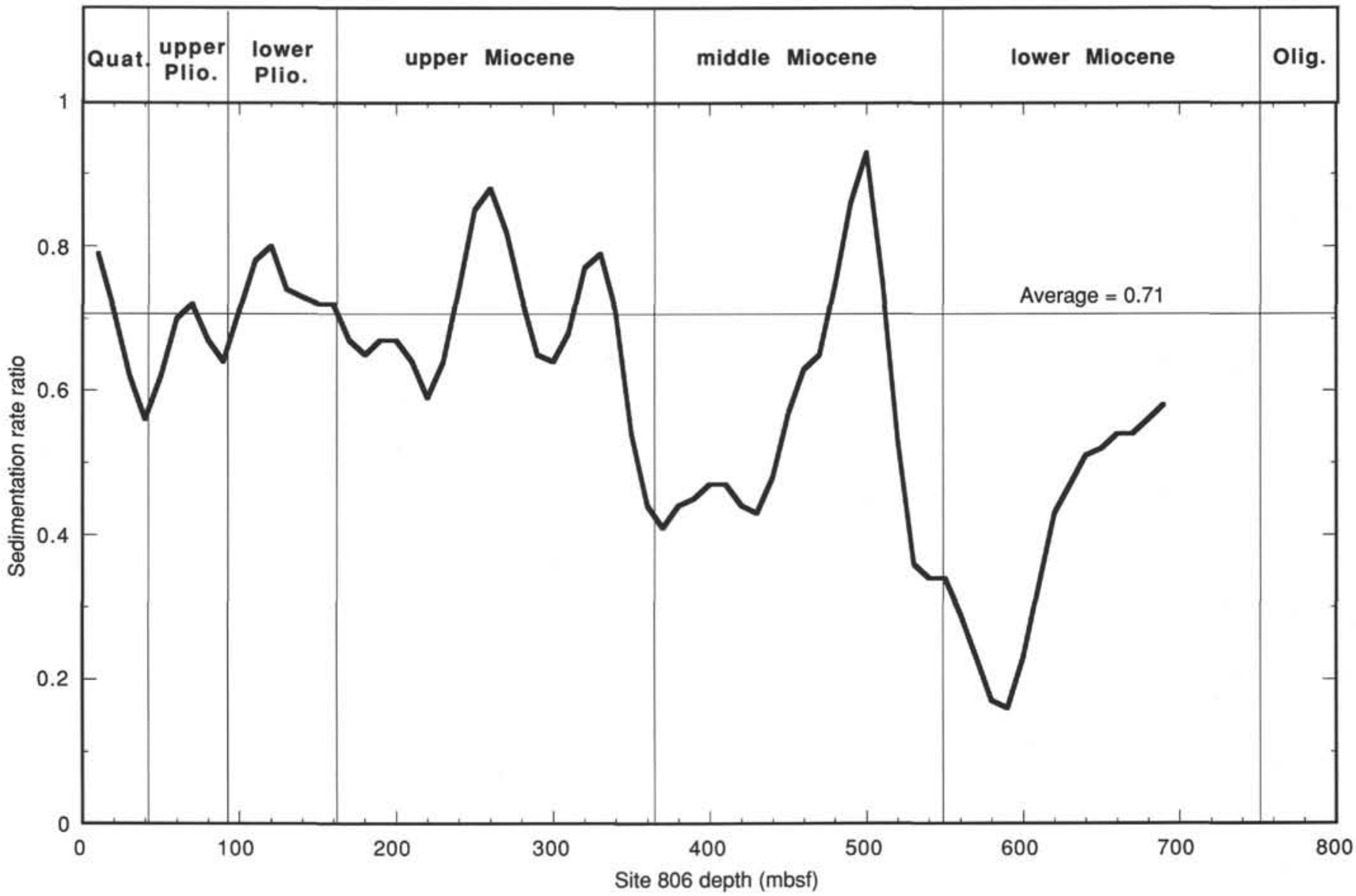

Figure 60. Sedimentation rate ratio between Sites 805 and 806, calculated on the basis of the match of carbonate curves shown in Figure 59. Note the similarity with the SRR curve based on biostratigraphy (Fig. 57) down to the upper middle Miocene. For older sediments, carbonate data are spotty.

is a tendency for a low SRR, presumably because of the equatorial position of Site 806. There are two substantial peaks and one valley in SRR within the interval with sufficient data for discussion (above 500 mbsf). The first peak is near 240 mbsf (6.5–7 Ma), the second is near 490 mbsf (14–15 Ma), and the valley is centered near 400 mbsf, in the upper middle Miocene (11 Ma). The peaks signify that sedimentation rates differed little between Sites 805 and 806 during those particular periods; the valley, on the other hand, indicates a major difference in sedimentation rates.

The first peak (near 240 mbsf) marks the time when Site 805 crossed the equator while Site 806 had moved off it. If we assume that Site 805 should have had a sedimentation rate 0.7 times that of 806, the discrepancy suggests that the difference in sedimentation rate between the equator and 1° to the south was a factor of 1.2. This appears reasonable for an equator-to-south comparison (a similar distance to the north would have virtually no effect). The period centered on 6–7 Ma falls in Hiatus Interval NH6 (Keller and Barron, 1987); perhaps this is why the equatorial effect is not expressed more strongly.

The second peak of SRR, near 490 mbsf, is centered on the Antarctic cooling event, as seen in oxygen isotopes (Savin et al., 1985; Vincent and Berger, 1985) and marks a time of substantial dissolution in Site 805. It is quite possible that this peak is spurious, at least in its extent above the average SRR. A slight adjustment of the match between Sites 805 and 806 could readily reduce the peak and at the same time fill the trough to its right, without eliminating it, of course. Not much credence can be given to the exact shape of the SRR minimum in the uppermost lower Miocene because the carbonate data base deteriorates quickly below 450 mbsf. The SRR minimum is most probably present (based on biostratigraphy, there is a condensed section in Site 805 centered at this period), but it does not necessarily extend to values below 0.3.

The broad SRR minimum in the upper middle Miocene, and extending into the lowermost upper Miocene, marks the end of the Antarctic cooling period (Savin et al., 1985) and contains two hiatus-prone periods (NH3 and NH4 of Keller and Barron, 1987), as well as evidence for major carbonate removal in the central Pacific (Barron et al., 1985). This coincidence suggests that the late-stage Antarctic cooling steps resulted in carbonate dissolution in the western equatorial Pacific, and that such dissolution affected Site 805 more than Site 806.

Discussion

A comparison of the carbonate-based stratigraphies is shown in Figure 61. The carbonate curves for Sites 805 and 806 are the same as in Figure 59 (showing only matching pairs). Note that correlation between the two curves is good to about 10 Ma ($R^2 = 0.81$), and becomes quite poor in sediments older than this ($R^2 = 0.16$). It is not clear to what extent this reflects a change in climate dynamics, and to what extent it is a function of poor data coverage. The matching technique also needs to be improved. Note for example that a slight shift of the Site 805 curve at 16 Ma to the left would improve the fit with the Site 806 curve between 15 and 17 Ma. This would have the beneficial effect of decreasing the apparent 15-Ma peak in the SRR (Fig. 60, 490

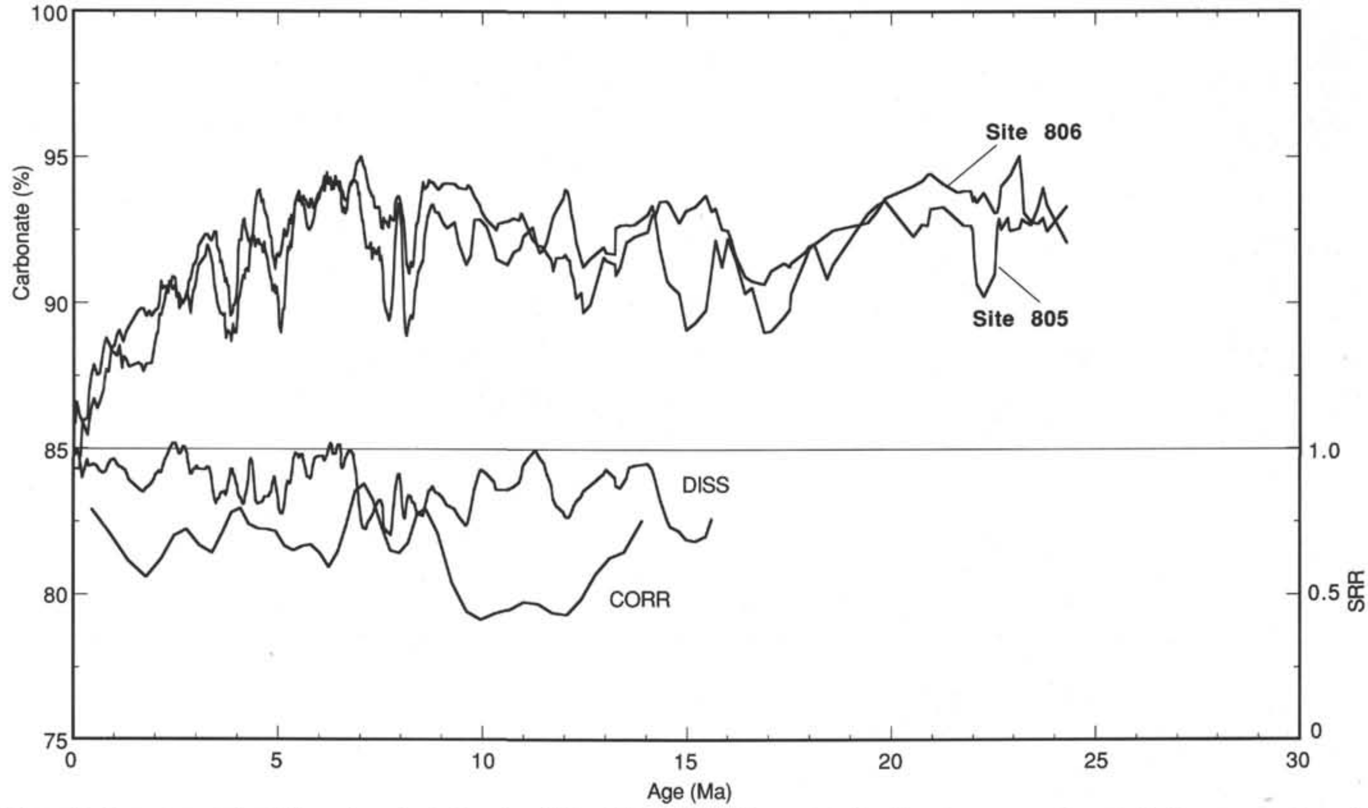

Figure 61. Summary graph of the carbonate stratigraphy of Sites 805 and 806. Top: matched carbonate curves, pairs only. Bottom: comparison of sedimentation rate ratios (SRR) between the two sites, one based on carbonate differences ("DISS"), the other on the match of the carbonate profiles ("CORR"). SRR values were left off for the deeper part of the section, where they are believed to be unreliable. Note that the two SRRs do not agree.

mbsf) while reducing the minimum in the SRR to the right (Fig. 60, 580 mbsf). Nevertheless, a strong dynamic component is believed to be present in the factors responsible for the change in carbonate correlation near 10 Ma, but this effect must be substantiated by work on shore.

The data density and the match based on it are thought to be quite good back to 13.5 Ma, so the two derivative curves are shown back to this time in the summary figure (Fig. 61). DISS is the SRR based on LOSS, where LOSS is calculated from the ratio of noncarbonate values (see equation above) (Fig. 59B), and CORR is the SRR based on matching the carbonate curves (Fig. 60). It is quite evident that the two independent SRR estimates only agree in three intervals: near 3.5–5, near 7–8.5, and near 14 Ma. These intervals contain well-defined periods of strong carbonate dissolution (CRE-V and CRE-VII, CRE-IX and CRE-X, and CRE-XVI; see Fig. 59A), all of which affect Site 805 much more than Site 806. During such times, then, the dissolution gradient dominates the differences in sedimentation rate. During the rest of the time (most of it, actually), changes in the carbonate dissolution gradient do not seem to be the controlling factor governing changes in sedimentation rates, or, if they are, carbonate dissolution does not result in sufficient reduction of carbonate percentages at the deeper site to allow calculation of the loss sustained.

The latter point was raised earlier, when discussing Figure 59B. The carbonate percentages in Site 805 are too similar to those of Site 806, considering the difference in sedimentation rates between the two sites. It is as though much noncarbonate loss occurred at Site 805 also, in addition to carbonate loss (which, of course, must bear the bulk of the difference between the two sites). An alternative hypothesis for explaining the discrepancy, namely, the addition of "trickle-down" carbonate from higher up the slope, cannot stand up to scrutiny. If sufficient nannofossil carbonate were to be added to Site 805 to bring the percentages back up, the rate of sedimentation would then go up proportionally, changing both SRR indexes in the same direction.

We need to find a mechanism that removes noncarbonate dilutants at the same time, and at the same measure, as carbonate is removed. Several mechanisms can be envisaged, as follows:

1. The reduction of carbonate accumulation from dissolution may lead to greater exposure of siliceous fossils, coupling their dissolution rate to that of carbonate. In this case, the diatoms at Site 805 should be less well preserved that those at Site 806, at least in the upper portion of the section, before diagenesis destroys the signal. The diatom preservation differences between Sites 805 and 806 are being checked for this predicted effect.

2. Dissolution of carbonate changes the physical properties of the sediment in such a fashion that mechanical removal of noncarbonate is more easily accomplished by a combination of biosuspension and current transport. In this case, the diatom-to-radiolarian ratio should be less in Site 805 than in Site 806, and there should also be less clay per radiolarian weight.

3. Much of the loss at Site 805 could be caused by solifluction, engendered by carbonate dissolution, which increases porosity and decreases shear strength. In this scenario, the bioturbated layer moves downslope during repeated short dissolution pulses and microhiatuses are produced, especially during earthquakes. Such a mechanism would result in loss of sediment without fractionating between carbonate and noncarbonate, reducing the "true" SRR, but not the one based on carbonate difference.

Evidence for the operation of these (or related) processes has to be collected onshore. It is unlikely that the raw grain size data available will throw light on the subject. The mean size values are higher in Site 806 than at Site 805, presumably because of the higher foraminifer content at the shallower site. This is the reverse of what would be expected if winnowing were the most important factor. However, breakdown of foraminifers from dissolution will produce a decrease in mean size in calcareous sediments (Johnson et al., 1977), overriding any effect from winnowing.

REFERENCES

Adelseck, C. G., Jr., 1977. Recent and late Pleistocene sediments from the eastern equatorial Pacific Ocean: sedimentation and dissolution [Ph.D. dissert.]. Univ. California, San Diego.

Backman, J., 1979. Pliocene biostratigraphy of DSDP Sites 111 and 116 from the North Atlantic Ocean and the age of the Northern Hemisphere Glaciation. *Stockholm Contrib. Geol.*, 32:115-137.

Barron, J. A., and Keller, G., 1982. Widespread Miocene deep-sea hiatuses: coincidence with periods of global cooling. *Geology*, 10:577-581.

Barron, J. A., Keller, G., and Dunn, D. A., 1985. A multiple microfossil biochronology for the Miocene. *In* Kennett, J. P. (Ed.), *The Miocene Ocean: Paleoceanography and Biogeography.* Mem. Geol. Soc. Am., 163:21-36.

Berger, W. H., 1979. Impact of deep-sea drilling on paleoceanography. *In* Talwani, M., Hay, W., and Ryan, W.B.F. (Eds.), *Deep Drilling Results in the Atlantic Ocean: Continental Margins and Paleoenvironment.* Am. Geophys. Union, Maurice Ewing Ser., 3:297-314.

Berger, W. H., and Johnson, T. C., 1976. Deep-sea carbonates: dissolution and mass wasting on Ontong Java Plateau. *Science*, 192:785-787.

Berger, W. H., Johnson, T. C., and Hamilton, E. L., 1977. Sedimentation on Ontong Java Plateau: observations on a classic "carbonate monitor." *In* Anderson, N. R., and Malahoff, A. (Eds.), *The Fate of Fossil Fuel CO_2 in the Oceans:* New York (Plenum Press), 543-567.

Berger, W. H., and Mayer, L. A., 1978. Deep-sea carbonates: acoustic reflectors and lysocline fluctuations. *Geology*, 6:11-15.

Berger, W. H., and Winterer, E. L., 1974. Plate stratigraphy and the fluctuating carbonate line. *In* Hsü, K. J., and Jenkyns, H. C. (Eds.), *Pelagic Sediments on Land and Under the Sea:* Spec. Publ., Int. Assoc. Sedimentol., 1:11-48.

Bukry, D., 1973. Low-latitude coccolith biostratigraphic zonation. *In* Edgar, N. T., Saunders, J. B., et al., *Init. Repts. DSDP*, 15: Washington (U.S. Govt. Printing Office), 685-703.

Davies, T. A., Hay, W. W., Southam, J. R., Worsley, T. R., 1977. Estimates of Cenozoic oceanic sedimentation rates. *Science*, 197:53-55.

Dunlop, D. J., 1981. The rock magnetism of fine particles. *Phys. Earth Planet. Inter.*, 26:1-26.

Elderfield, H., Gieskes, J. M., Baker, P. A., Oldfield, R. K., Hawkesworth, C. J., and Miller, R., 1982. $^{87}Sr/^{86}Sr$ and $^{18}O/^{16}O$ ratios, interstitial water chemistry and diagenesis in deep-sea carbonate sediments of the Ontong-Java Plateau. *Geochim. Cosmochim. Acta*, 46:2259-2268.

Emeis, K.-C., and Kvenvolden, K. A., 1986. Shipboard organic geochemistry on *JOIDES Resolution. ODP Tech. Note*, No. 7.

Farrell, J. W., and Prell, W. L., 1989. Climatic change and $CaCO_3$ preservation: an 800,000 year bathymetric reconstruction from the central equatorial Pacific Ocean. *Paleoceanography*, 4:447-466.

Gieskes, J. M., 1981. Deep-sea drilling interstitial water studies: implications for chemical alteration of the oceanic crust, Layers I and II. *In* Warme, J. E., Douglas, R. G., and Winterer, E. L. (Eds.), *The Deep Sea Drilling Project: A Decade of Progress.* Spec. Publ., Soc. Econ. Paleontol. Mineral., 32:149-167.

Hamilton, E. L., 1976. Variations in density and porosity with depth in deep-sea sediments. *J. Sediment. Petrol.*, 46:280-300.

Hussong, D. M., Wipperman, L. K., and Kroenke, L. W., 1979. The crustal structure of the Ontong Java and Manahiki oceanic plateaus. *J. Geophys. Res.*, 84:6003-6010.

Ingle, J. C., 1973. Summary comments on Neogene biostratigraphy, physical stratigraphy and paleo-oceanography in the marginal northeastern Pacific Ocean. *In* Kulm, L. D., von Huene, R., et al., *Init. Repts. DSDP*, 18: Washington (U.S. Govt. Printing Office), 949-960.

Johnson, T. C., Hamilton, E. L., and Berger, W. H., 1977. Physical properties of calcareous ooze: control by dissolution at depth. *Mar. Geol.*, 24:259-277.

Karlin, R., and Levi, S., 1983. Diagenesis of magnetic minerals in recent hemipelagic sediments. *Nature*, 303:327-330.

Karlin, R., and Levi, S., 1985. Geochemical and sedimentological control of the magnetic properties of hemipelagic sediments. *J. Geophys. Res.*, 90:10,373-10,392.

Keigwin, L. D., 1978. Pliocene closing of the Isthmus of Panama, based on biostratigraphic evidence from nearby Pacific and Caribbean sea cores. *Geology*, 6:630-634.

Keller, G., and Barron, J. A., 1987. Paleodepth distribution of Neogene deep-sea hiatuses. *Paleoceanography*, 2:697-713.

Kennett, J. P. (Ed.), 1985. *The Miocene Ocean: Paleoceanography and Biogeography.* Mem. Geol. Soc. Am., No. 163.

Kligfield, R., and Channell, J.E.T., 1981. Widespread remagnetization of Helvetic Limestones. *J. Geophys. Res.*, 86:1888-1900.

Kroenke, L., 1972. Geology of the Ontong Java Plateau [Ph.D. dissert.]. Univ. of Hawaii.

Lowrie, W., and Heller, F., 1982. Magnetic properties of marine limestones. *Rev. Geophys. Space Phys.*, 20:171-192.

Martini, E., 1971. Standard Tertiary and Quaternary calcareous nannoplankton zonation. *In* Farinacci, A. (Ed.), *Proc. 2nd Planktonic Conf. Roma:* Rome (Ed. Technosci.), 2:739-785.

Mayer, L. A., Shipley, T. H., Theyer, F., Wilkens, R. W., and Winterer, E. L., 1985. Seismic modelling and paleoceanography at DSDP Site 574. *In* Mayer, L. A., Theyer, F., Thomas, E., et al., *Init. Repts. DSDP*, 85: Washington (U.S. Govt. Printing Office), 947-970.

Mayer, L. A., Shipley, T. H., and Winterer, E. L., 1986. Equatorial Pacific seismic reflectors as indicators of global oceanographic events. *Science*, 233:761-764.

McDuff, R. E., and Gieskes, J. M., 1976. Calcium and magnesium profiles in DSDP interstitial waters: diffusion or reaction? *Earth Planet. Sci. Lett.*, 33:1-10.

Moore, T. C., Pisias, N. G., and Heath, G. R., 1977. Climate changes and lags in Pacific carbonate preservation, sea surface temperature and global ice volume. *In* Malahoff, A., and Anderson, N. (Eds.), *The Fate of Fossil Fuel CO_2 in the Oceans:* New York (Plenum Press), 145-165.

Okada, H., and Bukry, D., 1980. Supplementary modification and introduction of code numbers to the low latitude coccolith biostratigraphic zonation (Bukry, 1973; 1975). *Mar. Micropaleontol.*, 5:321-325.

Riedel, W. R., and Sanfilippo, A., 1978. Stratigraphy and evolution of tropical Cenozoic radiolarians. *Micropaleontology*, 24:61-96.

Rio, D., Fornaciari, E., and Raffi, I., 1990. Late Oligocene through early Pleistocene calcareous nannofossils from western equatorial Indian Ocean (ODP Leg 115). *In* Backman, J., Duncan, R. A., et al., *Proc. ODP, Sci. Results*, 115: College Station, TX (Ocean Drilling Program), .

Sager, W. W., 1988. Paleomagnetism of Ocean Drilling Program Leg 101 Sediments: magnetostratigraphy, magnetic diagenesis, and paleolatitudes. *In* Austin, J. A., Jr., Schlager, W., et al., *Proc. ODP, Sci. Results*, 101: College Station, TX (Ocean Drilling Program), 327-360.

Saito, T., Burckle, L. H., and Hays, J. D., 1975. Late Miocene to Pleistocene biostratigraphy of equatorial Pacific sediments. *In* Saito, T., and Burckle, L. H. (Eds.), *Late Neogene Epoch Boundaries.* Spec. Publ., Micropaleontol., 1:226-244.

Sallomy, J. T., and Briden, J. C., 1975. Palaeomagnetic studies of Lower Jurassic rocks in England and Wales. *Earth Planet. Sci. Lett.*, 24:369-376.

Savin, S. M., Abel, L., Barrera, E., Hodell, D., Kennett, J. P., Murphy, M., Keller, G., Killingley, J., and Vincent, E., 1985. The evolution of Miocene surface and near-surface marine temperatures: oxygen isotopic evidence. *In* Kennett, J. P. (Ed.), *The Miocene Ocean: Paleoceanography and Biogeography.* Mem. Geol. Soc. Am., 163:49-82.

Schlanger, S. O., and Douglas, R. G., 1974. The pelagic ooze-chalk-limestone transition and its implication for marine stratigraphy. *In* Hsü, K. J., and Jenkyns, H. C. (Eds.), *Pelagic Sediments: On Land and Under the Sea.* Spec. Publ., Int. Assoc. Sedimentol., 1:117-148.

Shackleton, N. J., Backman, J., Zimmerman, H., Kent, D. V., Hall, M. A., Roberts, D. G., Schnitker, D., Baldauf, J., Desprairies, A., Homrighausen, R., Huddlestun, P., Keene, J. B., Kaltenback, A. J., Krumsiek, K.A.O., Morton, A. C., Murray, J. W., and Westberg-Smith, J., 1984. Oxygen isotope calibration of the onset of ice-rafting in DSDP Site 552A: history of glaciation in the North Atlantic region. *Nature,* 307:620–623.

Shackleton, N. J., and Opdyke, N. D., 1976. Oxygen-isotope and paleomagnetic stratigraphy of Pacific Core V28-239: late Pliocene to latest Pleistocene. *In* Cline, R. M., and Hays, J. D. (Eds.), *Investigations of Late Quaternary Paleoceanography and Paleoclimatology.* Mem. Geol. Soc. Am., 145:449–464.

Shipboard Scientific Party, 1971. Site 64. *In* Winterer, E. L., Riedel, W. R., et al., *Init. Repts. DSDP,* 7: Washington (U.S. Govt. Printing Office), 473–606.

Shipboard Scientific Party, 1975a. Site 288. *In* Andrews, J. E., Packham, G., et al., *Init. Repts. DSDP,* 30: Washington (U.S. Govt. Printing Office), 175–229.

Shipboard Scientific Party, 1975b. Site 289. *In* Andrews, J. E., Packham, G., et al., *Init. Repts. DSDP,* 30: Washington (U.S. Govt. Printing Office), 231–398.

Shipboard Scientific Party, 1986a. Site 586. *In* Moberly, R., Schlanger, S. O., et al., *Init. Repts. DSDP,* 89: Washington (U.S. Govt. Printing Office), 213–281.

Shipboard Scientific Party, Leg 90, 1986b. Site 586: western equatorial Pacific. *In* Kennett, J. P., von der Borch, C. C., et al., *Init. Repts DSDP,* 90: Washington (U.S. Govt. Printing Office), 19–114.

Shipboard Scientific Party, 1989. Explanatory Notes. *In* Prell, W. L., Niitsuma, N., et al., *Proc. ODP, Init. Repts.,* 117: College Station, TX (Ocean Drilling Program), 11–33.

Thompson, P. R., 1976. Planktonic foraminiferal dissolution and the progress towards a Pleistocene equatorial Pacific transfer function. *J. Foraminiferal Res.,* 6:208–227.

van Andel, T. H., Heath, G. R., and Moore, T. C., Jr., 1975. Cenozoic history and paleoceanography of the central equatorial Pacific. *Mem. Geol. Soc. Am.,* No. 143.

Vincent, E., and Berger, W. H., 1985. Carbon dioxide and polar cooling in the Miocene: the Monterey Hypothesis. *In* Sundquist, E., and Broecker, W. S. (Eds.), *The Carbon Cycle and Atmospheric CO_2: Natural Variations Archean to Present:* Am. Geophys. Union, Geophys. Monogr. Ser., 32:455–468.

Whitman, J. M, 1989. Stable isotope record of foraminifera from Ontong Java Plateau for the last 6 million years, DSDP Site 586 [Ph.D. dissert.]. Univ. California, San Diego.

Wu, G., and Berger, W. H., 1989. Planktonic foraminifera: differential dissolution and the Quaternary stable isotope record in the west-equatorial Pacific. *Paleoceanography,* 4:181–198.

Ms 130A-108

NOTE: All core description forms ("barrel sheets") and core photographs have been printed on coated paper and bound as Section 5, near the back of the book, beginning on page 559.

Hole 806B: Resistivity-Sonic-Gamma Ray Log Summary

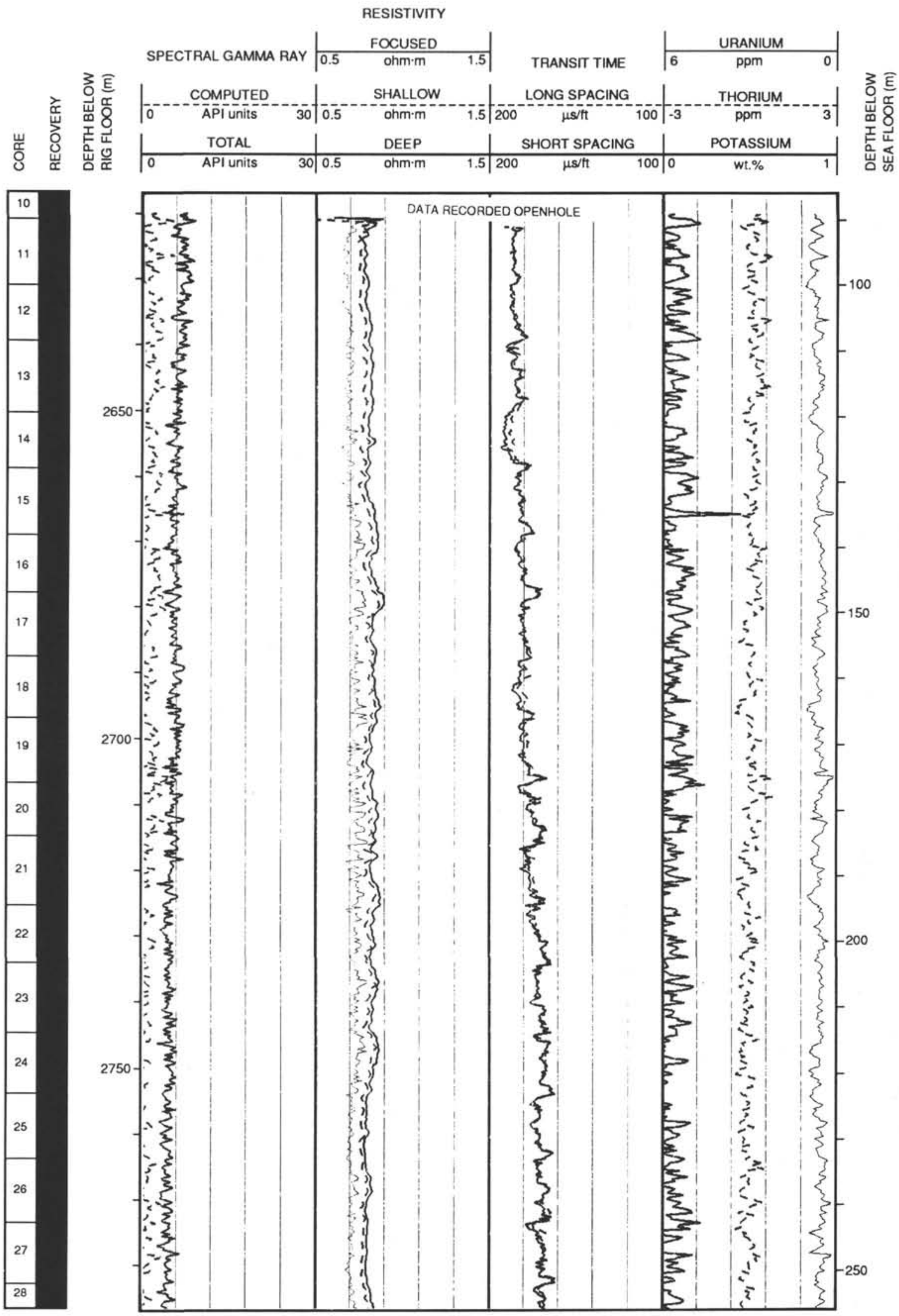

Hole 806B: Resistivity-Sonic-Gamma Ray Log Summary (continued)

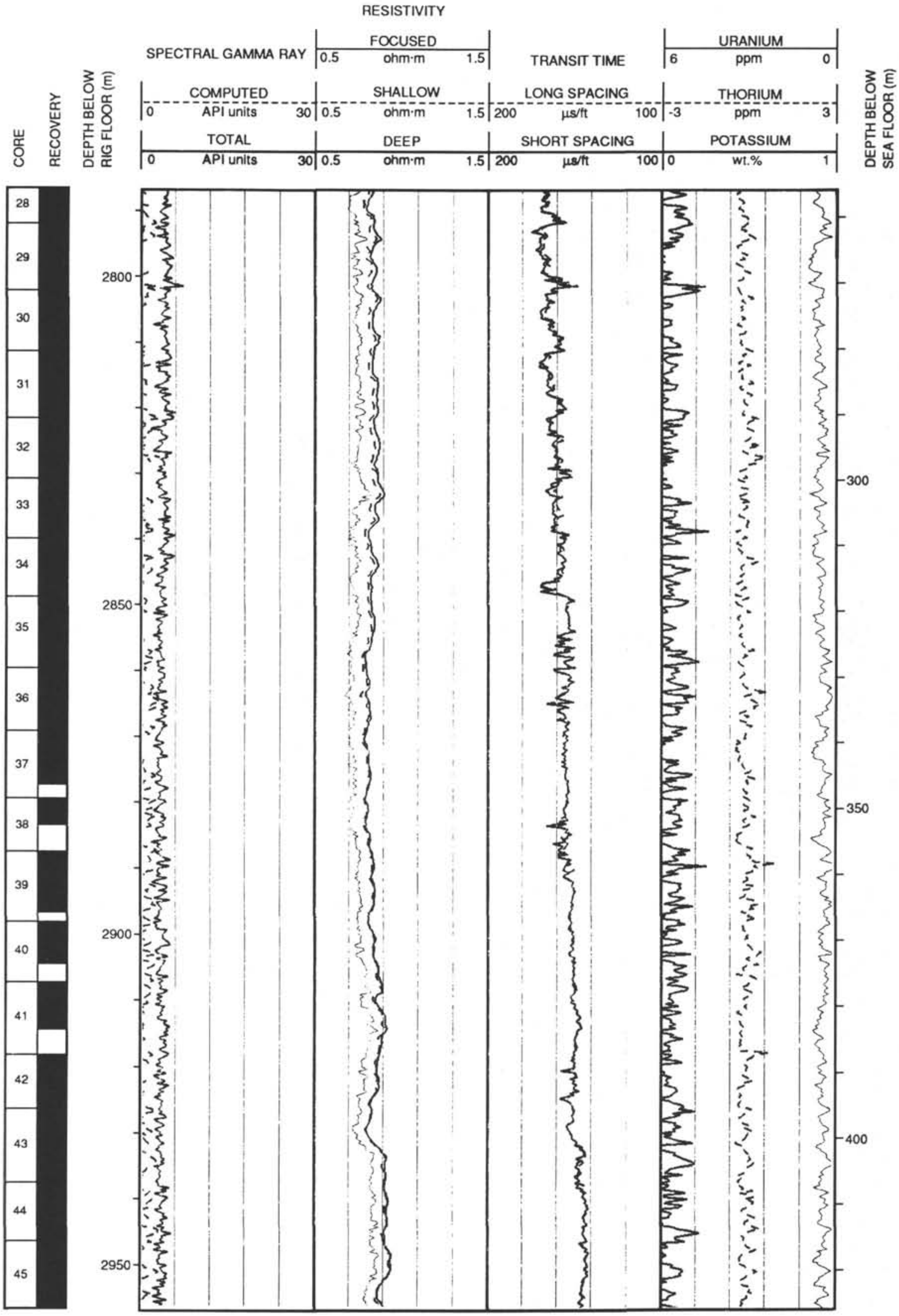

Hole 806B: Resistivity-Sonic-Gamma Ray Log Summary (continued)

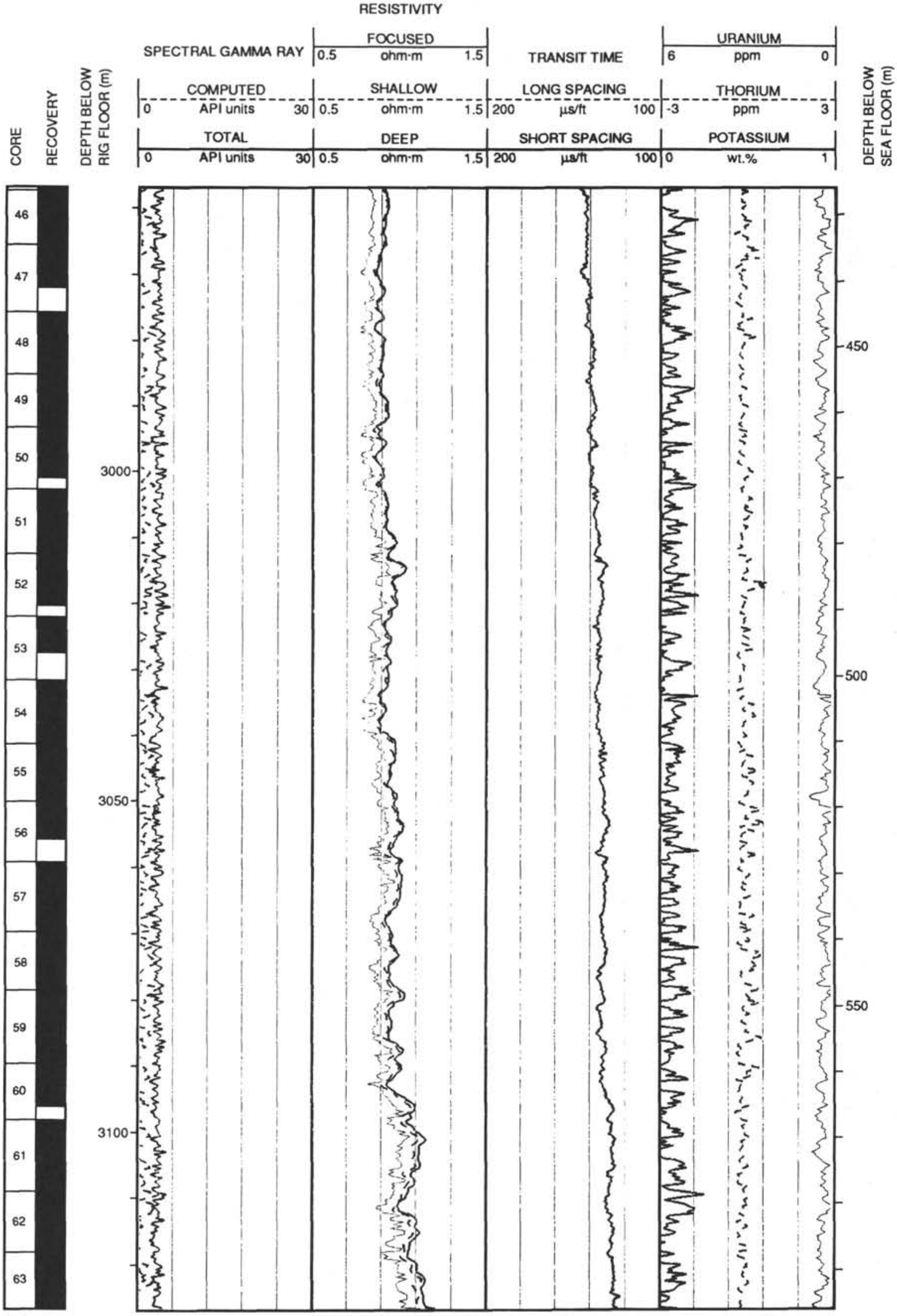

Hole 806B: Resistivity-Sonic-Gamma Ray Log Summary (continued)

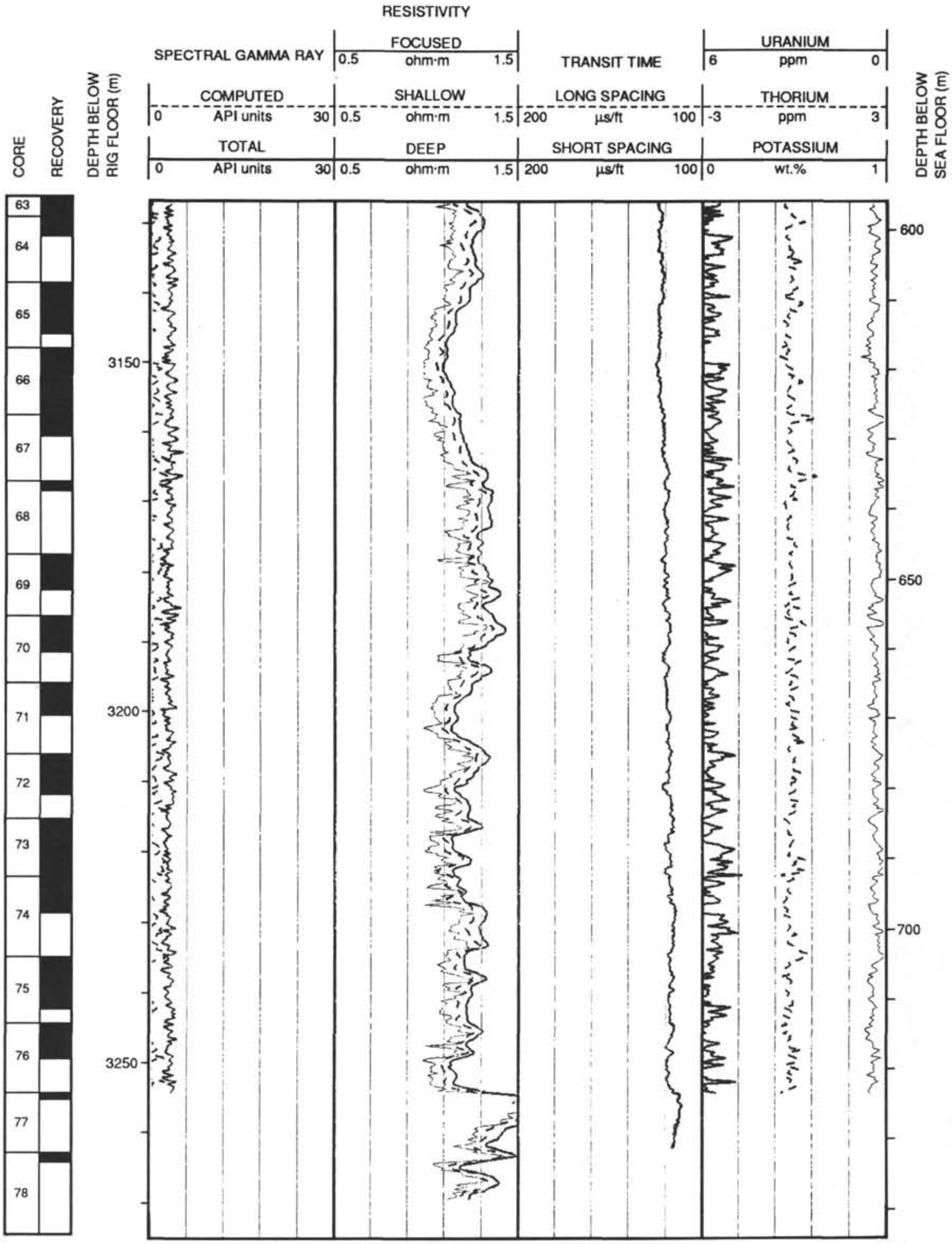

Hole 806B: Density-Gamma Ray Log Summary

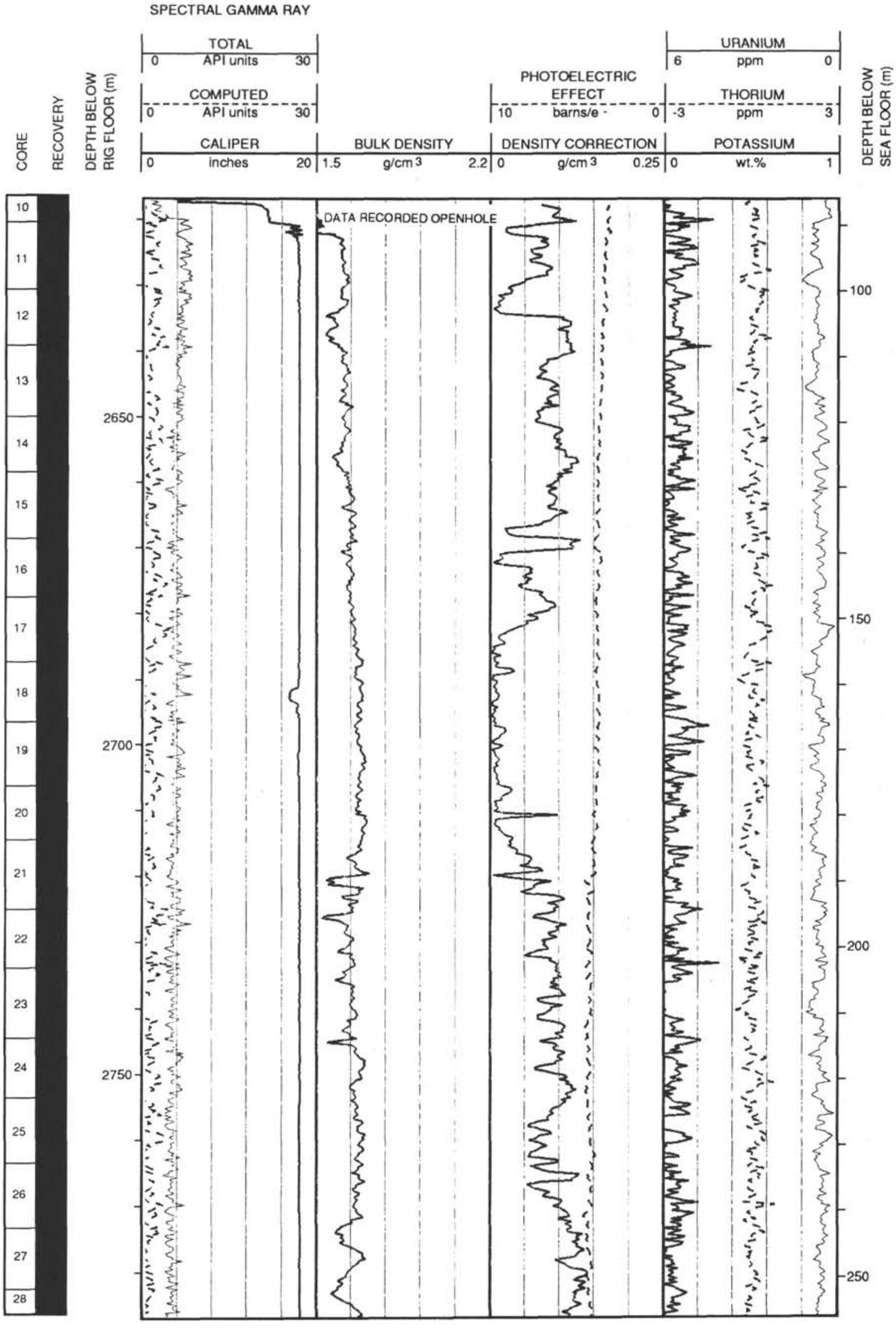

Hole 806B: Density-Gamma Ray Log Summary (continued)

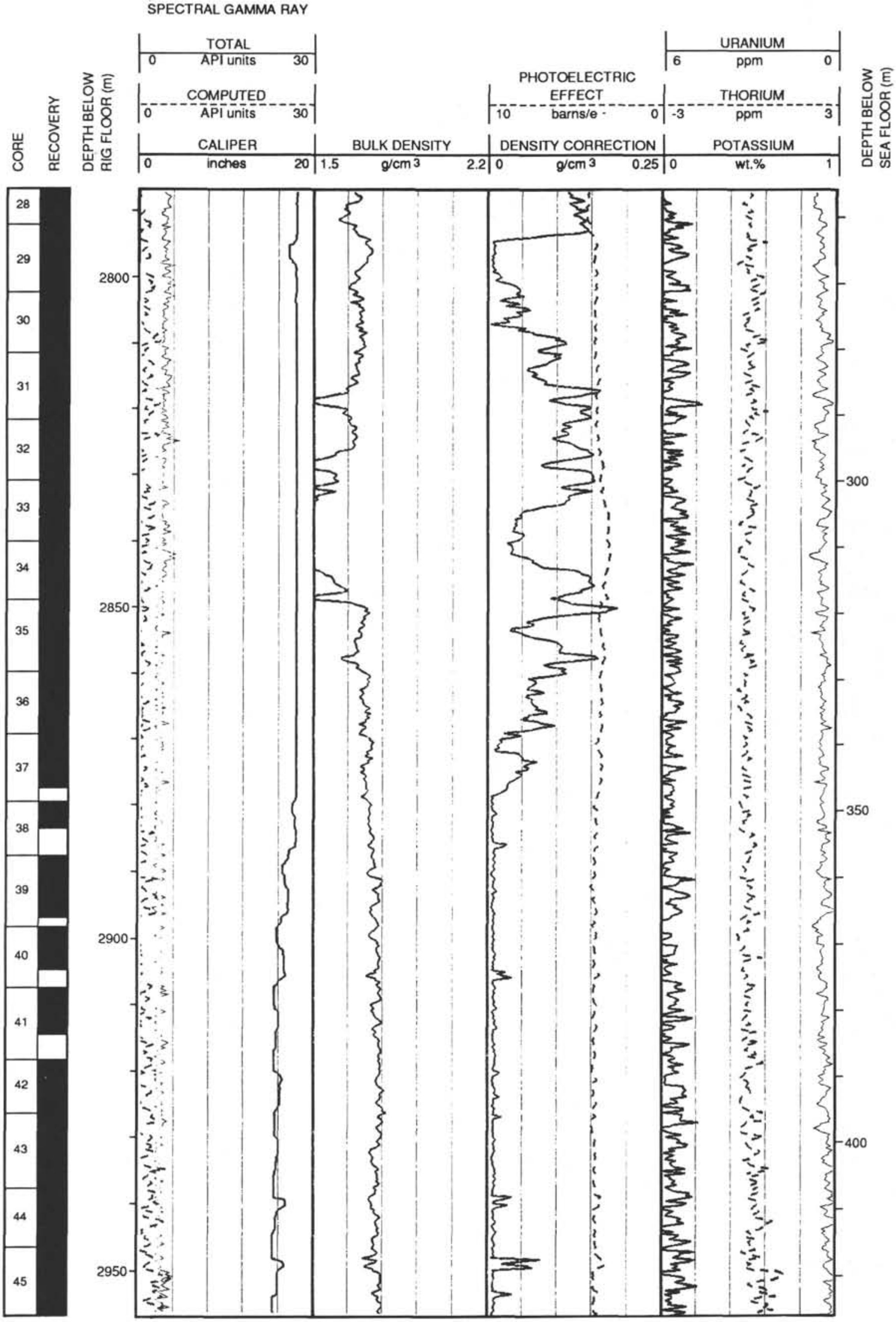

Hole 806B: Density-Gamma Ray Log Summary (continued)

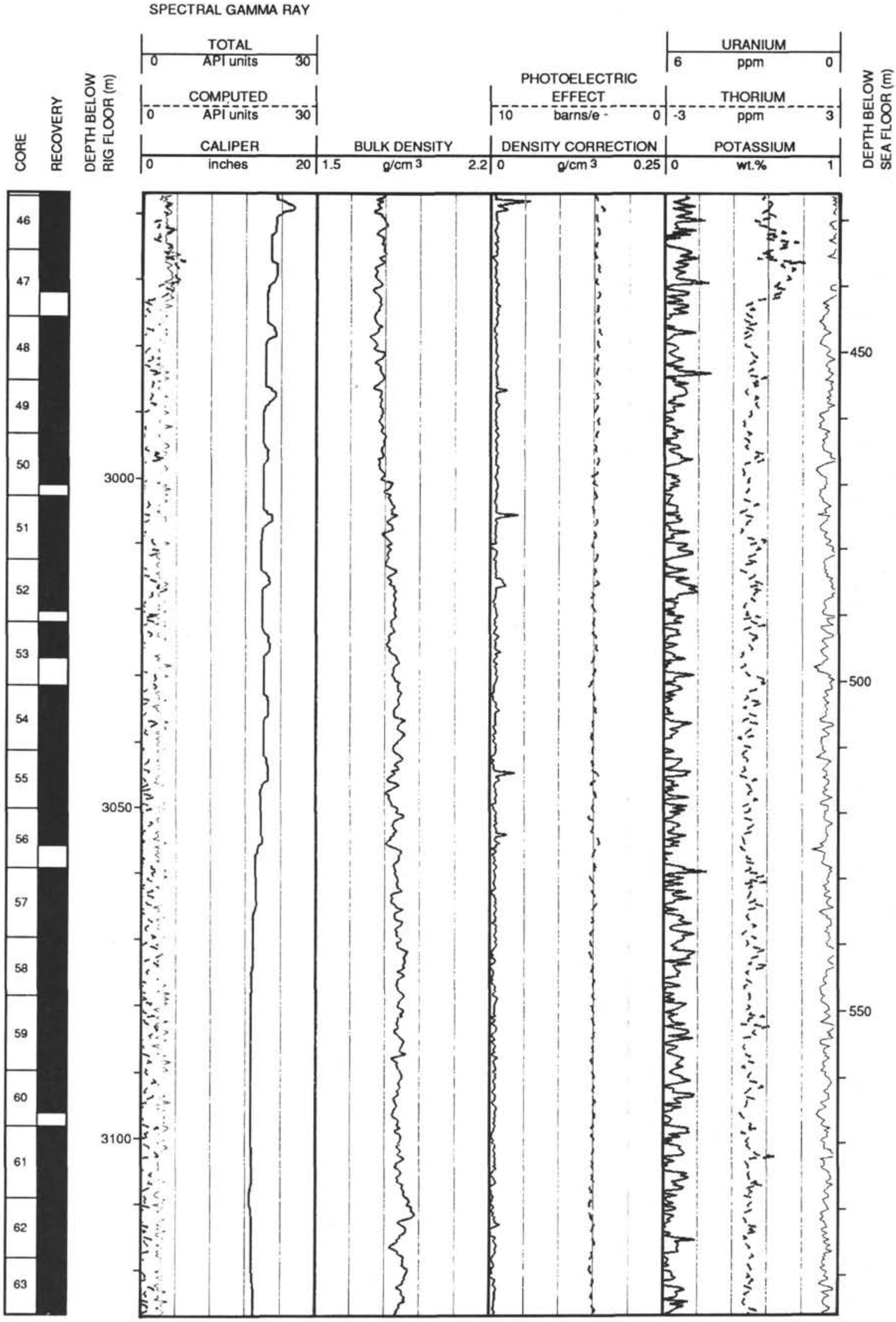

Hole 806B: Density-Gamma Ray Log Summary (continued)

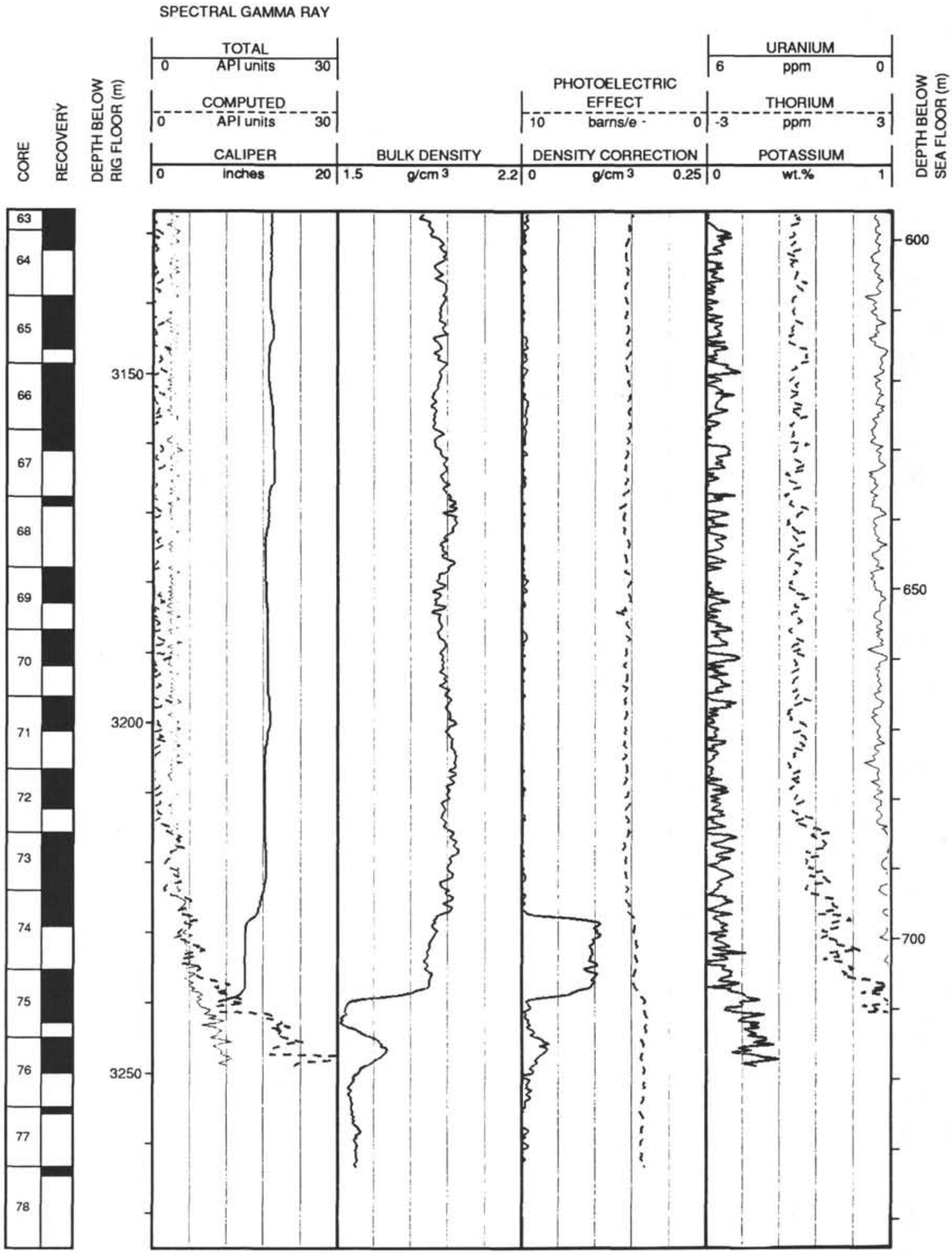

Hole 806B: Geochemical Log Summary

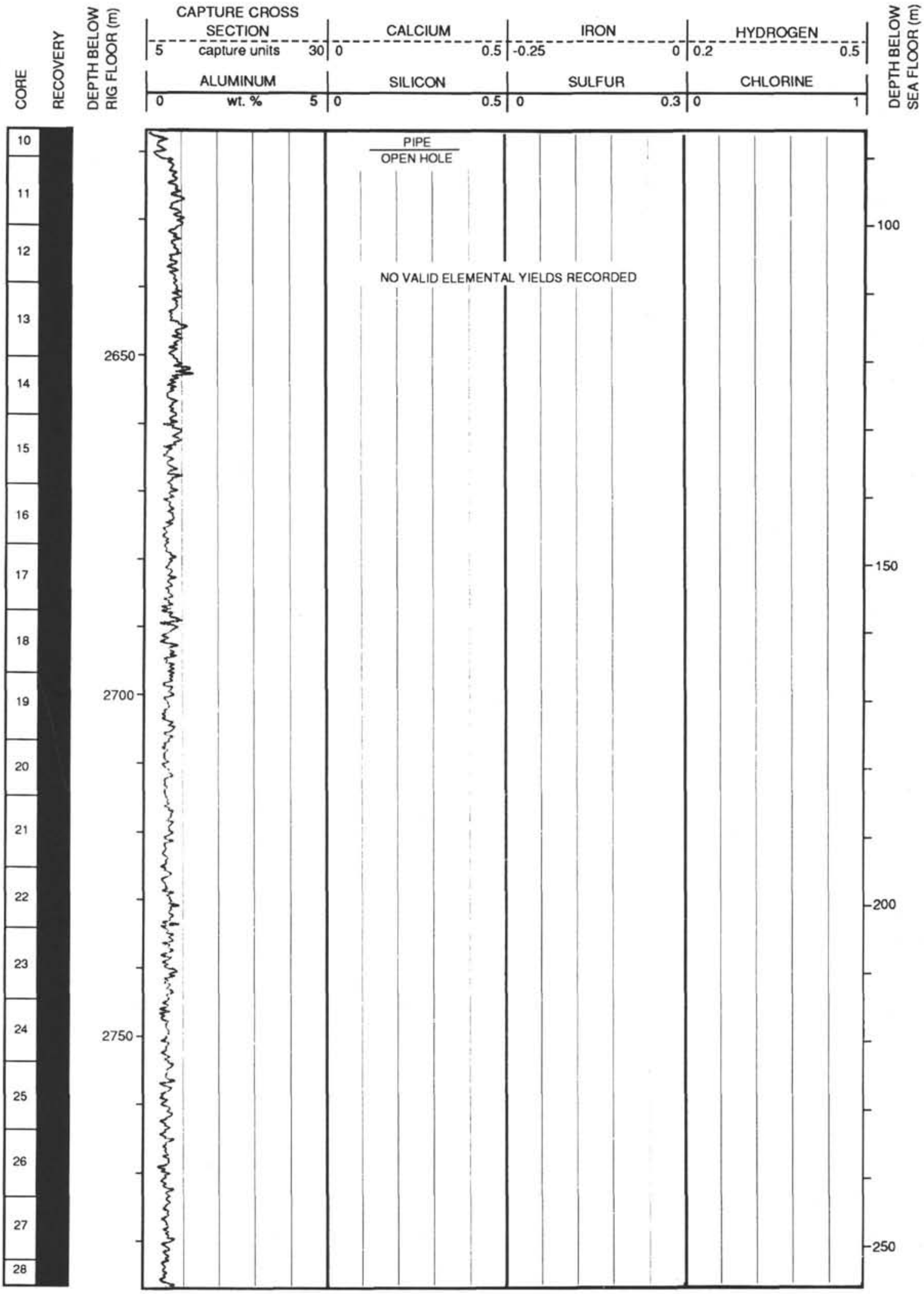

Hole 806B: Geochemical Log Summary (continued)

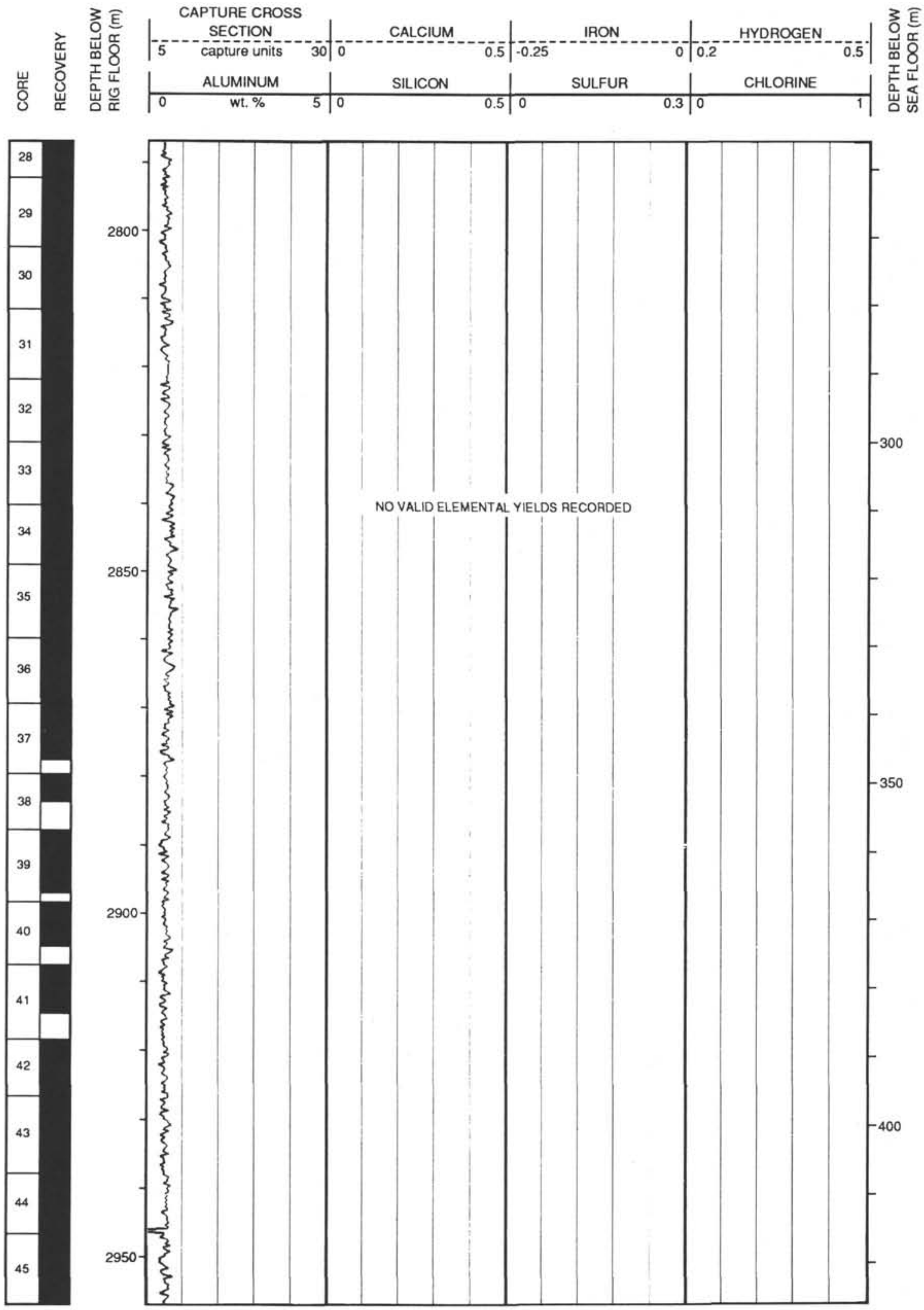

Hole 806B: Geochemical Log Summary (continued)

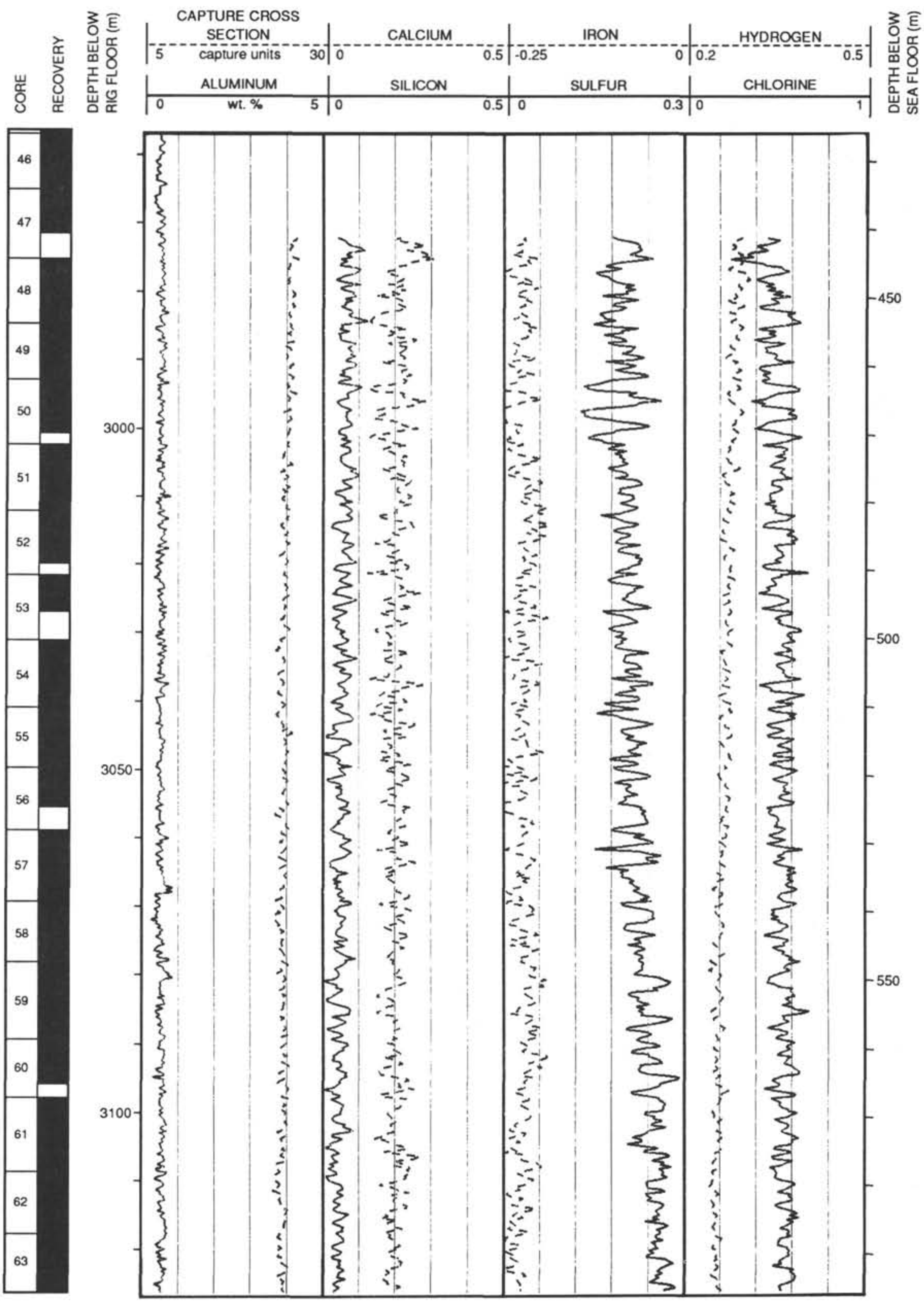

Hole 806B: Geochemical Log Summary (continued)